



THE UNIVERSITY OF QUEENSLAND
AUSTRALIA

Locomotive Traction and Rail Wear Control

Ye Tian

BEng Electrical Engineering and Automation Tianjin University, China

MSc Control Systems Imperial College London, UK

A thesis submitted for the degree of Doctor of Philosophy at

The University of Queensland in 2015

School of Mechanical and Mining Engineering

Abstract

Railways play one of the most important roles in today's transport systems throughout the world due to their safety, relatively high traction capacity and low operation and maintenance cost [1]. With the development of electric drive and power electronics technology, the capacity and efficiency of railway transport has been improved dramatically, giving birth to higher speed passenger trains and higher capacity heavy haul trains. In Australia, the development of the mineral resources industry drives further improvement of railway operational efficiency without bringing excessive burden to infrastructural maintenance. The purpose of this thesis is to provide the required modelling and simulation to determine appropriate traction system conditions and controllers to achieve this.

The first part of this thesis is focused on building a locomotive mathematical model including all the essential dynamic components and interactions to provide prediction of locomotive dynamic response. The overall model consists of locomotive dynamics, wheel/rail contact dynamics and electrical drive and control dynamics. The locomotive dynamics include longitudinal, vertical and pitch motions of the locomotive body, front and rear bogies and six axles. For the wheel/rail contact dynamics, the Polach model is used to obtain the amount of tractive force generated due to wheel/rail interaction on the contact patch. The simplified electric drive dynamics are designed according to the traction effort curves provided by industry using constant torque and constant power regions. Modes of oscillations have been identified by eigenmode analysis and show that all the vertical and pitch modes of the locomotive dynamics are stable. The modes that are most likely to contribute to dynamic behaviour are identified and it is shown that the locomotive body pitch mode is most excited by traction perturbations. The locomotive dynamic behaviour under changes in contact conditions is also examined.

The second part of this thesis is focused on achieving higher tractive force under different operating speed and wheel/rail contact conditions. The dynamic impact of a new control strategy is compared with that of a traditional fixed threshold creep/adhesion control strategy. A fuzzy logic based control strategy is employed to adjust the torque output of the motors according to the operating condition of the locomotive to achieve higher tractive force than that with the traditional constant creep control strategy. Simulation results show that by controlling the torque generated by the electric drives, tractive force can be maximized. However, the benefit in the tractive force increase is marginal under low speed operation at the cost of higher creep values. Under high speed operation, due to the impact of the electric drive traction effort characteristics, the dynamic responses with both control strategies are mostly identical.

The last part of this thesis is focused on specialized real-time traction control that regulates the wear to low levels, which is motivated by the increased amount of rail wear damage observed in the rail industry in recent years. In this thesis, a novel real-time approach of controlling wear damage on rail tracks is proposed based on a recent wear growth model. Simulation results show that under high speed operation the dynamic responses are mostly identical with two investigated control strategies due to the impact of the electric drive traction effort characteristics. However, the new control strategy can effectively reduce wear damage dramatically under other operation conditions, with a relatively small amount of tractive force decrease.

The work in this thesis explores various aspects of locomotive traction research. The most important contributions are the development of a mathematical/simulation model for predicting the dynamic response of a locomotive under change of operating conditions and its impact on wear damage on rail tracks. The impact of maximizing tractive effort on rail track wear damage is quantified, providing practical guidance on locomotive operation. In addition to this, the development and testing of a specialized real-time traction control strategy that regulates the wear to low levels based on a recent wear growth model is provided.

Declaration by author

This thesis is composed of my original work, and contains no material previously published or written by another person except where due reference has been made in the text. I have clearly stated the contribution by others to jointly-authored works that I have included in my thesis.

I have clearly stated the contribution of others to my thesis as a whole, including statistical assistance, survey design, data analysis, significant technical procedures, professional editorial advice, and any other original research work used or reported in my thesis. The content of my thesis is the result of work I have carried out since the commencement of my research higher degree candidature and does not include a substantial part of work that has been submitted to qualify for the award of any other degree or diploma in any university or other tertiary institution. I have clearly stated which parts of my thesis, if any, have been submitted to qualify for another award.

I acknowledge that an electronic copy of my thesis must be lodged with the University Library and, subject to the General Award Rules of The University of Queensland, immediately made available for research and study in accordance with the *Copyright Act 1968*.

I acknowledge that copyright of all material contained in my thesis resides with the copyright holder(s) of that material. Where appropriate I have obtained copyright permission from the copyright holder to reproduce material in this thesis.

Publications during candidature

The following publications are related to the research work conducted in this dissertation.

Paper A, Y. Tian, W.J.T. (Bill) Daniel, S. Liu and P.A. Meehan, 2013, “Dynamic Tractional Behaviour Analysis and Control for a DC Locomotive”, World Congress of Rail Research 2013.

Paper B, Y. Tian, W.J.T. (Bill) Daniel, S. Liu and P.A. Meehan, 2014, “Fuzzy Logic Creep Control for a 2D Locomotive Dynamic Model under Transient Wheel-rail Contact Condition”, 14th International Conference on Railway Engineering Design and Optimization, COMPRAIL 2014, Proceedings: Computers in Railways XIV: Railway Engineering Design and Optimization: WIT Press; 2014. 885-896.

Paper C, Y. Tian, W.J.T. (Bill) Daniel, S. Liu and P.A. Meehan, 2015, “Fuzzy Logic based Sliding Mode Creep Controller under Varying Wheel-Rail Contact Conditions”, International Journal of Rail Transportation, 3(1), 40-59.

Paper D, Y. Tian, W.J.T. (Bill) Daniel, S. Liu and P.A. Meehan, “Investigation of the impact of full scale locomotive adhesion control on wear under changing contact conditions”, accepted by Vehicle System Dynamics special issue, DOI: 10.1080/00423114.2015.1020815.

Paper E, Y. Tian, W.J.T. (Bill) Daniel, and P.A. Meehan, “Real-time rail/wheel wear damage control”, submitted to International Journal of Rail Transportation.

Paper F, (co-authored): Sheng Liu, Ye Tian, W.J.T. (Bill) Daniel and Paul A. Meehan, “Dynamic response of a locomotive with AC electric drives due to changes in friction conditions”, submitted to Journal of Rail and Rapid Transit.

Publications included in this thesis

None

Contributions by others to the thesis

My thesis supervisor Paul Meehan provided extensive assistance with drafting and revision of this thesis and each paper mentioned below so as to contribute to the interpretation. Specific assistance with individual papers is detailed below.

In **Paper A**, (Y. Tian, W.J.T. (Bill) Daniel, S. Liu and P.A. Meehan, 2013, “Dynamic Tractional Behaviour Analysis and Control for a DC Locomotive”, Proceedings of the 10th World Congress of Rail Research), Paul Meehan provided guidance and motivation for building a longitudinal-vertical-pitch locomotive dynamic model including the wheel-rail contact dynamics and simplified DC drive dynamics in Matlab and assistance in revision. Bill Daniel provided guidance and suggestions in multibody dynamics as well as contact mechanics. Sheng Liu provided help in proofreading the paper. Ye Tian was responsible for the remainder of the work.

In **Paper B**, (Y. Tian, W.J.T. (Bill) Daniel, S. Liu and P.A. Meehan, 2014, “Fuzzy Logic Creep Control for a 2D Locomotive Dynamic Model under Transient Wheel-rail Contact Condition”, 14th International Conference on Railway Engineering Design and Optimization, COMPRAIL 2014, Proceedings: Computers in Railways XIV: Railway Engineering Design and Optimization: WIT Press; 2014. P885-896.), Paul Meehan provided guidance and motivation for investigating a controller to achieve highest tractive force available. Bill Daniel provided assistance in modelling. Sheng Liu provided assistance in revision. Ye Tian was responsible for modelling, simulations and result analysis. The remainder of the work was done by Ye Tian.

In **Paper C**, (Y. Tian, W.J.T. (Bill) Daniel, S. Liu and P.A. Meehan, 2015, “Fuzzy Logic based Sliding Mode Creep Controller under Varying Wheel-Rail Contact Conditions”, International Journal of Rail Transportation, 3(1), 40-59), Paul Meehan provided guidance and motivation for investigating the controller achieving highest tractive effort and the practical control effect comparison between this controller and a traditional one. Ye Tian was responsible for modelling integration, simulations and result analysis. Bill Daniel and Sheng Liu provided assistance in proofreading. Ye Tian was responsible for the any remaining work.

In **Paper D**, (Y. Tian, W.J.T. (Bill) Daniel, S. Liu and P.A. Meehan, “Investigation of the impact of full scale locomotive adhesion control on wear under changing contact conditions”, accepted by Vehicle System Dynamics special issue, DOI: 10.1080/00423114.2015.1020815), Paul Meehan provided guidance and motivation for investigating the effect of traditional creep controller

threshold setting and its effect on wear growth rate. Ye Tian was responsible for modelling integration, simulations and result analysis. Bill Daniel and Sheng Liu provided assistance in proofreading. Ye Tian was responsible for the any remaining work.

In **Paper E**, Y. Tian, W.J.T. (Bill) Daniel, and P.A. Meehan, “Real-time rail/wheel wear damage control”, submitted to International Journal of Rail Transportation, Paul Meehan provided guidance and motivation for investigating the controller reducing wear damage and the practical control effect comparison between this controller and a traditional one. Ye Tian was responsible for modelling integration, simulations and result analysis. Bill Daniel provided assistance in proofreading. Ye Tian was responsible for the any remaining work.

In **Paper F**, (Sheng Liu, Ye Tian, W.J.T. (Bill) Daniel and Paul A. Meehan, “Dynamic response of a locomotive with AC electric drives due to changes in friction conditions”, submitted to Journal of Rail and Rapid Transit), Paul Meehan provided guidance and motivation for investigating the dynamic response of a locomotive with complex AC drives due to changes in friction conditions. Bill Daniel provided assistance in modelling. Ye Tian was responsible for modelling and implementing the model in Simulink/Matlab. The remainder of the work was done by Sheng Liu.

Statement of parts of the thesis submitted to qualify for the award of another degree

None.

Acknowledgements

I would like to thank Australian Government and the University of Queensland for the scholarship that enabled me to do this PhD.

I would like to thank both technical support and financial support of CRC for Rail Innovation under the project No. R3.119 Locomotive Adhesion.

I would like to thank my principal supervisor Associate Professor Paul Meehan for all the patient assistance and guidance he has given me. I would also like to thank my associate supervisor Dr. W.J.T. (Bill) Daniel for his help and support.

Finally I greatly acknowledge in particular my parents. They taught me to see the silver lining of every cloud; they gave me the heart to never stop hoping and believing; they gave me the courage to pursue my dream and happiness. I deeply appreciate them for all their love and support, and for giving me a family that is always there for me.

Keywords

real-time traction control, wear reduction, creep control, adhesion control, locomotive

Australian and New Zealand Standard Research Classifications (ANZSRC)

091307, Numerical Modelling and Mechanical Characterisation, 30%

091302, Automation and Control Engineering, 30%

091304, Dynamics, Vibration and Vibration Control, 40%

Fields of Research (FoR) Classification

0913, Mechanical Engineering, 100%

Contents

Chapter I: Introduction	18
1.1. Background and Motivation	18
1.2. Objectives and Scope of Research.....	20
1.2.1 Modelling of the locomotive dynamics	20
1.2.2 Theoretical and numerical analysis of creep control and locomotive dynamics	20
1.2.3 Design of specialized real-time traction control that regulates the wear to low levels.....	20
1.3. Thesis Outline.....	21
Chapter II: Literature Review.....	22
2.1. Review of Locomotive Dynamic Modelling/Simulation (Objective 1)	22
2.1.1. Review of Locomotive Multibody Dynamic Modelling	22
2.1.2. Review of Wheel-rail Contact Mechanics	26
2.1.3. Review of Locomotive Electric Drive Control Design	30
2.2. Review of Adhesion/Creep Control (Objective 2)	33
2.2.1. Pattern-based Slip Control Method	34
2.2.2. Disturbance Observer Based Slip Control.....	35
2.2.3. Slip Control with Bogie Oscillation Suppression	35
2.2.4. Other Control Strategies	36
2.3. Review of Wear Models in Railways (Objective 3).....	37
2.4. Summary.....	39
Chapter III: Methodology	40
3.1. Overview	40
3.2. Locomotive dynamic modelling and eigenmode analysis (Objective 1).....	41
3.2.1. Locomotive Multibody Dynamics	41
3.2.2. Contact Mechanics	45
3.2.3. Electric Drive Dynamics	48
3.3. Creep Controllers (Objective 2)	51
3.3.1. PI Controller	51
3.3.2. Fuzzy Logic Controller with Variable Creep Threshold	53
3.3.3. Modified Fuzzy Logic Controller.....	55
3.4. Wear Rate Control (Objective 3).....	58
3.5. Summary.....	61
Chapter IV: Results and Discussion	62
4.1. Locomotive Dynamic Simulation and Validation (Objective 1).....	62
4.1.1. Validation of Multibody Dynamics - Eigenmode Analysis.....	62
4.1.2. Validation of the Creep Model	66
4.1.3. Simulation Results of the Simplified and Detailed Drives	69

4.2. Investigations on Creep Controllers (Objective 2)	76
4.2.1. Axle Based PI Controller.....	76
4.2.2. Fuzzy Logic Adhesion Control.....	78
4.2.3. Modified Fuzzy Logic Controller.....	81
4.3. Impact of Locomotive Creep/Adhesion Control on Wear Index and Wear Control (Objective 3) ..	87
4.3.1. Impact of Locomotive Creep/Adhesion Control of Wear Index	87
4.3.2. Wear Growth Rate Control.....	91
4.4. Conclusion.....	99
Chapter V: Summary of Appended Papers.....	100
Chapter VI: Conclusions and Future work	102
6.1. Thesis Contributions.....	104
6.2. Suggestions for Future Work.....	104
References	106
Appended Papers.....	112

List of Tables

Table 1: Detailed parameters of the locomotive model	45
Table 2: Parameters for different contact conditions.....	48
Table 3: Fuzzy rule table.....	55
Table 4: Fuzzy rule table of the modified fuzzy controller.....	58
Table 5: Modal frequencies of the locomotive dynamic system vibrations, damping ratio, decay rates and corresponding eigenvalues.....	64
Table 6: Diagram of the mode motions.....	65
Table 7: Acceleration simulation and comparison with data in [91]	75
Table 8: Simulation cases.....	87

List of Figures

Figure 1: Australian heavy haul, intermodal and freight rail [3].....	18
Figure 2: Figure 2: Diagram showing the rail wear.....	19
Figure 3: The quarter rail vehicle model [9].....	23
Figure 4: FEM model of locomotive [11].....	23
Figure 5a: Locomotive & track modelling with Gensys software [13].....	24
Figure 5b: A typical ADAMS/Rail model [12].....	24
Figure 5c: A typical Vampire model screen [12].....	25
Figure 6: A typical Newton/Lagrangian full locomotive (vertical direction) [20].....	26
Figure 7: A wheel rolling over a rail [23].....	27
Figure 8: Assumption of distribution of normal and tangential stresses in the wheel-rail contact area [17].....	28
Figure 9: Calculated adhesion force-creep functions for typical parameters of real wheel [26].....	29
Figure 10: Single-phase equivalent circuit for a squirrel cage motor [35] (upper); and an AC Induction Motor with cut away showing squirrel cage rotor (lower).....	30
Figure 11: Basic scheme of FOC for the three-phase AC machine [45].....	32
Figure 12: A typical DTC controlled AC drive structure [48].....	33
Figure 13: Pattern re-adhesion control method [51].....	34
Figure 14: Estimation system of adhesion force coefficient [52].....	35
Figure 15: Re-adhesion control block based on [53]	36
Figure 16: Wear types identified during tests of BS11 Rail vs. Class D Tyre [69].....	38
Figure 17: The wear coefficient versus the frictional power density for UICB rail steel, running with class D wheel steel [81].....	39
Figure 18: Schematic diagram of the overall system.....	40
Figure 19: Locomotive longitudinal-vertical dynamic diagram.....	42
Figure 20: Standard 60kg rail profile [89].....	47
Figure 21: Schematic diagram of an AC machine with inverter (left) and instantaneous voltage vectors (right) [90].....	49
Figure 22: Optimum switching table and comparators [90].....	49
Figure 23: Diagram of the DTC induction machine.....	50
Figure 24: Diagram of basic PID adhesion/creep controller.....	51
Figure 25: The flow chart of the PI creep controller.....	52
Figure 26: Adhesion control diagram.....	53

Figure 27: (a) Membership functions of inputs and output; (b) fuzzy logic 3D input-output characteristics.....	54
Figure 28: Illustrative graph for the fuzzy rules	55
Figure 29: Schematic diagram of the overall system.....	56
Figure 30: (a) Membership functions of input; (b) Membership functions of output.....	57
Figure 31: (a) Creep only control diagram; (b) Creep and wear control diagram.....	60
Figure 32: Vertical displacements of axles under change of contact conditions.....	65
Figure 33: Locomotive car body pitch, vertical and bogies' vertical displacements.....	65
Figure 34: Tuned Polach creep-adhesion coefficient curve for oil condition at 20 km/h and data in [99].....	67
Figure 35: The form of adhesion coefficient-creep function and the influence of vehicle speed under dry wheel/rail contact condition.....	67
Figure 36: Polach tractive force curve at different speeds under (a) dry contact condition; and (b) under wet contact condition.....	68
Figure 37: (a) Comparison between traction force curve of AC model full locomotive (= single AC traction effort $\times 6$) and the GT46MAC data [104]; (b) Comparison between traction force curve of DC model full locomotive (= single DC traction effort $\times 6$) and the GT46C data [105].....	70
Figure 38: (a) Comparison between braking effort curve of AC model full locomotive (= single AC traction effort $\times 6$) and the GT46MAC data [102]; (b) Comparison between braking effort curve of DC model full locomotive (= single DC traction effort $\times 6$) and the GT46C data [105].....	72
Figure 39: (a) AC creep curves for all traction mode notches under transient state at 20km/h; (b) DC creep curves for all traction mode notches under transient state at 20km/h.....	74
Figure 40: Acceleration Simulation result (speed and $T_e \times 6$ with notch).....	75
Figure 41: Acceleration test speed curve under a change of friction condition using the axle based controller.....	77
Figure 42: Acceleration test creep curves under a change of friction condition using the axle based controller.....	77
Figure 43: Acceleration test tractive force curves under a change of friction condition using the axle based controller.....	78
Figure 44: Comparison of total tractive force with PI and fuzzy controllers.....	79
Figure 45: Comparison of creep response with PI control (a) and with fuzzy logic control (b).....	80
Figure 46: Comparison of total tractive forces with PI and fuzzy sliding mode control at low speed.....	82
Figure 47: Creep of the front axle under change of contact conditions at low speed.....	82
Figure 48: Bogie pitch motion during operation	83

Figure 49: Weight distribution on each axle.....	84
Figure 50: Comparison of total tractive forces with PI and fuzzy sliding mode control at high speed.....	84
Figure 51: Creep of the front axle under change of contact conditions at high speed.....	85
Figure 52: Bogie pitch motion during operation.....	85
Figure 53: Weight distribution on each axle.....	86
Figure 54: Front wheel tractive force comparison under different controller thresholds at low speed.....	88
Figure 55: Front wheel $T\gamma/A$ values comparison under different controller thresholds at low speed.....	89
Figure 56: Front axle creep response for medium speed simulation under change of contact conditions.....	89
Figure 57: Front wheel $T\gamma/A$ values at medium speed.....	90
Figure 58: Comparison of total tractive forces with creep and wear controllers.....	91
Figure 59: Comparison of front and rear bogie pitches with creep and wear controllers.....	92
Figure 60: Comparison of car body pitch with creep and wear controllers.....	93
Figure 61: Comparison of axle 1 creep with creep and wear controllers.....	94
Figure 62: Comparison of axle 1 friction power density with creep and wear controllers.....	94
Figure 63: Comparison of axle 1 mass loss rate with creep and wear controllers.....	95
Figure 64: Comparison of total tractive forces with creep and wear controllers.....	96
Figure 65: Comparison of front and rear bogie pitch with creep and wear controllers.....	96
Figure 66: Comparison of car body pitch with creep and wear controllers.....	97
Figure 67: Comparison of axle 1 creep with creep and wear controllers.....	98
Figure 68: Comparison of axle 1 friction power density with creep and wear controllers.....	98
Figure 69: Comparison of axle 1 mass loss rate with creep and wear controllers.....	99

Chapter I: Introduction

1.1. Background and Motivation

Rail offers one of the most efficient forms of land-based transport [2], providing great carrying capacity at relatively low energy cost. Figure 1 shows a typical Australian heavy haul rail system [3], where a train can reach a length of 2.5km and weights up to 40t/axle or more. The progressive development of AC traction motor and control technology based on power electronics has brought great benefits to the rail industry due to its high power capacity, reliability and low maintenance. As a result, the new AC traction motor has allowed locomotives to be operated with much higher continuous traction forces and adhesion levels than previously achieved on locomotives with DC motors.



Figure 1: Australian heavy haul, intermodal and freight rail [3]

Locomotives require precision traction control to achieve steady performance close to the adhesion limit, i.e. from 30% to 46% [4], to maximize capacity. Therefore it is important to the rail industry to investigate methods to make the most of the tractive capacity of modern electric motors to improve operation efficiency, by means of controlling the creep/adhesion on the wheel/rail contact patch. On the other hand, the increase of traction capacity of modern electric drives, particularly

with the goal of achieving the highest tractive force, is likely to cause an increase in maintenance costs due to wear at the wheel/rail contact patch, as shown in Figure 2. In Figure 2, W1 represents the rail head wear which is one of the most common types of wear damage and thus is the main focus of this thesis.

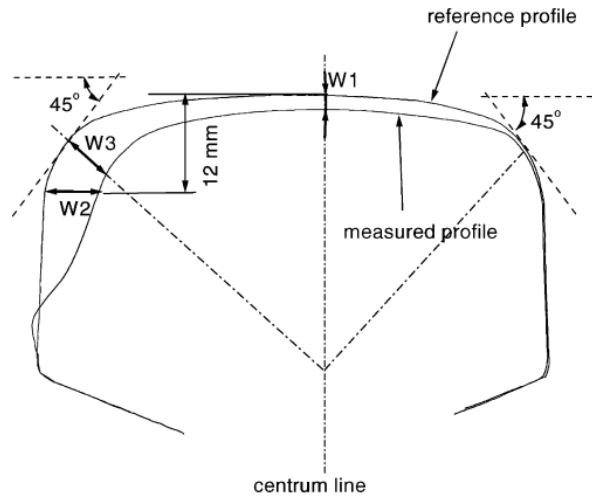


Figure 2: Diagram showing the rail wear

There is debate as to whether the more powerful AC motors contribute to considerable increases of rail track damage and track maintenance costs. Methods such as lubrication and surface coating have also been used, particularly in curves, to reduce wear damage [5]. A friction modifier (FM) has been employed on the rail/wheel contact patch to reduce such wear and rolling contact fatigue [6]. It works if applied properly. However, this method is reliant upon operator experience which can vary and the refilling of the FM applicators can be costly. The American Association of Railroads estimates that wear occurring at the wheel/rail interface as a result of ineffective lubrication costs in excess of \$US 2 billion per year [7]. The use of more durable rail materials has also been proposed to reduce the cost of wear damage. However, the implementation of these methods may also involve large cost. Therefore, it is necessary to understand how different operation conditions and creep/adhesion control strategies affect wear growth. Particularly, the transient state of locomotive operation due to external perturbations such as changes of wheel-rail contact conditions needs to be further investigated, as the most significant changes of locomotive dynamic responses and oscillations are likely to occur during this transient state. Thus rail damage due to wear could be controlled in a systematic way on board, potentially reducing or even excluding the use of friction modifiers for the purpose of wear reduction.

In order to study this, the vehicle/track dynamics, contact mechanics and traction and creep control behaviour of modern AC locomotive drives need to be integrated and assessed as a total dynamic

feedback interactive system. The dynamic response and its impact on wear growth under different control strategies and changes of contact conditions due to natural perturbations such as friction/lubrication, vehicle/track dynamics et al. need to be analysed. These problems will be addressed in this thesis. Moreover, a specialized novel real-time traction control system limiting rail track wear growth will also be proposed to provide a systematic approach to achieve the optimum balance between traction and wear.

1.2. Objectives and Scope of Research

The focus of this thesis is to develop a predictive integrated locomotive dynamic model, implement different creep/adhesion control strategies, and to propose and test a real-time control approach to limit rail damage caused by wear.

Specifically, the major objectives of this thesis are as follows.

1.2.1 Modelling of the locomotive dynamics

To develop a simplified predictive integrated mathematical model including locomotive longitudinal, vertical and pitch dynamics, wheel/rail contact mechanics and simplified electric drive dynamics. To investigate the oscillation modes of the locomotive multibody dynamics and consequently identify the modes those are more likely to be excited, and to examine the locomotive dynamic behaviour under changes in contact conditions.

1.2.2 Theoretical and numerical analysis of creep control and locomotive dynamics

To develop creep/adhesion controllers to achieve highest tractive force under changes of operating conditions such as wheel/rail contact conditions and operation speed. To investigate their influence on locomotive dynamic response compared to fixed creep threshold control by carrying out simulations.

1.2.3 Design of specialized real-time traction control that regulates the wear to low levels

To develop a novel real-time control strategy to reduce the wear damage on the tracks. To investigate and compare its impact on the locomotive dynamic response and the wear damage with that with fixed creep threshold control by simulation.

1.3. Thesis Outline

This thesis is divided into 6 chapters including this introduction. A summary of the remaining chapters is provided as follows.

Chapter 2 provides an overview of the current state of research regarding locomotive dynamic modelling. A review of creep/adhesion control and of wear growth modelling in railways is then described.

Chapter 3 presents the modelling methodology used to achieve the thesis objectives. Firstly, the simulation model for locomotive longitudinal-vertical-pitch dynamics, wheel/rail contact mechanics and electric drive dynamics are presented, followed by creep/adhesion control design. Finally the proposed wear rate control methodology is provided.

Chapter 4 describes the simulation results first, including single drive simulation results and results with the locomotive dynamic model under changes of operation conditions. Simulation results and the comparisons of dynamic responses between constant threshold creep control and various adjustable creep controls achieving higher tractive force are then provided. Subsequently simulation results showing the impact of wear control on wear growth rate and locomotive dynamic responses are provided, followed by results highlighting the effectiveness of the wear control strategy.

In Chapter 5, a summary of appended papers is provided.

Chapter 6 summarises the conclusions of this study, together with the recommendations for future research.

Chapter II: Literature Review

This chapter presents a detailed literature review of the locomotive dynamics and control research including five aspects which are categorized into locomotive dynamic modelling, wheel/rail contact mechanics, locomotive electric drive and control, locomotive adhesion/creep control, and wear models in railways. This leads to a summary statement of where the research performed in this thesis contributes to the body of knowledge on the development of locomotive traction and wear control technology.

2.1. Review of Locomotive Dynamic Modelling/Simulation (Objective 1)

This section provides literature research on the modelling of essential dynamic components of a locomotive, including the locomotive multibody dynamics, wheel/rail contact dynamics and electric drive dynamics. The reviews of the major dynamic components are detailed in the following sections.

2.1.1. Review of Locomotive Multibody Dynamic Modelling

Research into dynamic modelling and simulation of a locomotive based on mathematical models to represent certain complex railway vehicles varies significantly depending on the purpose of researchers and the cases being investigated. Most of the models can be categorised into (1) longitudinal and vertical dynamics on tangent tracks, (2) lateral dynamics on tangent tracks and (3) curving dynamics [8]. This study focuses on the first category as it is the most important dynamic part of locomotive dynamics which is closely related to traction/braking effort, passenger comfort and energy management. The modelling of rail vehicle longitudinal and vertical dynamics without consideration of traction or drive issues has been extensively studied for many years, and in different levels of complexity. In this section, a range of locomotive dynamic models are reviewed, including the quarter rail vehicle model, finite element models and longitudinal-vertical dynamic models for the whole locomotive built with Newton principles or Lagrangian method, and software packages that have been widely used for locomotive dynamic modelling.

The simplest model proposed to reveal the overall dynamics of a locomotive is a quarter rail vehicle model, which is preferred in many studies because of its simplicity and ease of application [9, 10]. This model is based on a quarter of a 4 wheelsets locomotive and consists of a primary and secondary suspension as shown in Figure 3.

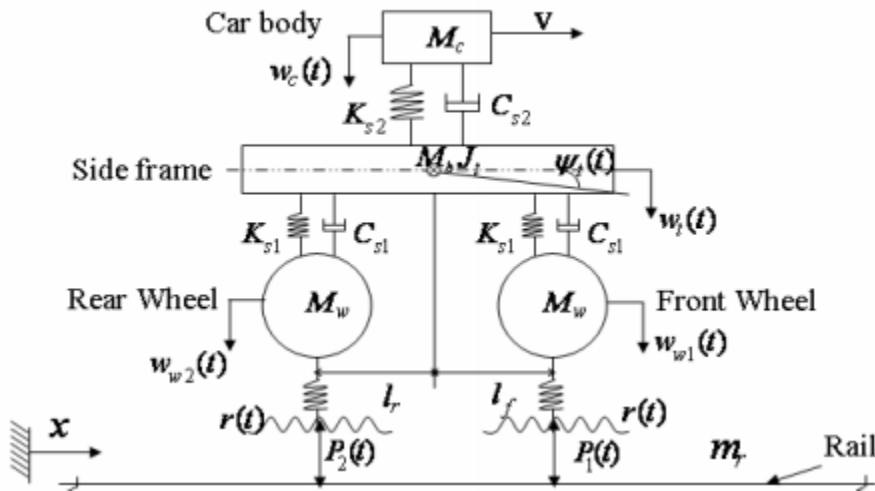


Figure 3: The quarter rail vehicle model [9]

The primary suspension connects the wheels and bogie frame, and the secondary suspension connects the bogie frame and the car body. Both are modelled as spring and damper elements. A rather complex locomotive model [11] has been built to investigate crashworthiness using the finite element method as shown in Figure 4. However, the FEM models are very time-consuming and computationally expensive.



Figure 4 : FEM model of locomotive [11]

Various multibody dynamics (MBD) software packages have been developed. Commonly used ones include Gensys, Vampire, Adams/Rail, NUCARS and Simpack [12]. These have also been employed to build locomotive dynamic models [13, 14] as shown in Figure 5a-5c below.

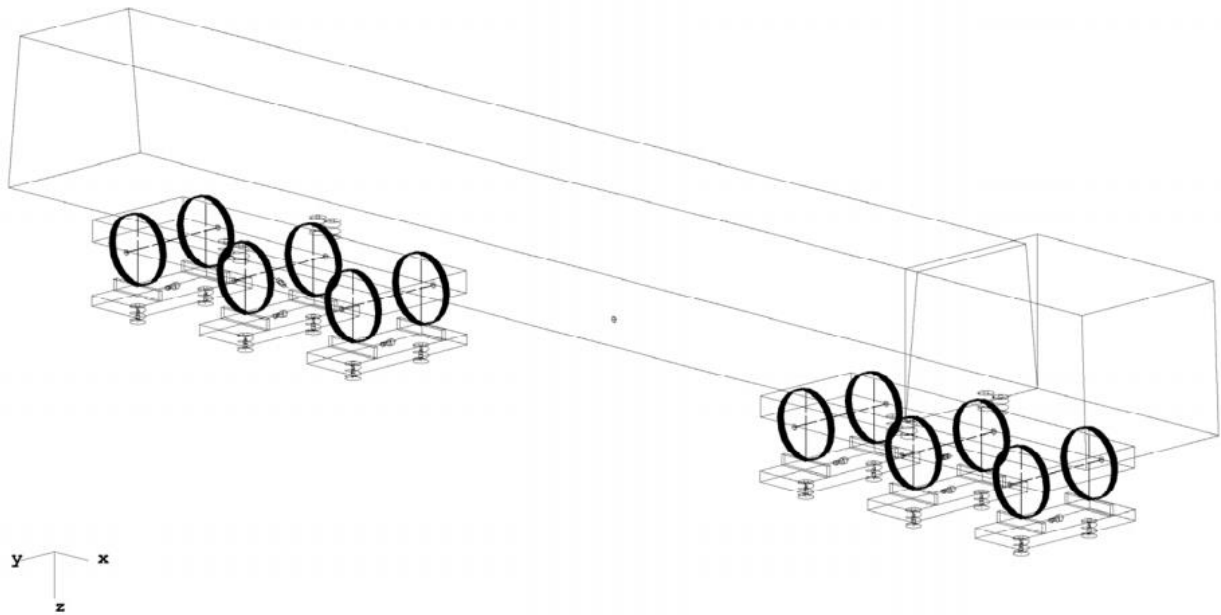


Figure 5a: Locomotive & track modelling with Gensys software [13]

Gensys has been used for dynamics analysis for vehicle components such as for rubber suspension [15], as well as for a whole locomotive and its interaction with the railway [14].

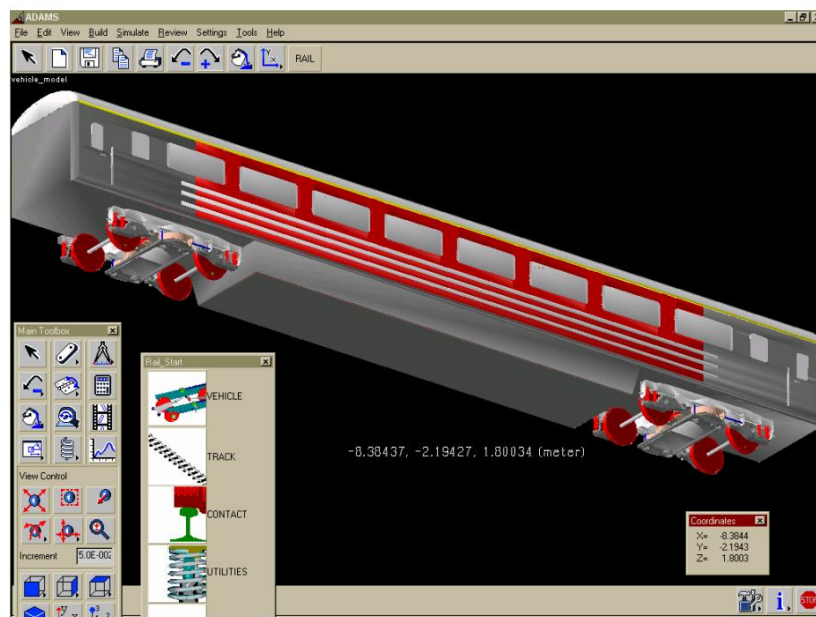


Figure 5b: A typical ADAMS/Rail model [12]

Other multi-body dynamics packages such as VAMPIRE, NUCARS, SIMPACK, LMS Dads and ADAMS/Rail have also been used to model and analyse the dynamics of freight vehicles [16, 17]. ADAMS/Rail has also been used as a part of co-simulations with contact mechanics software package FASTSIM [18].

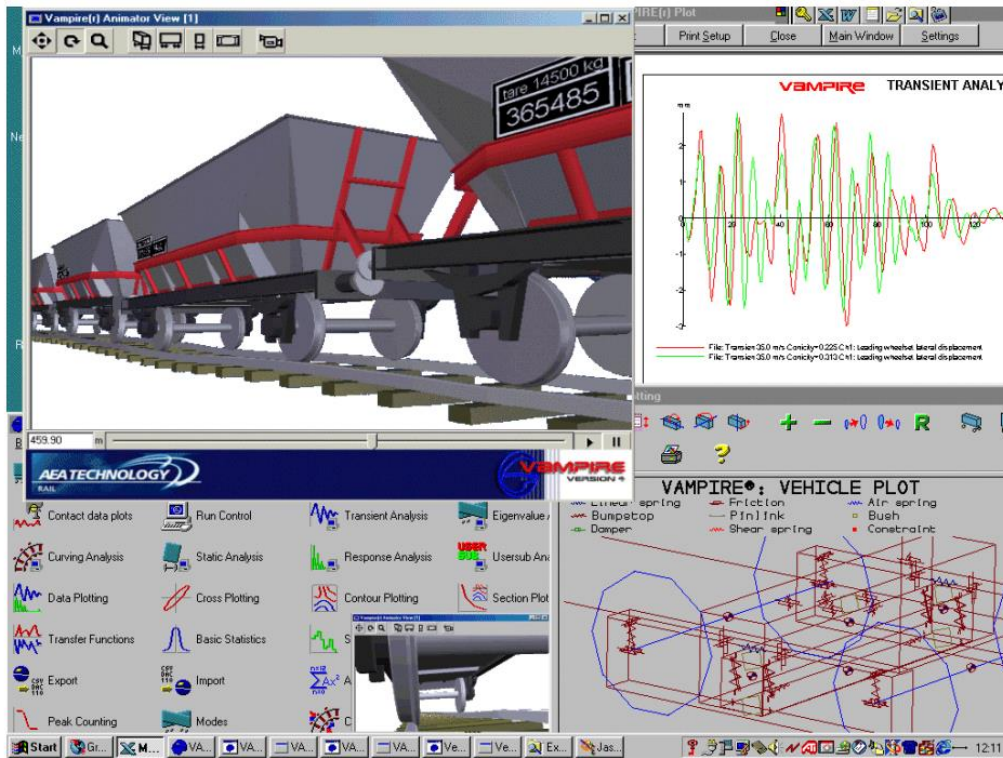


Figure 5c: A typical Vampire model screen [12]

This modelling method is less complicated to implement compared with mathematical modelling methods as the software packages do not require end users to perform the complex mathematical modelling. However, this method is rather restricted as a model built in a certain software environment is not likely to be able to be implemented directly in other software environments.

A Newton/Lagrangian full locomotive model for locomotive dynamic analysis is built by means of the basic Newton principle or by a Lagrangian method [19, 20]. A typical model is shown in Figure 6. The model has 10 degrees of freedom and it contains a locomotive body which is connected with two bogies by secondary suspensions. Each bogie is connected with two wheelsets by primary suspensions.

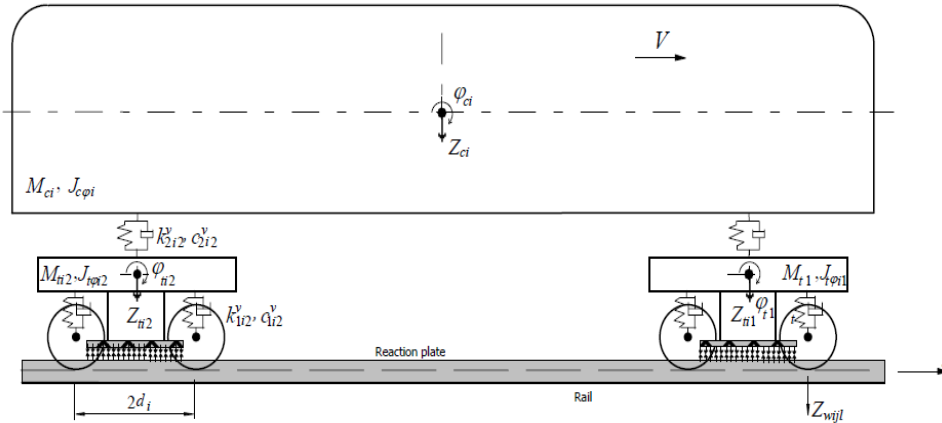


Figure 6: A typical Newton/Lagrangian full locomotive (vertical direction) [21]

Models built by this method can describe the dynamic response of the whole locomotive and the interaction between components and at the same time be not too computationally expensive. This method, although being not as detailed as the finite element modelling method, can reveal most of the locomotive dynamics and the interaction between different components. It is suitable to create a fast calculation dynamic model and is used in the thesis to develop the locomotive dynamic model subsystem.

2.1.2. Review of Wheel-rail Contact Mechanics

The wheel-rail contact characteristics calculate the dynamics of the interaction between the wheel and rail track, as illustrated in Figure 7. Wheel-rail contact mechanics focuses mainly on calculating tangential tractive/braking forces. In this section, contact mechanics methods that are used to calculate the tractive force are reviewed.

Early investigation on the creep forces in wheel/rail rolling contact has been initiated by Carter [22]. In his work, a two-dimensional model was proposed with an assumption that the contact area is comprised of an area of adhesion in the leading part and an area of slip in the trailing part. Johnson extended this model to three-dimensional by considering the lateral creepage [23]. Kalker's research on the rail/wheel contact modelling contributes to an important development in the area of fast and relatively accurate rail/wheel contact force calculation. The diagram of wheel/rail contact is shown in Figure 7.

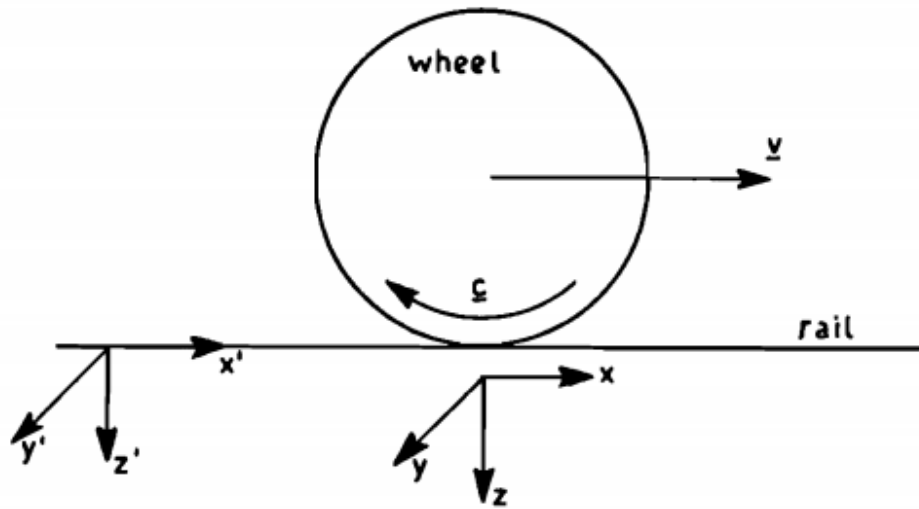


Figure 7: A wheel rolling over a rail [24]

Kalker [25] devised a contact mechanics method considering small creep conditions based on Hertz theory. Then he simplified the theory based on approximating the relation between the tangential surface traction and the tangential surface displacement by using compliance (flexibility) parameters [26]. Kalker then developed the theory further and published the FASTSIM algorithm with corresponding software. This is programmed in FORTRAN to calculate the longitudinal and lateral wheel-rail contact creep forces and can greatly shorten the calculation time compared to the original Kalker algorithm. However it is still considered too computationally expensive to use in complicated multibody systems [18]. Kalker's algorithm although being the first method that can calculate the traction force accurately, loses its accuracy at a high creepage condition. Several methods have been developed by improving Kalker's FASTSIM model such as by using tabulated data instead of calculation. Commercial software packages NUCARS and VAMPIRE use large pre-tabulated results to increase the calculation efficiency [5]. However, while small tables may affect the accuracy of the result, searching in large tables consumes calculation time [18].

In order to reduce computational time so that the calculation of wheel-rail contact force can be used in real-time vehicle dynamics simulations, Polach developed a fast algorithm. The computer code [18] calculates the wheel-rail contact forces with known contact geometry, creep and spin conditions. The assumption of the contact patch in his algorithm is based on Hertz contact and is shown in Figure 8.

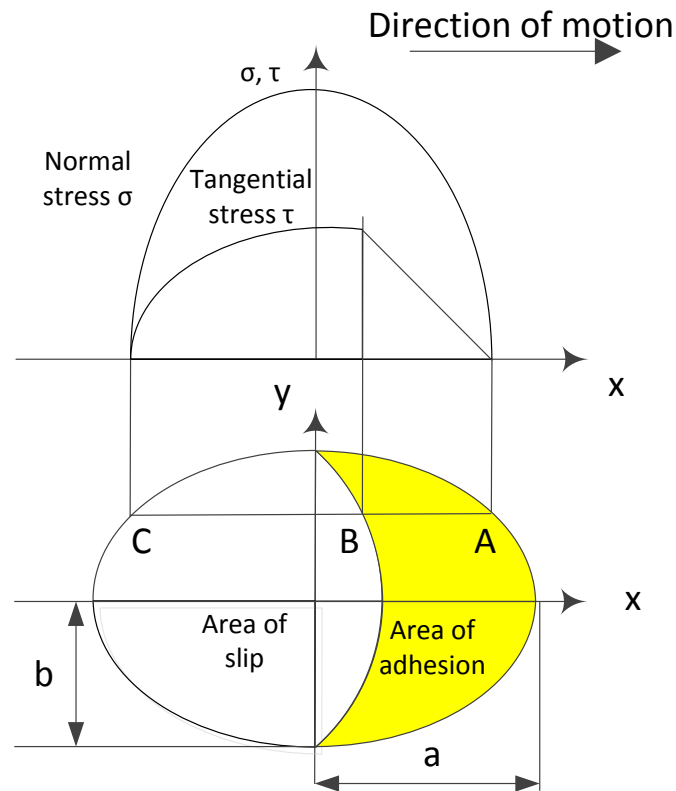


Figure 8: Assumption of distribution of normal and tangential stresses in the wheel-rail contact area [18]

This method is much faster than Kalker's method. However, it cannot reveal the adhesion characteristic under a high creep value condition. The author then modified the method by adding in extra tuning parameters k_a and k_s . This model's input includes the normal contact force, the speeds of the locomotive and the wheelsets and the contact condition parameters. The normal contact forces are calculated from the vertical wheels' accelerations, given the stiffness of the rail/wheel contact is known. The speeds of the wheels are obtained from the accelerometers. The locomotive speed can be measured by means of a GPS system. The contact condition parameters are from the Polach's model [18]. The adhesion force curves for a typical dry or wet condition are shown in Figure 9 with the horizontal axis representing creepage and vertical axis representing the ratio between tangential tractive force and normal loading. The model has been validated by the comparing with experimental data from various vehicles (including SBB460, 12X, SD45X, DB127 and S252) [27]. To clarify, the wet condition means an interfacial layer of liquid on the contact patch [27]. The wet rail conditions are obtained either when rain was falling or artificially spraying water to the rail surface ahead of the lead axle of the locomotive [27, 28].

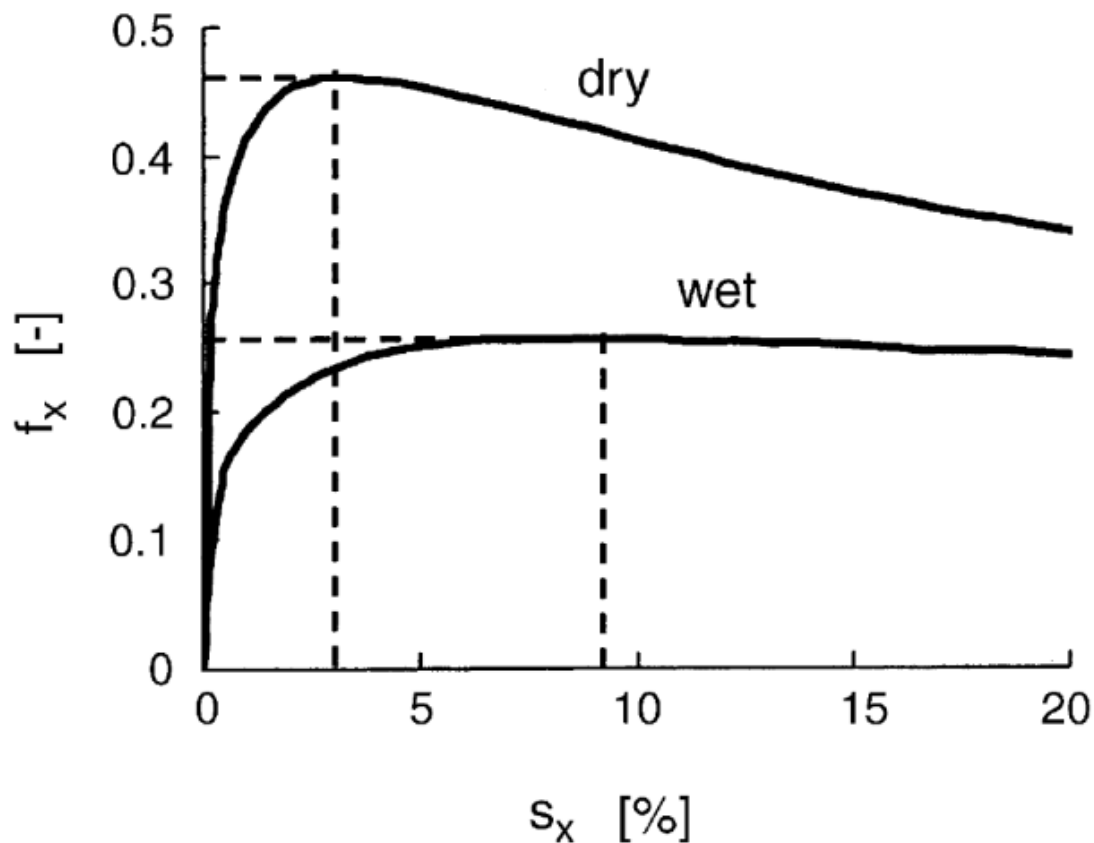


Figure 9: Calculated adhesion force-creep functions for typical parameters of real wheel [27]

The modified creep force formula does not increase much of the calculation burden but can be used to calculate creep force for both low and high creep conditions. Recent research on wheel/rail force study gives a variety of contact force models. Spiryagin's work introduced a contact model considering different contact conditions and the effect of contact temperature [29]. This model agrees well with their lab experimental data, however, it may increase the calculation time.

Research on non-elliptical rail/wheel contact has been carried out to solve normal contact problems when Hertzian geometric assumptions do not hold. Some novel virtual penetration based methods include Kik–Piotrowski's method [30], Linder's method [31] and Stripes method [32]. Burgelman has compared the results of these methods and the elliptical based method FASTSIM and has concluded that the non-elliptical models predict a better curving behaviour with 12% lower creepages and 3% lower creep force than the FASTSIM elliptical model; however, the difference on straight tracks is negligible [33].

To sum up, Polach's adhesion model is effective for both small and large values of longitudinal wheel-rail creep as well as representing the decreasing part of creep-force function exceeding the

adhesion limit [34]. Furthermore, it is used in this thesis as it has been verified to be relatively accurate for the application in the field of locomotive traction analysis [35].

2.1.3. Review of Locomotive Electric Drive Control Design

Locomotive drive and creep controller design is critical to the performance of the locomotive system and also is one of the main focuses of the thesis. A well-designed drive and control system can not only increase the operational reliability of the locomotive but also improve the driver/passenger comfort. In this section an introduction including the characteristics of an AC motor emphasizing the challenge of its control will be proposed first, followed by some AC drive control methods commonly used in industry especially on locomotives.

Dynamic analysis of an AC motor is shown in Figure 10. It is a highly coupled, non-linear, and multivariable structure compared to the simple structure of DC motors [36]. One of the major technology challenges is implementing precise control.

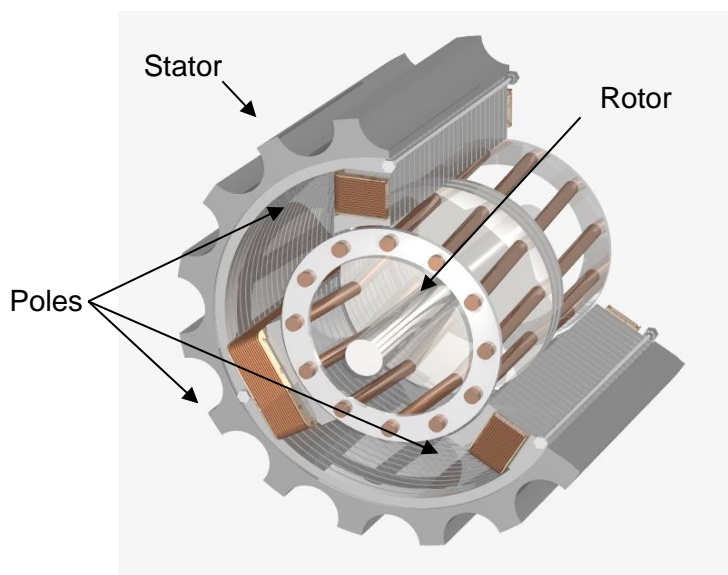
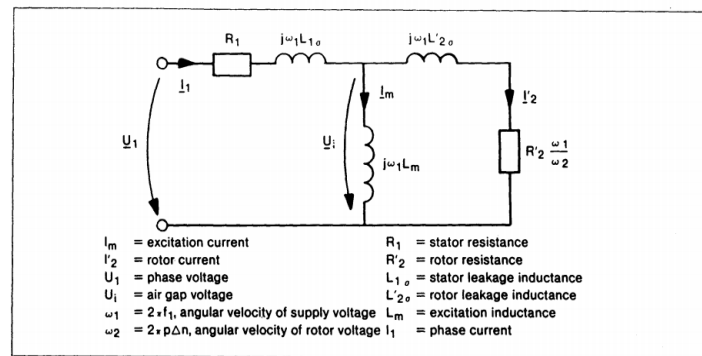


Figure 10: Single-phase equivalent circuit for a squirrel cage motor [37] (upper); and an AC Induction Motor with cut away showing squirrel cage rotor (lower)

Simple open loop control is possible with a fixed control frequency, via a variety of techniques such as switching of the number of active poles or varying the supply voltage. However such schemes do not provide good control over the system over a large range of speeds and slip [38]. AC drives do, however, naturally possess a steep torque slip curve near the synchronous speed of the motor, which is exploited in a number of control schemes based on varying the amplitude and waveform of the supplied voltage, enabling precise speed control [39]. The difficulties associated with this type of precise control over the full range of operating conditions is due to the nonlinear nature of the system and the practical challenge of generating the desired multiphase supply voltage with fine enough resolution to accurately reproduce the waveform as required for the control signal.

An induction motor drive is a complicated nonlinear system that has been the subject of a large body of research and their control schemes have reached a high state of development [38]. System modelling typically allows for nonlinear inversion into a linear model, allowing the use of well understood linear control techniques [39]. The principal challenges in implementing these techniques are then technical and financial, in that a reliable estimate must be available for the control model. Examples of these challenges are the difficulty of accurately estimating rotor fluxes and load torques [40] and the cost associated with installing high accuracy sensors to measure rotation speed [41]. Techniques have been developed to overcome these limitations, such as sliding mode nonlinear state estimation techniques [42], but the potential costs of poor estimates are degraded performance [43].

The importance of AC induction drives and their control in industrial applications has resulted in the development of accurate simulation packages capable of reproducing the dynamic behaviour of typical drive and control configurations [43]. MATLAB/Simulink based modelling is frequently encountered in research papers as a useful tool for evaluating the expected performance of AC drive systems (see for example [43-45]). In the following sections, some widely used AC drive control methods are separately explained.

This AC machine control method, also known as Field-Oriented Control (FOC), simulates the DC drive by means of complex transforms [46]. It achieves control performance as good as that of DC machines. The scheme is shown in Figure 11.

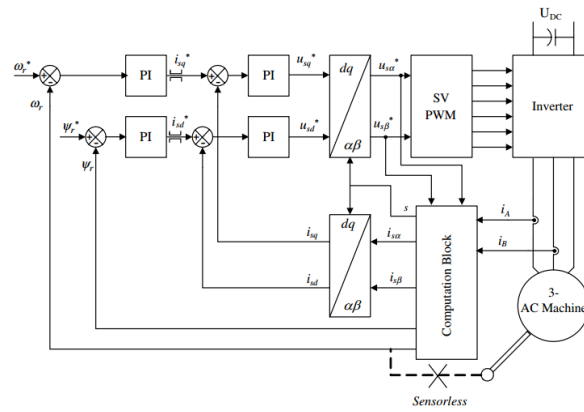


Figure 11: Basic scheme of FOC for the three-phase AC machine [47]

In the system, two motor phase currents and the DC bus voltage are measured and transformed using the Clarke transformation block (the transformations can be found in [48]) into a stationary reference frame. These last two components are further transformed, using the Park transformation, into rotating components (dq). The PI controllers compare the command values with the measured components (after transformation) and command proper values to establish the desired condition. The outputs of the controllers are transformed from a rotating to a stationary frame using the Park transformation. The commanded signals of the stator voltage are sent to the pulse width modulation (PWM) block. Although the flux vector AC machine control method can achieve good torque response with full torque at zero speed and has performance very close to a DC drive, it needs a feedback device which can be costly and can add complexity to the drive system. A modulator is also used, which will slow down communication between the incoming voltage and frequency.

The direct torque control (DTC) method was proposed by Manfred Depenbrok in U.S. Patent 4,678,248 in 1987 and firstly applied by ABB in German diesel-electric locomotives [49]. This method achieves field orientation without feedback calculating the motor torque directly and without using modulation. DTC is commonly used in controlling locomotive motors, for example DE502 and DE10023 diesel-electric locomotives, as well as some Siemens locomotives. The DTC technique is chosen to control the traction motor because it is fast in response and computationally inexpensive to simulate. The structure of a typical DTC controlled AC drive is shown as in Figure 12.

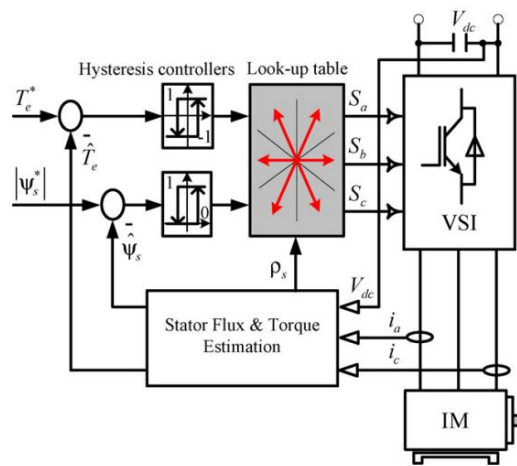


Figure 12: A typical DTC controlled AC drive structure [50]

Details of this method can be found in [51]. This method has the following advantages: no modulator is needed; no tachometer or position encoder which is to feedback the shaft speed or position is required; and the torque performance is faster than other AC or DC drives [52]. This induction machine control technique is used in this thesis to build the complex drive model and to compare with available data considering the above advantages over other methods.

2.2. Review of Adhesion/Creep Control (Objective 2)

Modern development of mechatronics systems provides the possibility of improving rail vehicle operation under various conditions. The traction control system, also known as an adhesion control system or anti-slip regulation system is essential for such systems to achieve operational efficiency and reliability. The traction control system is designed to regulate the torque applied to the vehicle wheelsets to prevent excessive wheel-slip and resulting loss of traction. A number of different methods have been proposed by researchers aiming to prevent excessive wheel-slip and to operate the rail vehicle at an optimum level of adhesion. Most of these require vehicle velocity and wheel-rail contact condition information. A terminology, creepage, needs to be introduced here. It is defined as the difference between wheelset velocity and locomotive velocity normalized by locomotive speed.

As mentioned in previous sections, AC motors can achieve higher traction/adhesion performance than their DC counterparts to theoretically achieve the optimum traction/adhesion operation of rail locomotives. However, due to its inherent complexity and non-linearity, the high performance can only be achieved by accurate state detection and/or estimation together with proper AC drive

control design. The performance under dynamic conditions has also not been investigated deeply. The following sections will review several recent adhesion control techniques.

2.2.1. Pattern-based Slip Control Method

There are several pattern-based adhesion control methods and derivations. A typical application is by Park et al. [53]. The idea of this method is to adjust the control command according to a pre-set command pattern by setting different thresholds and can be illustrated in Figure 13.

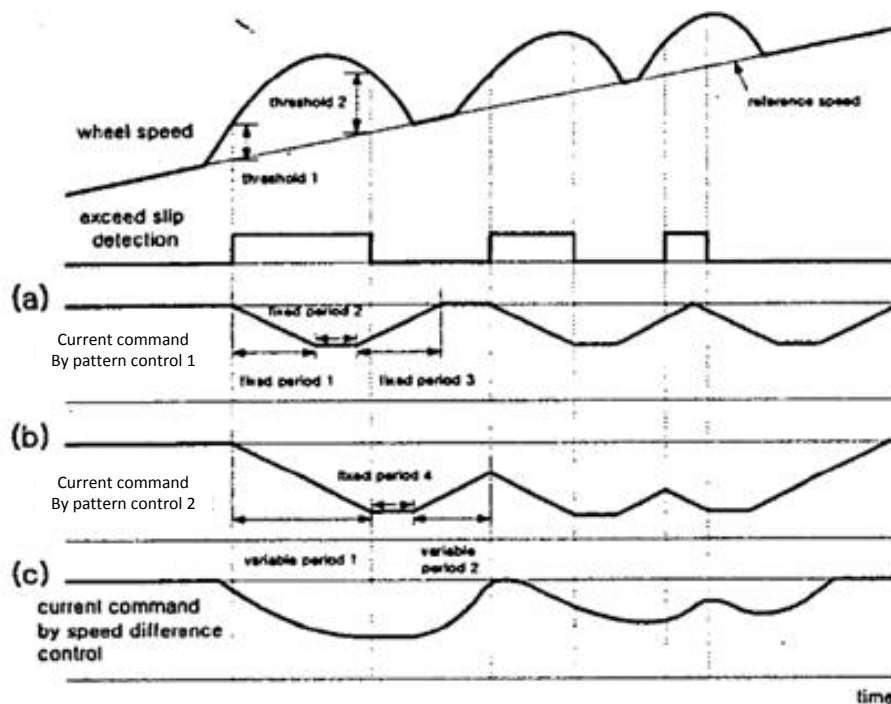


Figure 13: Pattern re-adhesion control method [53]

In this method, the speed difference control (c) is separately activated after the dead zone, which is determined by the speed sensor error. The second step by pattern control (a and b) begins if the first step failed to constrain the slip under pre-set threshold 1. This method, although being able to constrain the slip velocity within a certain range as the author claimed, cannot assure the achievement of maximum adhesion during locomotive operation since the maximum adhesion is determined by creepage rather than slip velocity.

2.2.2. Disturbance Observer Based Slip Control

Anti-slip control based on a disturbance observer was proposed by Ohishi et al. [54]. The method is to estimate the friction coefficient by using the estimated disturbance torque \hat{T}_L with an adhesion force coefficient estimation system in Figure 14.

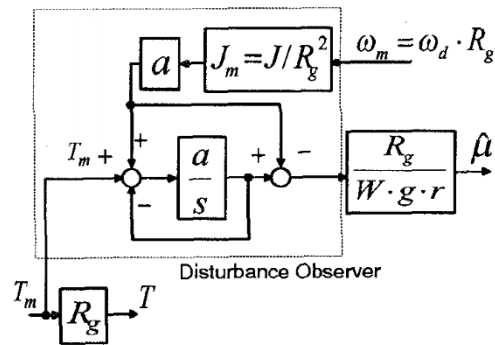


Figure 14: Estimation system of adhesion force coefficient [54]

The anti-slip control is then carried out by setting the torque command to the maximum value based on the estimated friction coefficient. This method which has also been claimed to be able to achieve maximum adhesion force operation and good anti-slip effect, does not take the speed sensor delay into account and has only been simulated as a single wheel. As a result the transient behaviour of the locomotive utilizing this method has not been deeply investigated.

2.2.3. Slip Control with Bogie Oscillation Suppression

Yasuoka et al. proposed a slip control method [55] which also takes into account bogie oscillation suppression. This control method consists of creep control, estimated traction force control, oscillation suppression control and all wheel slip suppression control. The control system diagram is as shown in Figure 15.

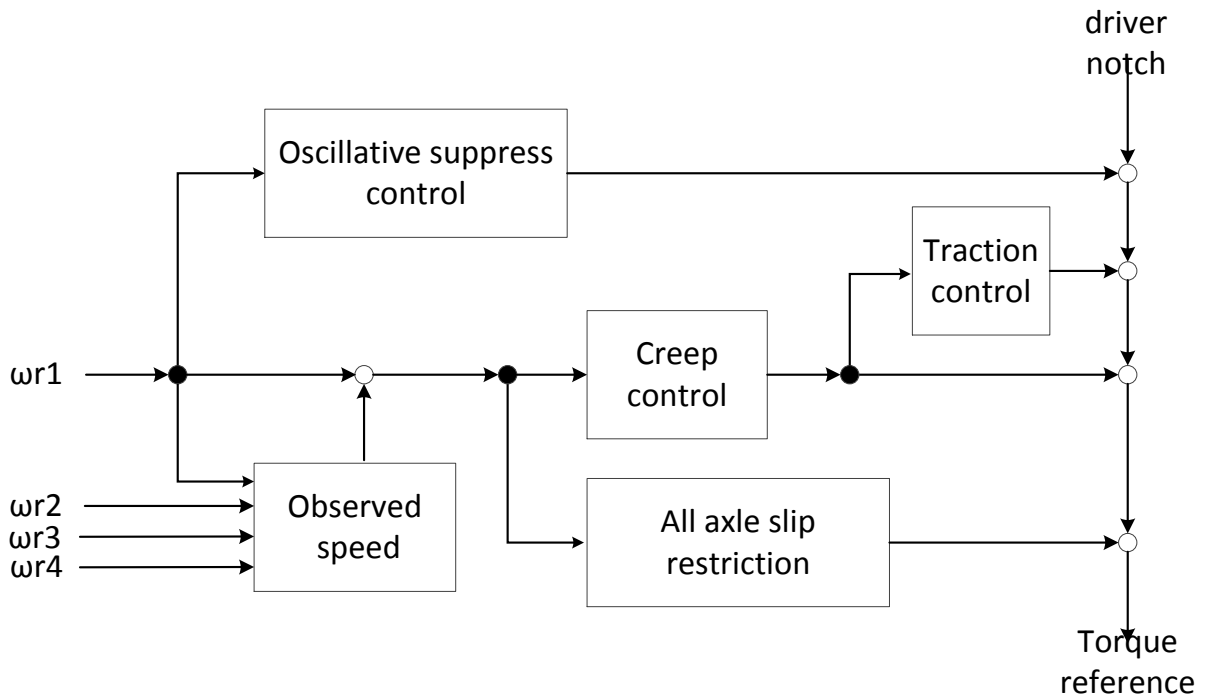


Figure 15: Re-adhesion control block based on [55]

The proposed creep controller in this method is to amplify the square of the slip velocity by a scale coefficient and use this as a torque reduction signal. The oscillation suppression control is by reducing the torque command to the leading wheel proportionally to the velocity difference between the leading and trailing wheels.

2.2.4. Other Control Strategies

Several advanced control strategies have been proposed on locomotive application for different purposes. An optimal control method has been proposed for cruise control [56] and energy management [57]. However, the optimal nature of this kind of controller may not be suitable for the application of traction dynamics improvement. The fuzzy logic method has also been proposed on locomotive applications [58, 59]. Fuzzy logic systems are based on fuzzy set theory [60]. Fuzzy sets derive from a grouping of elements into classes that do not possess sharply defined boundaries [61]. Since fuzzy logic uses fuzzy linguistic rules based on expert knowledge and specific numeric data without the existence of a suitable mathematical model [58], it has the ability to tackle uncertainties and nonlinearity [62]. This method can be applied to various real-life situations and is easy to design and implement. It is not a systematic way of control design and depends heavily on experience. Model predictive control (MPC) is a modern control method and has been applied on some slow process control situations [63]. However, the online optimal calculation for each time-step makes it difficult to apply on a complex fast sampling process. A mechatronic approach to

control the wheel slip based on the information on the torsional vibration of the wheelset is investigated by Mei et al. [64]. Nonlinear control design and its application has been proposed [65] on a simplified mass locomotive. The process of finding the Lyapunov function may be difficult if the whole complex locomotive dynamics is considered. In this thesis, PI and fuzzy logic based controllers are used to achieve creep and wear control.

2.3. Review of Wear Models in Railways (Objective 3)

Wear is the progressive loss of material from the operating surface of a body, caused by relative motion at the surface [66]. In the railway field it is a fundamental problem as the change of profile shape deeply affects the dynamic characteristics of railway vehicles such as stability or passenger comfort and, in the worst cases, can cause derailment [67]. Wear may be broadly classified according to the relative types of motion such as sliding, rolling and rolling-sliding, or types of wear mechanisms [68]. The wear phenomenon in the rail industry and its modelling has been studied for decades [67, 69-71]. However, the impact of locomotive dynamic response on wear phenomena under different conditions has not been investigated deeply.

Beagley et al. proposed patterns of wear behaviour [72], which is categorized into “mild” and “severe” regimes to describe wear characteristics on either side of a wear transition between sliding velocity regions observed in his experimental results. A third regime, defined as “catastrophic” regime of wear, was defined by Bolton et al. according to their test results [73]. A thorough review of this “catastrophic” wear phenomenon was performed by Markov et al. in [74]. Furthermore, three wear regimes for wheel/rail steels have also been observed by Danks et al. [75] with field and laboratory test results. Danks et al. also proposed to use the terms “type I wear”, “type II wear” and “type III wear” for describing the “stages” of the wear, which are characterised by: the wear rate; the worn surface features (particularly its roughness); and the size, morphology and colour of wear debris which are caused by wear modes identified in references [66, 72, 73, 75, 76]. According to Clayton [77], type I wear combines both oxidational and rolling-sliding modes of wear resulting in debris containing oxide and metal particles. It approaches a true oxidative wear, in which materials are removed by the progressive growth and mechanical breakdown of an oxide layer, at very low creep rate and contact pressures. At the creep rate beyond the creep saturation there is a significant contribution from the formation of rolled out, thin, metal flakes that eventually fracture. Type II is characterised by completely metallic wear debris, the occurrence of microscope ripples on the wear surfaces and some metal transfer. It has been concluded that this is a deformation and fracture process with no evidence of fatigue-like cracks at the surface. Type III wear involves an initial

break-in period that leads to the production of large pieces of wear debris. This causes self-inflicted wear of both contact surfaces.

For the wheel/rail steel, the material loss in the wear process is defined as wear rate. It is determined by the loss of material mass per rolling distance ($\mu\text{g}/\text{m}$) [75]; or by the total loss of material mass per rolling distance, per contact area ($\mu\text{g}/\text{m}/\text{mm}^2$) [76]. Both wheel and rail wear regimes can be illustrated in a similar mapping method [67, 71, 78-81]. According to Lewis et al. [71], the Type I, II and III wear regimes, corresponding to the mild, severe and catastrophic wear regimes respectively, can be presented by plotting wear rate against $T\gamma/A$ to allow a direct comparison, as shown in Figure 16.

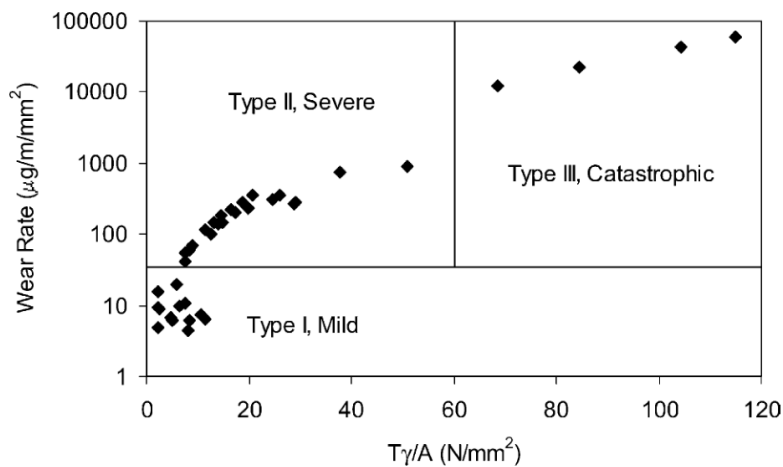


Figure 16: Wear types identified during tests of BS11 Rail vs. Class D Tyre [71]

According to the purpose of the study, wear rate can be plotted against the contact pressure and slip rate; multiplied by contact pressure and slip rate or even versus the ‘wear index’, $T\gamma/A$ [82] as shown in Figure 16 (in which T is the tangential force, γ is the creep rate and A is the nominal contact area). The correspondence between the laboratory and field results has been investigated in [58]. Comparison of the wear rate, wear surface and wear debris in laboratory and field showed that type I wear may be used to model the rail head wear, type II wear is most likely to model the rail gauge wear and type III wear closely simulates the rail gauge wear under unlubricated condition and heavy axle loads [58]. This model was used in the intermediate stage of this study. A new model based on recent experimental data was used for the purpose of wear control. The new wear model is specified in the following section.

A recent work on wear rate modelling has been carried out by Vuong et al. [66, 83], providing the relation between the frictional power density and the wear rate as shown in Figure 17 below. This wear model has also been used for the purpose of rail corrugation prediction and grinding cost analysis, which agrees with the field data from Queensland Rail [66].

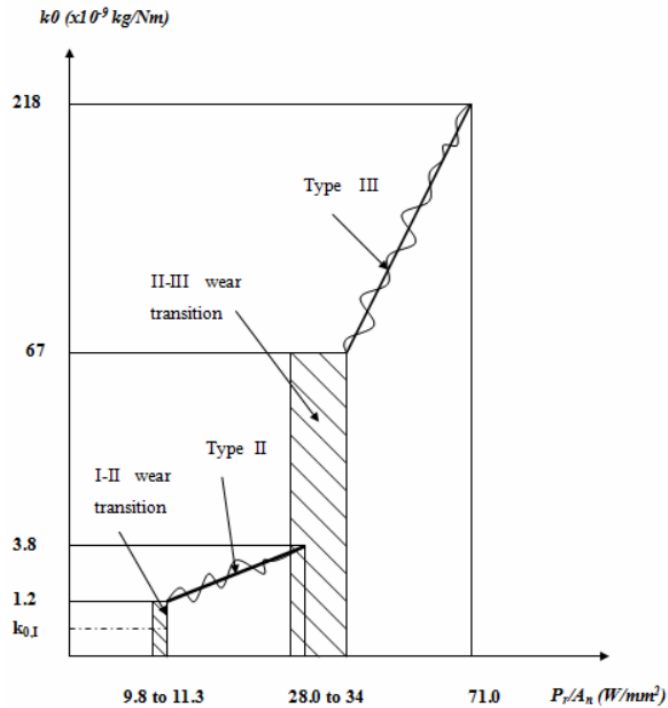


Figure 17: The wear coefficient versus the frictional power density for UICB rail steel, running with class D wheel steel [83]

In order to limit the wear damage on the rail tracks, the value P_r/A_n should be limited within a certain range. In this thesis the frictional power density threshold is chosen according to the experimental result as shown in Figure 17 above [83].

2.4. Summary

This chapter has examined the locomotive dynamic modelling efforts, rail-wheel contact mechanics, AC drive control techniques, adhesion/slip control methods and wear growth modelling. The available literature suggests that while there are seminal works with respect to each of the areas, there have been very few or emerging efforts that have tried to integrate these areas and establish a dynamic modelling framework for locomotive adhesion and wear control from a systems approach.

This thesis will combine the above mentioned subsystems by taking advantage of the above mentioned methods and investigate reliable fast adhesion/traction and wear control.

This section has identified the major research interests in this field in the period of the last 20 years and also identified the potential knowledge gap between control design and performance of locomotives and consequently established the objectives of the research.

Chapter III: Methodology

This chapter provides a summary of methodologies and models developed in this thesis for locomotive and electric drive modelling, wheel/rail contact mechanics modelling, creep/adhesion control and wear control. More specifically, section 3.1 mainly introduces the mathematical modelling for locomotive longitudinal, vertical and pitch dynamics; a detailed wheel/rail contact mechanics modelling; and electric drive dynamic modelling (Objective 1). Section 3.2 provides details of the fuzzy logic based creep/adhesion control methods aiming to achieve higher tractive force under a change of operating conditions (Objective 2). In section 3.3, details of wear rate control strategy are provided (Objective 3).

3.1. Overview

In order to study the dynamic response of a locomotive under a change of operating conditions, a model considering all essential dynamic components needs to be developed. In the proposed model, three major subsystems are taken into consideration for the modelling process; namely, a mathematical model representing the dynamics of a locomotive along longitudinal, vertical and pitch directions, electric drive/control dynamics, and contact mechanics. The interaction among the three modules is shown in Figure 18. The dynamic model of the mechanical system of an electric locomotive based on the Newton-Euler method [84] is developed. The wheel-rail contact in this model is based on Polach’s model [27]. And the simplified electric drive model with a PI creep controller is integrated into the electric drive/control dynamics block in this model.

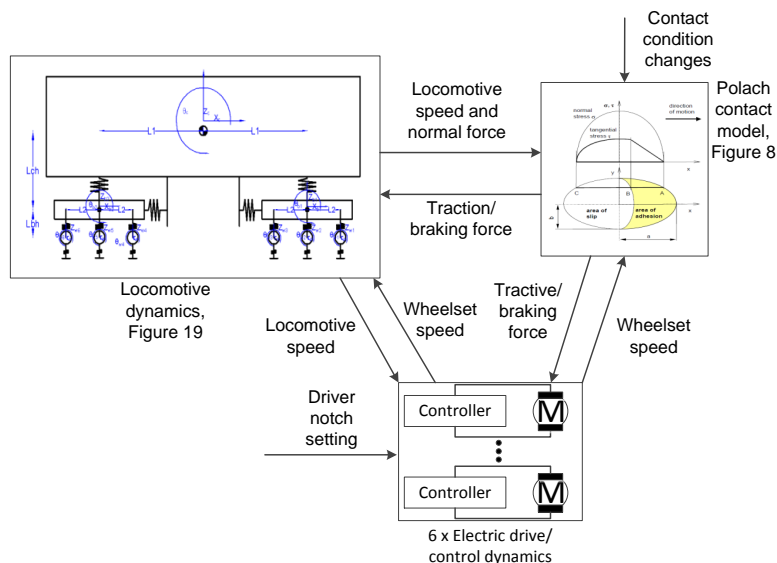


Figure 18: Schematic diagram of the overall system

The model may be described as a feedback system which takes creep as the major feedback signal. In the model, creep response is calculated directly from the rotational speed of the axles and the locomotive. The proposed system is also designed to be able to deploy into the field, where such speed information can be measured constantly. The rotational speeds of axles can be constantly measured by tachometers on the axles and used to generate reference creep. The position/speed information of the railway vehicle can be monitored by using a microwave ground speed sensor such as a Pegasem GSS20 [85, 86]. As a result, the creep value on each axle can be calculated as the relative difference between the speed of each axle and the locomotive speed. The controller then adjusts the amount of torque generated by each electric drive separately. The electric drive and control system provides a torque acting on the motor shaft in the locomotive model. Torque also results from the longitudinal force due to the interaction between wheel-rail track contact mechanics. The resultant creep changes the longitudinal tractive force calculated using the Polach model. The tractive force acts on the locomotive dynamic model and changes the displacements and velocities of the vehicle rigid bodies. Each of these components is detailed in the following sections.

3.2. Locomotive dynamic modelling and eigenmode analysis (Objective 1)

This section presents the modelling of essential locomotive dynamic components and eigenmode analysis (Objective 1). Specifically, the locomotive longitudinal, vertical and pitch dynamics modelling; the wheel/rail contact dynamics modelling; and the electric drive dynamics modelling are described respectively in detail.

3.2.1. Locomotive Multibody Dynamics

A 2-dimensional locomotive dynamic model is shown in Figure 19, which includes longitudinal, vertical and pitch dynamics of locomotive motion. An assumption has been made that the motors are fixed on the bogie evenly and no relative displacement occurs between the motors and the bogies, in order to simplify the model. The longitudinal motions between wheelsets and bogies are neglected to simplify the calculation and save simulation time while maintaining most of the essential dynamics. Also as for a typical three-piece freight vehicle bogie, axles are mounted on the bogies via axle boxes (Figure 3.37, [5]). The longitudinal stiffness between the axle box and bogie tends to be relatively higher than that of other parts, thus the relevant motion between the axles and bogies tends to be negligible.

Moreover, the main purpose of this study is to investigate the effect of creep and wear controllers. Therefore, taking longitudinal motion between bogies and axles into consideration will cause excessive computational cost and would not change the main conclusions of this study.

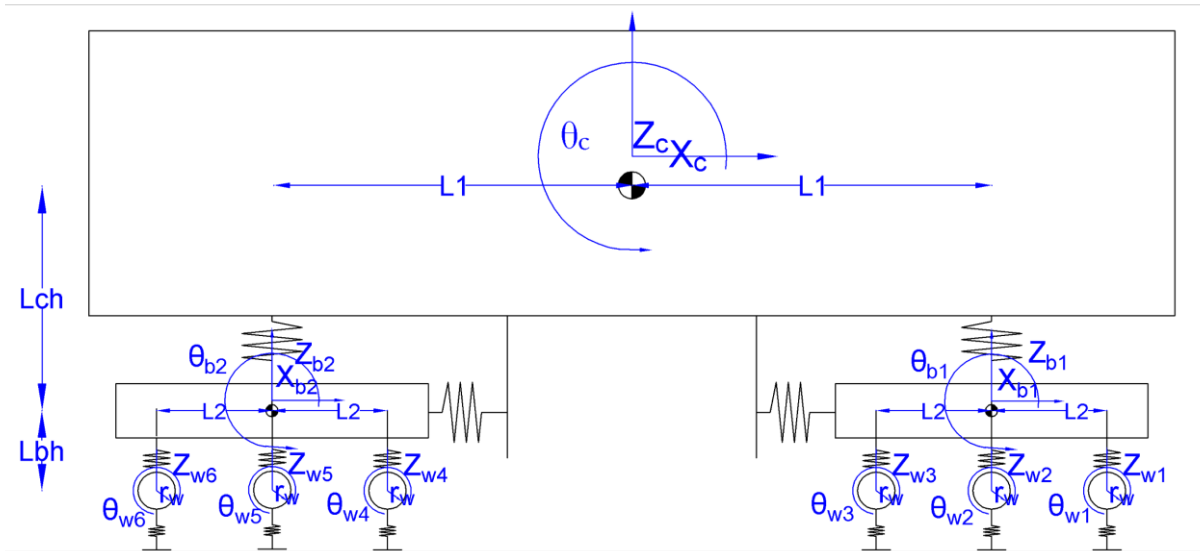


Figure 19: Locomotive longitudinal-vertical dynamic diagram

This model has 21 degrees of freedom (DOF), including 9 DOFs for the longitudinal, vertical and pitch motion of locomotive body and two bogies and 12 DOFs for vertical and rotating motion of the six wheelsets. The connection between the car body and bogies, i.e. the secondary suspension, contains a set of springs and dampers along both longitudinal and vertical directions. The connection between wheelsets and bogies, i.e. the primary suspension, contains a set of springs and dampers along only vertical direction as the longitudinal connections between the wheelsets and bogies are assumed to be rigid as the longitudinal stiffness of the primary suspension is usually much higher than that of the secondary suspensions [87]. The vertical wheel/track is modelled as a simple beam model [5], described by a stiffness coefficient. The longitudinal tractive force acting on the whole locomotive is caused by the friction force between the wheel and rail, providing a longitudinal acceleration/deceleration dynamic component of the bogie's motion and torque for bogie pitch motion. The relative motion between the bogies and car body provides the car body forces and torque for longitudinal, vertical and pitch motion.

The system variables are expressed as a vector containing 42 entries, representing the relative displacements and velocities between different nodes as:

$$X = [Z \quad \dot{Z}]^T, Z = [Z_c \quad Z_{bogie1} \quad Z_{bogie2} \quad Z_{axles}]^T, \quad (3.1)$$

in which $Z_c = [x_c \quad z_c \quad \theta_c]^T$ is a 3×1 vector representing the locomotive body longitudinal, vertical and pitch motion from the static positions, $Z_{bogie1} = [x_{b1} \quad z_{b1} \quad \theta_{b1}]^T$ and $Z_{bogie2} = [x_{b2} \quad z_{b2} \quad \theta_{b2}]^T$ are both 3×1 vectors representing longitudinal, vertical and pitch motion of the front and rear bogie separately, and $Z_{axles} = [z_{w1} \quad \theta_{w1} \quad z_{w2} \quad \theta_{w2} \quad \dots \quad z_{w6} \quad \theta_{w6}]^T$ is a 12×1 vector representing the vertical and rotating motion of wheelsets 1~6. The state space representation of the dynamics can be expressed as:

$$\begin{aligned} \dot{X} &= A_m \cdot X + B_m \cdot u \\ Y &= C \cdot X + D \cdot u \end{aligned} \quad (3.2)$$

where matrix A_m is defined as:

$$A_m = \begin{bmatrix} \theta & I \\ -M^{-1}K_m & -M^{-1}C_m \end{bmatrix}, \quad (3.3)$$

where u is the longitudinal tractive force resulted from the interaction between the wheelsets and rail tracks, Y is a vector of displacement or velocity of each node from its static position, θ is a zero matrix, I is an 21×21 identity matrix, K_m is the stiffness matrix, C_m is the damping matrix, and M is the diagonal mass and moment of inertia matrix in the form of,

$$M = \text{diag}(M_c \quad M_c \quad I_c \quad M_b \quad M_b \quad I_b \quad M_b \quad M_b \quad I_b \quad M_w \quad I_w \quad M_w \quad I_w \quad M_w \quad I_w \quad M_w \quad I_w \quad M_w \quad I_w \quad M_w \quad I_w). \quad (3.4)$$

Matrix D is defined as:

$$D = \theta_{21 \times 6}. \quad (3.5)$$

The detailed parameters of the locomotive are listed in Table 1.

Table 1: Detailed parameters of the locomotive model

Parameter	Value
Mass of each bogie frame (kg)	12121
Total mass of locomotive (t)	134
Load mass (kg/carriage \times no. of carriages)	90000×50
Load force (N)	4.8×10^6
Gear Ratio	17/90
Primary suspension springs (N/m)	89×10^6
Yaw viscous dampers stiffness (N/m)	45×10^6
Vertical viscous dampers stiffness (N/m)	44×10^6
Secondary suspension springs (N/m)	5.2×10^6
Longitudinal and lateral shear stiffness (N/m)	0.188×10^6
Central pivot longitudinal stiffness (N/m)	5×10^6
Wheel contact stiffness (N/m)	2.4×10^9
Primary suspension vertical damping (kg/s)	10×10^3
Secondary suspension vertical damping (kg/s)	2×10^4
Rail damping (kg/s)	1×10^6
Locomotive body length (m)	22
Locomotive body height – without bogie (m)	1.93
Bogie length (m)	3.7
Bogie height (m)	0.733
Horizontal distance between bogies mass centre (m)	13.7
Horizontal distance between axles (m)	1.3
Vertical distance between body bottom and bogie top (m)	0.3605
Vertical distance between bogie bottom and wheel top (m)	0.127
Wheel diameter (m)	1.016
Simulation time step (s)	5×10^{-6}
Wheelset mass (kg)	2850
Car body pitch moment of inertia (kg· m ²)	3610410
Front/rear bogie pitch moment of inertia (kg· m ²)	37007
Wheelset pitch moment of inertia (kg· m ²)	1200

The axle rotation dynamics is excluded from eigenmode (modal) analysis as the rotation of the axles is considered as linearly dependent on the motor shaft rotation, which is modelled as part of the motor dynamics. As a result the corresponding rows and columns are kept out from A_m to form a new matrix A_{modal} for the locomotive modal analysis. Since the matrix A_{modal} is the state space form of modal analysis [88, 89], the eigenvalues $\lambda_i = -\alpha_i \pm i\beta_i$ of matrix A_{modal} represent the modes of motion of the locomotive and the first 15 elements of the eigenvectors represent the corresponding mode shapes. The real part of the eigenvalues is the decay rate of the modes and the imaginary part is the corresponding damped natural frequency. The damping ratio is defined as $\zeta_i = \frac{-\alpha_i}{\sqrt{\alpha_i^2 + \beta_i^2}}$.

3.2.2. Contact Mechanics

The creep force is caused by the wheel-rail rolling contact and it is crucial in terms of the locomotive traction/braking operation. The Polach creep force model [27] is employed as it has been verified to be relatively accurate for locomotive traction analysis [35]. The contact area is assumed to be elliptical. The solution assumes a linear growth of the relative displacement between the bodies from the leading point A to the trailing point C along the edge of the contact area as shown in Figure 8. The tangential stress acts in the opposite direction of the creep and the value of stress grows linearly with the distance from the leading edge. The relative motion of the contact surfaces appears when the tangential stress reaches its maximum value according to [18]. The resulting creep force along the tangential direction is,

$$F = \frac{2Q\mu}{\pi} \left(\frac{k_A \varepsilon}{1+(k_A \varepsilon)^2} + \arctan(k_s \varepsilon) \right), \quad (3.6)$$

where F is the tangential force, Q is normal wheel load, k_A is the reduction factor in the area of adhesion and k_s is the reduction factor in the area of slip. ε is the gradient of the tangential stress in the area of adhesion which along the longitudinal direction (defined as x direction in Figure 8) can be calculated as,

$$\varepsilon_x = \frac{1}{4} \frac{G\pi abc_{11}}{Q\mu} S_x, \quad (3.7)$$

where G is the shear modulus and a and b are the half-axes of the contact ellipse as shown in Figure 8. The contact area is calculated as in [90] as $a = 8.6$ mm, $b = 4.4$ mm according to the dimension of the wheel in Table 1 and 60 kg rail profile from [91], c_{11} is derived from Kalker's work [25] and characterizes the longitudinal direction of the contact shear stiffness coefficient. Also s_x is the creep component in longitudinal direction defined as,

$$s_x = \frac{w_x}{V}, \quad (3.8)$$

where w_x is the slip velocity in longitudinal direction and V is the vehicle speed.

The Polach model employed is a regular form considering both longitudinal and lateral creep forces. However this is a simulation on a straight track, so only longitudinal dynamics need to be considered. Hence it is assumed the locomotive is tracking with no lateral displacement on the contact patch. As a result total creep s equals creep along longitudinal direction s_x . μ is the coefficient of friction calculated as:

$$\mu = \mu_0[(1 - A_p)e^{-B_p w} + A_p], \quad (3.9)$$

where μ_0 is the maximum friction coefficient at zero slip velocity, A_p is the ratio of friction coefficient at infinity slip velocity μ_∞ and μ_0 defined as:

$$A_p = \frac{\mu_\infty}{\mu_0}. \quad (3.10)$$

B_p is the coefficient of exponential friction decrease.

Details of the parameters are listed in the previous section. The axes can be calculated with elliptical point contact formulae as in Appendix 3 in [90].

$$\frac{a}{b} \approx \left(\frac{R'}{R''}\right)^{2/3}, \quad (3.11)$$

$$c = (ab)^{1/2} = \left(\frac{3PR_e}{4E^*}\right)^{1/3} F_1(R'/R''), \quad (3.12)$$

R' and R'' are major and minor relative radii of curvature. R_e is equivalent radius defined as $R_e = (R'/R'')^{1/2}$, P is normal load and E^* is the combined Young's modulus defined as $E^* = \left(\frac{1-\nu_1^2}{E_1} + \frac{1-\nu_2^2}{E_2}\right)^{-1}$ in which ν is the Poisson ratio. In this study under the assumption of straight tracks and cylindrical wheels, R' is the radius of the wheel and R'' is the radius of the rail head. The standard 60 kg rail profile [91] is considered, as shown in Figure 20:

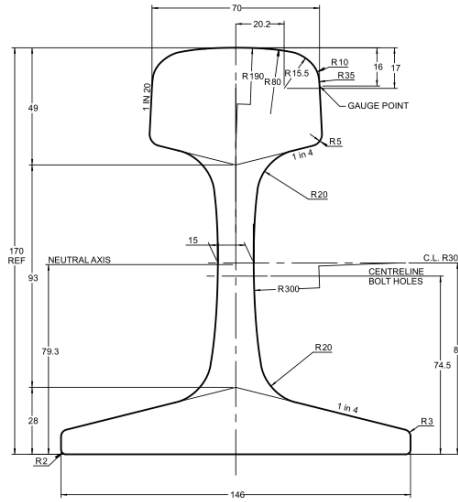


Figure 20: Standard 60kg rail profile [91]

The inputs of the Polach adhesion/traction model are locomotive velocity, normal contact force calculated by the locomotive dynamic model, wheel speed obtained from the electric drive shaft speed and the switchable parameter sets representing different contact conditions such as dry and wet wheel-rail contact circumstances. The parameters for dry and wet contact conditions are listed in Table 2, according to Polach's work [27], where A the ratio of friction coefficient is defined as $\frac{\mu_{\infty}}{\mu_0}$, B is the coefficient of exponential friction decrease (s/m), k_A is the reduction factor in the area of adhesion and k_S is the reduction factor in the area of slip. Rail tracks can be contaminated by oil. Compared with the dry and wet conditions, the oil contact condition tends to cause a large friction reduction. As a result, the wheelsets are more likely to lose traction under the oil condition than under the dry and wet conditions. Polach model parameters k_A and k_S will be tuned for an oil contact condition and the result will be shown in next chapter.

Table 2: Parameters for different contact conditions

Conditions Parameters	Dry	Wet
k_A	1	0.3
k_S	0.3	0.75
μ_0	0.55	0.3
A	0.4	0.4
B	0.25	0.09

3.2.3. Electric Drive Dynamics

This section provides details of the complex DTC drive and the simplified single drive AC drive and controller modelling.

The controlling variables are motor magnetising flux and motor torque. The electromagnetic torque generated by the induction machine can be expressed as [50],

$$T_e = \frac{3}{2}P \frac{L_m}{\sigma L_s L_r} \bar{\psi}_s \times \bar{\psi}_r = \frac{3}{2}P \frac{L_m}{\sigma L_s L_r} |\bar{\psi}_s| |\bar{\psi}_r| \sin(\delta) \quad (3.13)$$

where $\sigma = 1 - L_m^2/L_s L_r$ is the leakage factor, P is the number of pole pairs, $\delta = \rho_s - \rho_r$ is the torque angle where ρ_s and ρ_r are stator and rotor flux angles. L_m is the mutual inductance, L_s is the stator self-inductance and L_r is the rotor self-inductance. The dynamic model of an induction machine in the stationary reference frame can be written in $\alpha\beta$ frame variables. The stator and rotor flux linkage and their components can be written as,

$$\begin{aligned} \bar{\psi}_s &= L_s \bar{i}_s + L_m \bar{i}_r \\ \psi_{\alpha s} &= L_s i_{\alpha s} + L_m i_{\alpha r} , \\ \psi_{\beta s} &= L_s i_{\beta s} + L_m i_{\beta r} \end{aligned} \quad (3.14)$$

$$\begin{aligned} \bar{\psi}_r &= L_m \bar{i}_s + L_r \bar{i}_r \\ \psi_{\alpha r} &= L_r i_{\alpha r} + L_m i_{\alpha s} , \\ \psi_{\beta r} &= L_r i_{\beta r} + L_m i_{\beta s} \end{aligned} \quad (3.15)$$

where \bar{i}_s and \bar{i}_r are the stator and rotor current vectors. The three phase voltage is controlled by the switching of the voltage source inverter (VSI) on and off. The rotor flux is determined by loading and the stator flux is to be controlled nearly constant. As a result the torque can be controlled by changing the stator flux angle. As shown in Figure 21 (left), the three phases of the AC machine are connected to an inverter supplied with direct current voltage source. Each switch can be connected to upper position, indicated by '1', or lower position indicated by '0'. The line-to-neutral voltage v_{1a} , v_{1b} and v_{1c} are determined only by the switching mode of the inverter. Eight voltage vectors, including two zero voltage vectors can be generated by a different switching mode setting, as shown in Figure 21 (right).

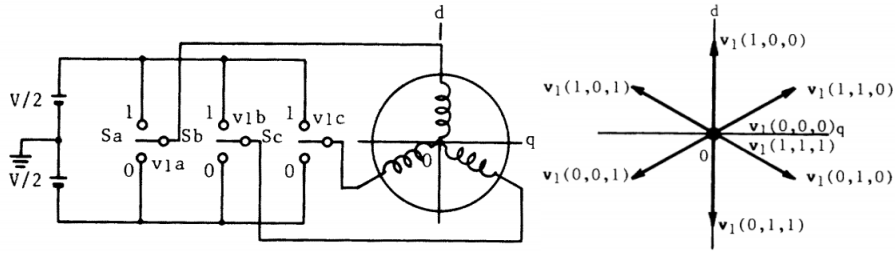


Figure 21: Schematic diagram of an AC machine with inverter (left) and instantaneous voltage vectors (right) [92]

The control signal is generated by the look-up table based on the stator voltage vectors generated by the inverter switching states as shown in Figure 21. The look-up table is as shown in Figure 22 below.

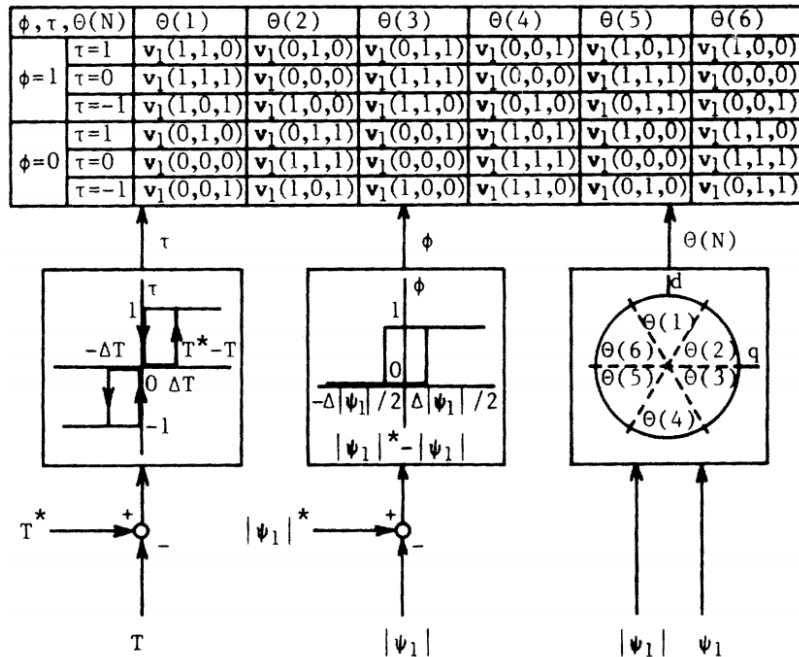


Figure 22: Optimum switching table and comparators [92]

It gives the selection of the voltage vectors for all the possible stator flux space vector positions in terms of sectors. The switching is determined by the status of errors of the primary (stationary) flux linkage vector ϕ and electromagnetic torque T_e .

The mechanical dynamics of the rotary motor is given by [93],

$$\dot{\omega} = \frac{1}{J}(T_e - T_l - T_f), \quad (3.16)$$

where ω is the angular velocity of the rotor, J is the moment of inertia of the rotor, T_e is the developed electromechanical torque, T_l is the load torque and T_f is the friction torque. In this thesis, the equivalent moment of inertia J_{eq} is introduced to represent the overall moment of inertia including the axles and gears. The gear ratio from the axle to the rotor is defined as R_g . The dynamics including the axles and the transmission mechanism is simplified as,

$$J_{eq}\dot{\omega} = T_e - R_g T_l - T_f. \quad (3.17)$$

The diagram of the DTC induction machine is as shown in Figure 23 below.

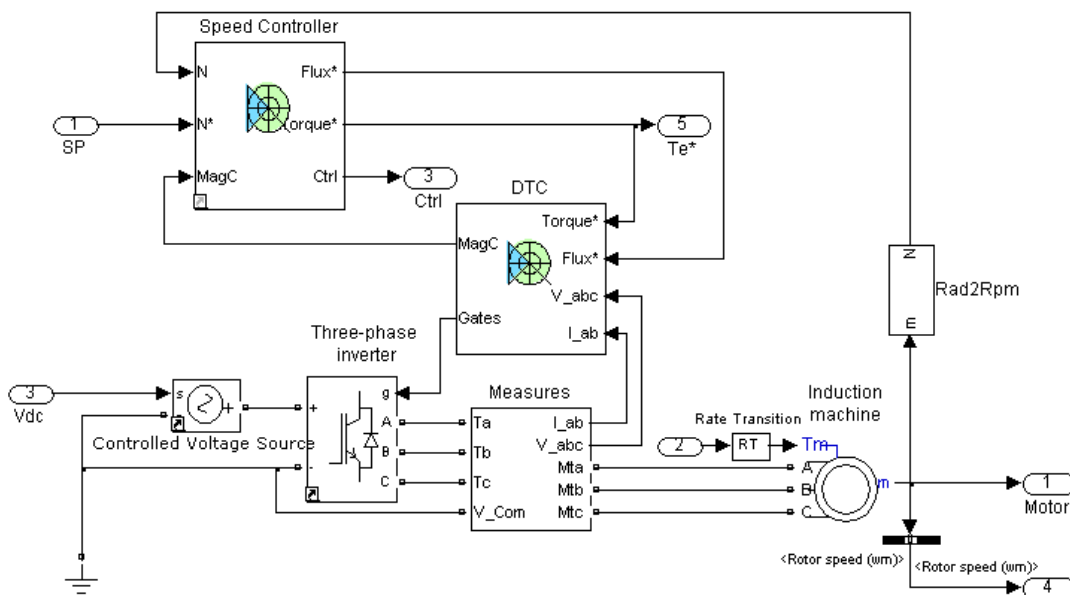


Figure 23: Diagram of the DTC induction machine

A simplified AC drive dynamic model has also been developed by excluding the electric dynamics of above procedure to simulate the low frequency dynamic response, and to reduce the simulation time. The simplified electric drive dynamics is as described by equation (3.17).

3.3. Creep Controllers (Objective 2)

In this section, several creep/adhesion control methods will be provided in detail, including a PI controller, a fuzzy logic based controller and a modified fuzzy controller.

3.3.1. PI Controller

A PI controller is adopted and tuned with a creep threshold setting and controller parameters to test the system stability and to reveal the transient dynamic behaviour of the model. In this way, the diagram of this basic method is shown in Figure 24:

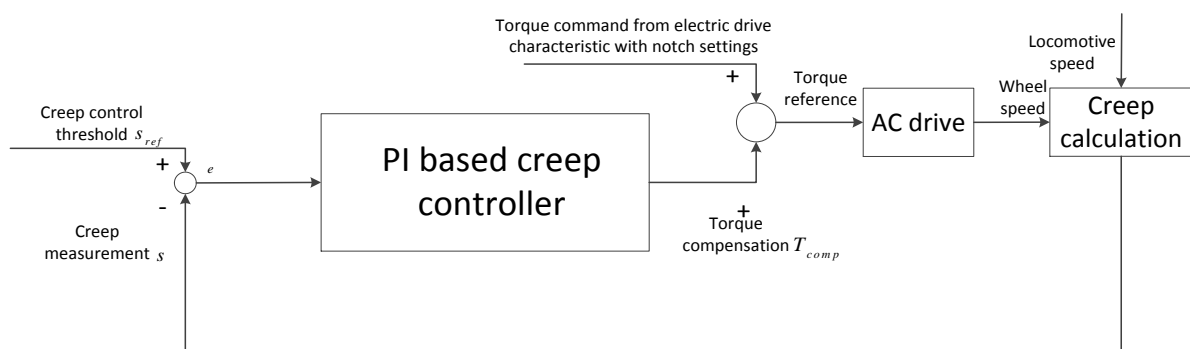


Figure 24: Diagram of basic PID adhesion/creep controller

The two main components of this subsystem are AC drives and the creep controller. The driver notch setting chooses different torque command levels. The torque reduction command is generated by the creep controller. The adjusted torque command then acts as the control input of the drives operating under torque control mode to generate electromagnetic torque acting on the shaft to drive the wheelset via a series of gears. The input electromagnetic torque command signal is the combination of the command signal given by driver notch setting and the compensation torque signal of the creep controller output. The PI controller compares the actual creep value to the pre-set threshold, which currently is chosen to be 7%. If the actual creep value is lower than the threshold, the controller outputs zero; otherwise, it generates a compensation value to reduce the overall torque command. In this way the AC motor tractive torque will be reduced and hence the creep will be controlled. A more advanced controller will be implemented in the following sections. The detailed model including electric AC drive dynamics would take approximately about 20 minutes to run 10 seconds simulation on a desktop workstation using Matlab/Simulink. In comparison, the

simplified model described in the previous section takes only 10 minutes for the same simulation. Figure 25 shows the flow chart of the PI creep controller.

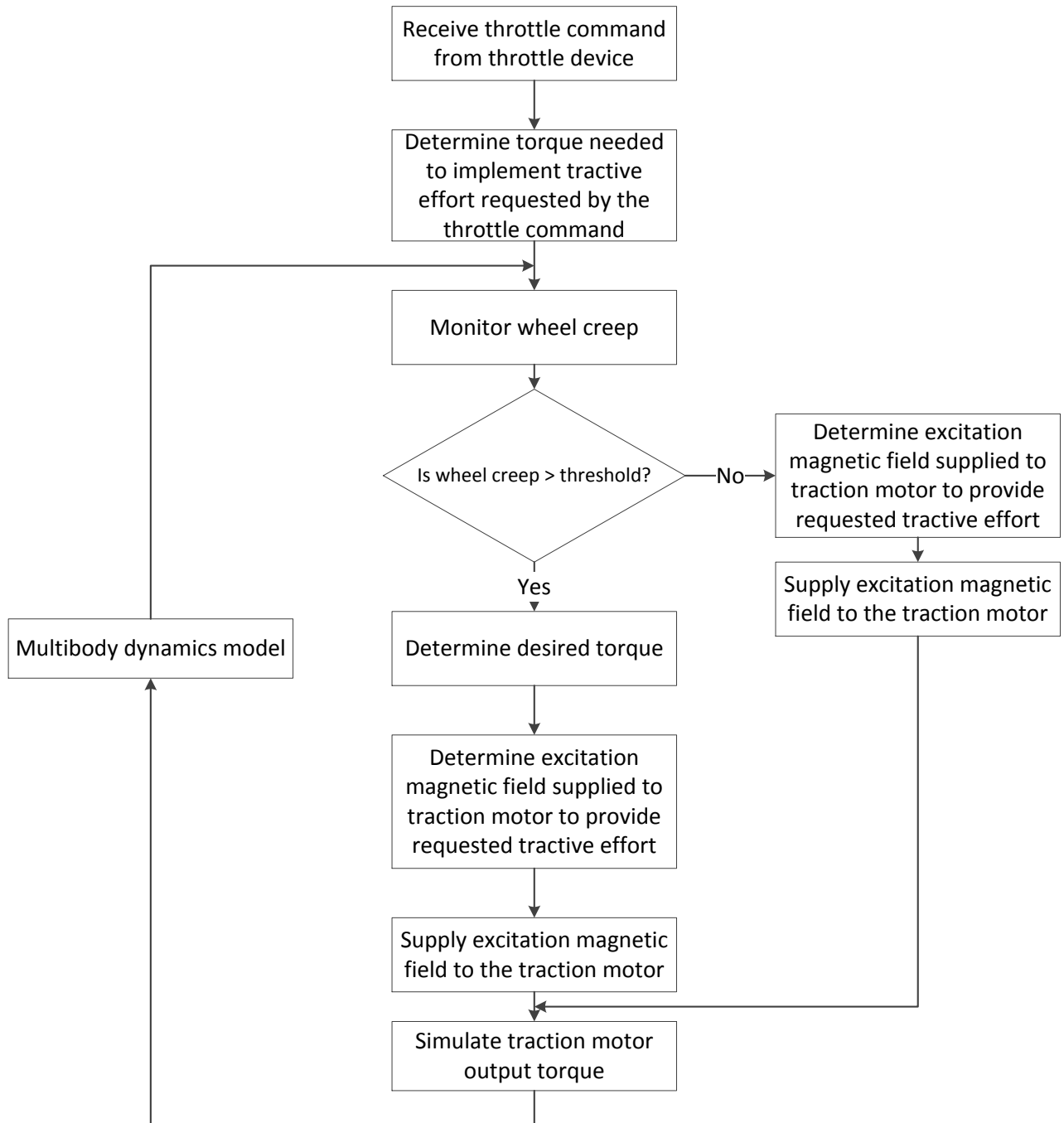


Figure 25: The flow chart of the PI creep controller

The creep controller is based on the creepage with maximum traction effort according to the creep curve. The design of the creep controller is very similar to the creep controller described in the patent document (US patent number 20130082626A [94]), which uses a

threshold value of 3%. Based on the design of GE’s PowerHaul Series locomotive [95], individual axle traction control technology is employed.

3.3.2. Fuzzy Logic Controller with Variable Creep Threshold

The proposed adhesion control system utilizes the method described in [96] to determine the locomotive speed which will be used to calculate the creep values of each axle. And an adhesion force coefficient observer proposed in [54] is adopted to generate the ‘optimum’ reference motor torque signal. The control system diagram is as shown in Figure 26.

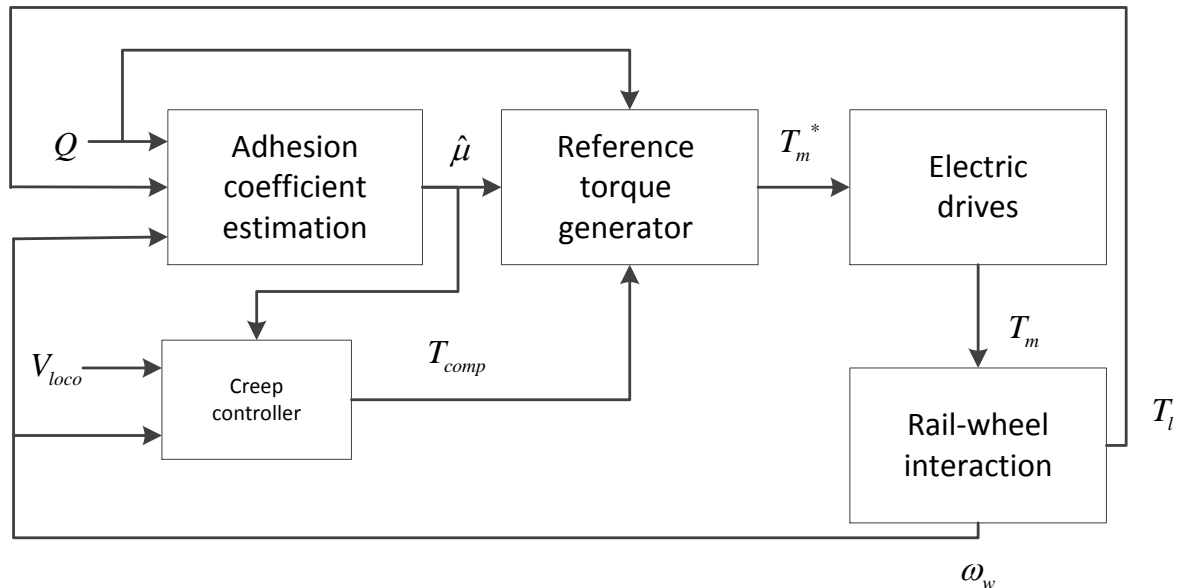


Figure 26: Adhesion control diagram

A fuzzy logic creep controller is adopted in this work due to its advantage of giving strong self-adaptive and robust performance without the need of an accurate mathematical model [97]. The proposed fuzzy logic controller uses the information of differentiation of each axle’s creep and the differentiation of each axle’s adhesion coefficient, which is estimated from the change in vehicle acceleration over one sample period as proposed in [98]. Each of the fuzzy inputs of derivative of creep and derivative of adhesion coefficient is expressed by 5 fuzzy membership functions, e.g. positive big (Pb), positive small (Ps), zero (0), negative small (Ns) and negative big (Nb). The output of the fuzzy logic controller is a torque compensation command to each of the motors, either to increase or reduce the

electromagnetic torque acting on the motors within the range of the traction limit. The controller output is described by,

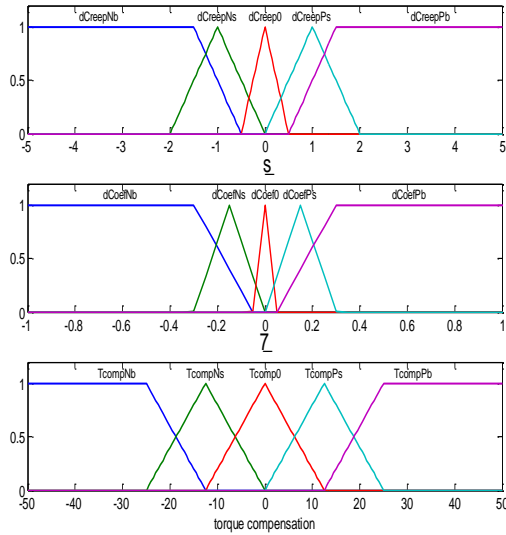
$$T_m^*(N) = T_m^*(N - 1) + T_{comp}(N). \quad (3.18)$$

The membership functions and control rules are in Table 3 and Figure 27 below.

Table 3: Fuzzy rule table

Derivative of creep (\dot{s})	Derivative of adhesion coefficient ($\dot{\mu}$)				
	Pb	Ps	0	Ns	Nb
Pb	Pb	Ps	Ns	Ns	Nb
Ps	Ps	Ps	0	Nb	Nb
0	Ps	0	0	Ps	Ps
Ns	Ns	Ns	Ps	Ps	Pb
Nb	Ns	Ns	Ps	Ps	Pb

(a)



(b)

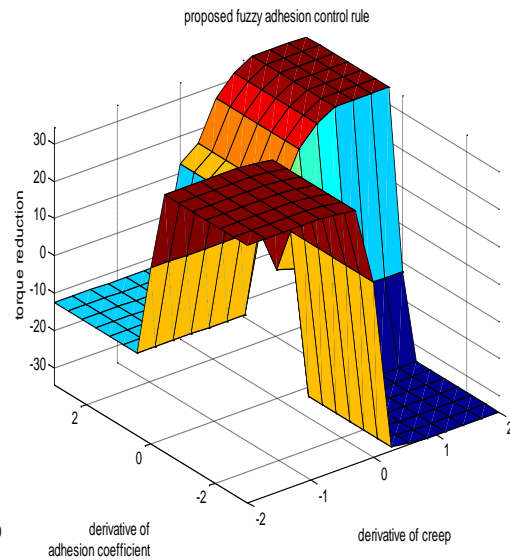


Figure 27: (a) Membership functions of inputs and output; (b) Fuzzy logic 3D input-output characteristics

The fuzzy rules are designed based on [98], i.e. dividing the creep-adhesion coefficient curve into four different sessions according to the value of \dot{s} and $\dot{\mu}$ (1~4 representing sessions of dry contact condition curve, 1*~4* representing sessions of wet contact condition curve), as shown in Figure 28:

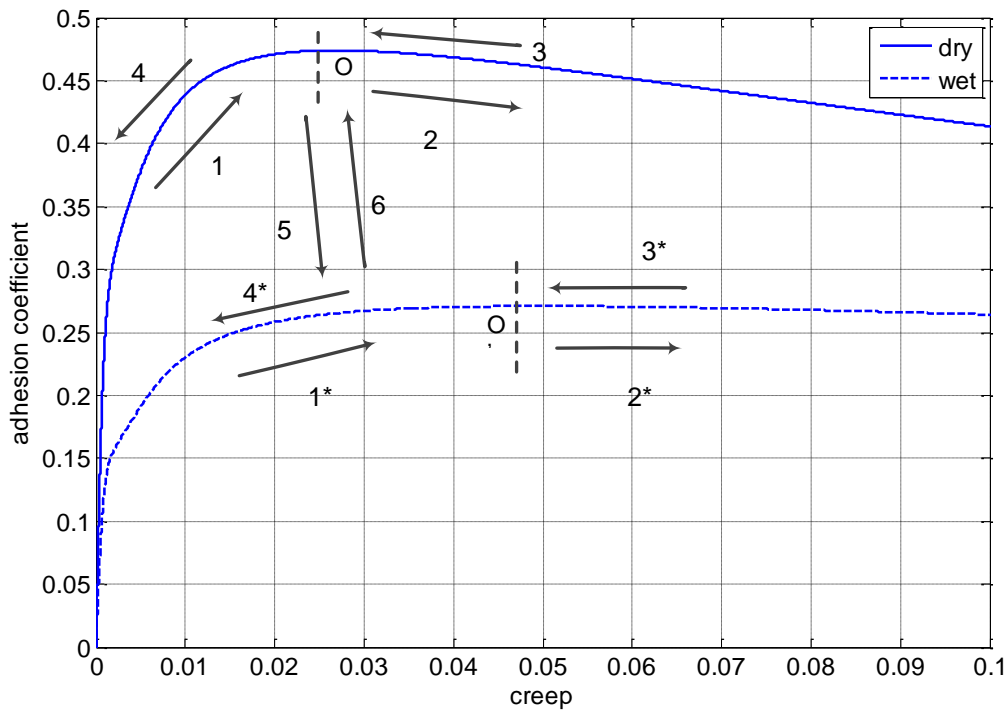


Figure 28: Illustrative graph for the fuzzy rules

The characteristics of the processes above in terms of \dot{s} and $\dot{\mu}$ are detailed below. In processes 1 and 1*, \dot{s} is positive and $\dot{\mu}$ is positive. In 2 and 2*, \dot{s} is positive and $\dot{\mu}$ is negative. In 3 and 3*, \dot{s} is negative and $\dot{\mu}$ is positive; and in 4 and 4*, \dot{s} is negative and $\dot{\mu}$ is negative. Moreover, the transient condition caused by the change of wheel-rail contact condition is also taken into consideration. Thus two additional sessions have been added. Process 5 is the transient from the dry curve to wet curve with a positive \dot{s} and a very large negative $\dot{\mu}$. Process 6 is the transient from wet curve to dry curve with a negative \dot{s} and a very large positive $\dot{\mu}$. The principle of the logic is to maintain the adhesion coefficient at a maximum value O for a dry contact condition or at O' for a wet contact condition, by reducing the torque command when the creep value is on the right hand side of a maximum value and increasing the torque command when on the left hand side of a maximum value.

3.3.3. Modified Fuzzy Logic Controller

The modified fuzzy controller differs from the one in the previous section in generating the reference slip instead of torque compensation signal. The controller from [99] is used to

regulate the torque output of the motor. The locomotive adhesion/traction control scheme that based on fuzzy logic is shown in Figure 29.

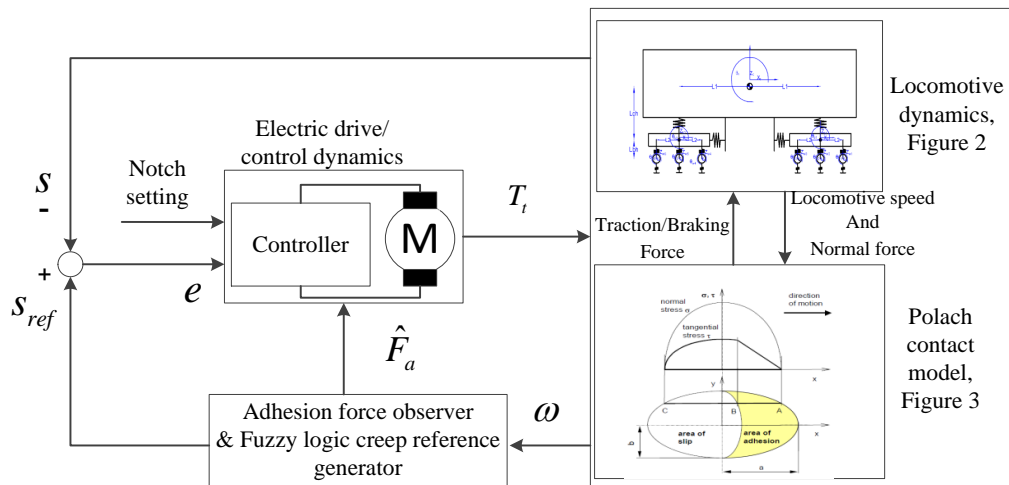


Figure 29: Schematic diagram of the overall system

The model may be described as a feedback system. The rotational speeds of axles are constantly measured and used to generate a reference creep. The creep value on each axle is also calculated with the information of the speed of each axle and the locomotive speed. The controller then adjusts the amount of torque generated by the electric drives accordingly. The electric drive and control system provides a torque acting on the motor shaft in the locomotive model. Torque also results from the longitudinal force due to the interaction between wheel-rail track contact mechanics. The resultant creep changes the longitudinal tractive force calculated as described in the Polach model, and the tractive force acts on the locomotive dynamic model and changes the displacements and velocities of the car bodies and bogies. The reference creep is calculated with the fuzzy logic method based on the derivative of creep \dot{s} and derivative of adhesion coefficient $\dot{\mu}(s)$. The updating law of reference slip is,

$$s_{ref}^k = s_{ref}^{k-1} + \Delta^k(\dot{s}, \dot{\mu}), \quad (3.19)$$

where updating term $\Delta^k(\dot{s}, \dot{\mu})$ is calculated with fuzzy logic. As the peak value of the adhesion coefficient occurs when $d\mu/ds = 0$, the update term can be chosen as $d\mu/ds$. For a discrete time system, it can be represented by,

$$\frac{\mu^k - \mu^{k-1}}{s^k - s^{k-1}}, \quad (3.20)$$

where the value of adhesion coefficient μ on the numerator is approximated with the ratio between \hat{F}_a and normal contact force between the wheel and the rail. The whole term in equation (3.20) is used as the input of the reference generator.

The fuzzy logic takes this as its input and calculates an updating term according to Table 4 and membership functions in Figure 30. Both input and output have four membership functions, i.e. negative big (NB), negative small (N), positive small (P) and positive big (PB). The output of the fuzzy system is the updating term Δ^k .

Table 4: Fuzzy rule table of the modified fuzzy controller

INPUT	OUTPUT
NB	NB
N	N
P	P
PB	PB

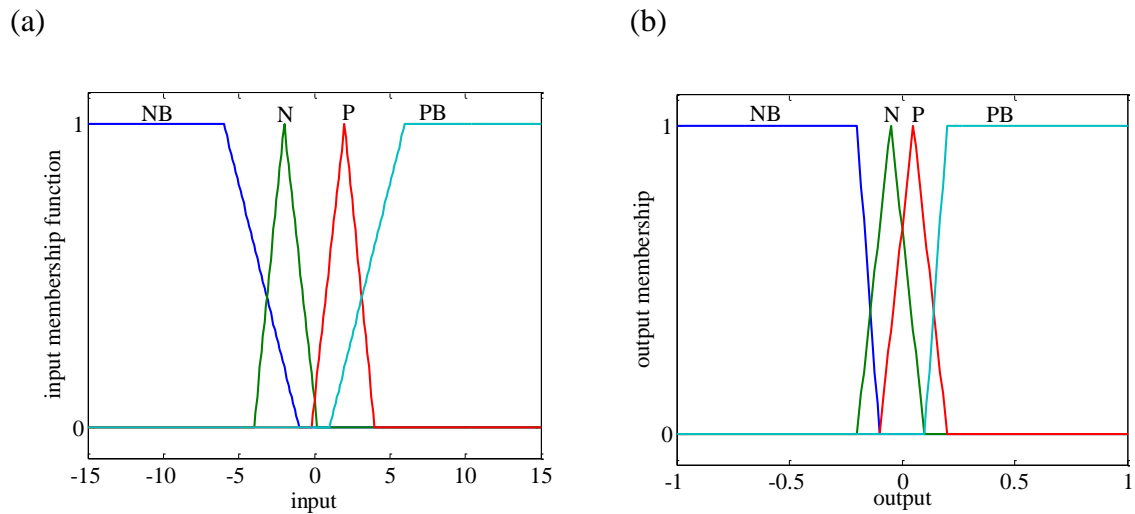


Figure 30: (a) Membership functions of input; (b) Membership functions of output

Values from equation (3.20) correspond with values of the input in Figure 30 (a), with which corresponding fuzzy values μ_{NB} , μ_N , μ_P and μ_{PB} can be obtained from the vertical axis in Figure 30 (b). Consequently, the centre of gravity method is employed as the defuzzification method. This method calculates the value z^* for a fuzzy number \tilde{C} as in [100],

$$z^* = \frac{\int z \mu_{\tilde{C}}(z) dz}{\int \mu_{\tilde{C}}(z) dz}, \quad (3.21)$$

where $\mu_{\tilde{C}}$ denotes the membership function of the fuzzy number \tilde{C} (NB, N, P and PB).

The sliding mode control law [99] is designed with a simplified system dynamic model with one axle and 1/6 of total dynamic mass and then integrated into the locomotive dynamics. The sliding surface $S(t)$ for the sliding mode controller is defined as,

$$S(t) = e + \gamma \int_0^t e dt, \quad (3.22)$$

with $e = s_{ref} - s$ represents the tracking error between the creep reference s_{ref} and the actual creep s . γ is a positive design parameter. The derivative of the sliding surface, after taking account of the simplified system dynamics, can be expressed as,

$$\dot{S} = \dot{s}_{ref} - \frac{r}{JV} T_t + \frac{r^2}{JV} F_a - \frac{1}{MV} (s + 1) F_a + \gamma e = -D_c s - K_s \text{sgn}(s). \quad (3.23)$$

The tractive force can be estimated by,

$$\hat{F}_a = \frac{1}{r} T_t - \frac{J}{r \tau s + 1} s, \quad (3.24)$$

where τ is the time constant of the first order filter in the adhesion force observer [99]. Thus the tractive torque can be obtained as,

$$T_t = \frac{JV}{r} \left\{ \dot{s}_{ref} + \gamma e + \left[\frac{r^2}{JV} - \frac{1}{MV} (s + 1) \right] \hat{F}_a + D_c s + K_s \text{sgn}(s) \right\}. \quad (3.25)$$

3.4. Wear Rate Control (Objective 3)

In this section, the wear rate control strategy based on a recent wear rate model [66] is provided in detail.

Wear of both rail and wheel can be categorized as Type I (Mild), Type II (Severe) and Type III (Catastrophic) regimes. Recent research [66, 83] has investigated wear transitions between

different types of wheel/rail steel and using different wear models and models have been proposed for various rail materials. The frictional power density P_r/A_n is defined by $\frac{P_r}{A_n} = \frac{F_t V_s}{A_n}$, where F_t is the traction force, V_s is the relative slip velocity and A_n is the nominal contact area. The wear coefficient k_0 is determined by,

$$k_0 = \frac{\Delta m}{\Delta W}, \quad (3.26)$$

where Δm is the mass loss of the rail disc after a certain time interval and ΔW is the frictional work dissipated in the rolling/sliding contact [66]. The wear coefficient under the dry conditions is about five times higher than that under the FM conditions [66].

In order to avoid excessive wear damage on the rail and wheel as in the Type III region in Figure 17, the friction power density value separating Type II and III regions of Figure 17 is chosen as the wear control threshold. In this study the threshold is set at 34 W/mm^2 .

This study employs a PI based creep controller to limit the creep values under pre-set creep thresholds at 4%. The block diagram of the creep control is shown in Figure 31 (a) and the diagram shown in 29 (b) is the block diagram of the wear and creep controller. Each wheelset has its own set of a controller and a motor so that the speed of the motors can be adjusted independently.

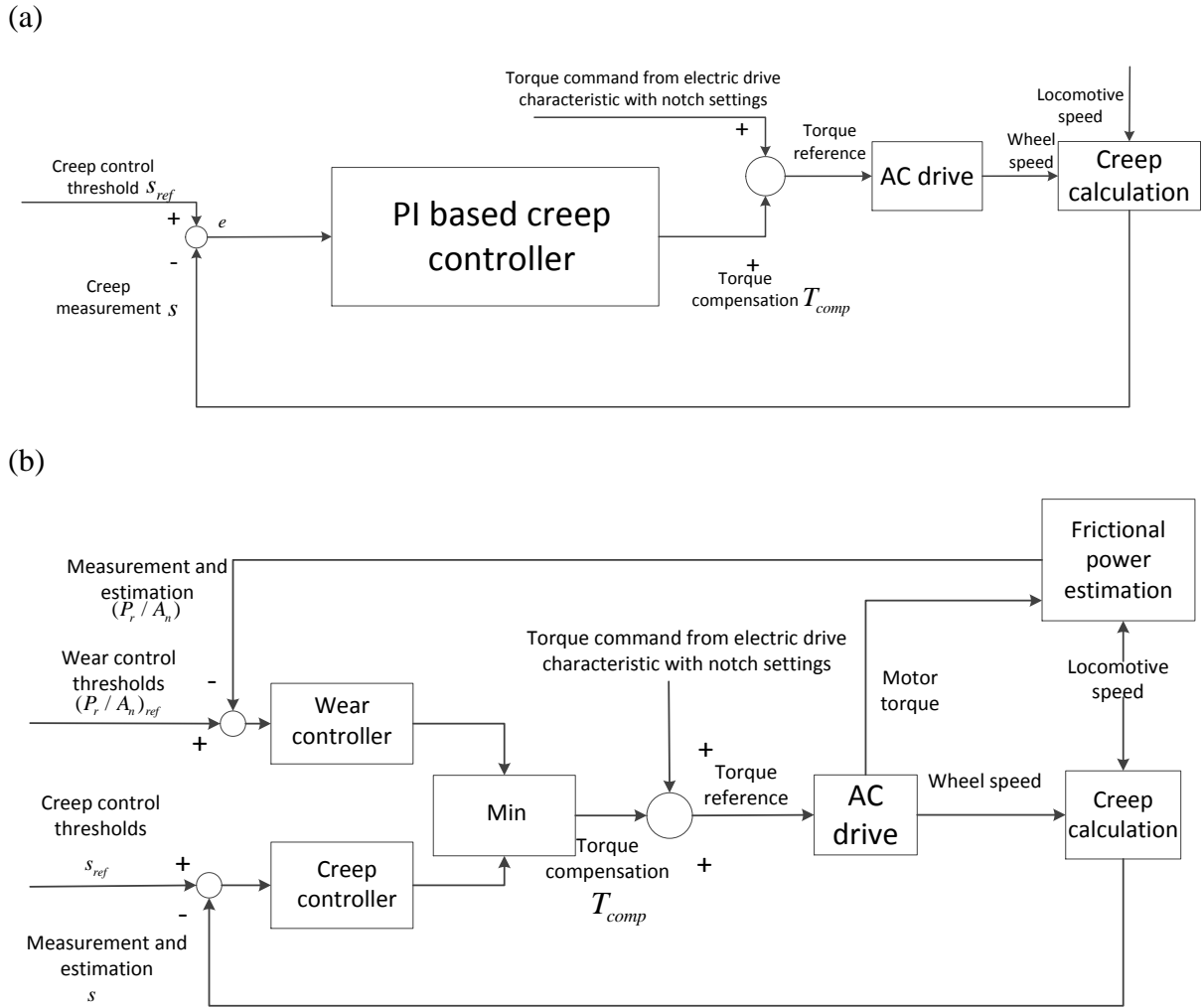


Figure 31: (a) Creep only control diagram; (b) Creep and wear control diagram

In this study the creep threshold setting is assumed to be adjustable to investigate its impact on wear growth rate under different contact conditions. Different notch settings adjust the level of power supply to the motors and are controlled by drivers. The creep controller adjusts the torque generated by the motor. If the creep measurement is lower than the pre-set threshold, the controller is not activated. Otherwise the creep controller gives a torque compensation signal to reduce the amount of torque generated by the electric drive. In this case, the parameter values of the PI controller are tuned to $P_{creep} = 1.5 \times 10^7$ and $I_{creep} = 2 \times 10^5$, for the proportional (P) and integral (I) constants respectively, with consideration of the ratio of $e = s_{ref} - s$ and the scale of torque to compensate. Hence the torque compensation can be calculated as,

$$T_{comp} = \begin{cases} 0 & \text{if } e \geq 0 \\ P_{creep} \times e + I_{creep} \times \int_{t_1}^{t_2} e dt & \text{if } e < 0 \end{cases} \quad (3.27)$$

Similarly, the wear controller adjusts the torque generated by the motor if either the frictional power density estimation exceeds the frictional power density threshold setting or the creep measurement exceeds the creep threshold setting. If both the creep measurement and the frictional power density estimation are lower than their corresponding pre-set thresholds, the controller is not activated; otherwise the controller outputs the smaller negative value of the two as the torque compensation. The parameter values of the creep control subsystem are the same as that of the creep only controller. The PI wear control subsystem control parameters are $P_{wear} = 1.25 \times 10^7$ and $I_{wear} = 8 \times 10^3$ respectively. The torque compensation generated by the wear and creep controller can be calculated as,

$$T_{comp} = \begin{cases} 0 & \text{if } e_s \geq 0 \text{ and } e_{P_r/A_n} \geq 0 \\ P_{creep} \times e_s + I_{creep} \times \int_{t_1}^{t_2} e_s dt & \text{if } e_s < 0 \text{ and } e_{P_r/A_n} \geq 0 \\ P_{wear} \times e_{P_r/A_n} + I_{wear} \times \int_{t_1}^{t_2} e_{P_r/A_n} dt & \text{if } e_s \geq 0 \text{ and } e_{P_r/A_n} < 0 \\ \min \left\{ P_{creep} \times e_s + I_{creep} \times \int_{t_1}^{t_2} e_s dt, P_{wear} \times e_{P_r/A_n} + I_{wear} \times \int_{t_1}^{t_2} e_{P_r/A_n} dt \right\} & \text{if } e_s < 0 \text{ and } e_{P_r/A_n} < 0 \end{cases} \quad (3.28)$$

3.5. Summary

The modelling and control methods used to complete the objectives in this thesis are detailed. In order to achieve Objective 1, the locomotive longitudinal, vertical and pitch dynamics are modelled using the Newton-Euler method. The eigenmode analysis method is also described. The wheel/rail contact dynamics is described with the Polach model, followed by a complex model of DTC electric drive dynamics and a simplified model. Objective 2 is achieved by using PI and fuzzy logic based control methods. A recent wear growth model is employed to control the wear damage to achieve Objective 3. With the modelling and control methodology identified and formulated, corresponding results were obtained, which are presented and discussed in the following chapter.

Chapter IV: Results and Discussion

This chapter presents a summary of the results of simulations in accordance with the thesis objectives. Firstly, simulation results of the individual dynamic subsystems, including the locomotive longitudinal, vertical and pitch dynamics, the wheel/rail contact mechanics and both simplified and complex electric drive dynamics, as well as the complete integrated system are presented and compared with available data from the literature. Eigenmode analysis has also been performed to validate the model and to identify the modes of oscillations that are more likely to be excited under external perturbations, to complete Objective 1. Secondly, the simulation results comparing the dynamic responses of the locomotive with a traditional creep controller and results with new creep controllers under changes of operating conditions are presented, highlighting the benefits and likely limitations of controllers aiming to achieve higher tractive forces to complete Objective 2. Lastly, simulation results showing the impact of different creep controller threshold settings on the wear index are presented, which give rise to the new real-time control strategy aiming to limit wear damage on the wheel/rail contact patch. Then the simulation results comparing the dynamic responses of the locomotive with the traditional creep controller and the new controller are presented to highlight the benefit of the new control strategy to complete Objective 3.

4.1. Locomotive Dynamic Simulation and Validation (Objective 1)

This section presents simulation results and analysis focusing on the individual dynamic subsystems respectively.

4.1.1. Validation of Multibody Dynamics - Eigenmode Analysis

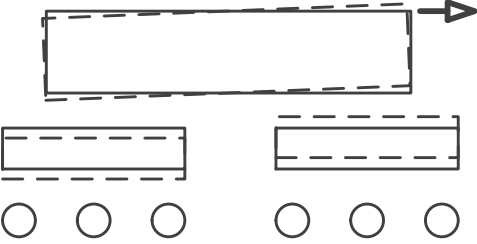
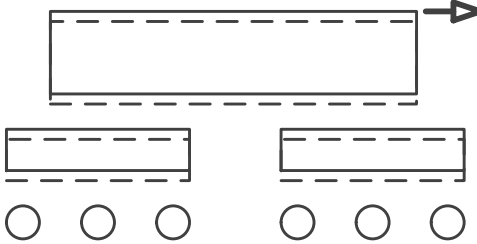
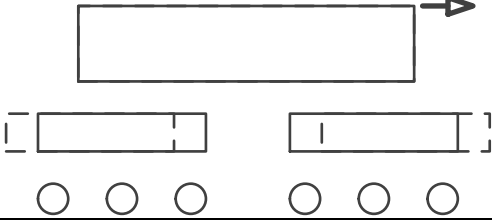
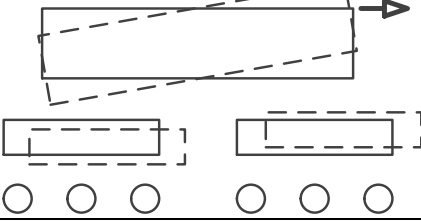
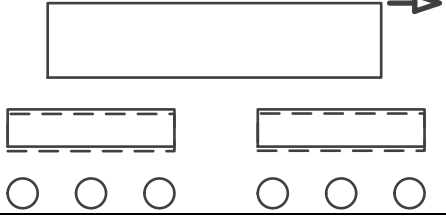
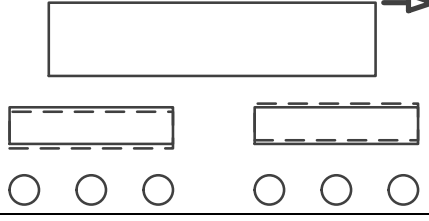
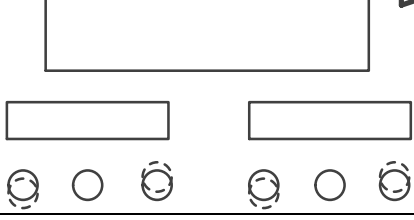
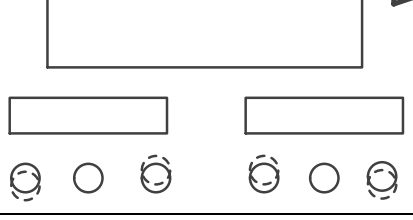
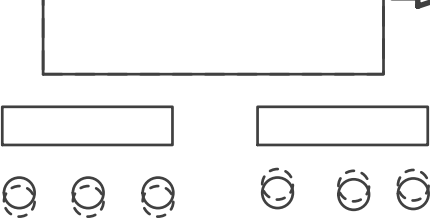
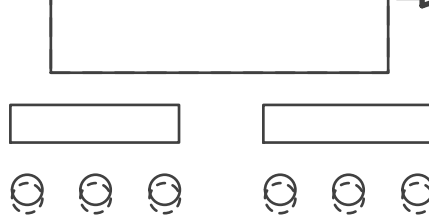
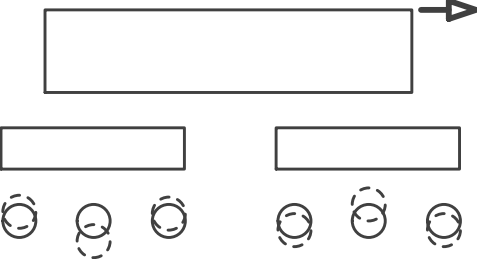
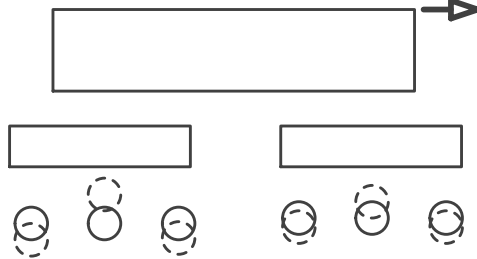
An eigenmode analysis was performed to identify all the dynamic modes of vibration and to determine the stability of the system. The system eigenvalues are provided in Table 5. An eigenvalue is obtained for each possible mode of vibration of the system. The negative real part shows that all vertical and pitch motions are stable. In other words, these modes of vibration are positively damped. Besides the modes listed in the table below, a rigid body mode is also identified with a zero frequency. This mode is associated with the longitudinal rigid body motion of the locomotive.

Table 5: Modal frequencies of the locomotive dynamic system vibrations, damping ratio, decay rates and corresponding eigenvalues

Modes	Frequency (Hz)	Damping ratio	Decay rate (s^{-1})	Eigenvalues
Mode 1	0.4	0.78	3.4624	$-3.4624 \pm 2.7499i$
Mode 2	0.45	0.72	2.9184	$-2.9184 \pm 2.8363i$
Mode 3	3.29	0.08	1.6874	$-1.6874 \pm 20.644i$
Mode 4	3.31	0.09	2.201	$-2.201 \pm 23.333i$
Mode 5	3.85	0.48	13.119	$-13.119 \pm 24.2i$
Mode 6	3.94	0.45	12.63	$-12.63 \pm 24.778i$
Mode 7	137.55	0.02	17.123	$-17.123 \pm 864.15i$
Mode 8	137.55	0.02	17.123	$-17.123 \pm 864.15i$
Mode 9	137.55	0.02	17.123	$-17.131 \pm 864.27i$
Mode 10	137.55	0.02	17.123	$-17.131 \pm 864.27i$
Mode 11	137.62	0.02	17.123	$-17.139 \pm 864.69i$
Mode 12	137.62	0.02	17.123	$-17.139 \pm 864.69i$

Table 6 graphically shows the motion of each mode. The amplitude of the displacements illustrates the tendency of the motion of the particular mode to be excited by external perturbations. From Table 5 and Table 6, it can be seen that modes 7~12 have the least damping. These modes are the vertical displacements of the axles with mostly identical frequency about 137.6 Hz, thus form a family of modes in terms of frequency similarity. Due to the low damping ratio in these modes of motion, the vibration energy dissipation is slow, which means this mode is easy to excite due to external perturbations. However, as shown in Table 5, these modes have the highest decay rate at $17.123 s^{-1}$, which means these modes of vibration die down quickly in time. Apart from this family of axle vertical modes, mode 3 and mode 4 have the least damping ratios at about 0.08 as well as low decay rates at about $1.7 s^{-1}$ and $2.2 s^{-1}$ respectively, which means these modes of vibration are relatively easy to be excited and are attenuated slowly. The major dynamic behaviour of mode 3 is the out of phase bogie longitudinal motion. Mode 4 includes the in phase locomotive body pitch, bogies' longitudinal motions and the out of phase bogies' vertical motions.

Table 6: Diagram of the mode motions

<p>Mode 1: 0.4 Hz</p> 	<p>Mode 2: 0.45 Hz</p> 
<p>Mode 3: 3.29 Hz</p> 	<p>Mode 4: 3.31 Hz</p> 
<p>Mode 5: 3.85 Hz</p> 	<p>Mode 6: 3.94 Hz</p> 
<p>Mode 7: 137.55 Hz</p> 	<p>Mode 8: 137.55 Hz</p> 
<p>Mode 9: 137.55 Hz</p> 	<p>Mode 10: 137.55 Hz</p> 
<p>Mode 11: 137.55 Hz</p> 	<p>Mode 12: 137.55 Hz</p> 

To investigate this further, Figure 32 shows the vertical displacements of the all axles under simultaneous change of contact conditions from dry to wet at 11 km/h.

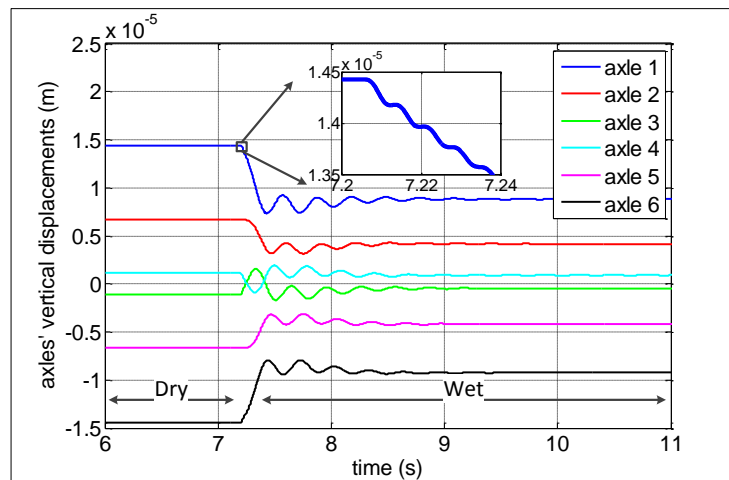


Figure 32: Vertical displacements of axles under change of contact conditions

As shown in Figure 32, the dynamic response of the axles has a frequency component of about 3.4 Hz, which is close to the frequency of Mode 4 in Table 6. The high frequency component in the axle response can be identified in the zoomed-in part in Figure 32. Figure 33 shows the pitch motion of the locomotive body, the vertical motions of bogies and the longitudinal motions of the bogies scaled down to 1/100 of the original displacements in order to make these displacements comparable. The vertical displacement of bogie 2 is plotted as its absolute value for the same reason.

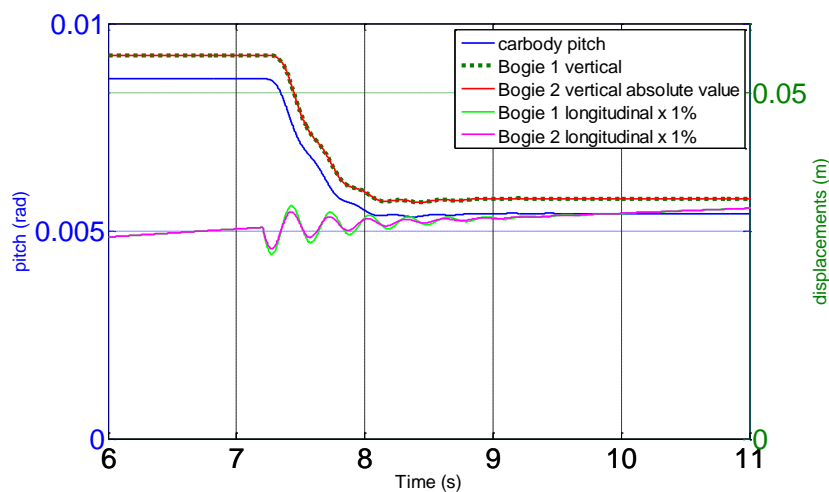


Figure 33: Locomotive car body pitch, vertical and bogies' vertical displacements

In Figure 33, the absolute value of bogie 2 vertical displacement (the vertical displacement itself is negative in the proposed coordinate) is mostly overlapped with the displacement of bogie 1 vertical displacement. It shows that the bogie vertical displacements are out of phase with a major frequency component of about 3.3 Hz. The locomotive body pitch motion and the vertical motion of bogie 1 are in phase with similar frequency of about 3.3 as shown in the zoomed-in part in the figure. These motions agree with the eigenmode analysis result of Mode 4 in Table 6. The tractive force reduces after the contact condition changes from dry to wet. The decline of the force causes the reduction of torque acting on the locomotive car body pitch motion, thus reducing its pitch angle. The corresponding change of bogies' vertical motion is caused by the resultant vertical displacements of the locomotive body pitch motion.

The eigenmode analysis result and the simulation result with a simultaneous wheel/rail contact condition change are consistent. This contributes to the validation of the dynamic modelling. It also highlights that the locomotive car body pitch mode is more likely to be excited by changes in friction conditions.

4.1.2. Validation of the Creep Model

The Polach creep model is mostly used for dry and wet wheel-rail contact conditions. In order to modify the Polach model to fit the creep-adhesion coefficient curve, the parameters were extended and tuned. As mentioned in previous chapter, the Polach model is of the form,

$$F = \frac{2Qu}{\pi} \left(\frac{k_A \varepsilon}{1 + (k_A \varepsilon)^2} + \arctan(k_s \varepsilon) \right) \text{ with } \mu = \mu_0 [(1 - A_p)e^{-Bw} + A_p]. \quad (4.1)$$

The parameter A_p is defined as the ratio of friction coefficients $\frac{\mu_\infty}{\mu_0}$, B is defined as the coefficient of exponential friction decrease, k_A is the reduction factor in the area of adhesion and k_s is the reduction factor in the area of slip. Additionally the original constraint on k_A and k_s is $k_s \leq k_A \leq 1$ to match the particular measured data for dry and wet contact conditions. The oily condition however, has a different shape of creep-adhesion coefficient curve for which the parameters need to be extended and modified to match. The data for the oil contact condition in [101] is used as the standard for the Polach parameter tuning for the oil condition. The parameters are tuned such that the curve fits the data, particularly in the region of creep involved in this study from 0 to 0.1. The tuned parameters for this condition

are $k_A = 1000$, $k_S = 0.025$, $\mu_0 = 0.22$, $A_p = 0.505$ and $B = -0.003$. The resulting Polach creep-adhesion coefficient curve comparing to the data in [101] is as in Figure 34.

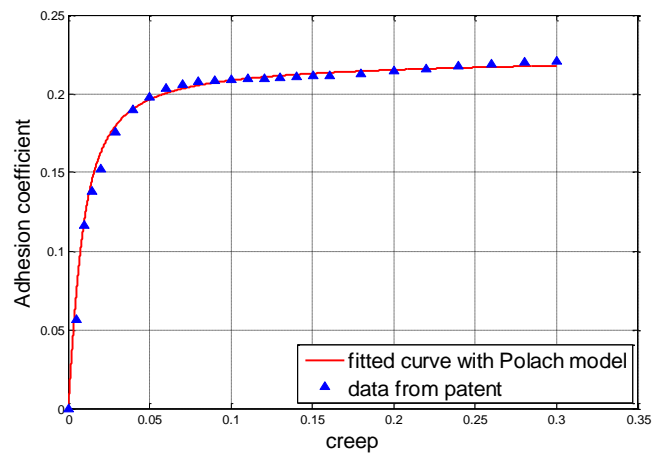


Figure 34: Tuned Polach creep-adhesion coefficient curve for oil condition at 20 km/h and data in [101]

It can be seen that the curve of the model is consistent with the data in [101]. Moreover, the data in [101] agrees with the friction region specified by the experimental data for the greasy/oily contact condition in [102]. Thus the Polach model is tuned for the oily condition. The parameters for dry and wet conditions are adopted from Polach’s work [27]. Figure 35 below shows the influence of the locomotive speed and creep on the adhesion coefficient under a dry wheel/rail contact condition.

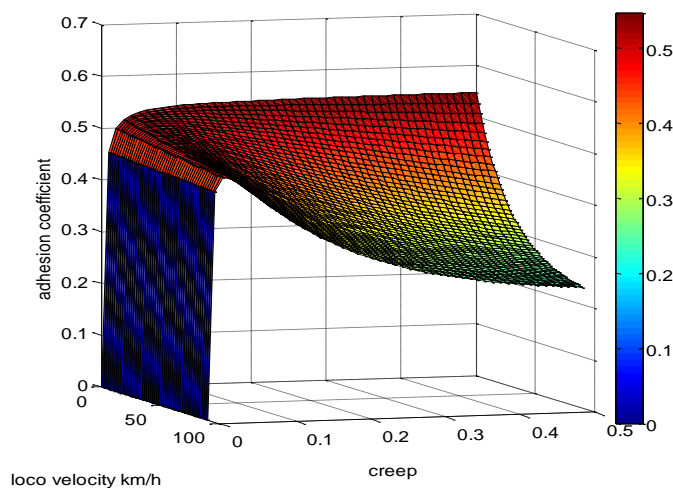


Figure 35: The form of adhesion coefficient-creep function and the influence of vehicle speed under dry wheel/rail contact condition

Under a constant locomotive speed, after the adhesion coefficient increases to a maximum value with the increase of creep, it decreases as the creep continues to increase. There is likely not yet a universally applicable explanation to this phenomenon for all contact conditions. However the change of the temperature on the contact patch results in locally varying material parameters [103]. The elastic modulus drops as the increase of temperature. Consequently the friction drops. The likely dependency of the friction coefficient on contact area temperature usually gives good agreement between theory and measurements for dry and clean contact conditions [27, 104]. The curves for dry and wet conditions under low and high speeds are as shown in Figure 36, in which the ratio between the longitudinal force and the normal force F/Q is also known as the adhesion coefficient. To clarify the definitions, friction is the general physical term describing the force resisting the relative motion of surfaces sliding against each other. Traction is mostly used to describe the tangential force in vehicle dynamics. Adhesion coefficient is the ratio between the tangential force and the normal force at the contact patch.

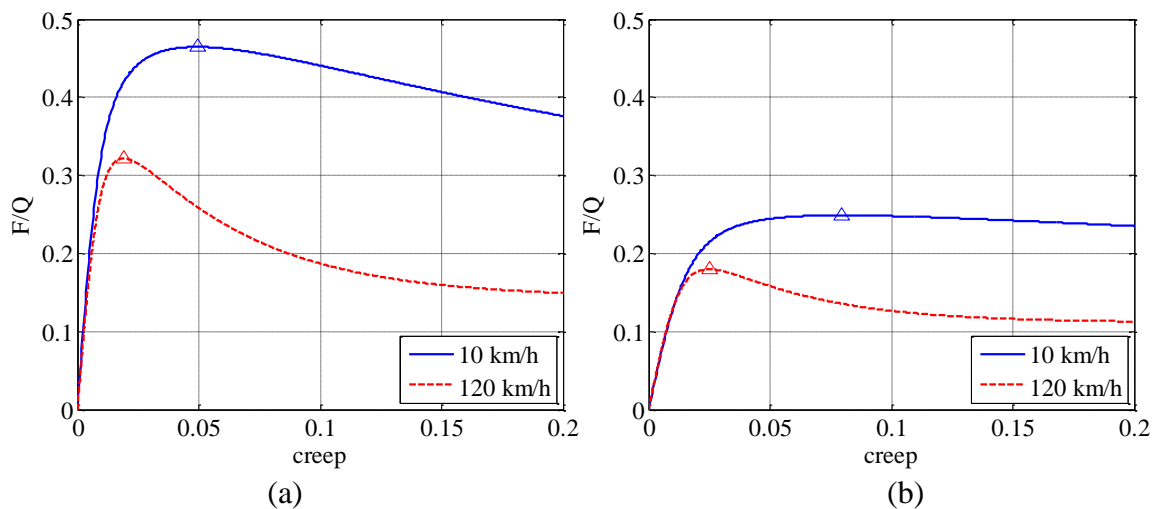


Figure 36: Polach tractive force curve at different speeds under (a) dry contact condition; and (b) under wet contact condition

The triangles in the figure mark the peak adhesion coefficient of the curves. It shows that under the same wheel-rail contact condition, the peak adhesion coefficient value shifts towards a low creep value as the locomotive speed is increased. This is due to the slip velocity dependent friction coefficient term in the Polach model. There is literature illustrating the dependency of friction coefficient on the slip velocity. Assumptions have been made that the dependency is caused by the high temperature at the contact patch under high speed. This causes material property changes and reduces the elastic modulus [103].

As shown above, the contact dynamics between the wheel and rail is complex and highly nonlinear. The adhesion coefficient, that is the ratio between longitudinal and normal force between the wheel and rail contact patch, varies significantly under different conditions such as different operating speeds or wheel/rail contact conditions. Thus it is crucial to adjust the wheel speed accordingly to avoid the occurrence of undesirable dynamics such as the loss of traction due to the excessive spin of the wheels.

4.1.3. Simulation Results of the Simplified and Detailed Drives

In order to validate the AC and DC drive and controller performances, simulations were carried out for single wheelset simplified locomotive models for a range of traction conditions. The following results will be detailed in the following subsections.

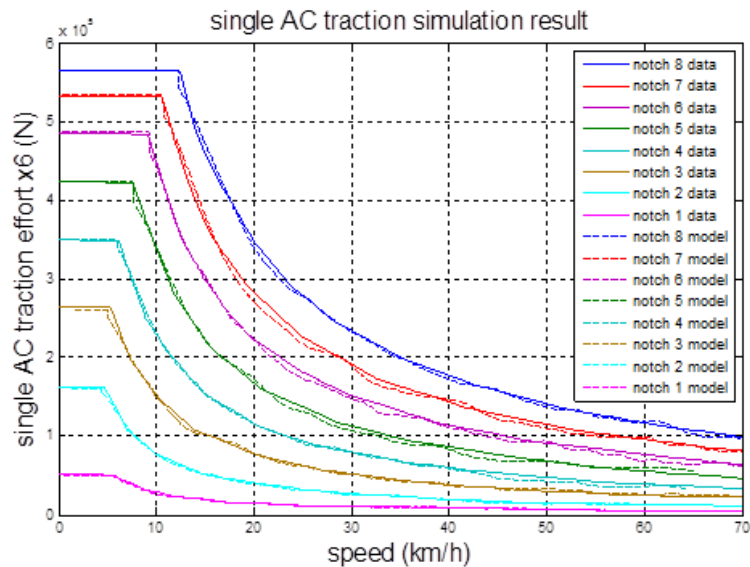
- Traction simulations for the dry condition to validate the tractive effort of the AC and DC drive and to compare to the traction curves in [101].
- A braking simulation for the dry condition to validate the braking effort of the AC and DC drive and to compare to the braking curve in [105].
- An acceleration simulation for the dry condition and comparison to data from [106].
- A transient contact condition simulation from the dry to the oil condition at 20km/h to validate the effectiveness of the creep controller.

In the simplified 1/6 locomotive model, the basic formula $f = ma$ has been employed where f is the traction/braking force caused by the interaction between the wheelset and rail tracks, m represents 1/6 of the total mass of the locomotive 134 tonnes and a is the acceleration of the mass. In order to verify the drive model's traction/braking performance without considering the vehicle structural dynamics, the dynamic model was simplified to a single mass of 1/6 of the total mass of the locomotive on an axle. Here a typical heavy haul locomotive GT46MAC mass and traction effort data are chosen for the simulation.

The simulations have been carried out for each traction notch by changing the driver notch setting as shown in Figure 37. The initial velocity of the locomotive is set to be 0.01km/h to avoid error due to an infinite initial creep value. For each notch a simulation is then carried out for the dry contact condition, from the initial speed to 70 km/h. Then the tractive force value is rescaled to calculate the total tractive force of the corresponding notch by being

multiplied by 6 (drives) and compared with the data for the total tractive force for the locomotive in [101].

(a)



(b)

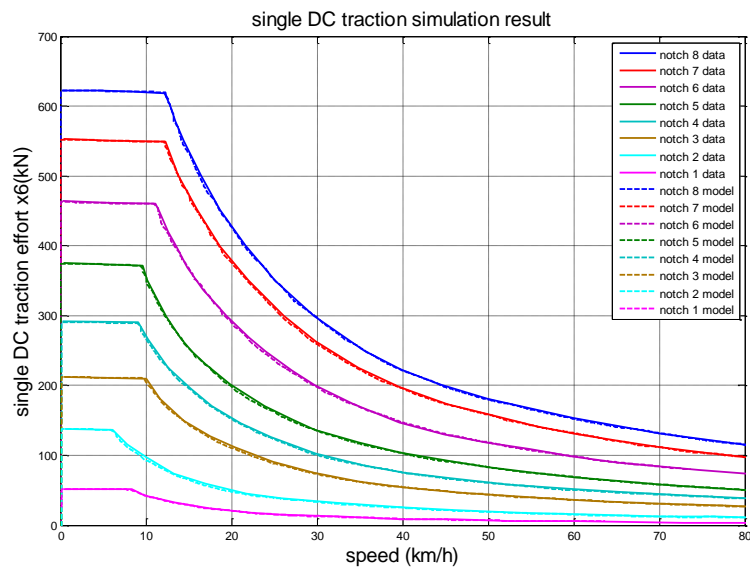
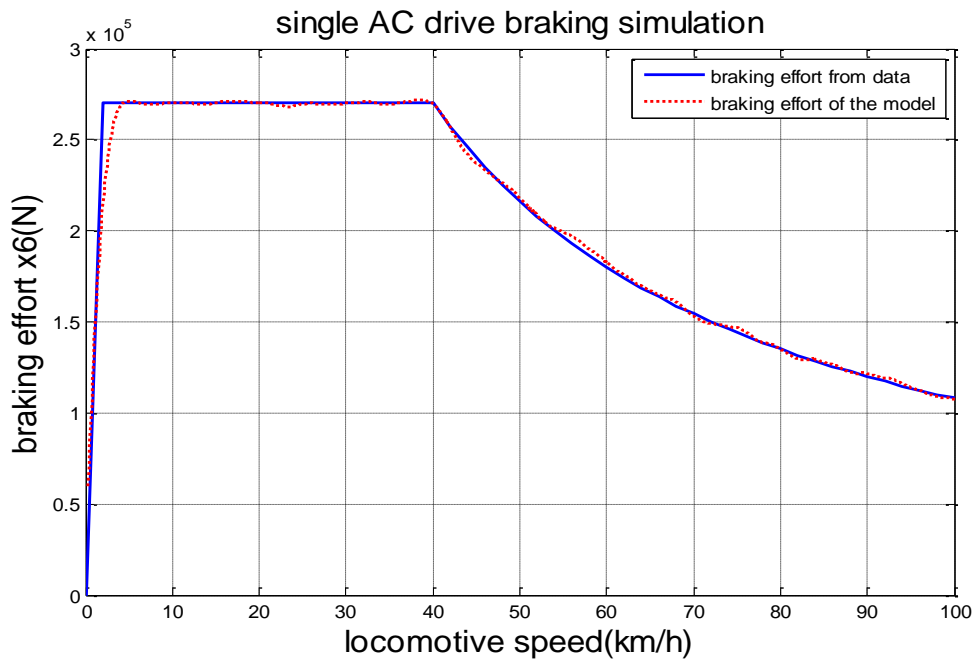


Figure 37: (a) Comparison between traction force curve of AC model full locomotive (= single AC traction effort $\times 6$) and the GT46MAC data [107]; (b) Comparison between traction force curve of DC model full locomotive (= single DC traction effort $\times 6$) and the GT46C data [108]

The solid lines in Figure 37 (a) and (b) are traction curves for all 8 notches from data in [107] and [108] respectively. The dashed lines in Figure 37 (a) and (b) are the mean value of the traction curves of the AC and DC drive model respectively. As seen from Figure 37 the traction efforts of the model for all notches are consistent with the available data. Thus the traction performance of the drive is verified. Note the curves are characterised by two parts,

which is typical of locomotive electric traction drive, providing approximately constant torque for low speeds until the maximum power for each notch is reached after which the curve is power limited ($= \text{torque} \times \text{speed}$). The dynamic braking simulation was performed to verify the braking effort of the model with comparison to the data in [105] and [108]. The simulations begin with a high initial locomotive speed and decelerate to 0.05 km/h.

(a)



(b)

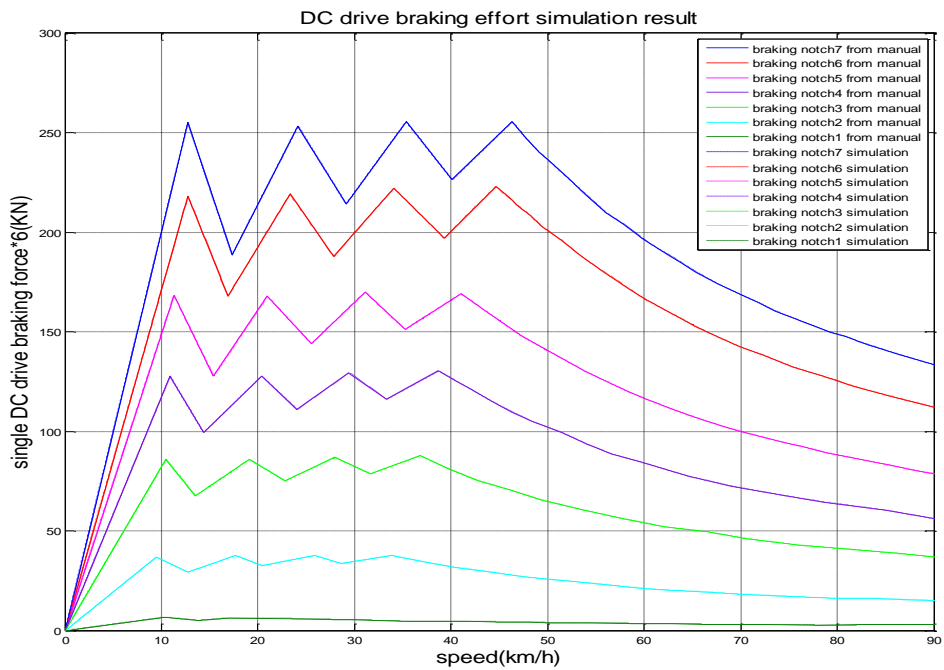


Figure 38: (a) Comparison between braking effort curve of AC model full locomotive (= single AC traction effort $\times 6$) and the GT46MAC data [105]; (b) Comparison between braking effort curve of DC model full locomotive (= single DC traction effort $\times 6$) and the GT46C data [108]

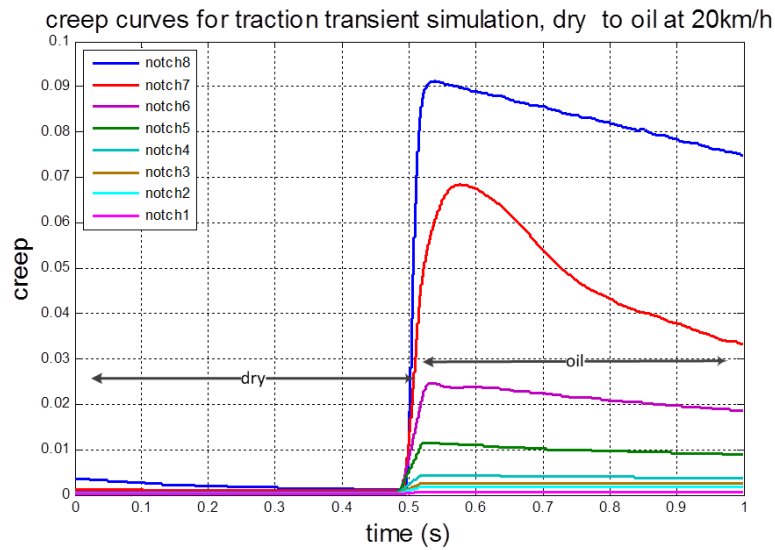
The solid lines in Figure 38 are the braking curve of GT46MAC and GT46C locomotive in [105] and [108] and the dashed lines are the mean values of the braking curves of the AC and

DC drive model. In Figure 38(b) the solid lines and the dashed lines are overlapped. As it can be seen from Figure 38 the braking effort of the model is consistent with the data in [105] and [108]. Thus the braking performance of the drive is verified. Note the AC curve follows a similar behaviour as the tractive force curves, providing constant braking effort at low speeds and an approximate power limited curve at higher speeds. For very low speeds, there is a sharp linear behaviour where the dynamic braking effort is limited to being proportional to speed as opposed to being controlled by the creep.

For the DC drive, the beginning velocity of the locomotive is set to be 90km/h. For each notch a simulation is then carried out for a dry contact condition, making the system run from the initial speed to 0.02 km/h rather than zero to avoid error due to the infinite creep value. The braking force is then calculated as described above and compared with the data for the total braking forces in [108]. The jagged nature of the curve is expected to maximise power dissipation given armature current limitations in the DC drive, i.e. the armature resistance is step changed. Note also that the slope at very low speeds is smaller to the AC case.

Simulations for transient contact condition from dry to oily have been carried out to show the effectiveness of the creep/slip controller for all traction notches. Here it is assumed the transient contact change occurs at 20km/h. The transient contact condition is implemented by the switching of Polach parameters mentioned in Table 2 to the parameters tuned for the oil condition.

(a)



(b)

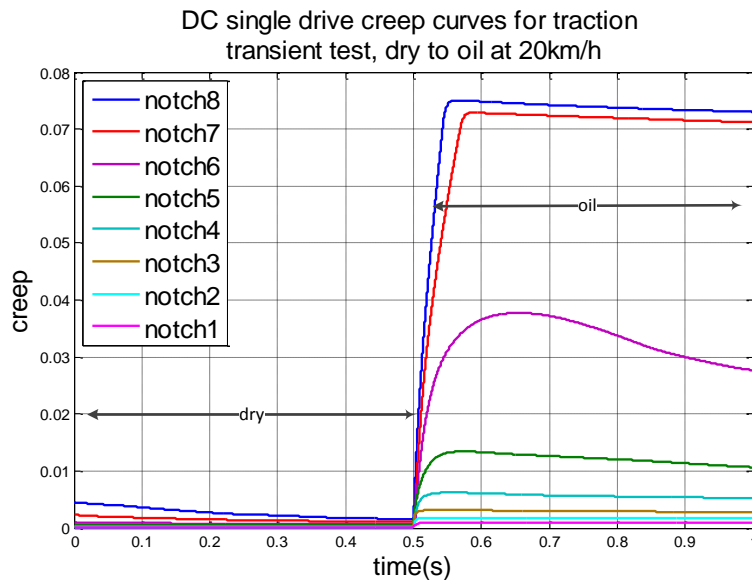


Figure 39: (a) AC creep curves for all traction mode notches under transient state at 20km/h; (b) DC creep curves for all traction mode notches under transient state at 20km/h

Figure 39 shows a part of the simulation when the contact transition happens. From Figure 39 (a), it can be seen that under higher notches, the peak creeps are higher than under lower notches. This is expected due to the high torque/tractive force command under high notches. The proposed creep controller is effective in constraining the creep to be under 10% for all conditions avoiding full sliding. It is noted that the response of notch 8 has a different shape to that of notch 7 because the creep controller has been activated above 7% creep. The shape of the response is dependent upon the vehicle dynamical, motor and controller parameters. The same transient simulation has also been conducted with a single DC drive on a same

simplified locomotive model as shown in Figure 39 (b). The creep curves of the DC drive are not smoothed while those of the AC drive have been smoothed due to the fact that the AC drive has high frequency torque ripples causing creep ripples. It is noted that the response of notches 8 and 7 has a different shape to that of notch 6 because the creep controller has been activated above 7% creep. The shape of the response is dependent upon the vehicle dynamical, motor and controller parameters.

The acceleration simulation was aimed to verify the acceleration capacity by comparing with the data in [106]. The initial locomotive velocity is the same to avoid the numerical error during simulation. The driver notch setting increases from notch 1 to notch 3 sequentially and the speed and tractive effort are plotted in Figure 40. The comparison between the data in [106] and the simulation data is shown in Table 7.

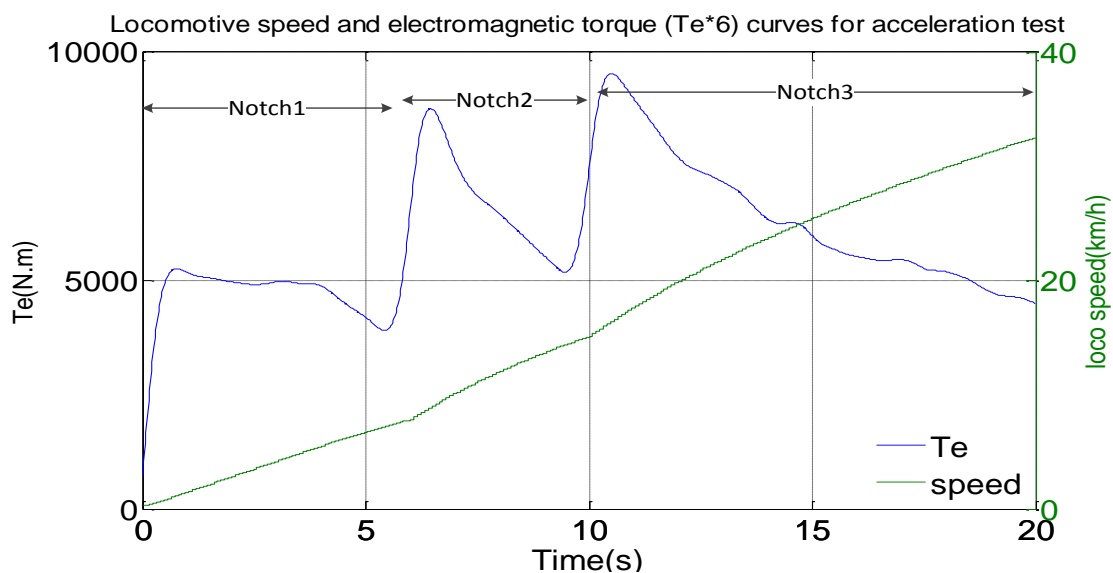


Figure 40: Acceleration Simulation result (speed and $Te \times 6$ with notch)

Table 7: acceleration simulation and comparison with data in [106]

Speed range (km/h)	Acceleration time(s) in [106]	Acceleration time(s) of the model
0→10 km/h	6.52 s	6.96 s
0→20 km/h	11.54 s	12.08 s
0→30 km/h	17.54 s	18 s

The starting procedure of the locomotive starts from notch 1 and then the notch setting increases sequentially to simulate the field testing procedure. It can be seen from Table 7 that the simulation result is consistent with the data in [106]. Also the locomotive speed (the green

solid line) increases almost linearly with time as expected. Each time the notch setting increases, the torque increases subsequently and then decreases gradually due to the increase of locomotive speed, which can be explained with Figure 37. In particular, the maximum tractive force decreases as the locomotive speed increases as the electric drives operate under constant power mode.

In this section, analysis and simulation results are provided for the essential dynamic subsystems of the locomotive. The eigenmode analysis reveals the frequency of vibration of each mode, as well as the modes which are most likely to be excited under external perturbations. The Polach model has been implemented and tuned for various contact conditions. The tuning results are compared with the data from literature, and they are in very good agreement. Additionally, the single drive model provided important validation information for the AC/DC drive module that can be adapted into the full locomotive model. The simulation results of AC and DC drives have confirmed that a creep controller is desired for the locomotives, as demonstrated in the result, that the maximum creep of the AC drive can exceed 9%, which is considerably large and is likely to cause a loss of tractive force.

4.2. Investigations on Creep Controllers (Objective 2)

Based on the full size co-co locomotive dynamics model presented in the previous section, a few different creep controllers are investigated for the purpose of preventing excessive creep from happening and achieving higher tractive force. All the simulations in this section are based on the simplified AC drive model which provides a detailed creep response. The creep controller is investigated under low speed acceleration operation with changes of friction conditions. The simulation is for the case when the locomotive runs into a wet rail section at 11km/h and back out to a dry rail section at 12.5km/h.

4.2.1. Axle Based PI Controller

The simulation is performed for the acceleration process with change of friction conditions using the axle based PI controller. The result is shown in Figure 41 - Figure 43. It is shown in these figures that the axle based PI controller is able to reduce the creep quickly in the acceleration process, as well as after the change of friction conditions.

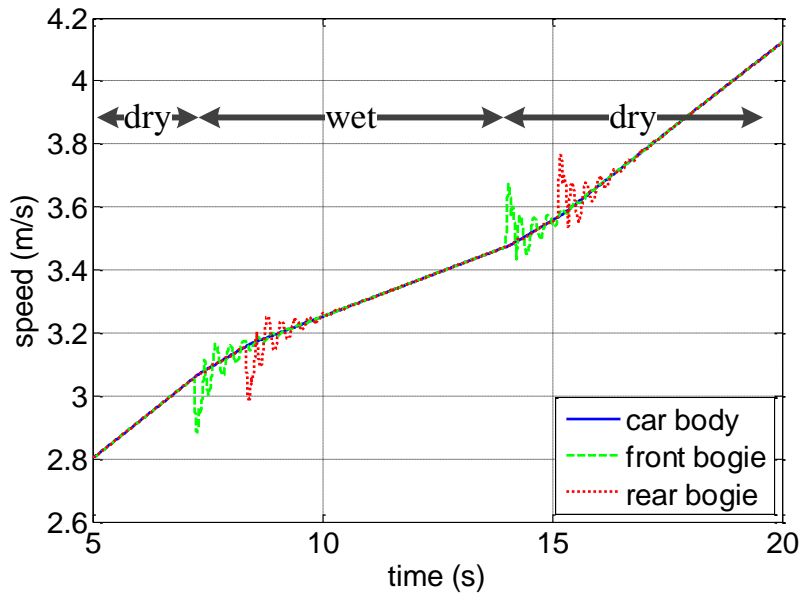


Figure 41: Acceleration test speed curve under a change of friction condition using the axle based controller

As shown in Figure 41, the overall horizontal speeds of the locomotive car body and bogies increase during this simulation. The acceleration under the wet contact condition is lower than that under the dry contact condition due to the change of maximum adhesion coefficient. The speeds of the bogies oscillate when the wheel/rail contact condition changes due to the dynamic coupling between the bogies and the locomotive car body.

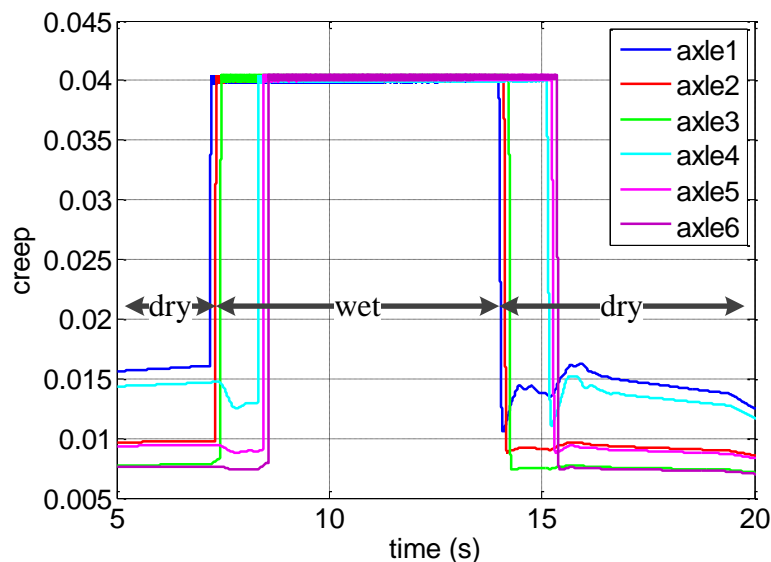


Figure 42: Acceleration test creep curves under a change of friction condition using the axle based controller

Figure 42 shows the creep of individual axles during the change of contact conditions. The creep increases significantly after the locomotive runs into the wet section. However, the axle

based PI creep controller can effectively restrain the creep to be about 4%. The creep drops when the locomotive runs to the dry section again due to the increase of the adhesion coefficient from the wet to the dry contact condition.

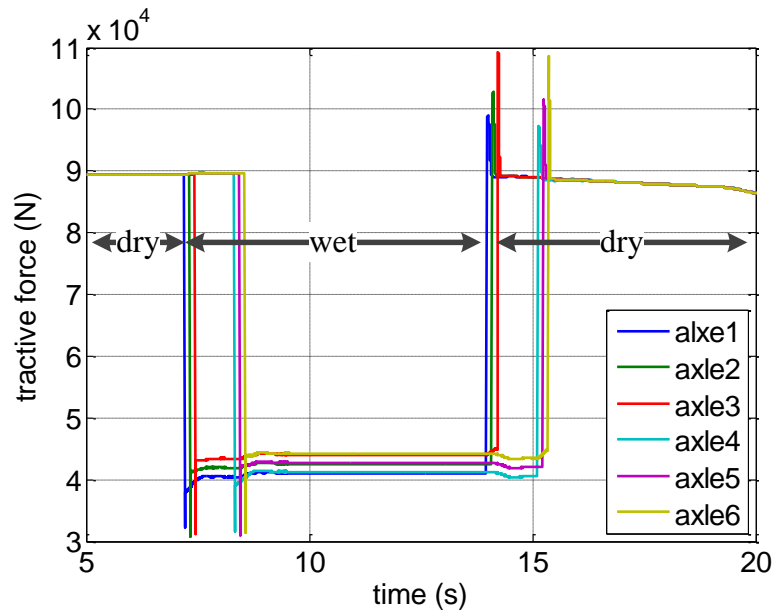


Figure 43: Acceleration test tractive force curves under a change of friction condition using the axle based controller

Figure 43 shows the tractive force of individual axles during the change of wheel/rail contact conditions. The axles provide higher tractive forces under dry wheel/rail contact condition than that under the wet condition. The spikes are caused by the dynamic process when the contact condition changes.

4.2.2. Fuzzy Logic Adhesion Control

Results of transient locomotive response with the proposed fuzzy logic controller are illustrated, including creep and tractive force. Initial operation speed was set at 10 km/h. Transient contact conditions are assumed to happen at 11km/h, from a dry contact condition to a wet condition, and change back from a wet to a dry contact condition at 12.5 km/h. The dynamic response comparison with PI and fuzzy controllers uses speed rather than time as the horizontal axis because the adhesion coefficient, under the same contact condition, is determined by the creep and locomotive speed. As a result the change of contact condition is assumed to happen at a certain speed to ensure the same force condition.

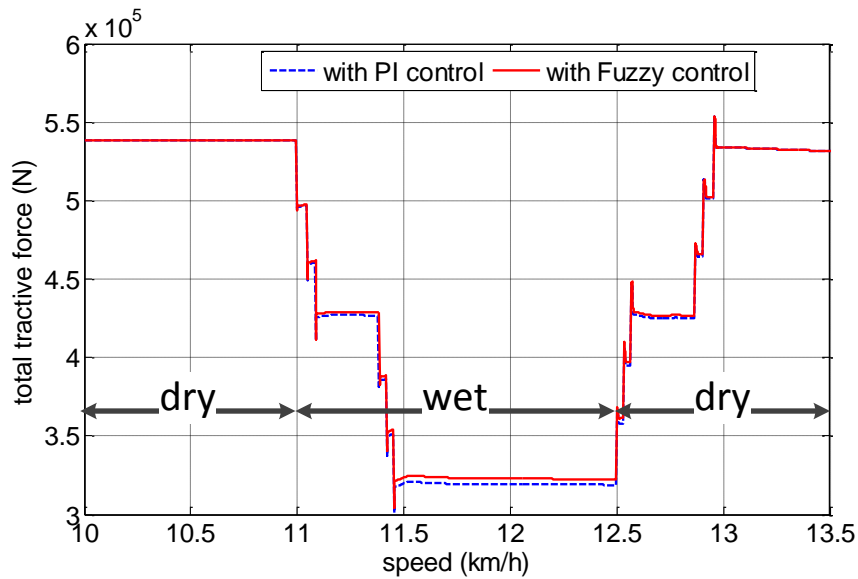
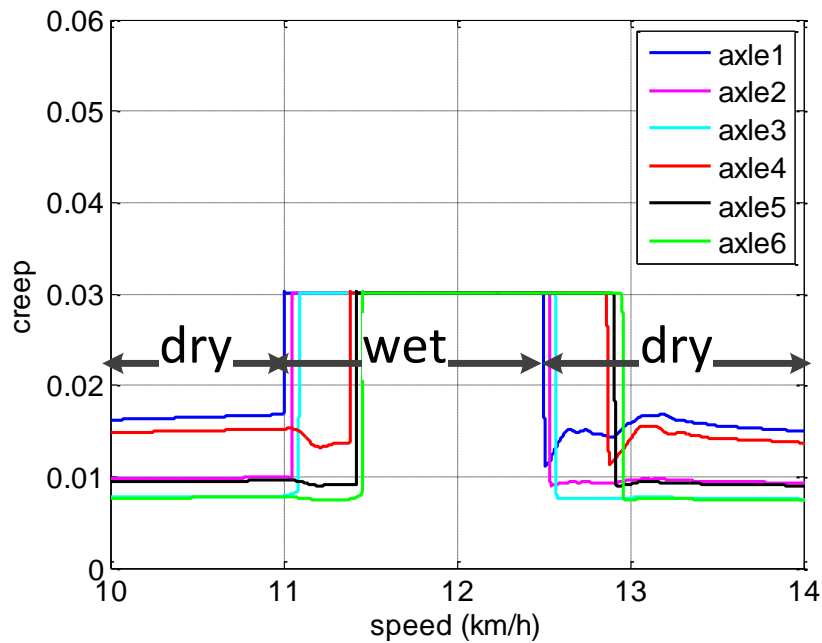


Figure 44: Comparison of total tractive force with PI and fuzzy controllers

It can be seen from Figure 44 that the tractive force with PI and fuzzy controllers under a dry contact condition is similar, while then the fuzzy controller can reach slightly higher tractive force than that with the PI controller under the wet contact condition. This can be explained as follows. As the threshold of the PI controller is chosen such that it can reach the maximum tractive force under the dry contact condition near the simulation speed, the tractive forces with controller are close to each other, both around the maximum tractive force the system can reach at the same speed. However, as the threshold of the PI controller is constant, it will not be able to adjust the control level according to the change of contact conditions and/or operating speed. On the other hand, the fuzzy controller searches for maximum tractive force with information of \dot{s} and $\dot{\mu}$. This causes higher tractive force under the wet contact condition with fuzzy controller than that with the PI controller.

(a)



(b)

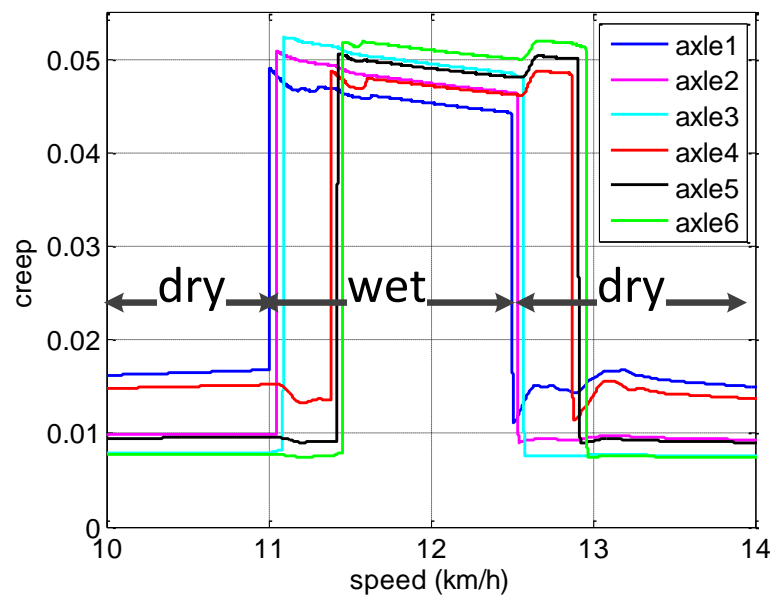


Figure 45: Comparison of creep response with PI control (a) and with fuzzy logic control (b)

In Figure 45(a), after the contact condition changes from the dry condition to the wet condition, the creep values have been limited at 0.03, as the pre-set threshold of the PI controller, whereas the creep values of the system with fuzzy logic are higher as in Figure 45(b), as the fuzzy controller adjusts the control effort according to the operation condition and intends to reach the maximum tractive force available.

The locomotive dynamic responses under transient contact conditions with PI and fuzzy logic creep controllers have been simulated. The comparison of the creep and total tractive force shows the advantage of the proposed fuzzy logic controller over the PI controller in term of realizing slightly higher tractive force under the change of contact conditions. While both controllers can limit the creep under a certain level, simulation results show that the fuzzy controller can reach slightly higher total tractive force than that with a constant threshold PI controller under the wet contact condition due to its ability to search for the maximum achievable force according to different contact conditions.

4.2.3. Modified Fuzzy Logic Controller

This section is also detailed in Appended Paper C. The proposed adhesion control system utilizes the method described in [99] with control torque acting on each axle. The following assumptions are made in the simulations.

1) A single powered locomotive is considered hauling a number of wagons, which are modelled as an equivalent trailing mass. No other resistance such as drag and air resistance is considered in this simulation.

2) A low speed simulation case is chosen to investigate the dynamic behaviour of highest tractive force case, namely the starting process of a locomotive.

3) The high speed simulation case is chosen below the maximum speed of the locomotive (about 128 km/h).

4) The tractive effort is limited by both the contact mechanics and the characteristic traction speed curve of the electric drive.

The results comparing locomotive response obtained with PI and fuzzy logic sliding mode controllers are presented, focussing on tractive force and speed/acceleration, at speeds of 10 km/h and 120km/h. Transient contact conditions are assumed to occur at 11km/h from dry to wet and at 12.5km/h from wet to dry for the low speed simulation. Similarly, for the high speed simulation case, the contact condition changes at 119.5km/h, and back to a dry condition at 120km/h.

In order to compare the tractive performance under the same condition, the change of contact conditions is considered to be triggered by speed, and thus the following figures showing forces and creep employ speed as the horizontal axis. In the first simulation, the contact

condition is assumed to change during a very low speed operation, namely starting from 11km/h. The transient tractive forces with different controllers are plotted in Figure 46.

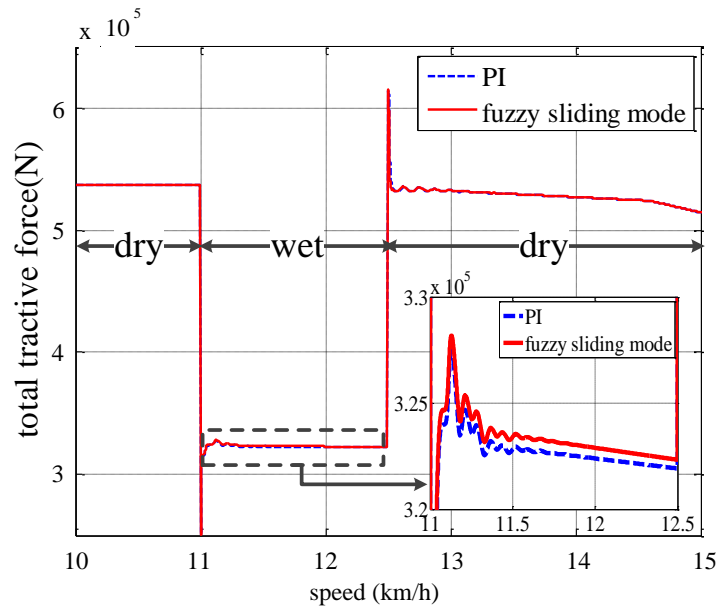


Figure 46: Comparison of total tractive forces with PI and fuzzy sliding mode control at low speed

At low speed, as shown in Figure 46, the tractive force with fuzzy sliding mode control is very similar to that with PI control, except under the wet condition when the fuzzy sliding mode control achieves marginally higher tractive force than PI control.

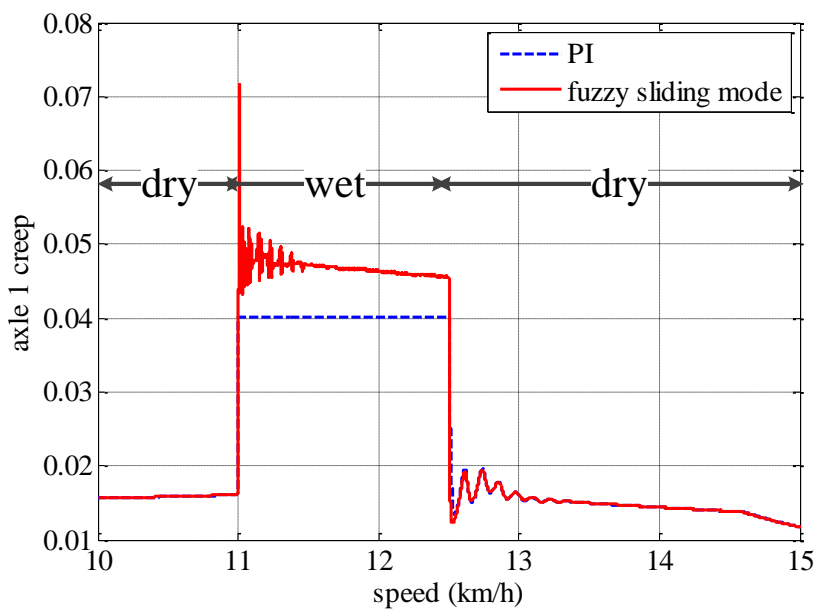


Figure 47: Creep of the front axle under change of contact conditions at low speed

The creep of all axles is similar with the same controller. The creep of the front axle is shown in Figure 47 to compare the creep response with the PI controller and with the fuzzy sliding mode one. It can be seen that at low speeds the creep of each axle with fuzzy sliding mode control is higher than that with PI control, however, the tractive force, as shown in Figure 46, is very similar. The similarity of the tractive force is caused by the relative flat area of the creep-tractive force curve as shown in Figure 36. In particular, the difference of the tractive force between when creep is 4% as with the PI control and about 4.5% with fuzzy logic sliding mode control is about 1%, as shown in Figure 36 (b). At such a low speed, the creep of each axle with fuzzy sliding mode control, however, is much higher than that with PI control, as shown in Figure 47. Therefore, in this case the fuzzy controller does not have an obvious advantage over the PI one in terms of tractive effort and creep control. Figure 48 shows front and rear bogie pitch motion during low speed operation.

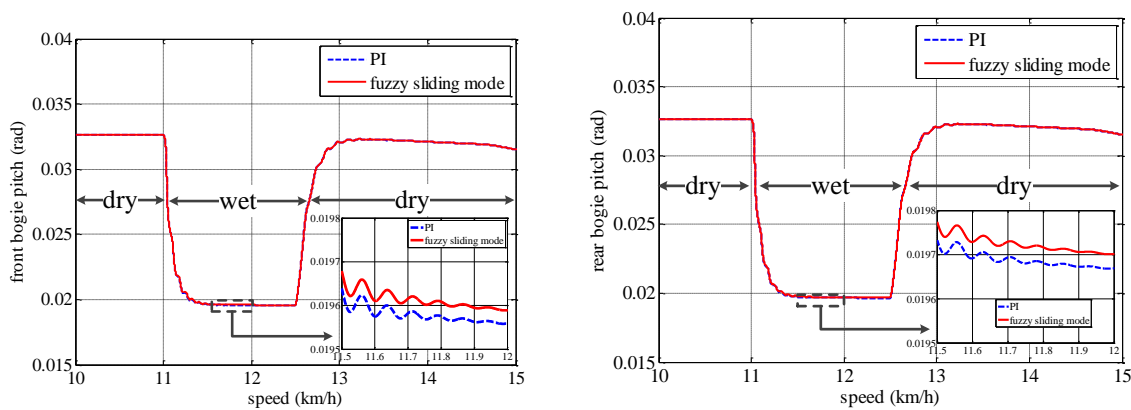


Figure 48: Bogie pitch motion during operation

As the tractive force with PI and fuzzy control is similar as shown in Figure 46, the bogie pitch motion has a similar dynamic response with the PI and the fuzzy controller as shown in Figure 48.

Figure 49 shows weight distribution on each axle during low speed operation.

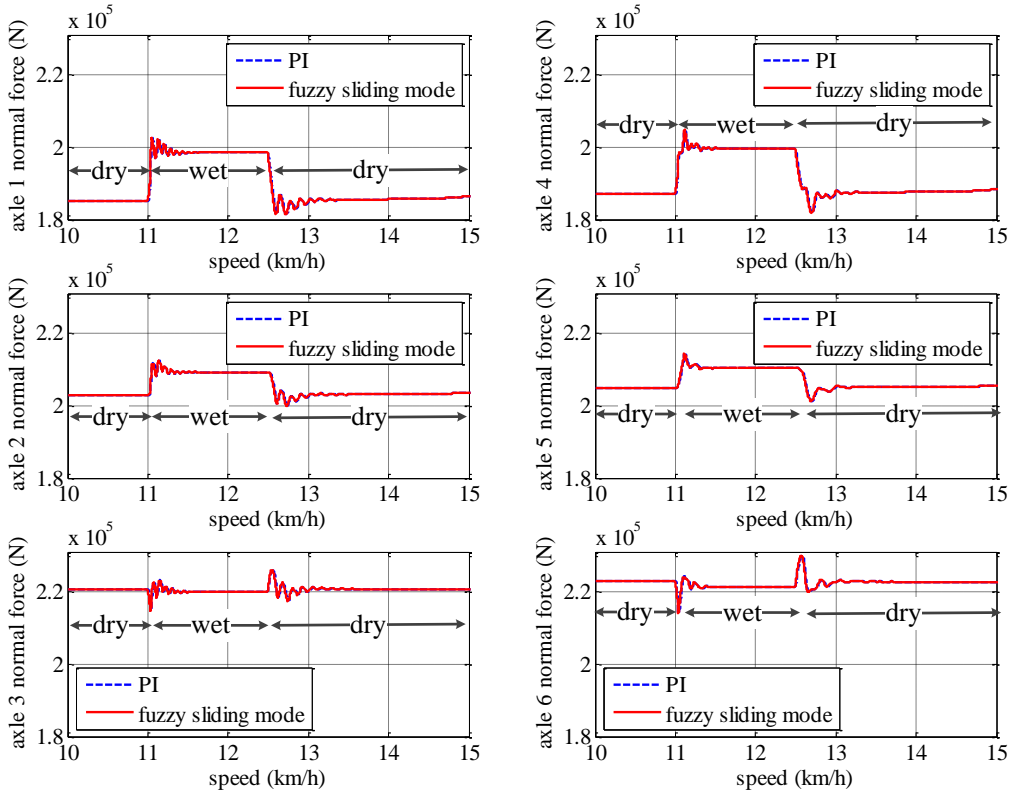


Figure 49: Weight distribution on each axle

Similar weight distribution dynamic responses with the PI and the fuzzy controllers are observed in Figure 49 due to the similar tractive force achieved with different controllers. As a result, the solid lines and the dashed lines mostly overlapped.

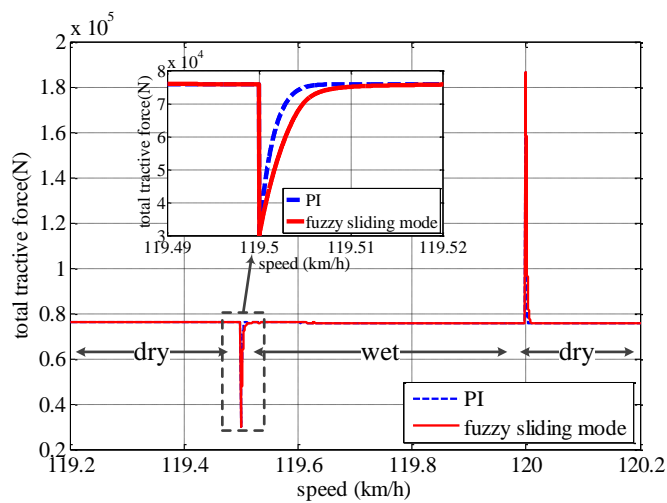


Figure 50: Comparison of total tractive forces with PI and fuzzy sliding mode control at high speed

At high operation speed, as shown in Figure 50, the tractive force with fuzzy sliding mode control is almost the same with that with PI control. This phenomenon is caused by the limit of electric drive tractive effort. As a result, the shift of the peak tractive force due to the change of operation speed will not affect the control effort.

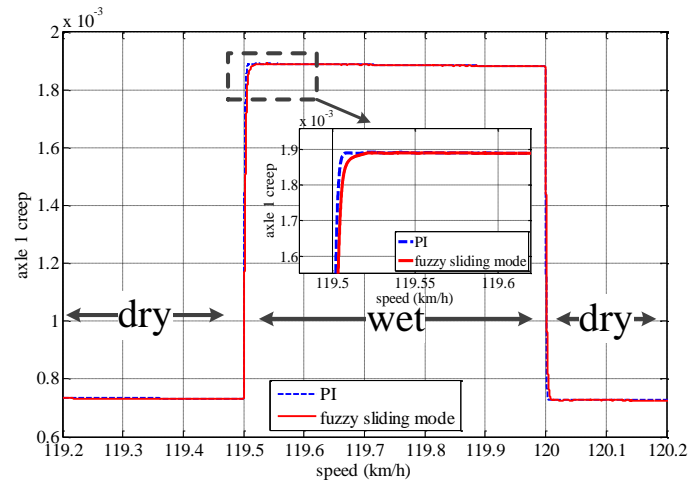


Figure 51: Creep of the front axle under change of contact conditions at high speed

Figure 51 shows the comparison of creep response of the front axle with a PI and a fuzzy sliding mode controller. Due to the constraint of electric drive tractive effort, at high speed, the creep of each axle with fuzzy sliding mode control is similar.

Figure 52 shows front and rear bogie pitch motion during operation.

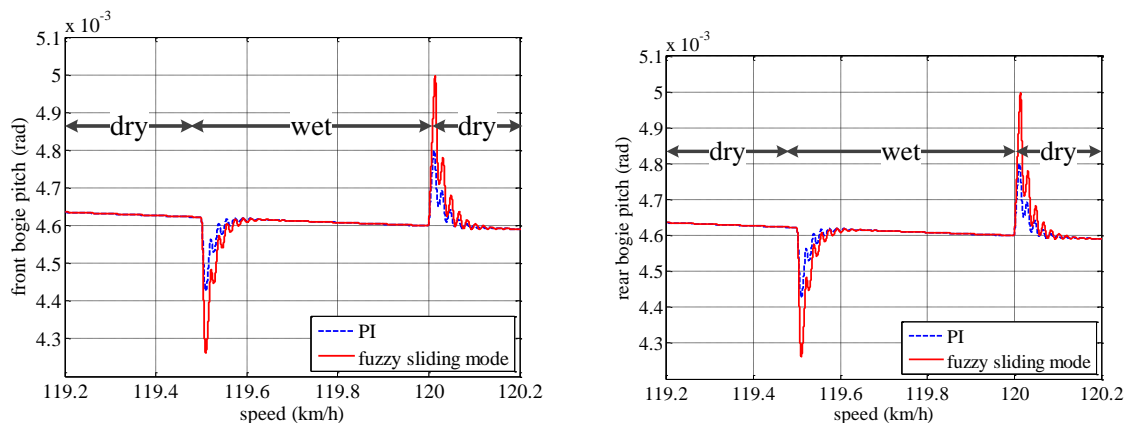


Figure 52: Bogie pitch motion during operation

The fuzzy control achieves higher tractive force spikes as shown in Figure 50, thus there are higher torque spikes that cause the bogie pitch motion. Consequently, the pitch angle spikes

of the fuzzy control are higher than those with the PI control. Figure 53 shows weight distribution on each axle during operation.

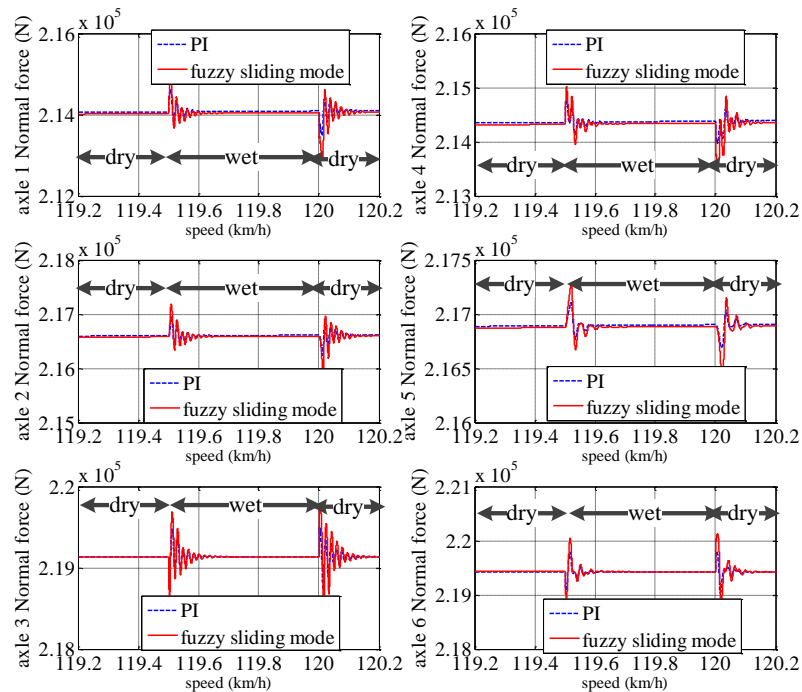


Figure 53: Weight distribution on each axle

As shown in Figure 53, normal force between the rear axle and track is the highest due to the pitch motion of the bogies.

In this section, simulation results of tractive performances and the dynamic responses with PI and fuzzy logic based creep controllers under transient contact conditions are provided. The PI controller was set a constant creep reference while the fuzzy controller searches continuously for a creep value that can achieve the maximum adhesion coefficient under various contact conditions. Results show that a PI controller can effectively limit the creep below a desired threshold. The proposed fuzzy logic based controllers have an advantage in maintaining a higher tractive force than PI controllers at a low operation speed but it is small for the conditions simulated. At high operation speed, the tractive effort is almost identical due to the limitations of the electric drive tractive effort. The simulation results inspire the investigation on the impact of different control settings on the wear damage on the wheel/rail contact patch and a control approach to reduce the wear damage.

4.3. Impact of Locomotive Creep/Adhesion Control on Wear Index and Wear Control (Objective 3)

The adhesion/creep controller has been investigated for decades and a number of different control approaches have been employed to improve the dynamic behaviour of the locomotives in various aspects. This section provides the simulation results to study the impact of different control strategies on wear damage.

4.3.1. Impact of Locomotive Creep/Adhesion Control of Wear Index

The parameter values of the PI controller are tuned to 1.5×10^7 and 2×10^5 , for the proportional (P) and integral (I) constants, respectively. Simulations have been carried out using the creep controller with different creep threshold settings in order to investigate its impact on rail damage due to wear. Detailed simulation cases are listed in Table 8.

Table 8: Simulation cases

Creep Threshold	Speed case (dry-wet-dry)	
	Low (≈ 10 km/h)	Medium (≈ 50 km/h)
0.03	Yes	Yes
0.04	Yes	No
0.06	Yes	No
0.08	Yes	No

A threshold higher than 0.03 is not simulated for the medium speed case since the creep response will not activate the creep controller due to the electric drive constraints. The locomotive acceleration operation is investigated to simulate high tractional conditions that typically occur on straight track. Thus other dynamics such as lateral and rolling dynamics are excluded from this study. The results comparing locomotive response obtained with different creep controller settings are presented, focussing on tractive force and the tractional power parameter $T\gamma/A$, which indicates the power expended through creepage [109], at speeds of about 10 km/h and 50km/h under the highest acceleration conditions. The $T\gamma/A$ value is relevant to wear rate according to the mapping relation [71], as shown in Figure 16 [41].

In order to avoid serious rail damage caused by wear, the $T\gamma/A$ value needs to be constrained below 60 N/mm^2 . Transient contact conditions are assumed to occur at 11km/h from dry to

wet and at 12.5km/h from wet to dry for the low speed simulation. Similarly, for the medium speed simulation case, the contact condition changes at 51km/h, and back to a dry condition at 52.5km/h.

Case 1: low speed simulation

Figure 54 shows the tractive force of the front wheel under a change of contact conditions during low speed conditions.

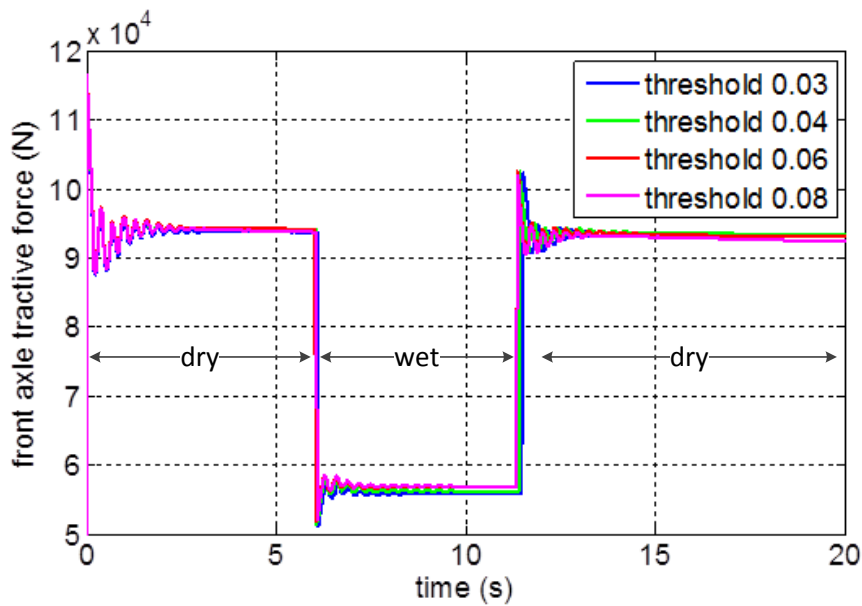


Figure 54: Front wheel tractive force comparison under different controller thresholds at low speed

The difference of tractive force under different creep control threshold settings is very small as shown in Figure 54. The reason is the gradient of the tractive force from creep values 0.03 to 0.08 is small, thus the change of tractive force is not sensitive to the change of creep value.

Figure 55 shows the front wheel $T\gamma/A$ value with different creep threshold settings under a change of contact conditions under low speed.

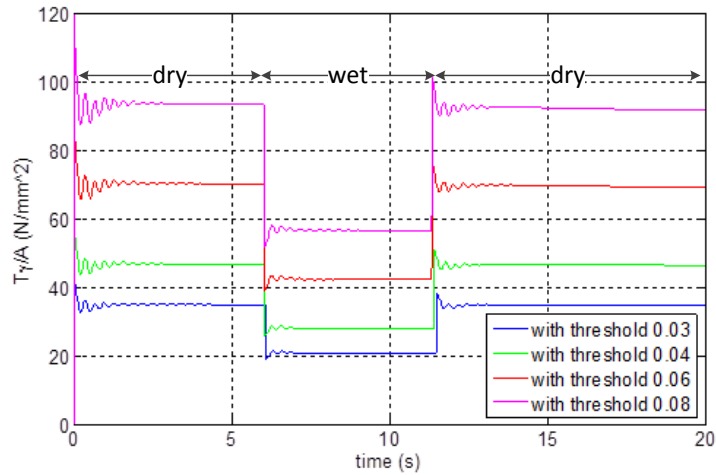


Figure 55: Front wheel $T\gamma/A$ values comparison under different controller thresholds at low speed

As is shown in Figure 55, the $T\gamma/A$ value is mostly proportional to the value of the creep threshold. From the simulation results, it can be seen that with a creep threshold below 0.04, the $T\gamma/A$ value is below 60 N/mm^2 and therefore according to Figure 16 the wear rate is constrained within the Type I and II (“mild” and “severe”) region. Similarly, with a creep threshold between 0.06 and 0.08, the wear rate is within the Type III (“catastrophic”) region, except under wet contact conditions. Therefore a creep controller threshold below 0.04 is desirable under low speed conditions.

Case 2: medium speed simulation

Figure 56 shows the front axle creep response for medium speed simulation under a change of contact conditions.

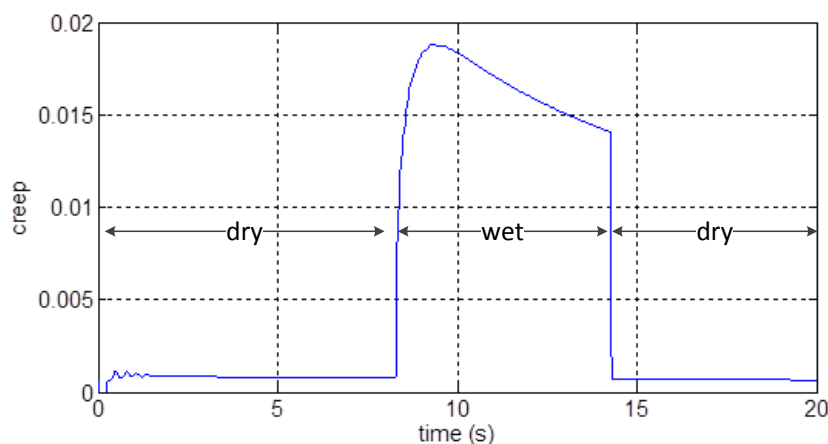


Figure 56: Front axle creep response for medium speed simulation under change of contact conditions

As it is shown in Figure 56, under the change of contact condition from dry to wet and from wet to dry for medium speed operation, the creep is always below 0.02. As a result, the creep controller will not be activated under the creep threshold settings in Table 8. Thus the dynamic response and wear rate with different controller threshold settings should be the same. Figure 57 below shows the corresponding $T\gamma/A$ response for medium speed simulation under the change of contact conditions.

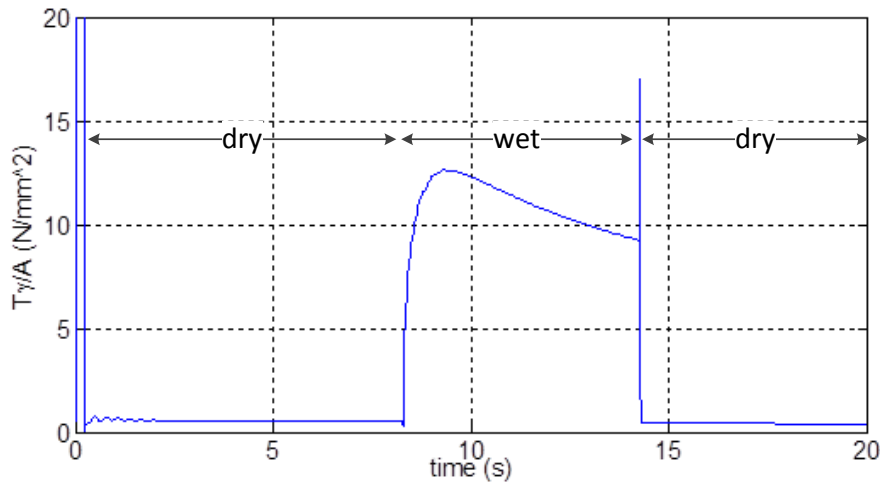


Figure 57: Front wheel $T\gamma/A$ values at medium speed

In Figure 57, the $T\gamma/A$ value at medium speed is always below 20 N/mm² due to the torque-speed characteristics of the electric drives, thus the wear rate is naturally within the Type I and Type II regions (see Figure 16).

In this section, the wear rate with different PI creep control threshold settings under transient contact conditions has been compared by using the locomotive dynamic model under different operation speeds. Simulations have been carried out to compare tractive force and wear rate, focusing on the impact of operation speed and creep controller setting. Results show that by designing the creep controller threshold parameter, the wear rate can be effectively constrained within Type I and Type II regions, avoiding Type III ‘Catastrophic’ wear. Under higher speed operation, such as Case 2 in this section, the wear rate is naturally constrained within region I and II due to the impact of the torque-speed characteristics of the electric drives, irrespective of the creep controller.

4.3.2. Wear Growth Rate Control

The dynamic response comparison with creep and wear controllers employs speed rather than time as the horizontal axis because the adhesion coefficient, under the same contact condition, is determined by the creep and locomotive speed. As a result the change of contact condition of the first axle is assumed to happen at a certain speed and sequentially the rest of axles change their contact condition to ensure the same force condition.

Case I: Low speed operation simulation:

The comparison of total tractive force with creep and wear controllers under a change of wheel/rail contact conditions between dry and friction modifier condition (FM) as listed in Table 2 under low speed operation is shown in Figure 58 below. Within the creep range between 0 and 0.04 in this study, the frictional modifier curve has a maximum adhesion coefficient of about 0.17. This is similar to the greasy condition in [102].

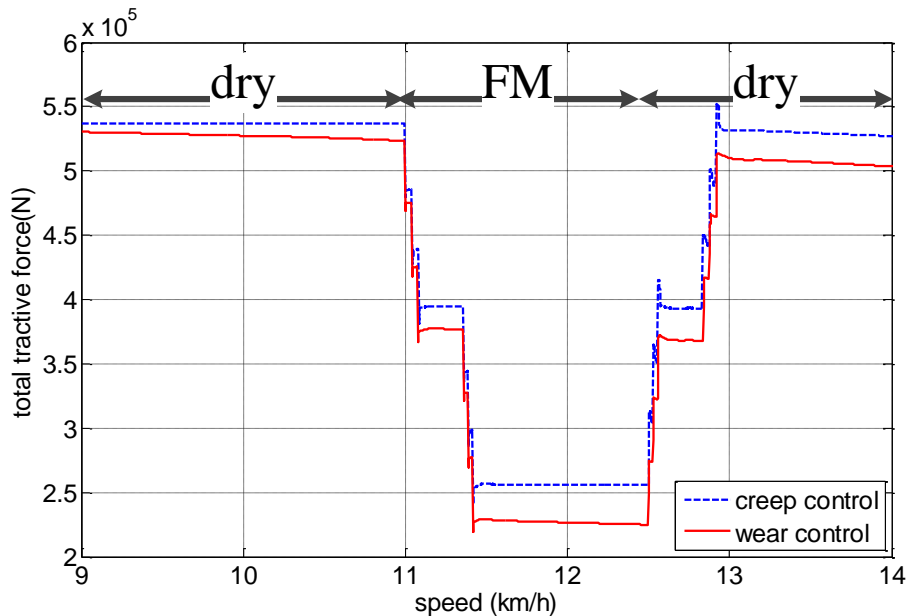


Figure 58: Comparison of total tractive forces with creep and wear controllers

It can be seen that under low speed operation, the total tractive force is about 4% lower with wear control than that with creep control under dry wheel/rail contact condition, and about 11% under the FM wheel/rail contact condition. Also, when the wheel/rail contact condition changes from FM back to dry, the total tractive force with the wear controller has less overshoot than that with the creep controller. It can be noticed with the increase of locomotive speed, the total tractive force difference increases between the case with creep control and that with wear control. The reason of this is that the creep control takes slip

velocity normalized by the speed of the locomotive as the control index; on the other hand, the wear control takes the frictional power density as the control index, which is directly affected by the slip velocity. As a result with the increase of the locomotive speed, the constant creep value means a larger slip velocity, which will result in a higher frictional power density ignoring the change of tractive force on the axle.

The comparison of front and rear bogie pitch with creep and wear controllers under the change of wheel/rail contact conditions under low speed operation is shown in Figure 59 below.

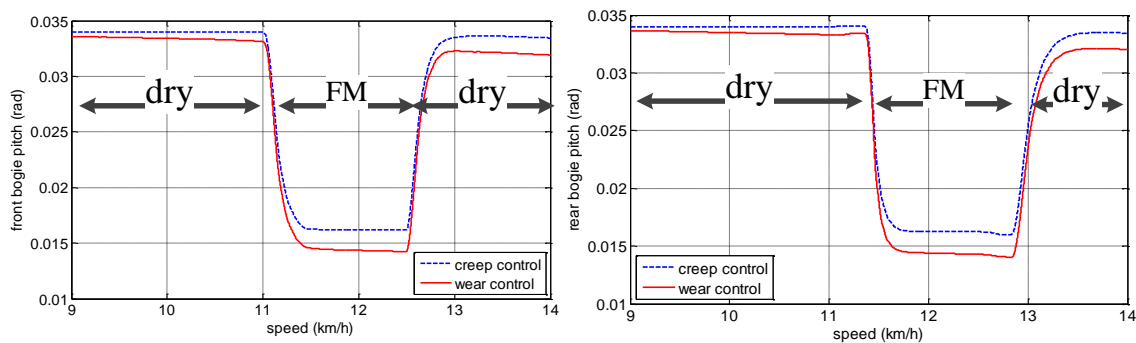


Figure 59: Comparison of front and rear bogie pitch with creep and wear controllers

The front and rear bogie pitch motions show similar dynamic responses to that of the total tractive force. The difference of pitch angles increases with the increase of locomotive speed at low speed operation.

The comparison of car body pitch with creep and wear controllers under a change of wheel/rail contact conditions under low speed operation is shown in Figure 60 below.

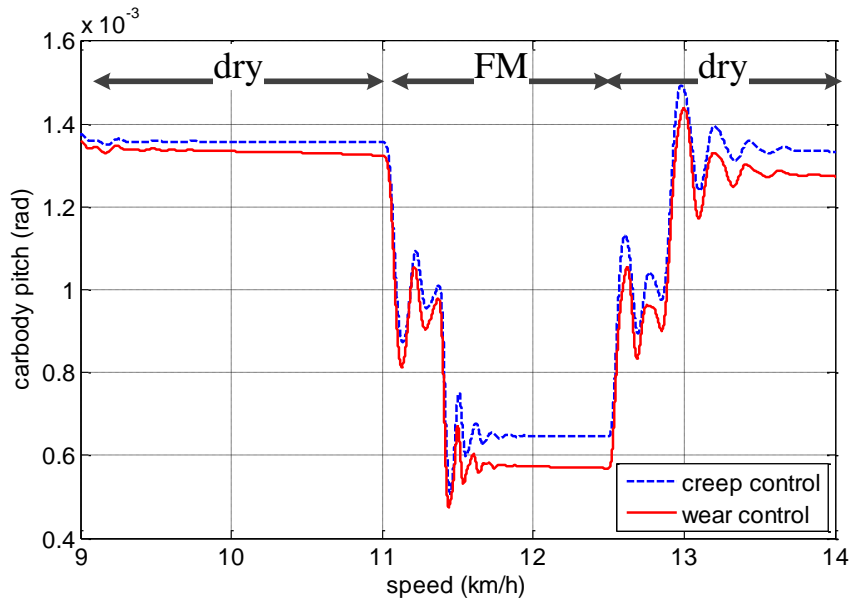


Figure 60: Comparison of car body pitch with creep and wear controllers

The response of the car body pitch angle is closely correlated with that of the total tractive force. The change in car body pitch angles increases with locomotive operating speed. In addition, there are noticeable oscillations during the change of the wheel/rail contact condition, particularly when all axles on the front/rear bogie finish their contact condition transition. The reason for this is that after the last axle of the front bogie has run into the FM rail and before the first axle of the rear bogie runs into the FM area the tractive force is relatively steady after a steep change, forming a step-like tractive force variation as shown in Figure 58. This step-like tractive force change excites the mode of vibration of the car body pitch motion.

The comparison of axle 1 creep response with creep and wear controllers under a change of wheel/rail contact conditions under low speed operation is shown in Figure 61 below.

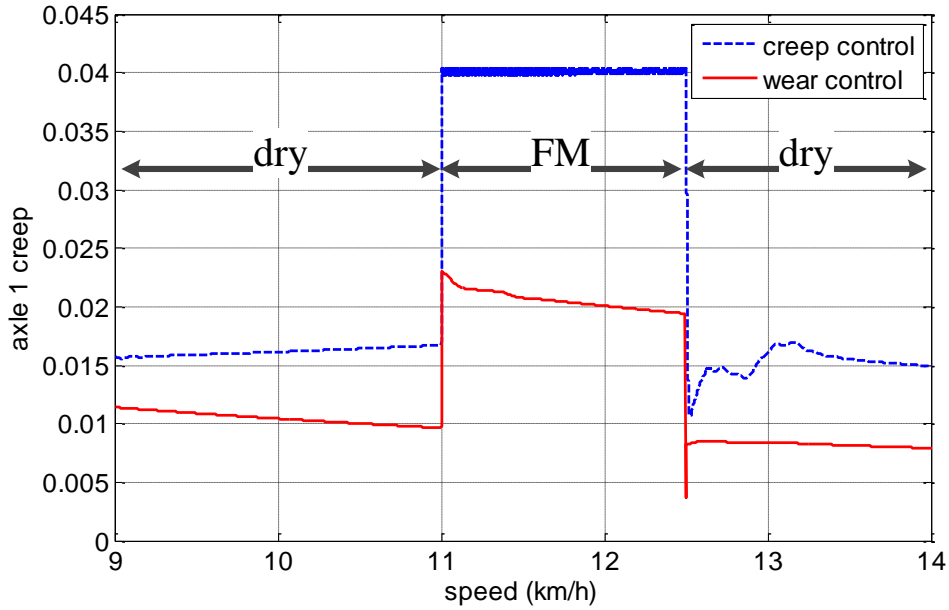


Figure 61: Comparison of axle 1 creep with creep and wear controllers

The creep of axle 1 with the wear controller is about 45.6% and 50% lower than that with the creep controller under dry and FM wheel/rail contact conditions respectively.

The comparison of axle 1 frictional power density with creep and wear controllers under a change of wheel/rail contact conditions under low speed operation is shown in Figure 62 below.

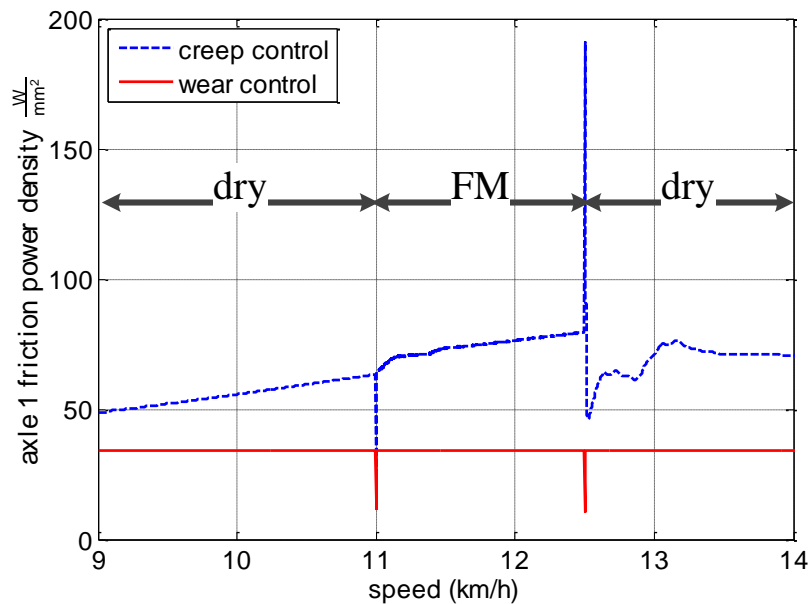


Figure 62: Comparison of axle 1 friction power density with creep and wear controllers

As the wear controller employs a constant frictional power density as the control threshold, the value of the frictional power density is effectively constrained despite of the change of wheel/rail contact conditions. The frictional power density of axle 1 with creep controller, on the other hand, is about 1.94 and 2.2 times that with wear controller under dry and FM contact conditions respectively.

The comparison of axle 1 mass loss rate with creep and wear controllers under a change of wheel/rail contact conditions under low speed operation is shown in Figure 63 below.

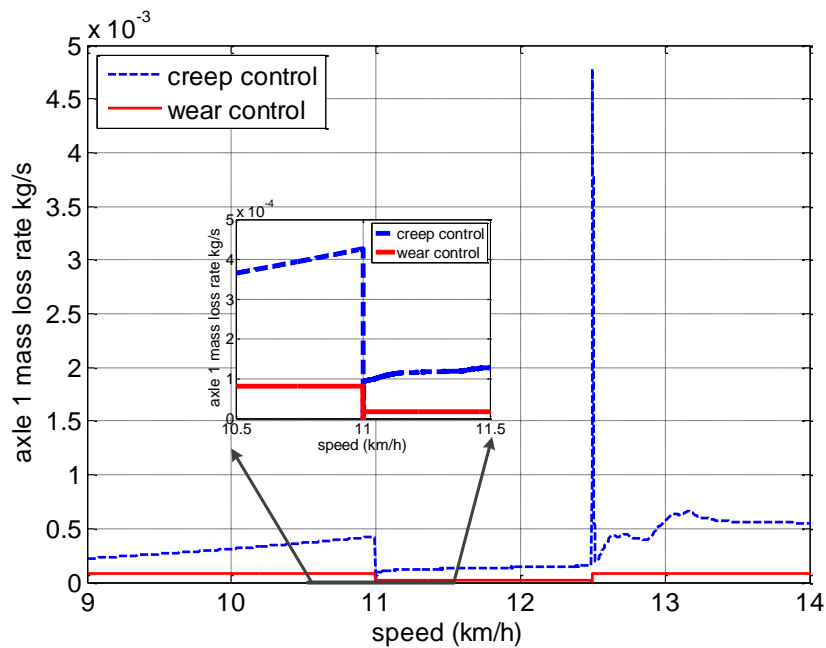


Figure 63: Comparison of axle 1 mass loss rate with creep and wear controllers

As it is shown in Figure 63, the mass loss rate with the wear controller has been reduced to about 18% and 13% that of the creep controller, under the dry and FM conditions respectively.

Case II: High speed operation simulation:

The comparison of total tractive force with creep and wear controllers under a change of wheel/rail contact conditions under high speed operation is shown in Figure 64 below.

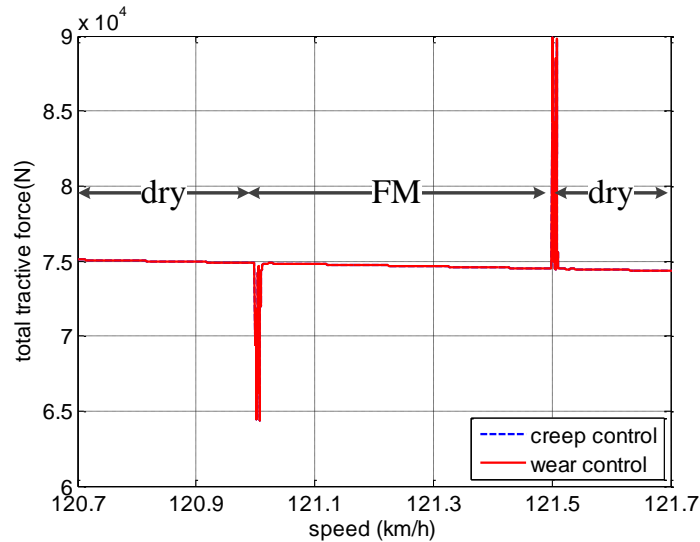


Figure 64: Comparison of total tractive forces with creep and wear controllers

Due to the impact of the electric drive tractive effort characteristic, the total tractive force is much lower at high speed than that at low speed. Consequently under high speed operation the controllers do not take effect and there is no difference between the total tractive force with the creep controller and that with the wear controller under both dry and FM wheel/rail contact conditions. Thus the curves with the creep controller and those with the wear controllers overlapped from Figure 64 to Figure 69.

The comparison of front and rear bogie pitch angles with creep and wear controllers under a change of wheel/rail contact conditions under high speed operation is shown in Figure 65 below.

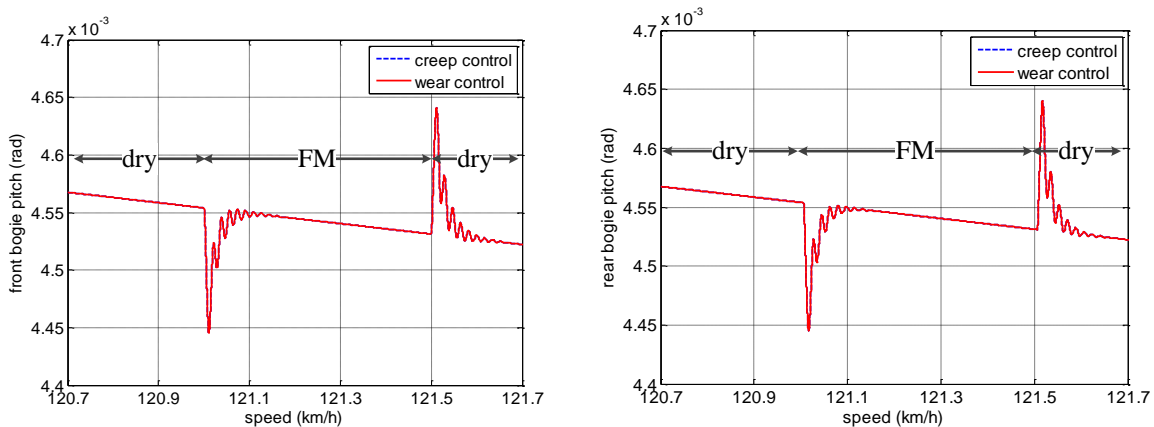


Figure 65: Comparison of front and rear bogie pitch with creep and wear controllers

Since the same amount of low tractive force is achieved under high speed operation, the actual creep and the frictional power density are below their control thresholds, as shown in

Figure 67 and Figure 68. As a result of neither controller being activated, the pitch motions of the front and rear bogies show the same dynamics with the creep and wear controllers.

The comparison of front and rear bogie pitch angles with creep and wear controllers under a change of wheel/rail contact conditions under high speed operation is shown in Figure 66 below.

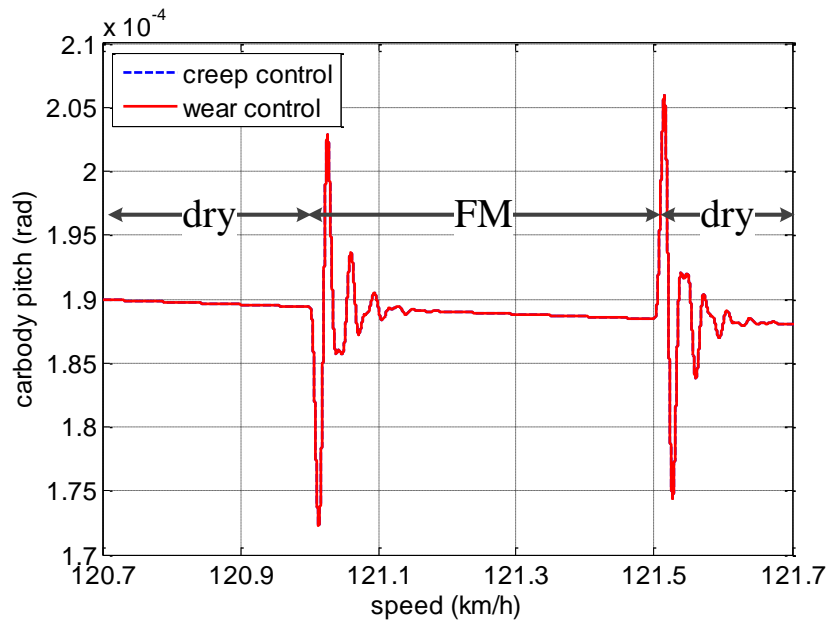


Figure 66: Comparison of car body pitch with creep and wear controllers

The dynamic response of the car body pitch motion with the creep controller shows the same behaviour with that with the wear controller due to the same amount of tractive force.

The comparison of axle 1 creep response with creep and wear controllers under a change of wheel/rail contact conditions under high speed operation is shown in Figure 67 below.

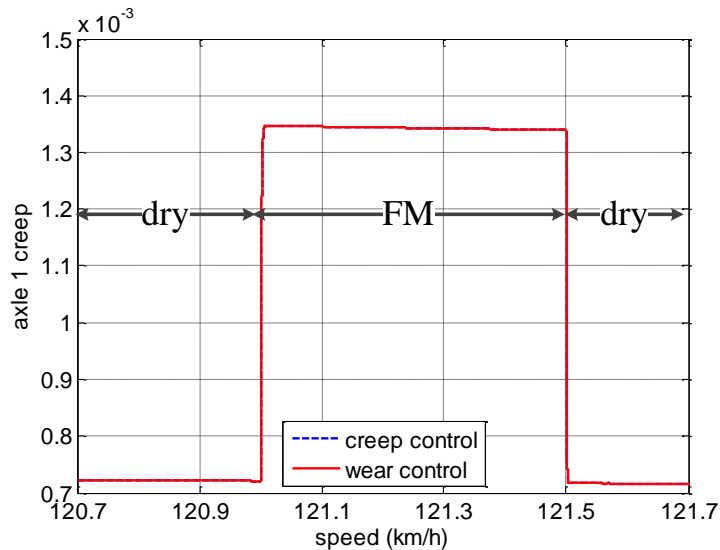


Figure 67: Comparison of axle 1 creep with creep and wear controllers

The dynamic response of the axle 1 creep with the creep controller shows the same behaviour as that with the wear controller due to the same amount of tractive force.

The comparison of axle 1 frictional power density with creep and wear controllers under a change of wheel/rail contact conditions under high speed operation is shown in Figure 68 below.

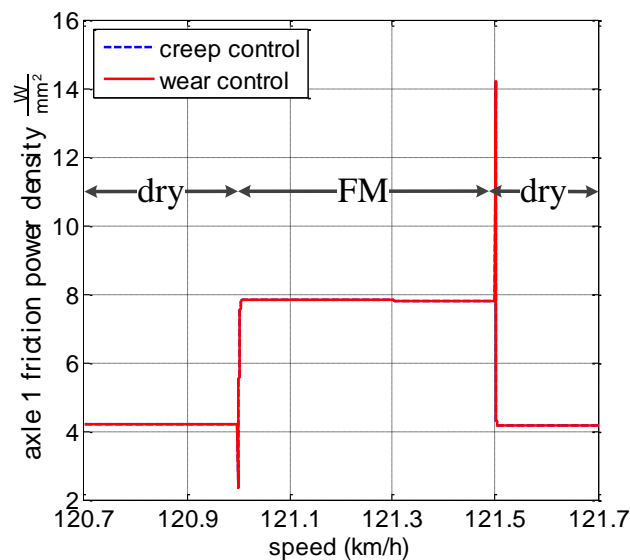


Figure 68: Comparison of axle 1 friction power density with creep and wear controllers

Again, the dynamic response of the axle 1 creep with the creep controller shows the same behaviour with that with the wear controller due to the same amount of tractive force.

The comparison of axle 1 mass loss rate with creep and wear controllers under change of wheel/rail contact conditions under high speed operation is shown in Figure 69 below.

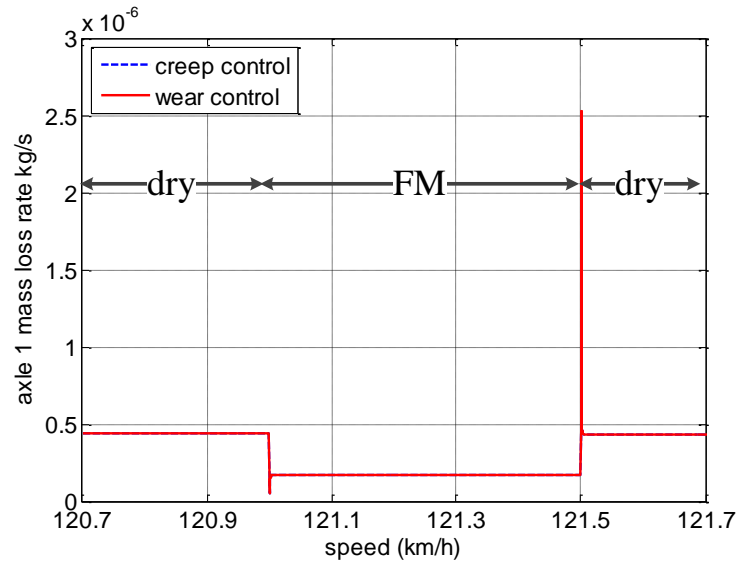


Figure 69: Comparison of axle 1 mass loss rate with creep and wear controllers

The response of mass loss rate has similar behaviour with both controllers. Comparing Figure 63 and 67, it can be seen that the mass loss rate at high speed operation is much lower than that at low speed operation.

4.4. Conclusion

The dynamic modelling has been validated by comparing the acceleration simulation results with data from available literature. The modes of locomotive vibration are identified, highlighting the modes that are more likely to be excited under external perturbations (Objective 1). Although a traditional control method is able to limit the creep under the scenarios investigated in this thesis, advanced adhesion/creep strategies such as the fuzzy logic based ones have the advantage of achieving marginally higher tractive effort under low speeds (Objective 2). Simulation results reveal the impact of different creep control settings on the wear rate under various wheel/rail contact conditions. Simulation results comparing the locomotive dynamic response with a creep controller and the newly developed specialized real-time traction controller show that the proposed specialized traction controller can reduce wear damage significantly, particularly under low speed operation. The corresponding tractive force reduction is reasonably small (Objective 3).

Chapter V: Summary of Appended Papers

In Paper A, (Y. Tian, W.J.T. (Bill) Daniel, S. Liu and P.A. Meehan, 2013, “Dynamic Tractional Behaviour Analysis and Control for a DC Locomotive”, World Congress of Rail Research 2013), the development of the mathematical model of a co-co locomotive including locomotive longitudinal, vertical and pitch dynamics, wheel/rail contact dynamics and simplified electric drive dynamics in Matlab as part of RailCRC Project No.R3.119 Locomotive Adhesion is detailed. Details of the sub-modules are provided. Modes of vibration of the locomotive are identified. Dynamic responses have been simulated under change of wheel/rail contact conditions.

In Paper B, (Y. Tian, W.J.T. (Bill) Daniel, S. Liu and P.A. Meehan, 2014, “Fuzzy Logic Creep Control for a 2D Locomotive Dynamic Model under Transient Wheel-rail Contact Condition”, 14th International Conference on Railway Engineering Design and Optimization, COMPRAIL 2014), a fuzzy logic creep/adhesion controller is developed and simulated with the locomotive mathematical model that has been developed previously. Dynamic responses have been compared with that with a traditional fixed creep threshold controller, highlighting the advantage of the fuzzy logic controller over the traditional one in terms of maintaining higher tractive force, particularly under wet wheel/rail contact condition.

In Paper C, (Y. Tian, W.J.T. (Bill) Daniel, S. Liu and P.A. Meehan, 2014, “Fuzzy Logic based Sliding Mode Creep Controller under Varying Wheel-Rail Contact Conditions”, International Journal of Rail Transportation, 3(1), 40-59), a creep controller based on the work of Park et al. [99] has been employed and modified to cope with the change of wheel/rail contact conditions. Dynamic responses have been compared with that with a traditional fixed threshold creep controller. Results show that the new controller has marginal advantage keeping higher tractive force over the traditional one under low speed operation. The responses are mostly identical under high speed operation. Simulation results also show that the control strategy intending to maximize tractive force will cause much higher creep under low speed operation, which is likely to cause more rail damage.

In Paper D, (Y. Tian, W.J.T. (Bill) Daniel, S. Liu and P.A. Meehan, “Investigation of the impact of full scale locomotive adhesion control on wear under changing contact conditions”, accepted by Vehicle System Dynamics special issue, DOI: 10.1080/00423114.2015.1020815), the impact of creep/adhesion controller on locomotive dynamic responses have been simulated and analysed. Dynamic responses with several creep threshold settings have been compared. Simulation results show that by properly choosing creep control threshold it is likely to avoid the locomotive operating in a Type III “Catastrophic” wear region under low speed operation, particularly under wet wheel/rail contact condition. The impact of the creep controller setting is minimized from medium speed operation due to the tractive effort characteristics of electric drives.

In Paper E, (Y. Tian, W.J.T. (Bill) Daniel, and P.A. Meehan, “Real-time rail/wheel wear damage control”, submitted to International Journal of Rail Transportation), a new real-time control strategy has been proposed to reduce wear damage. Simulation results show that the proposed control strategy can effectively reduce mass loss rate caused by wear, particularly under low speed operation. The consequent tractive force reduction is relatively small.

In Paper F (co-authored), (Sheng Liu, Ye Tian, W.J.T. (Bill) Daniel and Paul A. Meehan, Dynamic response of a locomotive with AC electric drives due to changes in friction conditions, submitted to Journal of Rail and Rapid Transit), locomotive dynamic response with detailed electric drive dynamics under change of contact conditions is simulated and analysed. Result shows that the detailed model is capable of simulating the dynamic fluctuations of creep and traction forces that is not presented in the simpler model. Such transient response may cause damage to the track and vehicle components.

Chapter VI: Conclusions and Future work

This thesis contains a new predictive integrated dynamic model containing 2D locomotive dynamics, wheel/rail contact dynamics and electric drive and control dynamics to investigate the dynamic response of a locomotive under a change of operation conditions. Moreover, eigenmode analysis has been performed to determine model stability and identify the modes of locomotive vibration and those that are most likely to be excited under external perturbations (Objective 1). Creep/adhesion controllers were developed to achieve the highest tractive force available in order to cope with the trend of maximizing locomotive operation efficiency, particularly in the heavy haul sector. Their influence on locomotive dynamic response has also been investigated and compared with that of a fixed creep threshold creep control strategy (Objective 2). Based on the results, a real-time strategy, aiming to reduce wear damage on the tracks is developed based on a recent wear growth model (Objective 3). Details of this work are summarised in the following.

In this thesis, an integrated mathematical model of the dynamics of a locomotive has been developed. The model includes the longitudinal, vertical and pitch motions of the locomotive body, front and rear bogies and six axles, as well as wheel/rail contact dynamics described by the Polach model and electric drive dynamics. Modes of vibrations of the locomotive have been identified with eigenmode analysis. The family of wheel vertical modes of vibration have the least damping and thus are the easiest to be excited under external perturbation, followed by the out of phase bogie longitudinal motion, the locomotive body pitch coupled with in phase bogie longitudinal motions and the out of phase bogie vertical motions. Research on a creep/adhesion controller has been carried out to investigate maximizing locomotive tractive force under various operation conditions including operating speeds and changes of wheel/rail contact conditions. Comparisons have been performed between the controller that achieves higher tractive force and a traditional one with a constant creep threshold. Simulation results show that under low speed operation the tractive forces with the traditional and the new control strategy under the dry contact condition are similar, while the new control strategy can reach higher tractive force than that with the traditional controller under wet contact conditions. Under high speed operation, the tractive force with the traditional controller and the new controller is similar under both dry and wet contact conditions. However, the simulation results also show that, by achieving marginally higher tractive force, the new control strategy causes higher creep under low speed operation. This

leads to the investigation as to how much more wear damage this new control strategy causes compared to the traditional creep control strategy.

Simulations have been carried out to compare the impact of creep controller threshold settings on tractive force and the amount of wear damage caused on rail tracks. Results show that the intention of maximizing tractive force can lead to excessive wear damage on rail tracks, providing only marginal tractive increase under low speed operation. Among the creep thresholds (3%, 4%, 6% and 8%) that have been tested under low speed locomotive operation, with the contact condition changing between dry and wet, only thresholds lower than 4% can avoid the wear damage entering the type III “Catastrophic” region. Compared to creep threshold settings 3% and 4%, the higher creep threshold setting does not have significant advantage in achieving higher tractive force (about 3%), while is likely to cause more wear damage (about 36%) on the rail tracks.

A new control strategy, aiming to reduce wear damage has been proposed based on a recent wear growth model. Simulation results show that, by controlling the wheel speed, the mass loss rate with the wear controller has been reduced to about 18% and 13% of the creep controller performance, at the cost of about 4% and 11% total tractive force decrease under the dry and FM conditions respectively. Under high speed operation, due to the constraint of the electric drive characteristic, the highest tractive force is significantly lower than that of low speed operation. The creep and friction power density are consequently lower so that neither controller will be triggered. Thus the dynamic responses are very similar. From the cost benefit point of view, the significant wear damage reduction is achieved by the proposed specialized real-time wear regulating traction controller under the low speed operation. The specialized traction controller is expected to reduce the wear damage on the rail tracks to about 20% of that with a creep controller. A simple regrinding model suggests that the optimum grind interval is inversely proportional to the wear/corrugation growth rate, which is approximately proportional to the steady wear coefficient [66]. Thus the grinding intervals with the wear controller under the dry and the FM conditions have been extended to 2.36 and 2.77 times of that with the creep controller. Consequently, the re-grinding cost is expected to be reduced to 42.4% and 36% of that with the creep control under the dry and the FM conditions respectively.

6.1. Thesis Contributions

The following are believed to be the novel contributions of this thesis to existing literature.

- An integrated locomotive dynamic model including locomotive longitudinal-vertical-pitch dynamics, wheel/rail contact dynamics and electric drive dynamics in Matlab has been developed for locomotive dynamic response and wear damage prediction under various operation conditions and control design.
- Locomotive modes of vibration have been investigated by eigenmode analysis and those most likely to be excited are identified. This provided insights into locomotive dynamic behaviour under external perturbations as well as validation of the stability of the system.
- Creep/adhesion controllers have been developed to achieve higher tractive force under change of operation conditions. The effectiveness has been compared with a traditional fixed threshold creep controller.
- Locomotive dynamic responses of the controllers achieving higher tractive forces and of the traditional controller are compared, highlighting the amount of tractive force benefit that can be achieved under various operating conditions.
- The impact of creep control setting on the tractive force and wear index $T\gamma/A$ has been quantified.
- The impact of operating condition such as operation velocity and change of contact conditions on creep, tractive force and wear on rail tracks has been quantified.
- A novel control strategy aiming to limit the wear damage on the rail tracks, based on a recent wear growth model has been developed. Simulation comparison has been carried out to validate its effectiveness in reducing wear damage, and to quantify the amount of trade off in terms of tractive forces under various operating conditions.

6.2. Suggestions for Future Work

The work presented in this thesis shows possible avenues of further study, some of which have already commenced. These are listed in the following.

- Modelling:
This research reveals the dynamic impact of different control strategies based on a simplified dynamic model. A more sophisticated model is preferable to

show more accurate dynamic responses with different control strategies under curving behaviour and under the influence of vertical/lateral track irregularities. This requires a 3D dynamic model which is beyond the scope of this research. Moreover, a better wear model is valuable to be included to provide more accurate wear damage quantification under different contact conditions and operation speeds.

- Experimental Validation:

- The experimental validation with a full scale locomotive experimental platform is necessary to verify the creep controller's performance. Under the acceleration operation on relatively straight tracks, the speeds of the locomotive and the axles need to be measured to calculate the creepage. Accelerations of the axles and the torque on the motor shaft need to be measured to obtain the tangential force.
- The measurement of the mass loss with the creep and the wear regulating traction controllers is necessary to validate the wear regulating traction controller's effect. The corresponding mass loss rate measurement can be carried out on the test rig in the lab environment. The upper and lower wheel speeds and the torque on the motor shaft need to be measured for the purpose of real-time control. The amount of contact surface deformation with the creep and the wear regulating traction control need to be measured and compared under the dry and the FM contact conditions.

References

- [1] B. Solomon, *American Diesel Locomotives*: Voyageur Press.
- [2] S. Hillmansen and C. Roberts, "Energy storage devices in hybrid railway vehicles: A kinematic analysis," *Proceedings of the Institution of Mechanical Engineers, Part F: Journal of Rail and Rapid Transit*, vol. 221, pp. 135-143, January 1, 2007 2007.
- [3] (2013). *Australian Trading Commission: Heavy haul, intermodal and freight rail*. Available: <http://www.austrade.gov.au/ArticleDocuments/2814/Heavy-Haul-Intermodal-and-Freight-Rail-2013-10.pdf.aspx>
- [4] N. Ramsey, *et al.*, "Introducing the next generation locomotive to the Australian rail network," presented at the Conference on Railway Engineering, Perth, 2008.
- [5] S. Iwnicki, *Handbook of railway vehicle dynamics*: CRC press, 2006.
- [6] D. T. Eadie, *et al.*, "The effects of top of rail friction modifier on wear and rolling contact fatigue: Full-scale rail-wheel test rig evaluation, analysis and modelling," *Wear*, vol. 265, pp. 1222-1230, 2008.
- [7] J. Mathew, *et al.*, *Engineering Asset Management: Proceedings of the First World Congress on Engineering Asset Management (WCEAM) 2006*: Springer-Verlag, 2008.
- [8] E. H. Law and N. K. Cooperrider, "A survey of railway vehicle dynamics research," *ASME Journal of Dynamic Systems, Measurement, and Control*, vol. 96, pp. 132-146, June 1974 1974.
- [9] R. U. A. Uzzal, *et al.*, "Dynamic Analysis of Pitch Plane Railway Vehicle-Track Interactions Due to Single and Multiple Wheel Flats," *ASME Conference Proceedings*, vol. 2008, pp. 89-97, 2008.
- [10] M. R. U. A. Uzzal, "ANALYSIS OF A THREE-DIMENSIONAL RAILWAY VEHICLE-TRACK SYSTEM AND DEVELOPMENT OF A SMART WHEELSET," PhD, Mechanical Engineering, Concordia University, 2012.
- [11] X. Xin, *et al.*, "Impact Analysis of an Innovative Shock Energy Absorber and Its Applications in Improving Railroad Safety."
- [12] J. Evans and S. D. Iwnicki, "Vehicle dynamics and the wheel/rail interface," in *Proceedings of the IMechE Seminar on Wheels on rails—an update, London, UK*, 2002.
- [13] M. Spiriyagin, *et al.*, "Development of traction control for hauling locomotives," ed.
- [14] M. Spiriyagin, *et al.*, "Co-simulation of a mechatronic system using Gensys and Simulink," *Vehicle System Dynamics*, vol. 50, pp. 495-507, 2012.
- [15] M. Berg, "A Non-Linear Rubber Spring Model for Rail Vehicle Dynamics Analysis," *Vehicle System Dynamics*, vol. 30, pp. 197-212, 1998/09/01 1998.
- [16] R. F. Harder, "Dynamic modeling and simulation of three-piece freight vehicle suspensions with nonlinear frictional behaviour using Adams/Rail," in *Railroad Conference, 2001. Proceedings of the 2001 IEEE/ASME Joint*, 2001, pp. 185-191.
- [17] P. Wang, *Design of High-Speed Railway Turnouts: Theory and Applications*: Elsevier Science, 2015.
- [18] O. Polach, "A Fast Wheel-Rail Forces Calculation Computer Code," *Vehicle System Dynamics*, vol. 33, pp. 728-739, 1999.
- [19] R. Guclu and M. Metin, "Fuzzy Logic Control of Vibrations of a Light Rail Transport Vehicle in Use in Istanbul Traffic," *Journal of Vibration and Control*, vol. 15, pp. 1423-1440, September 1, 2009 2009.
- [20] D. S. Garivaltis, *et al.*, "Dynamic Response of a Six-axle Locomotive to Random Track Inputs," *Vehicle System Dynamics*, vol. 9, pp. 117-147, 1980/05/01 1980.

- [21] H. Xia, *et al.*, "Dynamic interaction analysis of a LIM train and elevated bridge system," *Journal of Mechanical Science and Technology*, vol. 23, pp. 3257-3270, 2009/12/01 2009.
- [22] F. W. Carter, *On the Action of a Locomotive Driving Wheel* vol. 112, 1926.
- [23] K. Johnson, "The effect of spin upon the rolling motion of an elastic sphere on a plane," *Journal of Applied Mechanics*, vol. 25, pp. 332-338, 1958.
- [24] J. J. Kalker, "Survey of Wheel—Rail Rolling Contact Theory," *Vehicle System Dynamics*, vol. 8, pp. 317-358, 1979/09/01 1979.
- [25] J. Kalker, "On the Rolling Contact of Two Elastic Bodies in the Presence of Dry Friction," Ph. D Doctoral Thesis, Delft, 1967.
- [26] J. Kalker, "Simplified Theory of Rolling Contact," Delft, Progress Report 1973.
- [27] O. Polach, "Creep forces in simulations of traction vehicles running on adhesion limit," *Wear*, vol. 258, pp. 992-1000, 2005.
- [28] J. C. F. Logston and G. S. Itami, "Locomotive Friction-Creep Studies," *Journal of Engineering for Industry*, vol. 102, pp. 275-281, 1980.
- [29] M. Spiriyagin, *et al.*, "Modeling of Adhesion for Railway Vehicles," *Journal of Adhesion Science and Technology*, vol. 22, pp. 1017-1034, 2008/01/01 2008.
- [30] J. Piotrowski and W. Kik, "A simplified model of wheel/rail contact mechanics for non-Hertzian problems and its application in rail vehicle dynamic simulations," *Vehicle System Dynamics*, vol. 46, pp. 27-48, 2008/02/01 2008.
- [31] C. Linder, "Verschleiss von Eisenbahnrädern mit Unrundheiten," Ph.D., ETH, Zurich, 1997.
- [32] J. B. Ayasse and H. Chollet, "Determination of the wheel rail contact patch in semi-Hertzian conditions," *Vehicle System Dynamics*, vol. 43, pp. 161-172, 2005/03/01 2005.
- [33] N. Burgelman, *et al.*, "Influence of wheel–rail contact modelling on vehicle dynamic simulation," *Vehicle System Dynamics*, vol. 53, pp. 1190-1203, 2015/08/03 2015.
- [34] O. Polach, "Influence of Locomotive Tractive Effort on the Forces Between Wheel and Rail," *Vehicle System Dynamics*, vol. 35, pp. 7-22, 2001.
- [35] M. Spiriyagin, *et al.*, "Creep force modelling for rail traction vehicles based on the Fastsim algorithm," *Vehicle System Dynamics*, vol. 51, pp. 1765-1783, 2013/11/01 2013.
- [36] V. R. Moorthi, *Power electronics: devices, circuits and industrial applications*: Oxford University Press, 2005.
- [37] "Frequency controlled AC motor drive," Rockwell-Automation.
- [38] I. Boldea and S. A. Nasar, *The Induction Machine Handbook*: CRC Press, 2002.
- [39] R. Marino, *et al.*, *Induction Motor Control Design*: Springer, 2010.
- [40] D. J. Atkinson, *et al.*, "Observers for induction motor state and parameter estimation," *Industry Applications, IEEE Transactions on*, vol. 27, pp. 1119-1127, 1991.
- [41] S. Kadowaki, *et al.*, "Antislip Readhesion Control Based on Speed-Sensorless Vector Control and Disturbance Observer for Electric Commuter Train—Series 205-5000 of the East Japan Railway Company," *Industrial Electronics, IEEE Transactions on*, vol. 54, pp. 2001-2008, 2007.
- [42] A. Sabanovic and D. B. Izosimov, "Application of Sliding Modes to Induction Motor Control," *Industry Applications, IEEE Transactions on*, vol. IA-17, pp. 41-49, 1981.
- [43] K. L. Butler, *et al.*, "A Matlab-based modeling and simulation package for electric and hybrid electric vehicle design," *Vehicular Technology, IEEE Transactions on*, vol. 48, pp. 1770-1778, 1999.

- [44] L.-H. Hoang, "Modeling and simulation of electrical drives using MATLAB/Simulink and Power System Blockset," in *Industrial Electronics Society, 2001. IECON '01. The 27th Annual Conference of the IEEE*, 2001, pp. 1603-1611 vol.3.
- [45] K. L. Shi, *et al.*, "Modelling of the three-phase induction motor using SIMULINK," in *Electric Machines and Drives Conference Record, 1997. IEEE International*, 1997, pp. WB3/6.1-WB3/6.3.
- [46] V. Rafalko, *et al.*, "Dynamic Model Based Vector Control of Linear Induction Motor," DTIC Document 2012.
- [47] H. Abu-Rub, *et al.*, *High performance control of AC drives with Matlab/Simulink models*: Wiley, 2012.
- [48] TI, "Field Oriented Control of 3-Phase AC-Motors," Texas Instruments Europe February 1998.
- [49] M. Janecke, *et al.*, "Direct self-control, a novel method of controlling asynchronous machines in traction applications," in *Proc. of 3rd EPE'89 Conf*, 1989, pp. 75-81.
- [50] Y. Kumsuwan, *et al.*, "Modified direct torque control method for induction motor drives based on amplitude and angle control of stator flux," *Electric Power Systems Research*, vol. 78, pp. 1712-1718, 2008.
- [51] P. Wach, *Dynamics and Control of Electrical Drives*: Springer, 2011.
- [52] "Technical guide No.1 Direct torque control-the world's most advanced AC drive technology," ABB.
- [53] P. Doh-Young, *et al.*, "Hybrid re-adhesion control method for traction system of high-speed railway," in *Electrical Machines and Systems, 2001. ICEMS 2001. Proceedings of the Fifth International Conference on*, 2001, pp. 739-742 vol.2.
- [54] K. Ohishi, *et al.*, "Anti-slip control of electric motor coach based on disturbance observer," in *Advanced Motion Control, 1998. AMC '98-Coimbra., 1998 5th International Workshop on*, 1998, pp. 580-585.
- [55] I. Yasuoka, *et al.*, "Improvement of re-adhesion for commuter trains with vector control traction inverter," in *Power Conversion Conference - Nagaoka 1997., Proceedings of the*, 1997, pp. 51-56 vol.1.
- [56] P. Howlett, "The Optimal Control of a Train," *Annals of Operations Research*, vol. 98, pp. 65-87, 2000.
- [57] E. Khmelnitsky, "On an optimal control problem of train operation," *Automatic Control, IEEE Transactions on*, vol. 45, pp. 1257-1266, 2000.
- [58] M. Djukić, *et al.*, "A fuzzy model for an increase in locomotive traction force," *Transport*, vol. 25, pp. 36-45, 2010/01/01 2010.
- [59] R. Palm and K. Storjohann, "Torque optimization for a locomotive using fuzzy logic," presented at the Proceedings of the 1994 ACM symposium on Applied computing, Phoenix, Arizona, United States, 1994.
- [60] L. A. Zadeh, "Fuzzy sets," *Information and Control*, vol. 8, pp. 338-353, 1965.
- [61] P. Khatun, *et al.*, "Application of fuzzy control algorithms for electric vehicle antilock braking/traction control systems," *Vehicular Technology, IEEE Transactions on*, vol. 52, pp. 1356-1364, 2003.
- [62] M. Garcia-Rivera, *et al.*, "An antislipping fuzzy logic controller for a railway traction system," in *Fuzzy Systems, 1997., Proceedings of the Sixth IEEE International Conference on*, 1997, pp. 119-124 vol.1.
- [63] R. Sivakumar, *et al.*, "Application of Fuzzy Model Predictive Control in Multivariable Control of Distillation Column," *International Journal of Chemical Engineering and Applications*, vol. 1, pp. 39-42, 2010.

- [64] T. X. Mei, *et al.*, "A mechatronic approach for effective wheel slip control in railway traction," *Proceedings of the Institution of Mechanical Engineers, Part F: Journal of Rail and Rapid Transit*, vol. 223, pp. 295-304, May 1, 2009 2009.
- [65] Q. Song, *et al.*, "Adaptive backstepping control of train systems with traction/braking dynamics and uncertain resistive forces," *Vehicle System Dynamics*, vol. 49, pp. 1441-1454, 2011/09/01 2011.
- [66] T. Vuong, "Investigation for the wear coefficient of the frictional-work wear model and feasibility of friction modifiers for wear-type corrugation control," 2011.
- [67] F. Braghin, *et al.*, "A mathematical model to predict railway wheel profile evolution due to wear," *Wear*, vol. 261, pp. 1253-1264, 2006.
- [68] R. G. Bayer, *Wear Analysis for Engineers*: HNB Publishing, 2002.
- [69] T. Jendel, "Prediction of wheel profile wear—comparisons with field measurements," *Wear*, vol. 253, pp. 89-99, 2002.
- [70] T. G. Pearce and N. D. Sherratt, "Prediction of wheel profile wear," *Wear*, vol. 144, pp. 343-351, 1991.
- [71] R. Lewis and U. Olofsson, "Mapping rail wear regimes and transitions," *Wear*, vol. 257, pp. 721-729, 2004.
- [72] T. M. Beagley, "Severe wear of rolling/sliding contacts," *Wear*, vol. 36, pp. 317-335, 1976.
- [73] P. J. Bolton and P. Clayton, "Rolling—sliding wear damage in rail and tyre steels," *Wear*, vol. 93, pp. 145-165, 1984.
- [74] D. Markov and D. Kelly, "Mechanisms of adhesion-initiated catastrophic wear: pure sliding," *Wear*, vol. 239, pp. 189-210, 2000.
- [75] D. Danks and P. Clayton, "Comparison of the wear process for eutectoid rail steels: Field and laboratory tests," *Wear*, vol. 120, pp. 233-250, 1987.
- [76] S. Zakharov, *et al.*, "Wheel flange/rail head wear simulation," *Wear*, vol. 215, pp. 18-24, 1998.
- [77] P. Clayton, "Predicting the wear of rails on curves from laboratory data," *Wear*, vol. 181–183, Part 1, pp. 11-19, 1995.
- [78] M. Ignesti, *et al.*, "Development of a wear model for the prediction of wheel and rail profile evolution in railway systems," *Wear*, vol. 284–285, pp. 1-17, 2012.
- [79] R. Lewis, *et al.*, "Mapping railway wheel material wear mechanisms and transitions," *Proceedings of the Institution of Mechanical Engineers, Part F: Journal of Rail and Rapid Transit*, vol. 224, pp. 125-137, 2010.
- [80] J. Pombo, *et al.*, "A study on wear evaluation of railway wheels based on multibody dynamics and wear computation," *Multibody System Dynamics*, vol. 24, pp. 347-366, 2010/10/01 2010.
- [81] J. Pombo, *et al.*, "Development of a wear prediction tool for steel railway wheels using three alternative wear functions," *Wear*, vol. 271, pp. 238-245, 2011.
- [82] R. Lewisa and R. S. Dwyer-Joyce, "Wear mechanisms and transitions in railway wheel steels," *Proceedings of the Institution of Mechanical Engineers, Part J: Journal of Engineering Tribology*, vol. 218, pp. 467-478, June 1, 2004 2004.
- [83] T. T. Vuong and P. A. Meehan, "Wear transitions in a wear coefficient model," *Wear*, vol. 266, pp. 898-906, 2009.
- [84] M. D. Ardema, *Newton-Euler Dynamics*: Springer, 2006.
- [85] I. J. Guy, "An analysis of the interaction between the front and rear axles of a four-wheel-drive tractor, and its contribution to power delivery efficiency," Harper Adams University College, 2011.
- [86] Pegasem. Pegasem GSS series ground speed sensors [Online]. Available: http://www.pegasem.com/english/datasheets_uk/gss_uk.pdf

- [87] K. Abood and R. Khan, "Hunting phenomenon study of railway conventional truck on tangent tracks due to change in rail wheel geometry," *Journal of Engineering Science and Technology*, vol. 6, pp. 146-160, 2011.
- [88] A. Bhaskar, "Mode Shapes during Asynchronous Motion and Non-Proportionality Indices," *Journal of Sound and Vibration*, vol. 224, pp. 1-16, 1999.
- [89] G. Lallement and D. J. Inman, "A tutorial on complex eigenvalues," in *PROCEEDINGS-SPIE THE INTERNATIONAL SOCIETY FOR OPTICAL ENGINEERING*, 1995, pp. 490-490.
- [90] K. L. Johnson, *Contact Mechanics*: Cambridge University Press, 1985.
- [91] *Rail Track Material Catalogue A5*. Available: <https://www.scribd.com/doc/92072909/Rail-Track-Material-Catalogue-A5#download>
- [92] I. Takahashi and T. Noguchi, "A new quick-response and high-efficiency control strategy of an induction motor," *Industry Applications, IEEE Transactions on*, pp. 820-827, 1986.
- [93] F. Khorrami, *et al.*, *Modeling and adaptive nonlinear control of electric motors*: Springer Science & Business Media, 2003.
- [94] J. L. Daigle and J. McGarry, "System and method for traction motor control," ed: Google Patents, 2013.
- [95] *UGL Powerhaul Series Locomotive*. Available: http://cdn.ugllimited.com/Asset/cms/Freight_Product_brochures/084_Powerhaul_ProductSheet_V4_WEB.pdf
- [96] M. Spiryagin, *et al.*, "Control system for maximum use of adhesive forces of a railway vehicle in a tractive mode," *Mechanical Systems and Signal Processing*, vol. 22, pp. 709-720, 2008.
- [97] Y. Yuan, *et al.*, "The dynamic study of locomotives under saturated adhesion," *Vehicle System Dynamics*, vol. 49, pp. 1321-1338, 2011/08/01 2011.
- [98] M. Bauer and M. Tomizuka, "Fuzzy Logic Traction Controllers and their Effect on Longitudinal Vehicle Platoon Systems," *Vehicle System Dynamics*, vol. 25, pp. 277-303, 1996/04/01 1996.
- [99] S. Park, *et al.*, "Reference slip ratio generation and adaptive sliding mode control for railway rolling stocks," *International Journal of Precision Engineering and Manufacturing*, vol. 10, pp. 39-44, 2009/04/01 2009.
- [100] T. J. Ross, *Fuzzy Logic with Engineering Applications*: Wiley, 2004.
- [101] A. K. Kumar, "Method and system of limiting the application of sand to a railroad rail," U.S. Patent US7290807, 2007.
- [102] Y. Zhu, "Adhesion in the wheel-rail contact under contaminated conditions," Doctoral Thesis, KTH, 2011.
- [103] C. Tomberger, *et al.*, "Friction in wheel-rail contact: A model comprising interfacial fluids, surface roughness and temperature," *Wear*, vol. 271, pp. 2-12, 2011.
- [104] M. Ertz and F. Bucher, "Improved creep force model for wheel/rail contact considering roughness and temperature," *Vehicle System Dynamics*, vol. 37, pp. 314-325, 2003.
- [105] SIEMENS. Three-Phase AC Traction Technology for Diesel-Electric Locomotive WDG4 of India Railways [Online]. Available: <http://www.docstoc.com/docs/46726734/Three-Phase-ACTraction-Technology-for-Diesel-Electric-Locomotive-WDG4>
- [106] A. INDIA, "AUTOCAR Rail Test," IndiaSeptember 2009.
- [107] GM, "GT46MAC INDIAN STATE RAILWAYS LOCOMOTIVE SERVICE MANUAL," ed, 1999.
- [108] GM, "GT46C 3000 KW LOCOMOTIVE."

- [109] D. Berthe, *et al.*, *Tribological Design of Machine Elements*: Elsevier Science, 1989.
- [110] G. M. Corporation, "GT46C 3000KW LOCOMOTIVE," 2008.

Appended Papers

Paper A

**DYNAMIC TRACTIONAL BEHAVIOUR
ANALYSIS AND CONTROL FOR A DC
LOCOMOTIVE**

DYNAMIC TRACTIONAL BEHAVIOUR ANALYSIS AND CONTROL FOR A DC LOCOMOTIVE

Ye Tian^{1,2}, W.J.T. (Bill) Daniel^{1,2}, Sheng Liu¹, Paul A. Meehan^{1,2}

¹*School of Mechanical and Mining Engineering, the University of Queensland, Queensland, Australia 4072*

²*Cooperative Research Centre for Railway Engineering and Technology (CRC Rail), Queensland, Australia*

Abstract: In recent decades, advanced power-electronics-based control techniques have been widely used to upgrade direct current (DC) drives for the traction of locomotives. However the dynamic response of such upgraded DC locomotives under transient conditions due to external perturbations has not been fully investigated. In this work, an integrated dynamic model for a typical DC Co-Co locomotive/track system is developed to provide predictive simulations of the motion and forces transmitted throughout the DC locomotive dynamic system. The model integrates a 2D longitudinal-vertical locomotive structural vibration model, wheel/rail contact mechanics using Polach's creep force model, a generic DC dynamic traction model and a traditional creep controller to simulate the transient response to a change in friction conditions. It is found that although the largest creep is constrained below 10% there are large transient creep and traction fluctuations related to identified modes of vibration of the locomotive.

1. Introduction

The progressive adoption of high traction motors and control techniques based on power electronics has brought great benefits to rail industry due to its high power capacity and efficiency. Despite all the advantages, concerns arise as to the effects of operating at maximum adhesion and the possible impact of dynamic oscillations and resultant traction to the rail tracks. An electric locomotive is a complex system containing several nonlinear dynamic components coupled together when the locomotive operates. Its traction control performance and dynamic impact on the rail tracks are typically assessed under specific steady state conditions. However, the natural perturbations in friction/lubrication, wheel/rail profiles, track curvature, vehicle/track dynamics, wheel/track imperfections etc. are not comprehensively investigated yet. Among those perturbations, the transient changes in friction or lubrication can cause sudden changes of creep and often leads to over/under traction/braking. In order to investigate this issue, a predictive locomotive dynamic model combining crucial dynamic components such as locomotive rigid body dynamics, contact dynamics and electric drive and control is needed.

Locomotive traction simulations have been investigated by several researchers. A simulation package for simulation of rail vehicle dynamics has been developed in Matlab environment by Chudzikiewicz [1] for Poland railway specifications. Traction simulation considering bogie vibration has been provided by Shimizu et al. and a disturbance observer based anti-slip controller is also proposed [2]. Spiriyagin et al. employed co-simulation approach with the Gensys multibody code and Simulink to investigate the heavy haul train traction dynamics [3]. Fleischer proposed a modal state controller to reduce drive train oscillation during the traction simulation [4]. Bakhvalov et al. combined electrical and mechanical processes for locomotive traction simulation [5]. Senini et al. has also performed some locomotive traction and simulation on electric drive level [6]. These works however, haven't focused investigation on the effect of transient contact conditions on the locomotive dynamic response. In this work, we focus on longitudinal and vertical dynamics on tangent tracks as it is the most important part of locomotive dynamics closely related with traction/braking effort, passenger comfort and energy management [7]. Newton-Euler method [8, 9] is used to obtain the motion equations of the locomotive model. For the contact mechanics, Polach's adhesion model [10] is adopted as it has been verified to be effective for both small and large values of longitudinal wheel-rail creep as well as the decreasing part of creep-force function exceeding the adhesion limit [11]. Modern development of mechatronics systems has improved rail vehicle operation under various conditions. The traction control system, also known as an adhesion or anti-slip control system is essential for the operational efficiency and reliability in these systems. A pattern-based slip control method has been applied and modified by Park et al. [12]. Anti-slip control based on a disturbance observer was proposed by Ohishi et al. [13]. Yasuoka et al. proposed a slip control method [14] involving bogie oscillation suppression. All these methods claim the effectiveness of their proposed creep/traction controller; however, these conclusions were not validated on a comprehensive locomotive dynamic model.

In this paper, a full scale locomotive dynamic model with a basic creep controller combining all crucial dynamic components is developed and implemented using Matlab/Simulink to investigate creep and dynamic oscillation control. In addition, a traction control system is proposed and embedded into the dynamic model to prevent inefficient traction caused by perturbations. Eigenmode and frequency analysis is also performed to identify important structural behaviour.

2. Modelling details

The locomotive model is comprised of three major dynamic components: locomotive longitudinal-vertical-pitching dynamics, electric drive/control dynamics, and contact mechanics. The structure of the model is shown in Figure 1. A dynamics model of the mechanical system of an electric locomotive based on the Newton-Euler method is developed. The wheel-rail contact in this model is based on Polach's model. And a simplified electric drive model with a basic creep controller is proposed and integrated into the electric drive/control dynamics block in this model.

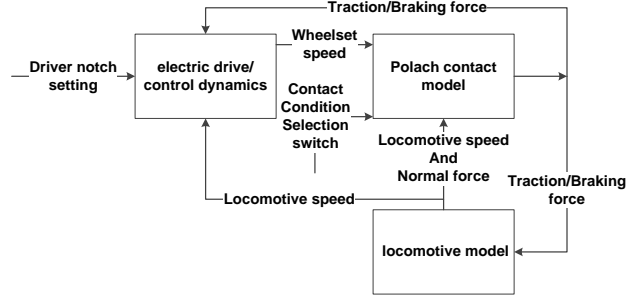


Figure 1: Overall model structure of a locomotive

The model may be described as a feedback system. The electric drive and control system provides a torque acting on the motor shaft in the locomotive model. Torque also results from the longitudinal force due to the interaction between wheel-rail track contact mechanics. The resultant creep changes the longitudinal tractive force calculated using the Polach model, and the tractive force acts on the locomotive dynamic model and changes the displacements and velocities of the rigid bodies. Each of those components is detailed in the following sections.

Locomotive 2D dynamic model

The locomotive dynamic model is illustrated in Figure 2. In this model longitudinal, vertical and pitching dynamics are taken into consideration. The simplified Co-Co locomotive has two bogies. Each bogie has three wheelsets attached. Key parameters including geometry, degrees of freedom etc., are marked in Figure 2.

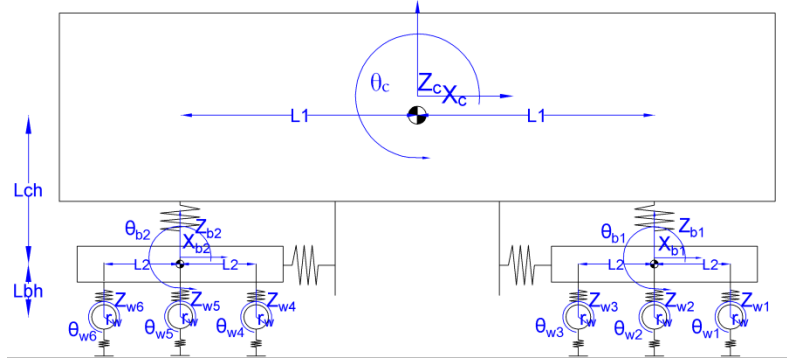


Figure 2: Diagram of simplified locomotive multibody structure

This simplified dynamic model has 21 degrees of freedom (DOF), including 9 DOF on the longitudinal, vertical and pitching motion of locomotive body and two bogies, and 12 DOF on vertical and rotating motion of six wheelsets. The system variables are expressed as a vector containing 42 entries, representing the relative displacements and velocities between different nodes as,

$$X = [Z \quad \dot{Z}]^T, \quad Z = [Z_{carbody} \quad Z_{bogie1} \quad Z_{bogie2} \quad Z_{axles}]^T \quad (1)$$

in which $Z_{carbody} = [x_c, z_c, \theta_c]^T$ is a 3×1 vector representing the locomotive body longitudinal, vertical and pitching motion from the static positions, $Z_{bogie1} = [x_{b1}, z_{b1}, \theta_{b1}]^T$ and $Z_{bogie2} = [x_{b2}, z_{b2}, \theta_{b2}]^T$ are both 3×1 vectors representing longitudinal, vertical and pitching motion of front and rear bogie separately, and $Z_{axles} = [z_{w1}, \theta_{w1}, z_{w2}, \theta_{w2}, \dots, z_{w6}, \theta_{w6}]^T$ is a 12×1 vector representing the vertical and rotating motion of wheelset 1~6. The state space representation of the simplified dynamics can be expressed as:

$$\begin{aligned} \dot{X} &= A \cdot X + B \cdot u \\ Y &= C \cdot X + D \cdot u \end{aligned}, \quad A = \begin{bmatrix} \Theta & I \\ M^{-1}K & M^{-1}C \end{bmatrix} \quad (2)$$

where u is the longitudinal tractive force resulted from the interaction between the wheelsets and rail tracks, Y is a vector of displacement or velocity of each node from its static position, Θ is a zero matrix, I is an identity matrix of certain dimensions, and M is the diagonal mass and moment of inertia matrix in the form of,

$$M = \text{diag}(M_c, M_c, I_c, M_t, M_t, I_t, M_t, M_t, I_t, M_w, I_w, M_w, I_w, M_w, I_w, M_w, I_w, M_w, I_w, M_w, I_w). \quad (3)$$

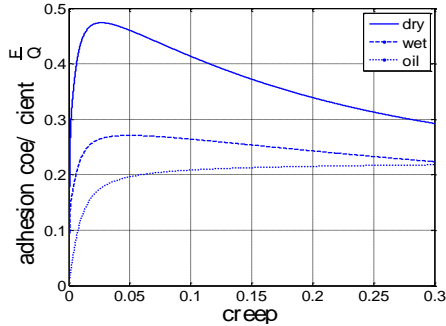
Contact mechanics

The Polach model [10] is employed in the contact mechanics component to determine the longitudinal tractive force resulted from the interaction between the wheelsets and rail tracks. In the model, the longitudinal tractive force can be expressed as,

$$F = \frac{2Q\mu}{\pi} \left(\frac{k_A \varepsilon}{1+(k_A \varepsilon)^2} + \arctan(k_s \varepsilon) \right) \quad (4)$$

where $\mu = \mu_0 \left[(1-A)e^{-B\omega} + A \right]$, $A = \frac{\mu_\infty}{\mu_0}$, $\varepsilon = \varepsilon_x = \frac{1}{4} \frac{G\pi abc_{11}}{Q\mu} s_x$, $s_x = \frac{w_x}{V}$ for longitudinal direction. Parameters are defined as in [10]: F is tractive force, Q is normal wheel load, μ is the coefficient of friction, k_A is the reduction factor in the area of adhesion, k_s is the reduction factor in the area of slip, ε is the gradient of the tangential stress in the area of adhesion, ε_x is the gradient of the tangential stress in the longitudinal direction, μ_0 is the maximum friction coefficient at zero slip velocity, μ_∞ is the friction coefficient at infinite slip velocity, A is the ratio of friction coefficients, B is the coefficient of exponential friction decrease, ω is the total creep (slip) velocity, ω_x is the creep (slip) velocity in the longitudinal direction, G is the shear modulus, a, b are half-axes of the contact ellipse, c_{11} is a coefficient from Kalker's linear theory and V is vehicle speed. The implemented Polach model gives simulation results plotted in Figure a) and ideal tractive force versus speed curves for all 8 traction notches is as shown in Figure 3 b).

a)



b)

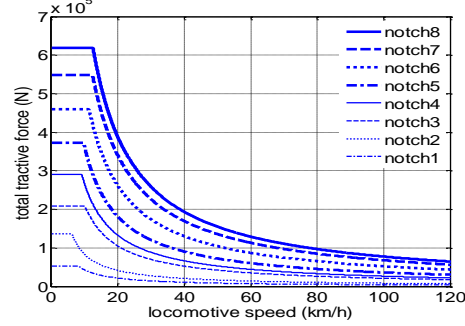


Figure 3: a) Adhesion coefficient for dry wet, and oil conditions; b) Tractive effort curves of GT46C[110]

In the figure, adhesion coefficients in dry, wet and oil conditions are plotted as a function of creep rate for locomotive speed of approximately 10 km/h. Note that Polach's experiments show adhesion variation of about $\pm 20\%$. This can be also seen from Table 5 in [16] which has larger variations. The curves in Figure for dry and wet conditions agree with those in Polach's work [10], and the curve for oil contact condition agrees with the data from a US patent [17]. As a result, the contact mechanics component is considered reliable when applied on those three contact conditions.

Electric drive and controller dynamics

A simplified electric drive dynamic model has been adopted in the paper to reduce the simulation time. The relation between the speed of axle and maximum tractive force for different notch settings is presented by means of a look-up table. The rotor speed is determined by the electromagnetic torque generated by the motor and the loading torque from the contact mechanics.

$$I_w \cdot \ddot{\theta}_{wi} = T_{ei} \cdot G - T_{li} \quad i = 1 \sim 6 \quad (7)$$

I_w is moment of inertia of an axle, $\ddot{\theta}_{wi}$ is angular acceleration of axle i ($i: 1 \sim 6$), G is gear ratio and T_{ei} is torque generated by electric drive i ($i: 1 \sim 6$). The index i represents the specific axle from the leading to the rear. A PI controller is also used in this study to act as the creep controller. It compares the measured creep value with the threshold setting providing torque compensation when the measured maximum creep value of the axles of a bogie exceeds the threshold setting at 6%. If the maximum creepage of all axles on a bogie exceeds the threshold, the creep controller reduces the torque acting on all axles on the bogie; otherwise the creep controller

stays idle without providing a torque reduction signal. The effect of the high frequency electronics of the electric drive have not been simulated in this case but will be investigated in future research.

3. Results

Eigenmode analysis

An eigenmode analysis was performed in Matlab to identify all the dynamic modes of vibration and to determine the stability of the system. The system eigenvalues are provided in

Table. An eigenvalue is obtained for each possible mode of vibration of the system. The first part (real value) of each complex eigenvalue represents the amount of damping (if negative) of each mode of vibration. The second part (imaginary number) represents the part from which the frequency of vibration can be calculated. From the eigenvalues of the system, it can be seen that except for the car body horizontal mode, all modes of vibration have positive damping (negative real parts) which implies that the system is stable. The car body horizontal mode with zero damping is expected due to the rigid body longitudinal motion of the train.

Table 1: Modal frequencies of the locomotive dynamic system vibration (Hz) and corresponding eigenvalues

Modes	Frequency (Hz)	Eigenvalues	Modes	Frequency (Hz)	Eigenvalues
Car body vertical	0.8	$-0.3 \pm 4.9i$	Bogie 2 vertical	7.2	$-6.5 \pm 45.3i$
Car body pitching	1.4	$-1.0 \pm 8.9i$	Bogie pitching	12	$-4.9 \pm 75.7i$
Bogie 1 horizontal	2.8	$-4.6 \pm 17.1i$	Bogie pitching	12	$-4.9 \pm 75.7i$
Bogie 2 horizontal	2.9	$-5 \pm 17.8i$	Wheelset vertical	216	$-1.6 \pm 1361.3i$
Bogie 1 vertical	7.2	$-6.2 \pm 45.4i$	Wheelset vertical	216	$-1.6 \pm 1361.3i$
Wheelset vertical	216	$-1.6 \pm 1361.3i$	Wheelset vertical	216	$-1.6 \pm 1361.3i$
Wheelset vertical	216	$-1.6 \pm 1361.3i$	Car body horizontal	0	0
Wheelset vertical	216	$-1.6 \pm 1361.3i$			

In the subsequent section full Simulink simulations are performed from which the dominant modes of vibration in the response can be compared to the eigenvalue analysis.

Simulation results

Simulation results for the transient response to changing contact conditions from dry to oily are provided in this section. The structure of the simulation block is as shown in Figure 1. The whole system combines the locomotive dynamics, Polach contact mechanics and electric drive & creep controller dynamics as described in the previous sections. The manual input of the system is from notch settings by the driver which control the level of torque command to the electric drives. The torque generated by the electric drive together with the effect of the longitudinal force acting on the axle from the rail tracks determines the angular acceleration of the rotor and consequently that of the axle. The change in creep in the transient response directly affects the longitudinal traction force and causes the dynamic change of acceleration, speed and position of all nodes in the system. Initial locomotive velocity and creep rate are set at 10 km/h and 0.5% respectively. The locomotive is operating on traction notch 8, i.e. high acceleration.

Figure 4 a) and b) show the creep response of each axle in response to the change in contact condition and the corresponding tractive force on each axle respectively.

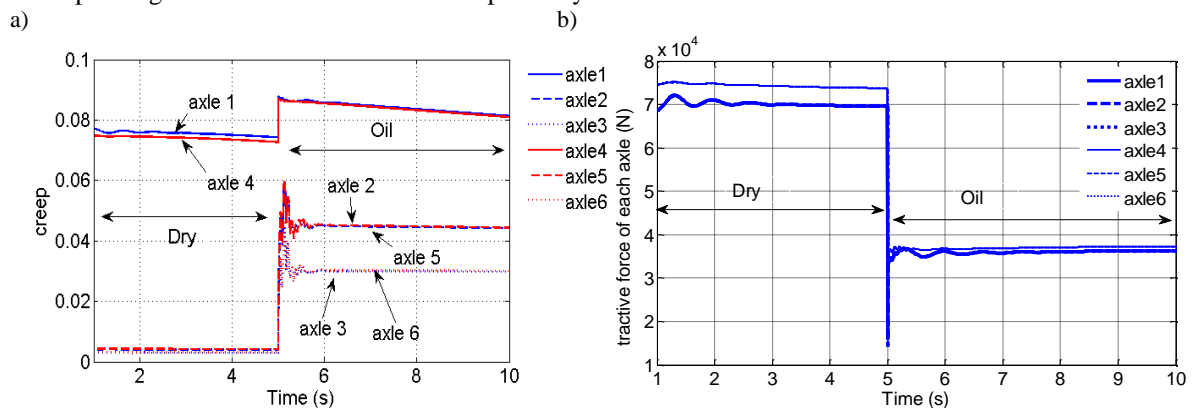


Figure 4: a) creep of all axles during the change of contact condition; b) tractive force on each axle

It can be seen that the creep response of each axle on each bogie is very similar to that of its matching axle at the same location on the other bogie. Also the leading axle of each bogie has a different response compared to the other two axles on the same bogie. This is maybe because the creep controller uses the maximum value of all

axles on a bogie as a control index and reduces the torque of all axles on the bogie based on this maximum response. As the creeps of the middle and rear axles are generally lower than the leading axles during locomotive acceleration, the creep controller is triggered and determined only by the leading axles during the acceleration tests. This explanation could be confirmed by further investigation into the signal generated by the creep controller. From Figure 4 b) it can be seen that the middle and rear axles have a drop of tractive force beginning with a shape of spike, while the tractive forces on the leading axles drop without a spike. This is likely because the creep value the leading axles are operating on, when the contact condition changes, is on a relatively flat part on the creep-adhesion coefficient curve. In contrast, the middle and rear axles are operating on a steep part of the creep-adhesion coefficient curve. Hence when the creep value increases the tractive forces increase steeply as spikes. The middle and rear axles dynamic creep overshoots are about 33% and 50% compared to their steady state creep values under an oily contact condition respectively. The tractive force overshoot of middle axles is about 47% and that of rear axles is about 58%.

Figure 5 a) shows the vertical displacement of each axle on the same bogie has similar dynamic responses during the change of contact condition.

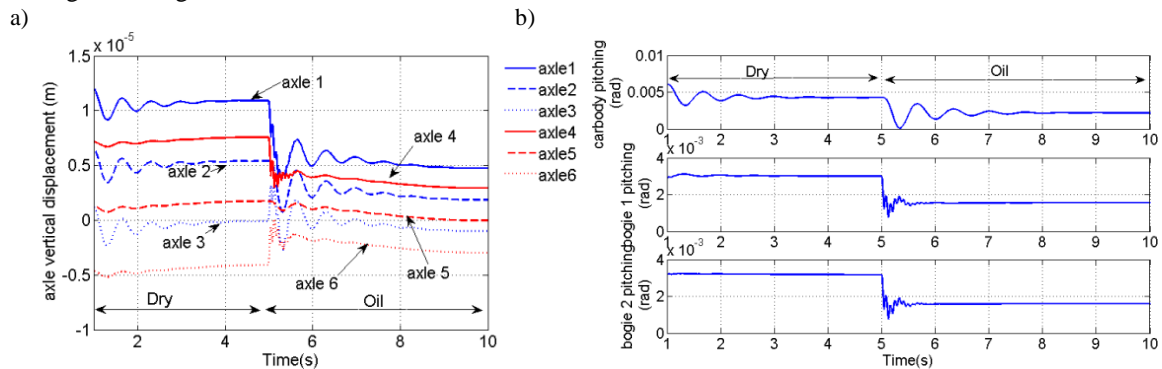


Figure 5: a) vertical displacement of all axles during the change of contact condition; b) pitching angles of car body and two bogies during the change of contact condition

The front and rear axle vertical displacements are dominated by the corresponding bogie pitching and the middle axle vertical displacements are dominated by the vertical motion of the bogies. The frequency of the car body pitching is about 1.5 Hz which is close to the eigenmode analysis result of 1.4 Hz. Also the pitching frequency seen in the response of Figure 5 b) is close to 12 Hz as found in the eigenmode analysis of

Table. The transient oscillations, between 1 to 4 seconds are caused by the system simulation initialization and stabilization. The bouncing motion of axles also affect the transient tractive force responses by varying the normal contact force between the axles and rail tracks as seen in Figures 4 b) and 5 a). Figure 5 b) shows the pitching angle of the car body and two bogies respectively. Comparing to previous figures, it can be seen that vertical displacement of the front and rear axles of each bogie is mainly affected by the pitching motion of each bogie. In addition, the sudden change of contact condition causes a decrease of tractive forces such that the torques acting on bogies and the locomotive body decrease consequently. This is the reason that the pitching angles of bogies and locomotive body are smaller under an oily contact condition than those under a dry contact condition.

4. Conclusion

In this work, an integrated dynamic model for a typical DC Co-Co locomotive/track system is developed. By simulating the transient response to a change in contact conditions from dry to oil under traction, the dynamic responses of all components are successfully generated. The resultant modes of those vibrations were validated by matching an eigenmode analysis of the structural dynamics model. It is found that the proposed creep controller is able to constrain the largest creep rate effectively but transient dynamic oscillations occur in response. In particular, the simulation shows that there is a substantial transient creep force response to changes in friction conditions which are shown to be associated with bouncing modes of the bogies and pitching of the bogies and locomotive body.

5. Acknowledgement

The authors are grateful to the CRC for Rail Innovation (established and supported under the Australian Government's Cooperative Research Centres program) for the funding of this research Project No. R3.119 "Locomotive Adhesion". The authors acknowledge the support of the Centre for Railway Engineering, Central Queensland University and the many industry partners that have contributed to this project, in particular staff from RailCorp, Fortescue Metals Group (FMG) and Brookfield Rail.

References

- [1] A. Chudzikiewicz, "Simulation of Rail Vehicle Dynamics in MATLAB Environment," *Vehicle System Dynamics*, vol. 33, pp. 107-119, 2000/02/01 2000.
- [2] Y. Shimizu, et al., "Anti-slip/skid Re-adhesion Control Based on Disturbance Observer Considering Bogie Vibration," in *Power Conversion Conference - Nagoya, 2007. PCC '07, 2007*, pp. 1376-1381.
- [3] M. Spiryagin, et al., "Development of traction control for hauling locomotives," ed.
- [4] M. Fleischer, "Modal state control in the frequency domain for active damping of mechanical vibrations in traction drive-trains," in *Advanced Motion Control, 2004. AMC'04. The 8th IEEE International Workshop on, 2004*, pp. 171-176.
- [5] Y. Bakhvalov, et al., "Mathematical Modelling of Electromechanical Processes in Electric Locomotive," presented at the 16th IMACS World Congress, Lausanne (Switzerland), 2000.
- [6] S. Senini, et al., "Dynamic simulation of wheel-rail interaction for locomotive traction studies," in *Railroad Conference, 1993., Proceedings of the 1993 IEEE/ASME Joint, 1993*, pp. 27-34.
- [7] E. H. Law and N. K. Cooperrider, "A survey of railway vehicle dynamics research," *ASME Journal of Dynamic Systems, Measurement, and Control*, vol. 96, pp. 132-146, June 1974 1974.
- [8] R. Guclu and M. Metin, "Fuzzy Logic Control of Vibrations of a Light Rail Transport Vehicle in Use in Istanbul Traffic," *Journal of Vibration and Control*, vol. 15, pp. 1423-1440, September 1, 2009 2009.
- [9] D. S. Garivaltis, et al., "Dynamic Response of a Six-axle Locomotive to Random Track Inputs," *Vehicle System Dynamics*, vol. 9, pp. 117-147, 1980/05/01 1980.
- [10] O. Polach, "Creep forces in simulations of traction vehicles running on adhesion limit," *Wear*, vol. 258, pp. 992-1000, 2005.
- [11] O. Polach, "Influence of Locomotive Tractive Effort on the Forces Between Wheel and Rail," *Vehicle System Dynamics*, vol. 35, pp. 7-22, 2001.
- [12] P. Doh-Young, et al., "Hybrid re-adhesion control method for traction system of high-speed railway," in *Electrical Machines and Systems, 2001. ICEMS 2001. Proceedings of the Fifth International Conference on, 2001*, pp. 739-742 vol.2.
- [13] K. Ohishi, et al., "Anti-slip control of electric motor coach based on disturbance observer," in *Advanced Motion Control, 1998. AMC '98-Coimbra., 1998 5th International Workshop on, 1998*, pp. 580-585.
- [14] I. Yasuoka, et al., "Improvement of re-adhesion for commuter trains with vector control traction inverter," in *Power Conversion Conference - Nagaoka 1997., Proceedings of the, 1997*, pp. 51-56 vol.1.
- [15] G. M. Corporation, "GT46C 3000KW LOCOMOTIVE," 2008.
- [16] R. S. S. Board, "Guidance on Wheel/Rail Low Adhesion Measurement," ed, 2008.
- [17] A. K. Kumar, "Method and system of limiting the application of sand to a railroad rail," U.S. Patent US7290807, 2007.

Paper B

Fuzzy Logic Creep Control for 2D Locomotive Dynamic Model under Transient Wheel-rail Contact Condition

Fuzzy Logic Creep Control for 2D Locomotive Dynamic Model under Transient Wheel-rail Contact Condition

Y.Tian^{1,2}, W.J.T. (Bill) Daniel¹, Sheng Liu¹, P.A. Meehan^{1,2}

¹*School of Mechanical and Mining Engineering, the University of Queensland, Australia*

²*Cooperative Research Centre for Railway Engineering and Technology (CRC Rail), Australia*

Abstract

In recent decades, advanced power-electronics-based control techniques have been widely used to electric drives for the traction of modern locomotives. However the dynamic response of such locomotives under transient conditions due to external perturbations has not been fully investigated. In this work, an integrated dynamic model for a typical Co-Co locomotive/track system is developed to provide predictive simulations of the motion and forces transmitted throughout the whole locomotive dynamic system. The model integrates a 2D longitudinal-vertical locomotive structural vibration model, wheel/rail contact mechanics using Polach's creep force model, a simplified dynamic traction model and a fuzzy logic creep controller to simulate the transient response to a change in friction conditions. It is found that the proposed fuzzy logic controller has the advantage over a PI controller in terms of achieving higher tractive force under transient contact conditions.

Keywords: locomotive creep control, fuzzy logic, transient contact conditions.

1 Introduction

The progressive adoption of high traction motors and control techniques based on power electronics has brought great benefits to rail industry due to its high power capacity and efficiency. Despite all the advantages, concerns arise as to the effects of operating at maximum adhesion and the possible impact of dynamic oscillations and resultant traction to the rail tracks. An electric locomotive is a complex system containing several nonlinear dynamic components coupled together when the locomotive operates. Its traction control performance and dynamic impact on the rail tracks are typically assessed under specific steady state conditions. However, the natural perturbations in friction/lubrication, wheel/rail profiles, track curvature, vehicle/track dynamics, wheel/track imperfections etc. are not comprehensively investigated yet. Among those perturbations, the transient changes in friction or lubrication can cause sudden changes of creep and often leads to over/under traction/braking. In order to investigate this issue, a predictive locomotive dynamic model combining crucial dynamic components such as locomotive rigid body dynamics, contact dynamics and electric drive and control is needed.

Locomotive traction simulations have been investigated by several researchers. A simulation package for simulation of rail vehicle dynamics has been developed in Matlab environment by Chudzikiewicz [1] for Poland railway specifications. Traction simulation considering bogie vibration has been provided by Shimizu et al. and a disturbance observer based anti-slip controller is also proposed [2]. Spiriyagin et al. employed co-simulation approach with the Gensys multibody code and Simulink to investigate the heavy haul train traction dynamics [3]. Fleischer proposed a modal state controller to reduce drive train oscillation during the traction simulation [4]. Bakhvalov et al. combined electrical and mechanical processes for locomotive traction simulation [5]. Senini et al. has also performed some locomotive traction and simulation on electric drive level [6]. These works however, haven't focused investigation on the effect of transient contact conditions on the locomotive dynamic response. In this work, we focus on longitudinal and vertical dynamics on tangent tracks as it is the most important part of locomotive dynamics closely related with traction/braking effort, passenger comfort and energy management [7]. Newton-Euler method [8,9] is used to obtain the motion equations of the locomotive model. For the contact mechanics, Polach's adhesion model [10] is adopted as it has been verified to be effective for both small and large values of longitudinal wheel-rail creep as well as the decreasing part of creep-force function exceeding the adhesion limit [11]. Modern development of mechatronics systems has improved rail vehicle operation under various conditions. The traction control system, also known as an adhesion or anti-slip control system is essential for the operational efficiency and reliability in these systems. A pattern-based slip control method has been applied and modified by Park et al. [12]. Anti-slip control based on a disturbance observer was proposed by Ohishi et al. [13]. Yasuoka et al. proposed slip control method [14] involving bogie

oscillation suppression. All these methods claim the effectiveness of their proposed creep/traction controller; however, these conclusions were not validated on a comprehensive locomotive dynamic model.

In this paper, a full scale locomotive dynamic model with a fuzzy logic creep controller combining all crucial dynamic components is developed and implemented using Matlab/Simulink to investigate creep and dynamic oscillation. In addition, a traction control system is proposed and embedded into the dynamic model to prevent inefficient traction caused by perturbations. Eigenmode and frequency analysis is also performed to identify important structural behaviour.

2 Modelling details

The locomotive model is comprised of three major dynamic components: locomotive longitudinal-vertical-pitching dynamics, electric drive/control dynamics, and contact mechanics. The structure of the model is shown in Figure 1. A dynamics model of the mechanical system of an electric locomotive based on the Newton-Euler method is developed. The wheel-rail contact in this model is based on Polach's model. And a simplified electric drive model with a basic creep controller is proposed and integrated into the electric drive/control dynamics block in this model.

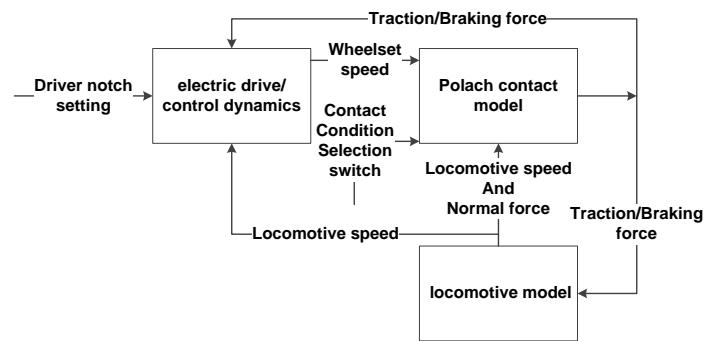


Figure 1: Overall model structure of a locomotive

The model may be described as a feedback system. The electric drive and control system provides a torque acting on the motor shaft in the locomotive model. Torque also results from the longitudinal force due to the interaction between wheel-rail track contact mechanics. The resultant creep changes the longitudinal tractive force calculated using the Polach model, and the tractive force acts on the locomotive dynamic model and changes the displacements and velocities of the rigid bodies. Each of those components is detailed in the following sections.

2.1 Locomotive 2D dynamic model

The locomotive dynamic model is illustrated in Figure 2. In this model longitudinal, vertical and pitching dynamics are taken into consideration. The simplified Co-Co locomotive has two bogies. Each bogie has three wheelsets attached. Key parameters including geometry, degrees of freedom etc., are marked in Figure 2.

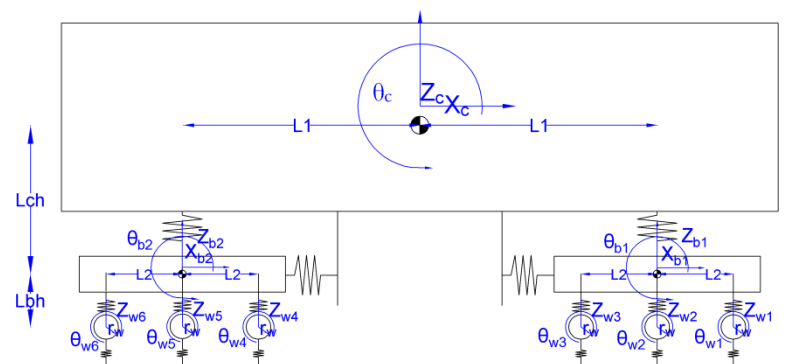


Figure 2: Diagram of simplified locomotive multibody structure

This simplified dynamic model has 21 degrees of freedom (DOF), including 9 DOF on the longitudinal, vertical and pitching motion of locomotive body and two bogies, and 12 DOF on vertical and rotating motion of six

wheelsets. The system variables are expressed as a vector containing 42 entries, representing the relative displacements and velocities between different nodes as,

$$X = [Z \quad \dot{Z}]^T, \quad Z = [Z_{carbody} \quad Z_{bogie1} \quad Z_{bogie2} \quad Z_{axles}]^T \quad (1)$$

in which $Z_{carbody} = [x_c, z_c, \theta_c]^T$ is a 3×1 vector representing the locomotive body longitudinal, vertical and pitching motion from the static positions, $Z_{bogie1} = [x_{b1}, z_{b1}, \theta_{b1}]^T$ and $Z_{bogie2} = [x_{b2}, z_{b2}, \theta_{b2}]^T$ are both 3×1 vectors representing longitudinal, vertical and pitching motion of front and rear bogie separately, and $Z_{axles} = [z_{w1}, \theta_{w1}, z_{w2}, \theta_{w2}, \dots, z_{w6}, \theta_{w6}]^T$ is a 12×1 vector representing the vertical and rotating motion of wheelset 1~6. The state space representation of the simplified dynamics can be expressed as:

$$\begin{aligned} \dot{X} &= A \cdot X + B \cdot u \\ Y &= C \cdot X + D \cdot u \end{aligned}, \quad A = \begin{bmatrix} \Theta & I \\ M^{-1}K & M^{-1}C \end{bmatrix} \quad (2)$$

where u is the longitudinal tractive force resulted from the interaction between the wheelsets and rail tracks, Y is a vector of displacement or velocity of each node from its static position, Θ is a zero matrix, I is an identity matrix of certain dimensions, and M is the diagonal mass and moment of inertia matrix in the form of

$$\begin{aligned} M &= \\ &diag(M_c, M_c, I_c, M_t, M_t, I_t, M_t, M_t, I_t, M_w, I_w, \\ &M_w, I_w, M_w, I_w, M_w, I_w, M_w, I_w, M_w, I_w) \end{aligned} \quad (3)$$

2.2 Contact mechanics

The Polach model [10] is employed in the contact mechanics component to determine the longitudinal tractive force resulted from the interaction between the wheelsets and rail tracks. In the model, the longitudinal tractive force can be expressed as,

$$F = \frac{2Q\mu}{\pi} \left(\frac{k_A \varepsilon}{1 + (k_A \varepsilon)^2} + \arctan(k_s \varepsilon) \right) \quad (4)$$

where $\mu = \mu_0 \left[(1 - A) e^{-B\omega} + A \right]$, $A = \frac{\mu_\infty}{\mu_0}$, $\varepsilon = \varepsilon_x = \frac{1}{4} \frac{G\pi abc_{11}}{Q\mu} s_x$, $s_x = \frac{w_x}{V}$ for longitudinal direction.

Parameters are defined as in [10]: F is tractive force, Q is normal wheel load, μ is the coefficient of friction, k_A is the reduction factor in the area of adhesion, k_s is the reduction factor in the area of slip, ε is the gradient of the tangential stress in the area of adhesion, ε_x is the gradient of the tangential stress in the longitudinal direction, μ_0 is the maximum friction coefficient at zero slip velocity, μ_∞ is the friction coefficient at infinite slip velocity, A is the ratio of friction coefficients, B is the coefficient of exponential friction decrease, ω is the total creep (slip) velocity, ω_x is the creep (slip) velocity in the longitudinal direction, G is the shear modulus, a, b are half-axes of the contact ellipse, c_{11} is a coefficient from Kalker's linear theory and V is vehicle speed.

Parameters describing dry and wet contact conditions have been adopted from Polach's work [10] as below:

Table 1: parameters for different contact conditions

Conditions	Parameters	Dry	Wet
	k_A	1	0.3
	k_S	0.3	0.75
	μ_0	0.55	0.3
	A	0.4	0.4
	B	0.25	0.09

The resulting creep-adhesion characteristics under dry and wet conditions are as in figure 3 a) and b) respectively,

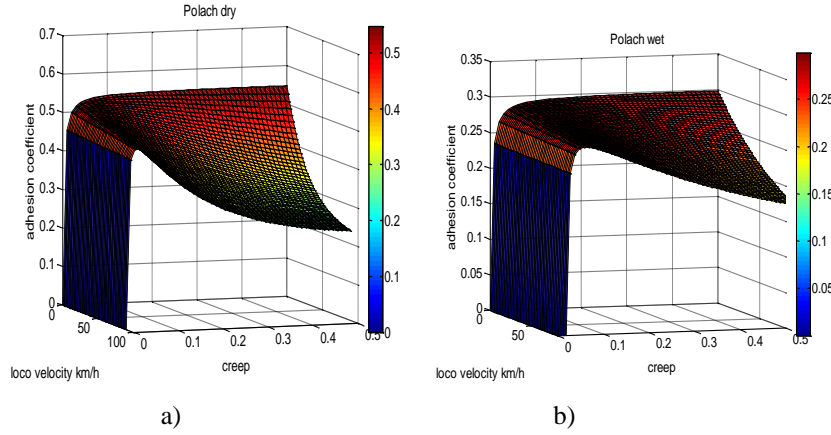


Figure 3: a) Creep, speed and adhesion coefficient relation under dry contact condition; b) Creep, speed and adhesion coefficient relation under wet contact condition

2.3 Simplified motor dynamic modelling

A simple motor dynamic model characterizing the electromagnetic torque T_e , mechanical loading T_l , the equivalent moment of inertia of the axles with the motor rotor J_m and the angular acceleration of axles $\dot{\omega}_w$ can be written as [15]

$$J_m \dot{\omega}_w = T_m - T_l \quad (5)$$

3 Proposed control system

The proposed adhesion control system utilizes the method described in [16] to determine the locomotive speed which will be used to calculate the creep values of each axle. And an adhesion force coefficient observer proposed in [13] is adopted to generate the ‘optimum’ reference motor torque signal. The control system diagram is as shown in figure 4.

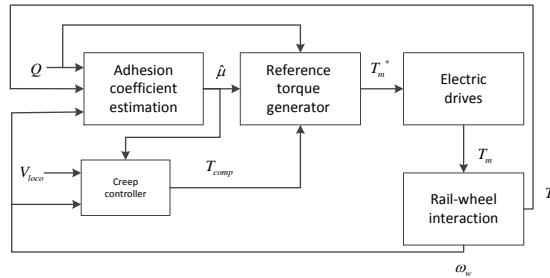


Figure 4: Adhesion control diagram

A fuzzy logic creep controller is adopted in this work as its advantage of giving strong self-adaptive and robust performance without the need of accurate mathematical model [17]. The proposed fuzzy logic controller uses the information of differentiation of each axle’s creep of and the differentiation of each axle’s adhesion coefficient, which is estimated from the change in vehicle acceleration over one sample period as proposed in [18]. Each of the fuzzy inputs of derivative of creep and derivative of adhesion coefficient are expressed by 5 fuzzy membership functions, e.g. positive big (Pb), positive small (Ps), zero (0), negative small (Ns) and negative big (Nb). The output of the fuzzy logic controller is torque compensation command to each of the motors, either to increase or reduce the electromagnetic torque acting on the motors within the range of traction limit.

Controller output:

$$T_m^*(N) = T_m^*(N-1) + T_{comp}(N) \quad (6)$$

The membership functions and control rules are in Table 2 and Figure 5 below.

Table 2: Fuzzy rule table

Derivative of creep (\dot{s})	Derivative of adhesion coefficient ($\dot{\mu}$)				
	<i>Pb</i>	<i>Ps</i>	<i>0</i>	<i>Ns</i>	<i>Nb</i>
<i>Pb</i>	<i>Pb</i>	<i>Ps</i>	<i>Ns</i>	<i>Ns</i>	<i>Nb</i>
<i>Ps</i>	<i>Ps</i>	<i>Ps</i>	<i>0</i>	<i>Nb</i>	<i>Nb</i>
<i>0</i>	<i>Ps</i>	<i>0</i>	<i>0</i>	<i>Ps</i>	<i>Ps</i>
<i>Ns</i>	<i>Ns</i>	<i>Ns</i>	<i>Ps</i>	<i>Ps</i>	<i>Pb</i>
<i>Nb</i>	<i>Ns</i>	<i>Ns</i>	<i>Ps</i>	<i>Ps</i>	<i>Pb</i>

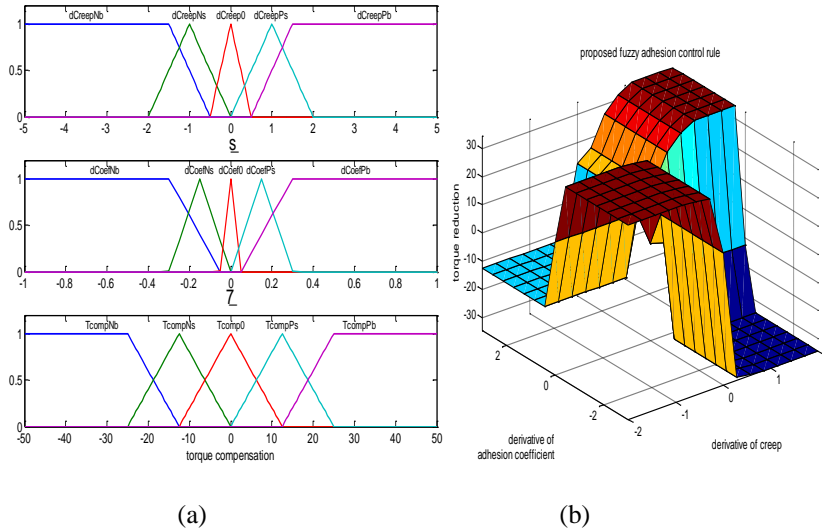


Figure 5: (a) Membership functions of inputs and output; (b) fuzzy logic 3D input-output characteristics

The fuzzy rules are designed based on [18], i.e. dividing the creep-adhesion coefficient curve into four different sessions according to the value of \dot{s} and $\dot{\mu}$ (1~4 representing sessions of dry contact condition curve; 1*~4* representing sessions of wet contact condition curve), as shown in Figure 6:

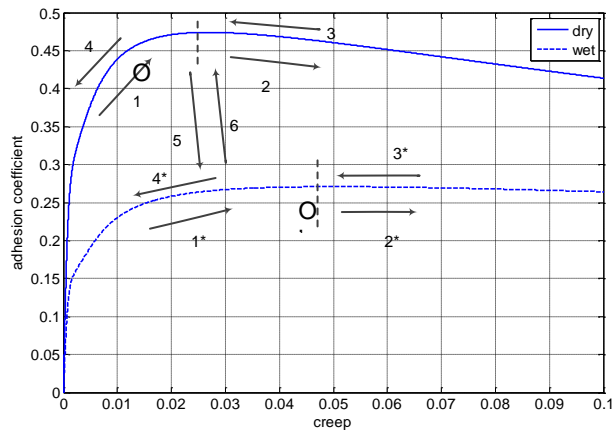


Figure 6: illustrative graph for the fuzzy rules

- 1 and 1*: \dot{s} is positive and $\dot{\mu}$ is positive
- 2 and 2*: \dot{s} is positive and $\dot{\mu}$ is negative
- 3 and 3*: \dot{s} is negative and $\dot{\mu}$ is positive
- 4 and 4*: \dot{s} is negative and $\dot{\mu}$ is negative

Moreover, transient condition caused by the change of wheel-rail contact condition is also taken into consideration. Thus two additional sessions have been added:

5: Transient from high curve to low curve- \dot{s} positive and $\dot{\mu}$ negative very large

6: Transient from low curve to high curve- \dot{s} negative and $\dot{\mu}$ positive very large

The principle of the logic is to maintain the adhesion coefficient at maximum value O for dry contact condition or O' for wet contact condition, by reducing the torque command when creep value is on the right hand side of maximum values and increasing the torque command when on the left hand side of maximum values.

4 Results

Results of transient locomotive response with proposed fuzzy logic controller are illustrated, including creep and tractive force. Initial operation speed was set at 10 km/h. Transient contact conditions are assumed to happen at 11km/h, from dry contact condition to wet condition, and change back from wet to dry contact condition at 12.5 km/h.

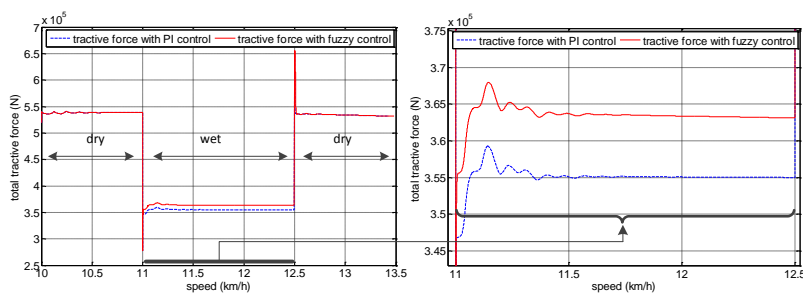


Figure 7: Comparison of total tractive force with PI and fuzzy controller (left); magnification of tractive force comparison under wet contact condition (right)

It can be seen from Figure 7 that the tractive force with PI and fuzzy controller under dry contact condition is similar, while then the fuzzy controller can reach higher tractive force than that with PI controller under wet contact condition. This can be explained as follow. As the threshold of the PI controller is chosen such that it can reach the maximum tractive force under dry contact condition near the simulation speed, the tractive force with controller are close to each other, both around the maximum tractive force the system can reach at the same speed. However, as the threshold of the PI controller is constant, it will not be able to adjust the control level according to the change of contact conditions and/or operating speed. On the other hand, the fuzzy controller search for maximum tractive force with information of \dot{s} and $\dot{\mu}$. This causes higher tractive force under wet contact condition with fuzzy controller than that with PI controller.

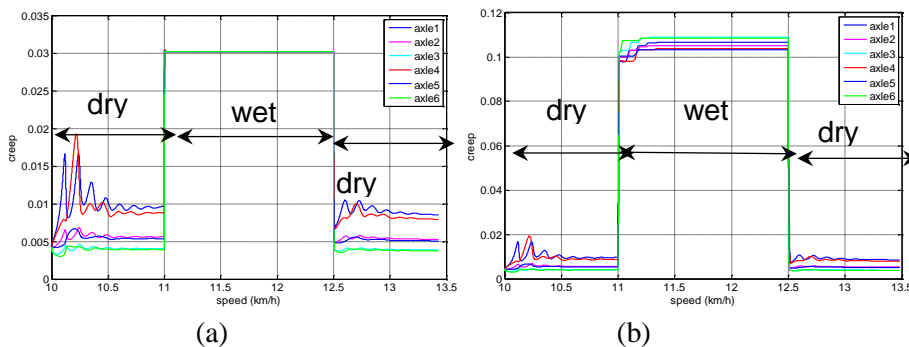


Figure 8: Comparison of creep response with PI control (a) and with fuzzy logic control (b)

In Figure 8(a), after the contact condition changes from dry condition to wet condition, the creep values have been limited at 0.03, as the pre-set threshold of the PI controller, whereas the creep values of the system with fuzzy logic are higher as in Figure 8(b), as the fuzzy controller adjusts the control effort according to the operation condition and intends to reach maximum tractive force available.

5 Conclusions

External perturbations such as the change of rail-wheel contact conditions often cause undesirable locomotive dynamic responses. In this paper, the locomotive dynamic responses under transient contact conditions with PI and fuzzy logic creep controller have been simulated with an integrated 2D Co-Co locomotive/track dynamic model. The comparison of the creep and total tractive force shows the advantage of proposed fuzzy logic controller over PI controller in term of realizing higher tractive force under the change of contact conditions. While both controllers can limit the creep under a certain level, simulation results show that the fuzzy controller can reach higher total tractive force than that with a constant threshold PI controller under wet contact condition thanks to its ability to search for the maximum achievable force according to different contact conditions.

Acknowledgement

The authors are grateful to the CRC for Rail Innovation (established and supported under the Australian Government's Cooperative Research Centres program) for the funding of this research Project No. R3.119 "Locomotive Adhesion". The authors acknowledge the support of the Centre for Railway Engineering, Central Queensland University and the many industry partners that have contributed to this project, in particular staff from RailCorp, Fortescue Metals Group (FMG) and Brookfield Rail.

References

- [1] Chudzikiewicz, A., Simulation of Rail Vehicle Dynamics in MATLAB Environment, *Vehicle System Dynamics*, vol. 33, pp. 107-119, 2000/02/01 2000.
- [2] Shimizu, Y., et al., Anti-slip/skid Re-adhesion Control Based on Disturbance Observer Considering Bogie Vibration, in *Power Conversion Conference - Nagoya, 2007. PCC '07*, pp. 1376-1381, 2007.
- [3] Spiryagin, M. et al., Development of traction control for hauling locomotives, ed.
- [4] Fleischer, M., Modal state control in the frequency domain for active damping of mechanical vibrations in traction drive-trains, in *Advanced Motion Control. AMC'04. The 8th IEEE International Workshop on*, 2004, pp. 171-176, 2004.
- [5] Bakhvalov, Y. et al., Mathematical Modelling of Electromechanical Processes in Electric Locomotive, presented at the 16th IMACS World Congress, Lausanne (Switzerland), 2000.
- [6] Senini, S. et al., Dynamic simulation of wheel-rail interaction for locomotive traction studies, in *Railroad Conference, 1993., Proceedings of the 1993 IEEE/ASME Joint*, pp. 27-34, 1993.
- [7] Law, E. H. and Cooperrider, N.K., A survey of railway vehicle dynamics research, *ASME Journal of Dynamic Systems, Measurement, and Control*, vol. 96, pp. 132-146, June 1974.
- [8] Guclu, R. and Metin, M., Fuzzy Logic Control of Vibrations of a Light Rail Transport Vehicle in Use in Istanbul Traffic, *Journal of Vibration and Control*, vol. 15, pp. 1423-1440, September 1, 2009.
- [9] Garivaltis, D. S. et al., Dynamic Response of a Six-axle Locomotive to Random Track Inputs, *Vehicle System Dynamics*, vol. 9, pp. 117-147, 1980/05/01 1980.
- [10] Polach, O., Creep forces in simulations of traction vehicles running on adhesion limit, *Wear*, vol. 258, pp. 992-1000, 2005.
- [11] Polach, O., Influence of Locomotive Tractive Effort on the Forces Between Wheel and Rail, *Vehicle System Dynamics*, vol. 35, pp. 7-22, 2001.
- [12] Doh-Young, P. et al., Hybrid re-adhesion control method for traction system of high-speed railway, in *Electrical Machines and Systems, 2001. ICEMS 2001. Proceedings of the Fifth International Conference on*, pp. 739-742 vol.2, 2001.
- [13] Ohishi, K. et al., Anti-slip control of electric motor coach based on disturbance observer, in *Advanced Motion Control, 1998. AMC '98-Coimbra., 1998 5th International Workshop on*, pp. 580-585, 1998.
- [14] Yasuoka, I. et al., Improvement of re-adhesion for commuter trains with vector control traction inverter, in *Power Conversion Conference - Nagaoka 1997., Proceedings of the*, pp. 51-56 vol.1, 1997.
- [15] Marino, R. et al., *Induction Motor Control Design*: Springer, 2010.
- [16] Spiryagin, M. et al., Control system for maximum use of adhesive forces of a railway vehicle in a tractive mode, *Mechanical Systems and Signal Processing*, vol. 22, pp. 709-720, 2008.
- [17] Yuan, Y. et al., The dynamic study of locomotives under saturated adhesion, *Vehicle System Dynamics*, vol. 49, pp. 1321-1338, 2011/08/01 2011.
- [18] Bauer, M. and Tomizuka, M., Fuzzy Logic Traction Controllers and their Effect on Longitudinal Vehicle Platoon Systems, *Vehicle System Dynamics*, vol. 25, pp. 277-303, 1996/04/01 1996.

Paper C

**Fuzzy Logic based Sliding Mode Creep
Controller under Varying Wheel-Rail Contact
Conditions**

Comparison of PI and fuzzy logic based sliding mode locomotive creep controls with change of rail-wheel contact conditions

Ye Tian^{a,*}, W.J.T. (Bill) Daniel^{a,b}, Sheng Liu^a and Paul A. Meehan^{a,b}

^a*School of Mechanical and Mining Engineering, the University of Queensland, Queensland, Australia 4072;*

^b*Cooperative Research Centre for Rail Innovation (CRC Rail), Queensland, Australia*

This paper presents locomotive traction controllers based on PI and sliding mode control with a fuzzy logic creep reference generator; and compares their performance based on tractive efforts under various operation speeds. The effect of change of wheel-rail friction conditions under different controllers is also investigated. In particular, a sliding mode traction controller based on a fuzzy logic creep reference generator is developed to tackle nonlinearity and uncertainty due to the contact conditions and operation speeds. It is shown that at high speed operation, the fuzzy logic based sliding mode controller can achieve higher tractive force with lower creep values.

Keywords: fuzzy logic; sliding mode control; traction control

Nomenclature

x_c	Locomotive body longitudinal displacement
z_c	Locomotive body vertical displacement
θ_c	Locomotive body pitch angle
$x_{b1,2}$	Locomotive front/rear bogie longitudinal displacement
$z_{b1,2}$	Locomotive front/rear bogie vertical displacement
$\theta_{b1,2}$	Locomotive front/rear bogie pitch displacement
$z_{w1\sim6}$	Wheelset 1~6 vertical displacement
$\theta_{w1\sim6}$	Wheelset 1~6 rotation angle
M_c, M_t, M_w	Mass of locomotive body, bogie and axle
I_c, I_t, I_w	Moment of inertia of locomotive body, bogie and axle along pitch direction
Q	Wheel load
μ	Friction coefficient
ε	Gradient of the tangential stress in the area of adhesion
k_A, k_S	Reduction factor in the area of adhesion, reduction factor in the area of slip
μ_∞	Friction coefficient at infinity slip velocity
μ_0	Maximum friction coefficient at zero slip velocity
s_x	Creep in longitudinal (x) directions
V	Vehicle speed
w_x	Creep (slip) velocity in longitudinal (x) direction
a, b	Half-axes of the contact ellipse
c_{11}	Coefficient from Kalker's linear theory
F, G	Tractive force, Shear modulus
T_{ti}	Torque generated by electric drive $i=1\sim6$
T_{li}	Torque acting on axle $i=1\sim6$ generated by longitudinal contact force

1. Introduction

The progressive application of high traction motors and control techniques based on power electronics has brought great benefits to the rail industry due to its high power capacity and efficiency. Therefore, an effective control system is demanded to suit the contemporary high speed railway network. Traditionally, traction controller performance and its dynamic impact on rail are typically assessed under specific steady state conditions. In particular, traction controller performance under natural perturbations in friction/lubrication, wheel/rail profiles, track curvature, vehicle/track dynamics, wheel/track imperfections etc. has not been comprehensively investigated yet. Among those perturbations, the transient changes in friction or lubrication can cause sudden changes of creep and often lead to over/under traction/braking. In order to investigate this issue, a predictive locomotive dynamic model combining crucial dynamic components such as locomotive rigid body dynamics, contact dynamics and electric drive and control is needed.

Locomotive traction simulations have been investigated by several researchers. Spiriyagin et al. employed a co-simulation approach with the Gensys multibody code and Simulink to investigate the heavy haul train traction dynamics [1]. Bakhvalov et al. combined electrical and mechanical processes for locomotive traction simulation [2]. Senini et al. has also performed some locomotive traction simulation on a simplified single wheel model [3]. These works, however, haven't focused investigation on the effect of transient contact conditions on the locomotive dynamic response. Modern development of mechatronics systems has improved rail vehicle operation under various conditions. The traction control system, also known as an adhesion or anti-slip control system is essential for the operational efficiency and reliability of these systems. A pattern-based slip control method has been applied and modified by Park et al. [4]. Anti-slip control based on a disturbance observer was proposed by Ohishi et al. [5]. Yasuoka et al. proposed a slip control method [6] involving bogie oscillation suppression. All these methods claim the effectiveness of their proposed creep/traction control; however, these conclusions were not validated on a comprehensive locomotive dynamic model. Fuzzy logic control has also been used to control the traction / braking force of locomotive vehicles due to its robustness. Garcia-Rivera et al. have proposed a fuzzy logic controller to constrain the slip velocity [7]. The results show the effectiveness of limiting the slip velocity. However, that method cannot guarantee the achievement of maximum force. Cheok et al. proposed a fuzzy logic controller and validated its effectiveness by experiment comparing it with a traditional PID method [8]. However their research mainly focused on constant contact conditions and hence the control performance was not tested under a change of contact conditions. Khatun et al proposed a fuzzy logic controller for an electric vehicle antilock braking system and simulations have been performed for icy to dry contact condition changes [9]. However it was only tested on a single axle model and the transient response from dry to other conditions was not investigated. Park et al. [10] proposed an adaptive sliding mode controller in order to deal with system uncertainties. A fuzzy logic method was used to generate a reference slip ratio. Although the method has been simulated with a simplified rolling stock quarter model, the performance on a whole locomotive dynamic model with dynamic interaction throughout the structural/controller system during the change of contact condition were not addressed.

In this paper, a full scale locomotive longitudinal-vertical-pitch dynamic model with a PI creep controller and a fuzzy logic sliding mode controller combining all crucial dynamic components is developed and implemented using Matlab/Simulink. The tractive performance is compared during a change of contact conditions. We focus on longitudinal and vertical dynamics on tangent tracks, as it is the most important part of locomotive dynamics closely related with traction/braking effort, passenger comfort and energy management [11]. A Newton-Euler method [12, 13] is used to obtain the motion equations of the locomotive model. For the contact mechanics, Polach's adhesion model [14] is adopted as it has been verified to be effective for both small and large values of longitudinal wheel-rail creep as well as the decreasing part of the creep-force function exceeding the adhesion limit [15]. The tractive performance and transient dynamics in creep and motion, particularly at different locomotive speeds, are compared and analysed.

2. Simulation modelling

In order to study the dynamics and interactions between different components of the overall locomotive dynamics, three major subsystems are taken into consideration for the modelling process; namely, locomotive multi-body dynamics, electric drive/control dynamics and contact mechanics. The structure of the model is shown in Figure 1. A dynamics model of the mechanical system of an electric locomotive based on the Newton-Euler method [16] is developed. The wheel-rail contact in this model is based on Polach's model [14]. A simplified electric drive model with a basic PI creep controller and a fuzzy logic sliding mode creep controller is proposed and integrated into the electric drive/control dynamics block in this model.

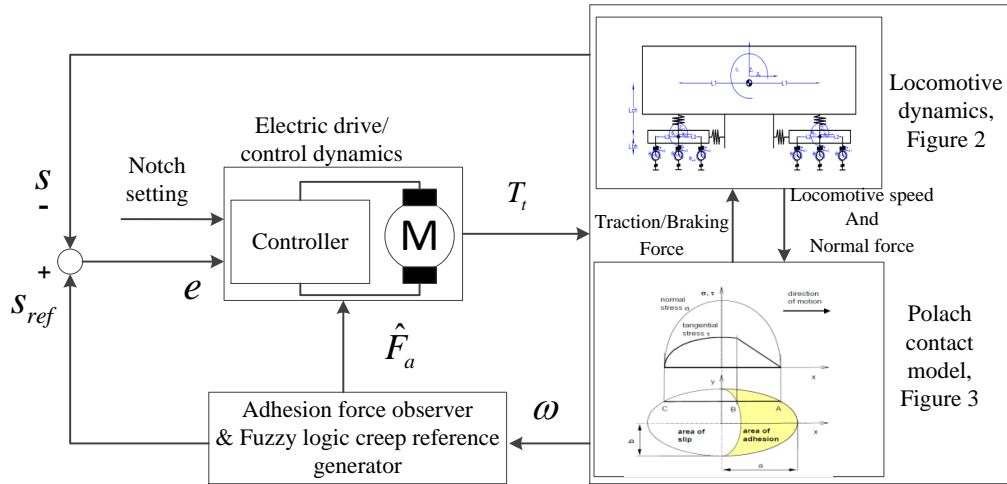


Figure 1. Schematic diagram of the overall system.

The model may be described as a feedback system. The rotational speeds of axles are constantly measured and used to generate a reference creep. The creep value on each axle is also calculated with the information of the speed of each axle and the locomotive speed. The controller then adjusts the amount of torque generated by the electric drives accordingly. The electric drive and control system provides a torque acting on the motor shaft in the locomotive model. Torque also results from the longitudinal force due to the interaction between wheel-rail track contact mechanics. The resultant creep changes the longitudinal tractive force calculated using the Polach model, and the tractive force acts on the locomotive dynamic model and changes the displacements and velocities of the rigid bodies. Each of those components is detailed in the following sections.

2.1. Locomotive longitudinal-vertical-pitch dynamic modelling

A 2-dimensional locomotive dynamic model is shown in Figure 2, which emphasizes longitudinal, vertical and pitch dynamics of locomotive operation. An assumption has been made that the motors are fixed on the bogie evenly and no relative displacement between the motors and bogie is considered in order to simplify the model. The pitch motions of the wagons and car body (θ_{b1} , θ_{b2} and θ_c) will be affected by the traction motor dynamics. In particular, the torque generated by the motor changes the contact creep which determines the tractive torque causing pitch motions of the wagons and car body. A commonly used Newton-Euler approach was used to obtain the locomotive dynamic equations in a similar manner as previous research [19-22].

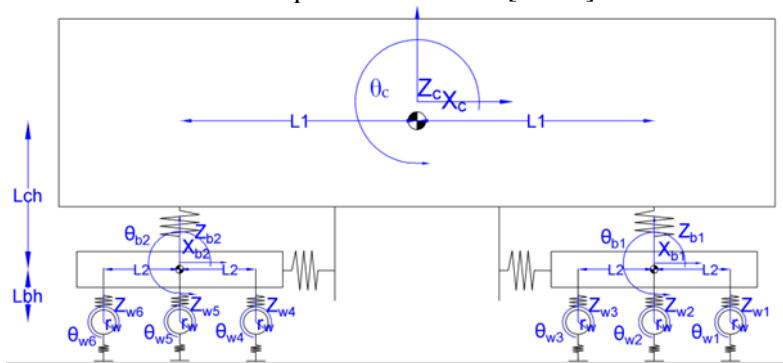


Figure 2. Locomotive longitudinal-vertical dynamic diagram.

This model has 21 degrees of freedom (DOF), including 9 DOF of the longitudinal, vertical and pitch motions of the locomotive body and its two bogies, and 12 DOF of vertical and rotating motions of six wheelsets. The system variables are expressed as a vector containing 42 entries, representing the relative displacements and velocities between different nodes as,

$$X = [Z \ \dot{Z}]^T, Z = [Z_{carbody} \ Z_{bogie1} \ Z_{bogie2} \ Z_{axles}]^T, \quad (1)$$

in which $Z_{carbody} = [x_c \ z_c \ \theta_c]^T$ is a 3×1 vector representing the locomotive body longitudinal, vertical and pitch motions from the static positions, $Z_{bogie1} = [x_{b1} \ z_{b1} \ \theta_{b1}]^T$ and $Z_{bogie2} = [x_{b2} \ z_{b2} \ \theta_{b2}]^T$ are both 3×1 vectors representing longitudinal, vertical and pitch motions of the

front and rear bogie separately, and $Z_{axles} = [z_{w1} \ \theta_{w1} \ z_{w2} \ \theta_{w2} \ \dots \ z_{w6} \ \theta_{w6}]^T$ is a 12×1 vector representing the vertical and rotating motions of wheelset 1~6. The state space representation of the dynamics can be expressed as:

$$\begin{aligned} \dot{X} &= A \cdot X + B \cdot u, \\ Y &= C \cdot X + D \cdot u, \end{aligned} \quad A = \begin{bmatrix} \Theta & I \\ M^{-1}K & M^{-1}C \end{bmatrix}, \quad (2)$$

where u is the longitudinal tractive force resultant from the interaction between the wheelsets and rail tracks, Y is a vector of displacement or velocity of each node from its static position, Θ is a zero matrix, I is an identity matrix of certain dimensions, and M is the diagonal mass and moment of inertia matrix in the form of,

$$M = \text{diag}(M_c \ M_c \ I_c \ M_t \ M_t \ I_t \ M_t \ M_t \ I_t \ M_w \ I_w \ M_w \ I_w \ M_w \ I_w \ M_w \ I_w \ M_w \ I_w \ M_w \ I_w). \quad (3)$$

Detailed locomotive parameters are shown in Appendix A as provided by industry partners. The terms $M^{-1}K$ and $M^{-1}C$ are defined as A_{21} and A_{22} separately and are provided in Appendix B.

Eigenmode analysis

An eigenmode analysis was performed in Matlab to identify all the dynamic modes of vibration and to determine the stability of the system. The system eigenvalues are provided in Table 1. An eigenvalue is obtained for each possible mode of vibration of the system. The first part (real value) of each complex eigenvalue represents the amount of damping (if negative) of each mode of vibration. The second part (imaginary number) represents the part from which the frequency of vibration can be calculated. From the eigenvalues of the system, it can be seen that except for the car body horizontal mode, all modes of vibration have positive damping (negative real parts) which implies that the system is stable. A car body horizontal mode with zero damping is expected due to the rigid body longitudinal motion of the train.

Table 1. Modal frequencies of the locomotive dynamic system vibrations (Hz) and corresponding eigenvalues.

Modes	Frequency (Hz)	Eigenvalues	Modes	Frequency (Hz)	Eigenvalues
Car body vertical	0.3	$-2.9 \pm 1.9i$	Bogie 1 vertical	3.1	$-2.9 \pm 20.6i$
Car body pitching	1.8	$-2.1 \pm 11.4i$	Bogie 2 vertical	3.3	$-1.7 \pm 20.8i$
Bogie pitching	3.3	$-1.7 \pm 20.8i$	Wheelset vertical	137.5	$-17 \pm 864i$

2.2. Creep force modelling

The creep force is caused by the rolling contact of wheel-rail interaction and is crucial in terms of locomotive traction/braking operation. Polach determined the tangential force along the rail tracks based on his experimental data as [16],

$$F = \frac{2Q\mu}{\pi} \left(\frac{k_A \varepsilon}{1 + (k_A \varepsilon)^2} + \arctan(k_S \varepsilon) \right), \quad (4)$$

where F is the tangential force, Q is normal wheel load, k_A is the reduction factor in the area of adhesion and k_S is the reduction factor in the area of slip. ε is the gradient of the tangential stress in the area of adhesion which along the longitudinal direction (defined as x direction in figure 1) can be calculated as,

$$\varepsilon_x = \frac{1}{4} \frac{G\pi abc_{11}}{Q\mu} S_x, \quad (5)$$

where G is the shear modulus, a and b are the semi-axes of the contact ellipse as shown in Figure 3, c_{11} is derived from Kalker's work [23] and characterizes the longitudinal direction of the contact shear stiffness coefficient. Also S_x is the creep component in longitudinal direction defined as

$$S_x = \frac{w_x}{V}, \quad (6)$$

where w_x is the slip velocity in longitudinal direction and V is the vehicle speed.

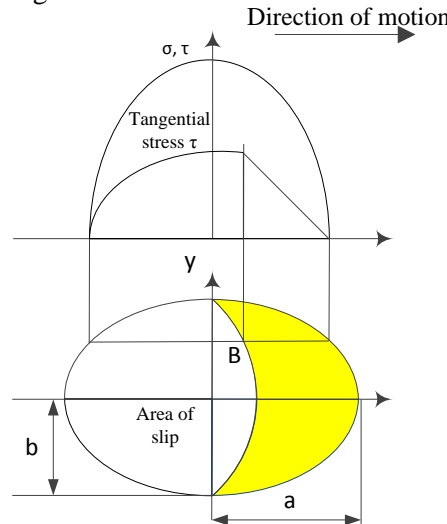


Figure 3. : Wheel-rail contact area and distribution of normal and tangential stresses [27].

As lateral dynamics is not considered in this paper, total creep s equals creep along the longitudinal direction s_x . The coefficient of friction μ is calculated as

$$\mu = \mu_0[(1 - A)e^{-Bw} + A], \quad (7)$$

where μ_0 is the maximum friction coefficient at zero slip velocity, A is the ratio of friction coefficient at infinity slip velocity μ_∞ and μ_0 , B is the coefficient of exponential friction decrease. Typical model parameters have been provided by Polach [16], as listed in Table 2. The contact patch dimensions shown in Figure 3 are specified as $a = 6 \times 10^{-3} \text{ m}$ and $b = 6 \times 10^{-3} \text{ m}$.

Table 2. Typical parameters for dry and wet contact condition [16].

Parameters	Contact condition	
	Dry	Wet
k_A	1.00	0.30
k_s	0.40	0.10
μ_0	0.55	0.30
A	0.40	0.40
B	0.60	0.20

As it is shown in Figure 4, the critical creep- at which maximum tractive force occurs shifts towards the lower creep values as the speed of locomotive increases. As a result, setting the reference creep to be constant will cause traction performance degradation over different locomotive operation speeds.

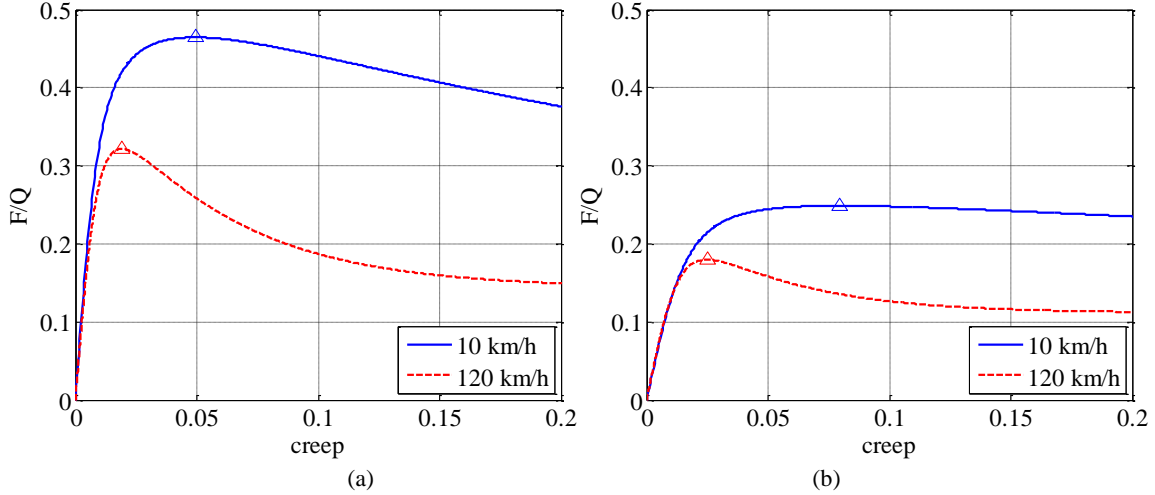


Figure 4. Polach tractive force curve at different speeds under (a) dry contact condition; and (b) under wet contact condition.

2.3. Wheel traction dynamic modelling

A simple wheel traction dynamic model characterizing the traction torque acting from the electric motor on a wheelset T_{ti} , external loading T_{li} , the equivalent moment of inertia of the axle with the motor rotor J , and the angular acceleration of axle $\dot{\omega}_{wi}$ can be written as [24]

$$J\dot{\omega}_{wi} = T_{ti} - T_{li}, i = 1, 2, \dots, 6 \quad (8)$$

3. Proposed control system

The proposed adhesion control system utilizes the method described in [9] with control torque acting on each axle.

3.1. Fuzzy logic

Fuzzy logic systems are based on fuzzy set theory [25]. Fuzzy sets derive from a grouping of elements into classes that do not possess sharply defined boundaries [8]. Since fuzzy logic uses fuzzy linguistic rules based on expert knowledge and specific numeric data without the existence of a suitable mathematical model [26], it has the ability to tackle uncertainties and nonlinearity [6].

The conventional locomotive adhesion/traction control scheme and that based on fuzzy logic are shown in Figure 5.

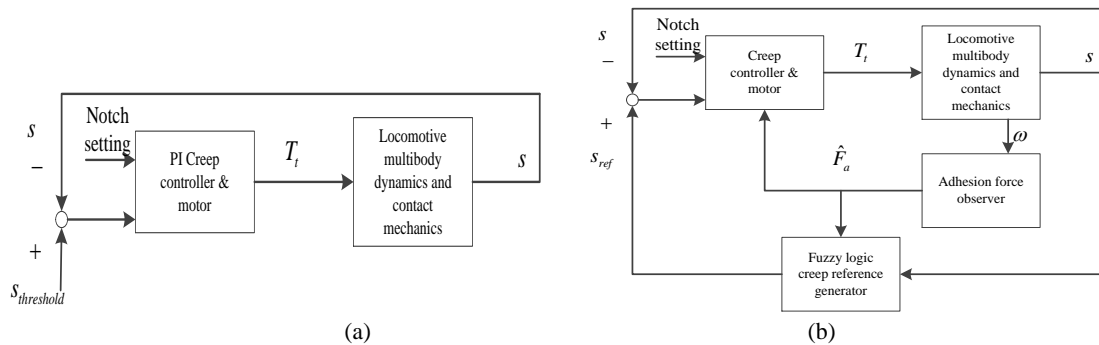


Figure 5. Adhesion control diagram (a) with a PI creep controller; (b) with fuzzy logic based sliding mode controller.

The reference creep is calculated with the fuzzy logic method based on the derivative of creep \dot{s} and derivative of adhesion coefficient $\dot{\mu}(s)$. The updating law of reference slip is,

$$s_{ref}^k = s_{ref}^{k-1} + \Delta^k(\dot{s}, \dot{\mu}), \quad (9)$$

where updating term $\Delta^k(\dot{s}, \dot{\mu})$ is calculated with fuzzy logic. As the peak value of the adhesion coefficient occurs when $d\mu/ds = 0$, the update term can be chosen as $d\mu/ds$. For a discrete time system, it can be represented by,

$$\frac{\mu^k - \mu^{k-1}}{s^k - s^{k-1}}, \quad (10)$$

where the value of adhesion coefficient μ on the numerator is approximated with the ratio between \hat{F}_a and normal contact force between the wheel and the rail. The whole term in equation (10) is used as the input of the reference generator.

The fuzzy logic takes this as its input and calculates an updating term according to Table 3 and membership functions in Figure 6. Both input and output has four membership functions, e.g. negative big (NB), negative small (N), positive small (P) and positive big (PB). The output of the fuzzy system is the updating term Δ^k .

Table 3. Fuzzy rule table.

INPUT		OUTPUT
NB		NB
N		N
P		P
PB		PB

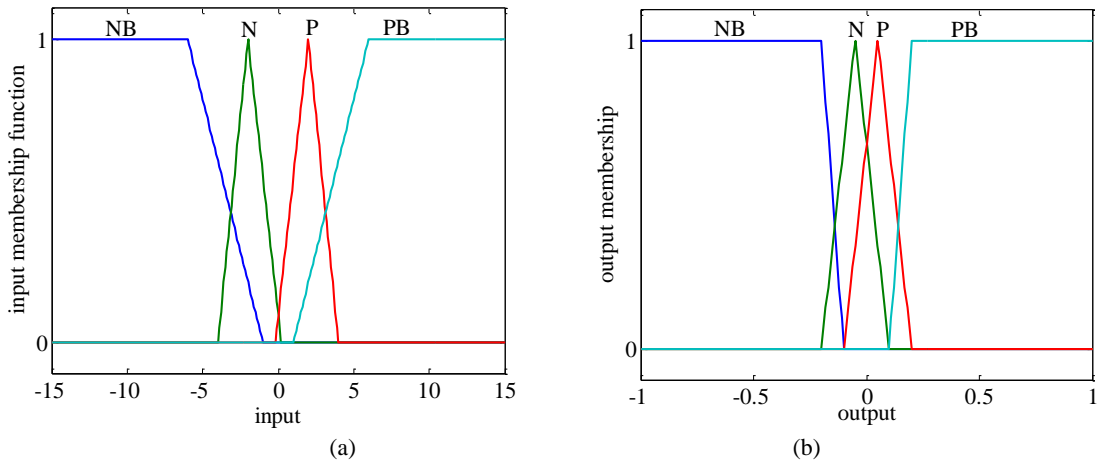


Figure 6. (a) Membership functions of input; (b) Membership functions of output.

Values from equation (10) correspond with values of the input in Figure 6 (a), with which corresponding fuzzy values μ_{NB} , μ_N , μ_P and μ_{PB} can be obtained from the vertical axis in Figure 6 (b). Consequently, the centre of gravity method is employed as the defuzzification method in this paper. This method calculates the value z^* for a fuzzy number \tilde{C} as in [100]27]

$$z^* = \frac{\int z \mu_{\tilde{C}}(z) dz}{\int \mu_{\tilde{C}}(z) dz}, \quad (11)$$

where $\mu_{\tilde{C}}$ denotes the membership function of the fuzzy number \tilde{C} (NB, N, P and PB).

The sliding mode control law [9] is designed with a simplified system dynamic model with one axle and 1/6 of total dynamic mass and then integrated into the locomotive dynamics. The sliding surface $S(t)$ for the sliding mode controller is defined as,

$$S(t) = e + \gamma \int_0^t e dt, \quad (12)$$

with $e = s_{ref} - s$ represents the tracking error between the creep reference s_{ref} and the actual creep s . γ is a positive design parameter. The derivative of the sliding surface, after taking account of the simplified system dynamics, can be expressed as,

$$\dot{S} = \dot{s}_{ref} - \frac{r}{JV} T_t + \frac{r^2}{JV} F_a - \frac{1}{MV} (s + 1) F_a + \gamma e = -D_c s - K_s \text{sgn}(s). \quad (13)$$

The tractive force can be estimated by:

$$\hat{F}_a = \frac{1}{r} T_t - \frac{J}{r \tau s + 1} s, \quad (14)$$

where τ is the time constant of the first order filter in the adhesion force observer [9]. Thus the tractive torque can be obtained as,

$$T_t = \frac{JV}{r} \left\{ \dot{s}_{ref} + \gamma e + \left[\frac{r^2}{JV} - \frac{1}{MV} (s + 1) \right] \hat{F}_a + D_c s + K_s \text{sgn}(s) \right\}. \quad (15)$$

3.2. PI controller

PI controllers are widely used in many industries [28]. They use feedback to reduce the effects of disturbance. Usually the feedback is compared with a reference value to obtain an offset. Through integral action it can eliminate steady-state offsets. It can also anticipate the future through derivative action [29].

In this work, a PI controller is tuned which employs pre-set creep as a reference. With the offset between the reference and actual creep value, it generates the torque command accordingly. The PI controller parameters are tuned as $1.5 \times 10^7 N \cdot m$ and $2 \times 10^5 N \cdot m/s$ for the proportional and integral coefficients respectively.

4. Results

The following assumptions are made in the simulations: 1) A single powered locomotive is considered hauling a number of wagons, which are modelled as an equivalent trailing mass. No other resistance such as drag and air resistance is considered in this simulation; 2) A low speed simulation case is chosen to investigate the dynamic behaviour of highest tractive force case, namely the starting process of a locomotive; 3) The high speed simulation case is chosen below the maximum speed of the locomotive (about 128 km/h); 4) The tractive effort is limited by both the contact mechanics and the characteristic traction speed curve of the electric drive.

The dynamic response comparison with PI and fuzzy controllers employs speed rather than time as the horizontal axis because the adhesion coefficient, under the same contact condition, is determined by the creep and locomotive speed. As a result the change of contact condition is assumed to happen at a certain speed to ensure the same force condition.

The results comparing locomotive response obtained with PI and fuzzy logic sliding mode controllers are presented, focussing on tractive force and speed/acceleration, at speeds of 10 km/h and 120km/h. Transient contact conditions are assumed to occur at 11km/h from dry to wet and at 12.5km/h from wet to dry for the low speed simulation. Similarly, for the high speed simulation case, the contact condition changes at 119.5km/h, and back to a dry condition at 120km/h.

Figure 7 shows the creep and normalized tractive force curve at high speed (120km/h) under both dry and wet contact conditions. Maximum tractive forces are marked as a triangle.

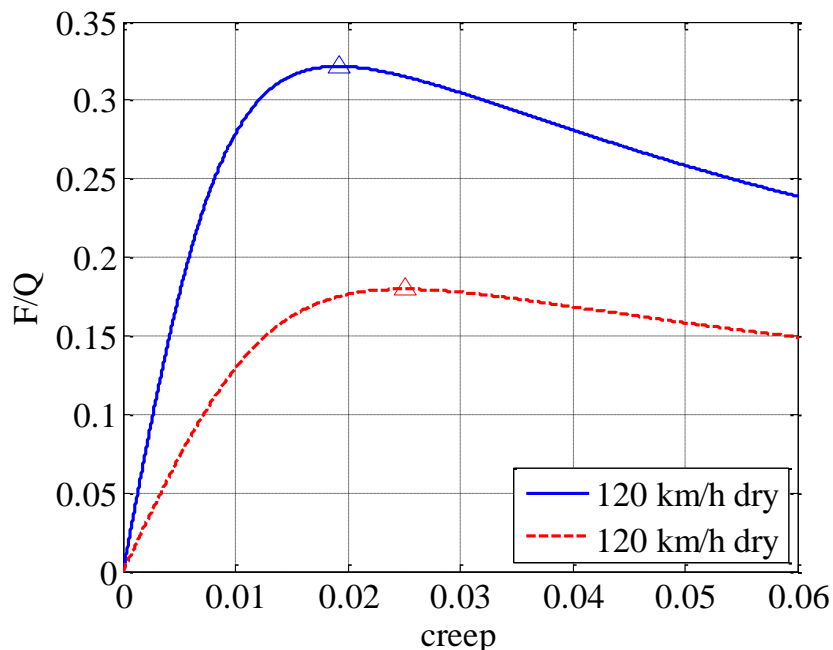


Figure 7. Polach tractive force curve at 120km/h under dry and wet contact conditions.

As shown in Figure 4, the characteristic curve of the creep and adhesion coefficient relation varies under different operation speeds. In order to compare the tractive performance under the same condition, the change of contact conditions is considered to be triggered by speed, and thus the following figures showing forces and creep employ speed as the horizontal axis.

In the first simulation, the contact condition is assumed to change during a very low speed operation, namely starting from 10km/h. The transient tractive forces with different controllers are plotted in Figure 8:

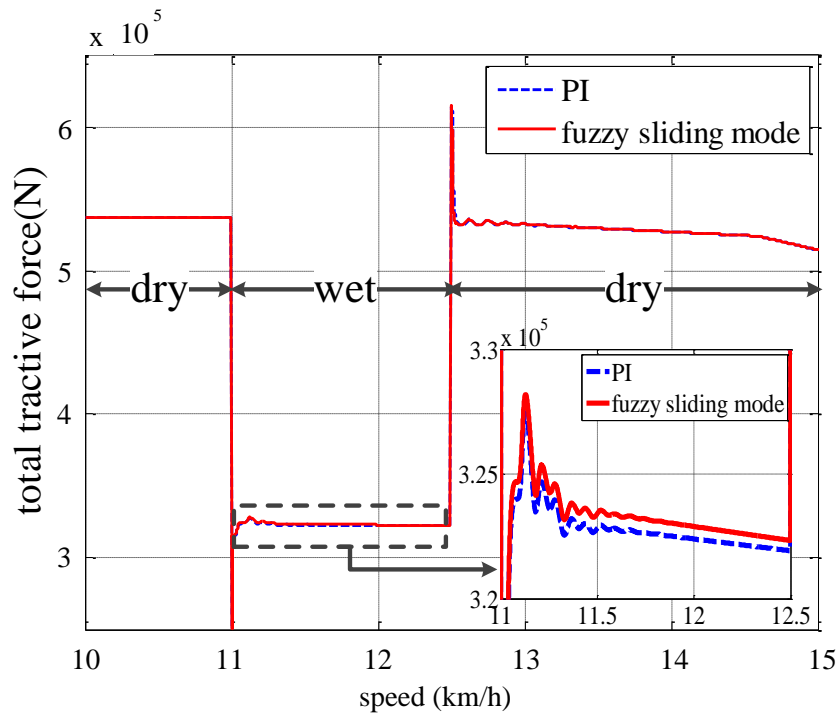


Figure 8. Comparison of total tractive forces with PI and fuzzy sliding mode control at low speed.

At low speed, as shown in Figure 8, the tractive force with fuzzy sliding mode control is very similar to that with PI control, except under the wet condition when the fuzzy sliding mode control achieves marginally higher tractive force than PI control.

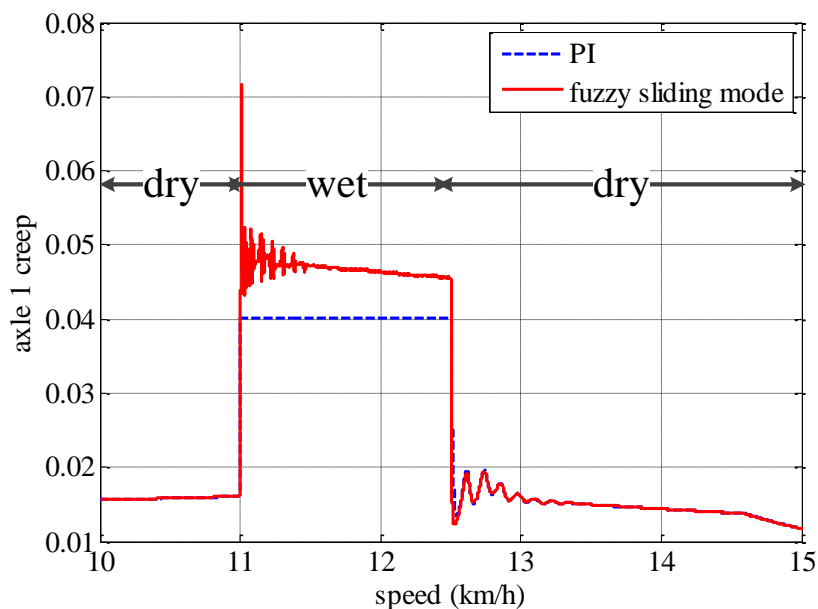


Figure 9. Creep of the front axle under change of contact conditions at low speed.

The creep of all axles is similar with the same controller. The creep of the front axle is shown in Figure 9 to compare the creep response with the PI controller and with the fuzzy sliding mode one. It can be seen that at low speeds the creep of each axle with fuzzy sliding mode control is higher than that with PI control, however, the tractive force, as shown in Figure 8, is very similar. The similarity of the tractive force is caused by the relative flat area of the creep-tractive force curve in Figure 4. In

particular, the difference of the tractive force between when creep is 4% as with the PI control and about 4.5% with fuzzy logic sliding mode control is about 1%, as shown in Figure 4 (b). At such a low speed, the creep of each axle with fuzzy sliding mode control, however, is much higher than that with PI control, as shown in Figure 9. Therefore in this case the fuzzy controller does not have an apparent advantage over the PI one in terms of tractive effort and creep control. Figure 10 shows front and rear bogie pitch motion during low speed operation.

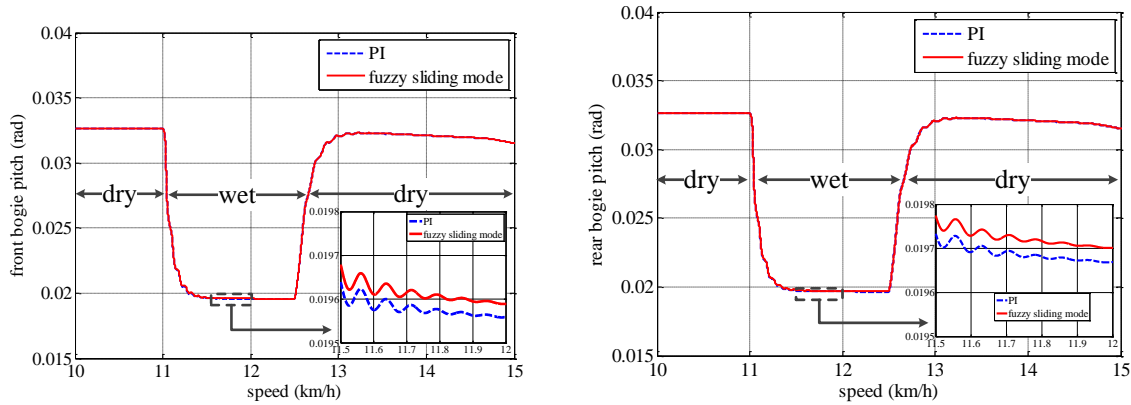


Figure 10. Bogie pitch motion during operation.

As the tractive force with PI and fuzzy control is similar as shown in Figure 8, the bogie pitch motion has a similar dynamic response with PI and the fuzzy controller as shown in Figure 10. Figure 11 shows weight distribution on each axle during low speed operation.

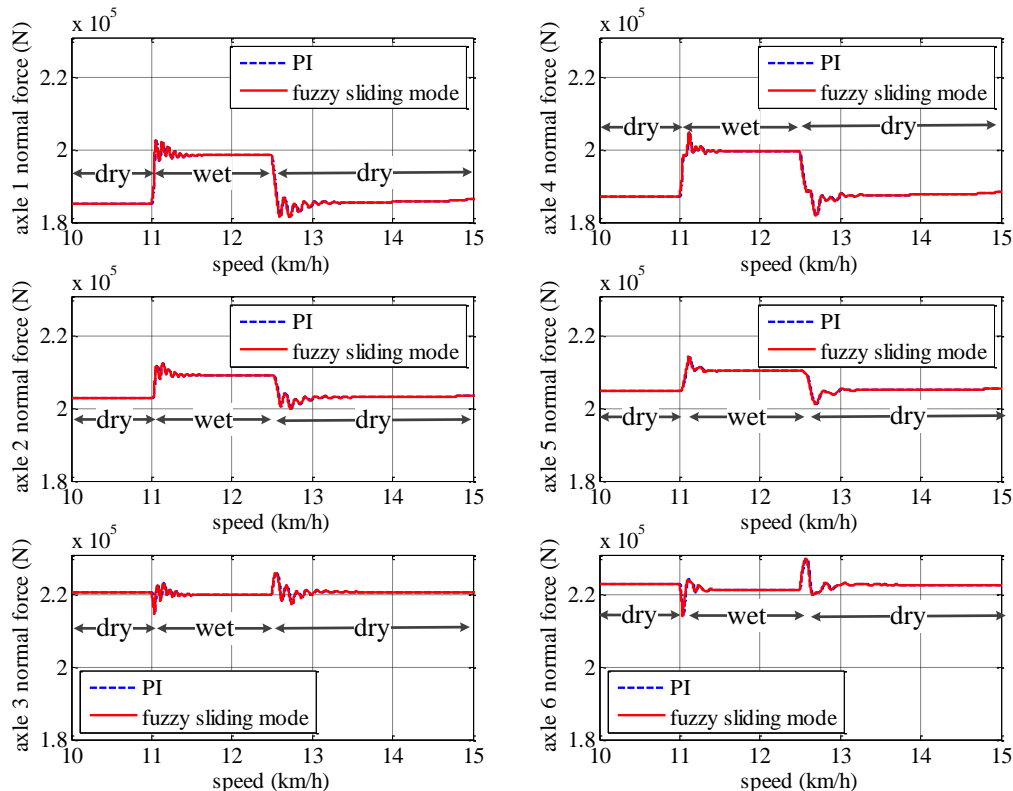


Figure 11. Weight distribution on each axle.

Similar dynamic responses are observed in Figure 11 due to the similar tractive force achieved with different controllers.

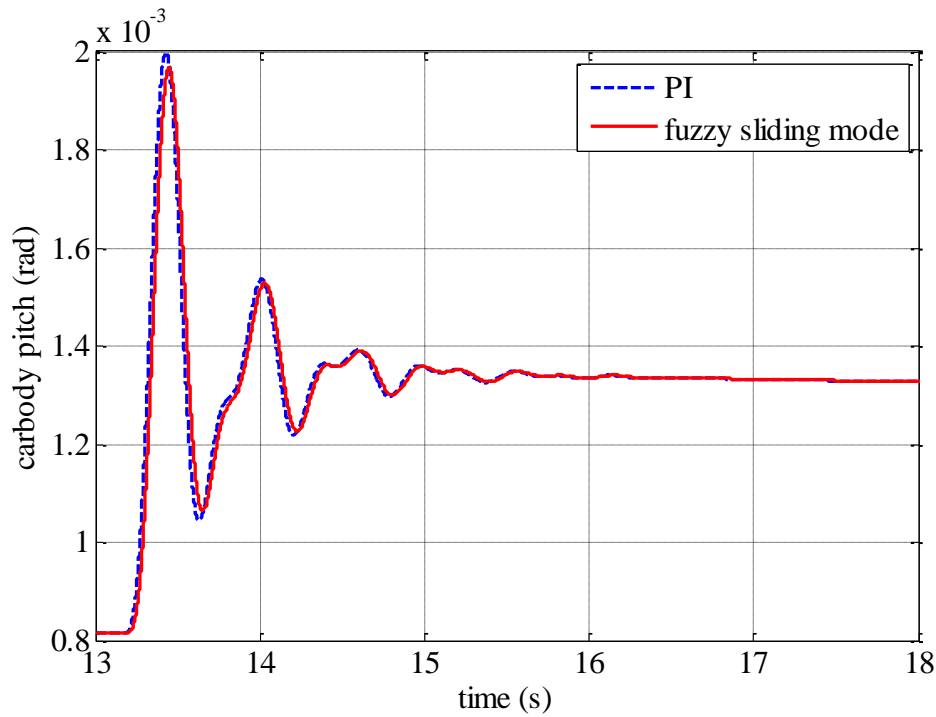


Figure 12. Car body pitch motion at low speed.

The pitch motion of the car body, when the contact condition changes from dry to wet, is as shown in Figure 12. The pitch motions with different control methods are mostly identical to each other, due to the similarity of tractive force dynamics with different control. The major frequency component of the car body pitch dynamic is 1.8 Hz which agrees with the modal frequency analysis as in Table 1. The pitch motion of the locomotive body is also affected by bogie pitch motion with a frequency about 3.3 Hz.

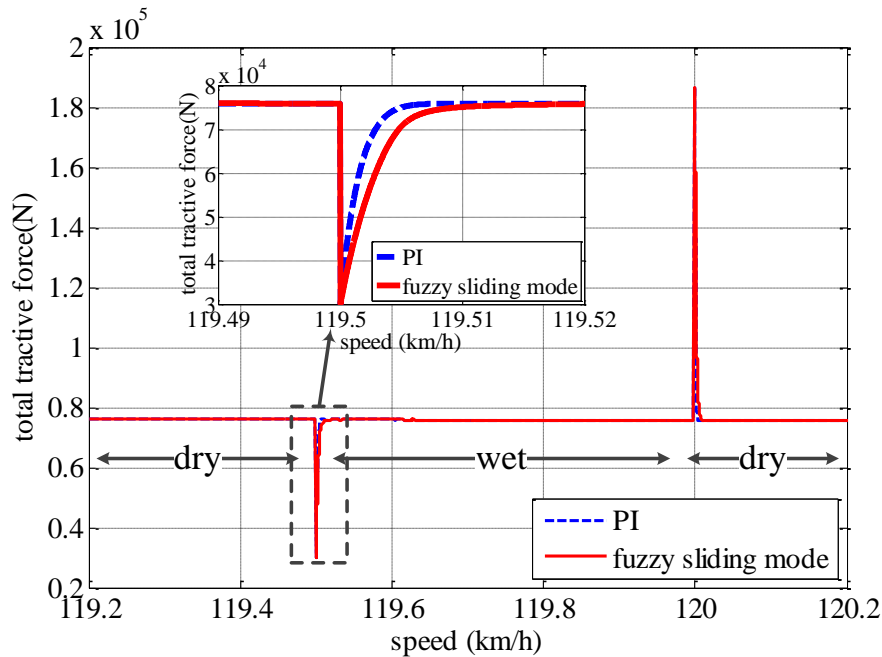


Figure 13. Comparison of total tractive forces with PI and fuzzy sliding mode control at high speed.

At high operation speed, as shown in Figure 13, the tractive force with fuzzy sliding mode control is almost the same with that with PI control. This phenomenon is caused by the limit of

electric drive tractive effort. As a result, the shift of the peak tractive force due to the change of operation speed, as shown in Figure 7 will not affect the control effort.

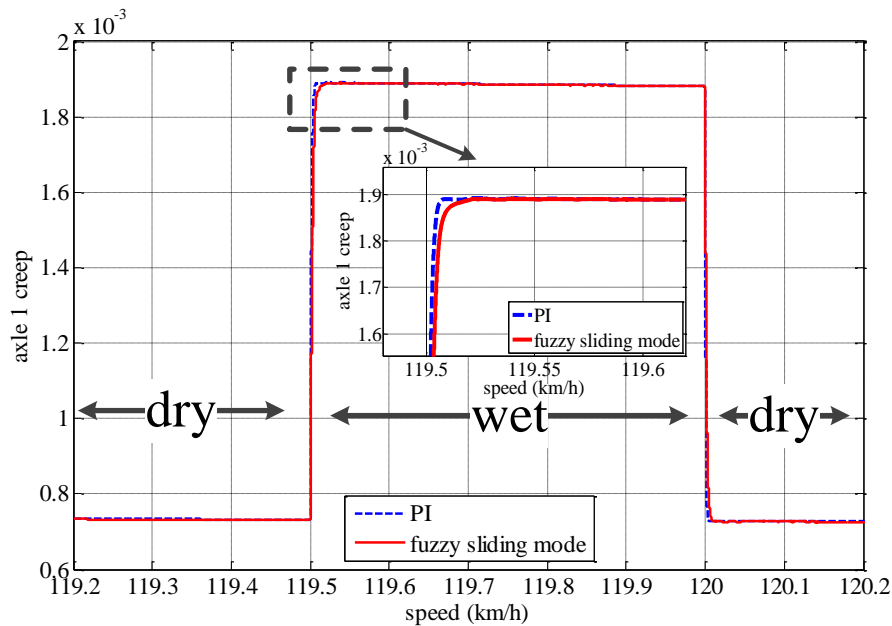


Figure 14. Creep of the front axle under change of contact conditions at high speed.

Figure 14 shows the comparison of creep response of the front axle with a PI and a fuzzy sliding mode controller. Due to the constraint of electric drive tractive effort, at high speed, the creep of each axle with fuzzy sliding mode control is similar.

Figure 15 shows front and rear bogie pitch motion during operation.

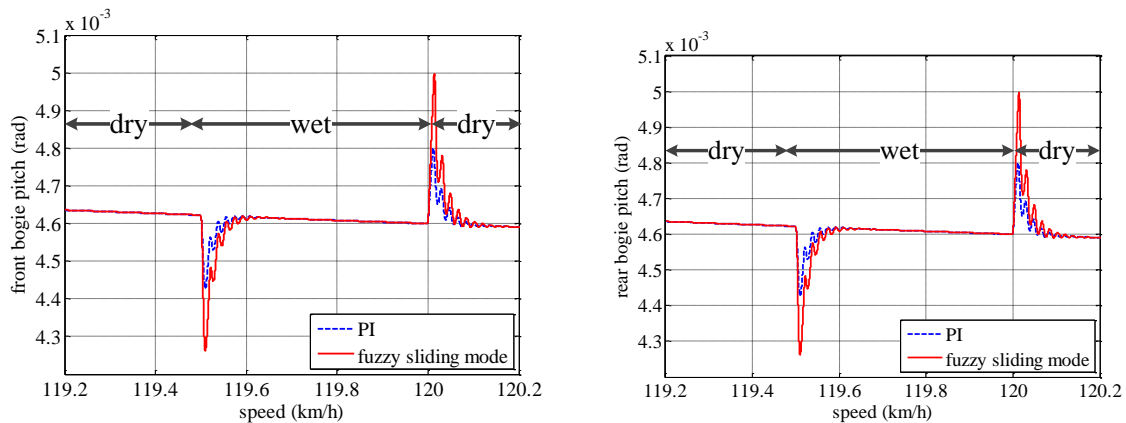


Figure 15. Bogie pitch motion during operation.

The fuzzy control achieves higher tractive force spikes as shown in Figure 13, thus higher torque spikes that cause the bogie pitch motion. Consequently, the pitch angle spikes of the fuzzy control are higher than those with the PI control. Figure 16 shows weight distribution on each axle during operation.

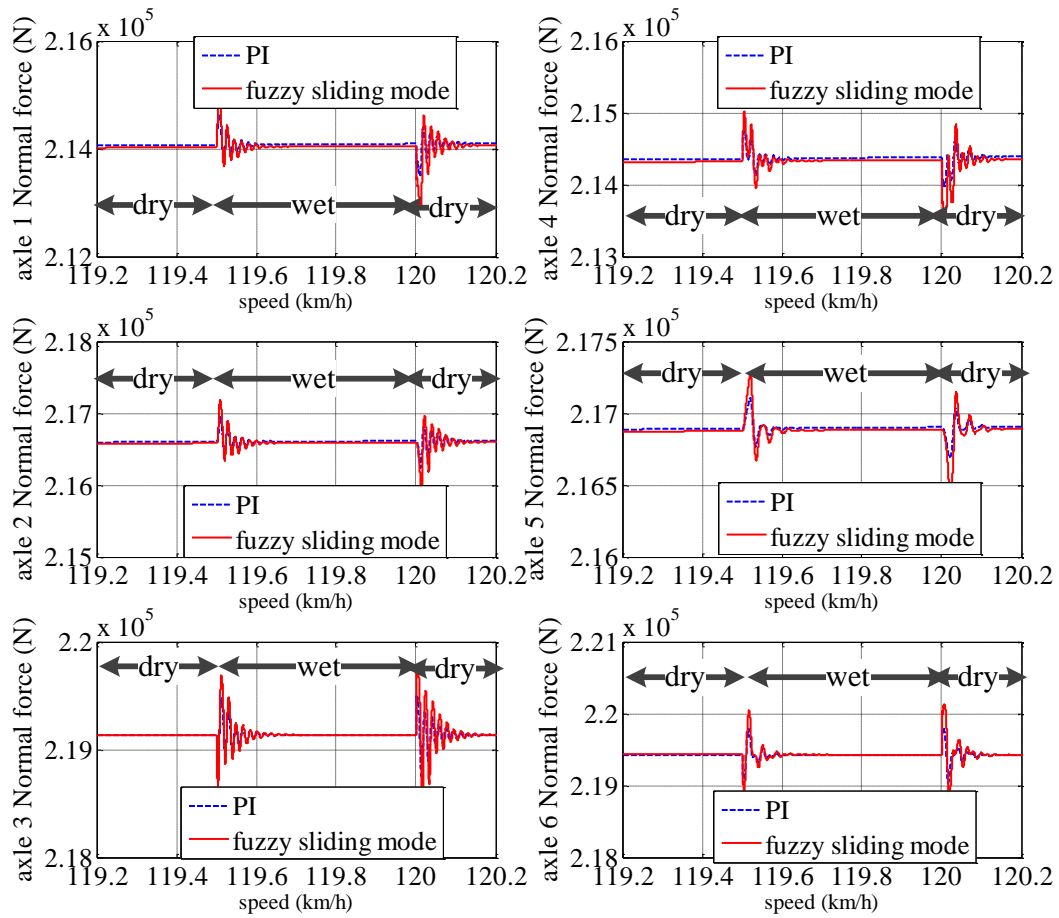


Figure 16. Weight distribution on each axle.

As shown in Figure 16, normal force between the rear axle and track is the highest due to the pitch motion of the bogies.

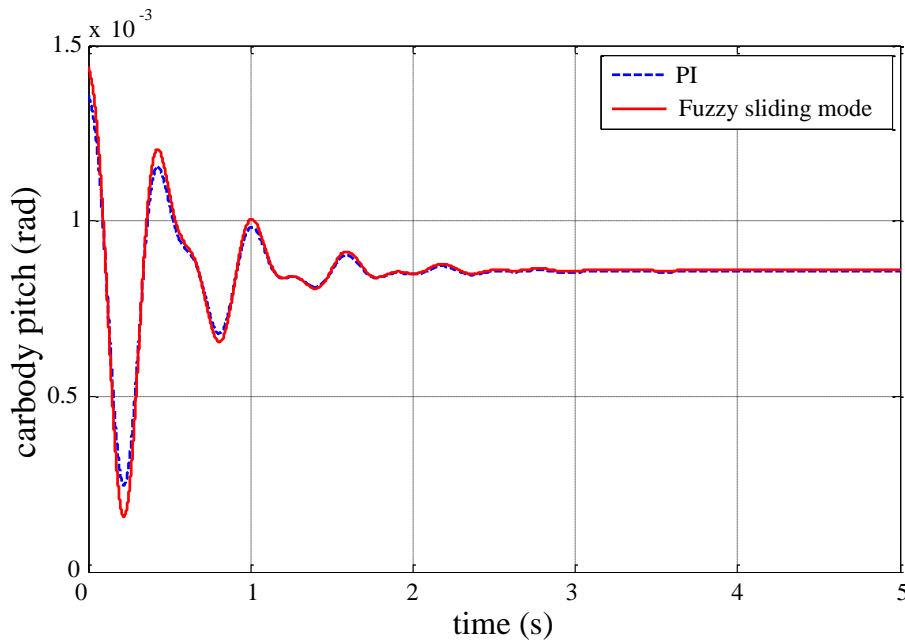


Figure 17. Car body pitch motion at high speed.

The car body pitch motion at high speed, when the contact condition changes from dry to wet, is shown in Figure 17. The responses with sliding mode control and PI control are similar, except that the amplitude of pitch angle spikes with fuzzy sliding mode control is higher than that with PI control. From Figure 13, the fuzzy sliding mode control provides similar tractive force with the PI control. The higher tractive force spikes provide the car body a larger torque about the pitch direction, and thus causes higher pitch angle spikes than those with PI control.

5. Conclusion

In this paper, total tractive performances and the dynamic responses with PI and fuzzy sliding mode creep controllers under transient contact conditions have been compared by using a proposed 21 DOF locomotive dynamic model. The PI controller was set a constant creep reference while the fuzzy controller searches continuously for a creep value that can achieve the maximum adhesion coefficient under various contact conditions.

Simulations have been carried out to compare total tractive performance with PI and fuzzy sliding mode controllers under transient contact conditions. Results show that the proposed fuzzy sliding mode controller has an advantage in maintaining a higher tractive force than PI controllers at a low operation speed but it is small for the conditions simulated. At high operation speed, the tractive effort is almost identical due to the limitations of the electric drive tractive effort.

Acknowledgements

The authors are grateful to the CRC for Rail Innovation (established and supported under the Australian Government's Cooperative Research Centres program) for the funding of this research Project No. R3.119 "Locomotive Adhesion". The authors acknowledge the support of the Centre for Railway Engineering, Central Queensland University and the many industry partners that have contributed to this project, in particular staff from RailCorp, Fortescue Metals Group (FMG) and Brookfield Rail.

References

- [1] Bakhvalov Y, Kolpahchyan P, Plokhov E, Yanov V, Zarifian A. Mathematical modelling of electromechanical processes in electric locomotive. 16th IMACS World Congress; 2000; Lausanne, Switzerland.
- [2] Senini S, Flinders F, Oghanna W. Dynamic simulation of wheel-rail interaction for locomotive traction studies. Proceedings of the 1993 IEEE/ASME Joint Railroad Conference; 1993 Apr 6-8; Pittsburgh, Pennsylvania.
- [3] Doh-Young P, Moon-Sup K, Don-Ha H, Joo-Hoon L, Yong-Joo K. Hybrid re-adhesion control method for traction system of high-speed railway. Proceedings of the 5th International Conference on Electrical Machines and Systems; 2001 Aug 18-20; Shenyang, China.
- [4] Ohishi K, Nakano K, Miyashita I, Yasukawa S. Anti-slip control of electric motor coach based on disturbance observer. The 5th International Workshop on Advanced Motion Control; 1998 Jun 29- Jul 1; Coimbra, Portugal.
- [5] Yasuoka I, Henmi T, Nakazawa Y, Aoyama I. Improvement of re-adhesion for commuter trains with vector control traction inverter. Proceedings of the Power Conversion Conference; 1997 Aug 3-6; Nagaoka, Japan.
- [6] Garcia-Rivera M, Sanz R, Perez-Rodriguez JA. An antislipping fuzzy logic controller for a railway traction system. Proceedings of the 6th IEEE International Conference on Fuzzy Systems; 1997 Jul 1-5; Barcelona, Spain .
- [7] Cheok AD, Shiomi S. Combined heuristic knowledge and limited measurement based fuzzy logic antiskid control for railway applications. IEEE Transactions on Systems, Man, and Cybernetics, Part C: Applications and Reviews. 2000; 30(4):557-568.
- [8] Khatun P, Bingham CM, Schofield N, Mellor PH. Application of fuzzy control algorithms for electric vehicle antilock braking/traction control systems. IEEE Trans Veh Technol. 2003; 52(5):1356-1364.
- [9] Park S, Kim J, Choi J. Reference slip ratio generation and adaptive sliding mode control for railway rolling stocks. Int J Precis Eng Manuf. 2009; 10(2):39-44.
- [10] Spiriyagin M, Simson S, Cole C, Persson I. Co-simulation of a mechatronic system using Gensys and Simulink. Vehicle Syst Dyn. 2012; 50(3):495-507.
- [11] Spiriyagin M, Lee KS, Yoo HH. Control system for maximum use of adhesive forces of a railway vehicle in a tractive mode. Mech Syst Signal Pr. 2008; 22(3):709-720.
- [12] Spiriyagin M, Cole C, Sun YQ. Adhesion estimation and its implementation for traction control of locomotives. Int J Rail Transport. 2014; 2(3):187-204.
- [13] Law EH, Cooperrider NK. A survey of railway vehicle dynamics research. J Dyn Syst-T ASME. 1974; 96(2):132-146.
- [14] Guclu R, Metin M. Fuzzy logic control of vibrations of a light rail transport vehicle in use in istanbul traffic. J Vib Control. 2009; 15(9):1423-1440.
- [15] Garivaltis DS, Garg VK, D'Souza AF. Dynamic response of a six-axle locomotive to random track inputs. Vehicle Syst Dyn. 1980; 9(3):117-147.
- [16] Polach O. Creep forces in simulations of traction vehicles running on adhesion limit. Wear 2005, 258(7-8):992-1000.
- [17] Spiriyagin M, Polach O, Cole C. Creep force modelling for rail traction vehicles based on the FastSim algorithm. Vehicle Syst Dyn. 2013; 51(11):1765-1783.
- [18] Ardena MD. Newton-Euler Dynamics: Springer; 2006.
- [19] Hou K, Kalousek J, Dong R. A dynamic model for an asymmetrical vehicle/track system. J Sound Vib. 2003; 267(3):591-604.
- [20] Lei X, Noda NA. Analyses of dynamic response of vehicle and track coupling system with random irregularity of track vertical profile. J Sound Vib. 2002; 258(1):147-165.
- [21] Chang EH, Garg VK, Goodspeed CH, Singh SP. Comparative study of the linear and non-linear locomotive response. J Dyn Syst Meas Control. 1979; 101(3):263-271.
- [22] Xia H, Guo WW, Xia CY, Pi YL, Bradford MA. Dynamic interaction analysis of a LIM train and elevated bridge system. J Mech Sci Technol. 2009; 23(12):3257-3270.
- [23] Kalker J. On the rolling contact of two elastic bodies in the presence of dry friction. Doctoral Thesis. Delft; 1967.
- [24] Marino R, Tomei P, Verrelli CM. Induction motor control design: Springer; 2010.
- [25] Zadeh LA. Fuzzy sets. Inform Control. 1965; 8(3):338-353.
- [26] Djukić M, Rusov S, Mitrović Z. A fuzzy model for an increase in locomotive traction force. Transport. 2010; 25(1):36-45.
- [27] Ross TJ. Fuzzy logic with engineering applications: Wiley; 2004.
- [28] Astrom KJ. PID controllers: theory, design and tuning. Instrument Society of America 1995.
- [29] Åström KJ, Hägglund T. Advanced PID control: ISA-The Instrumentation, Systems, and Automation Society; 2006.

APPENDIX A

Detailed parameters of the locomotive model:

Parameter	Value
mass of each bogie frame (kg)	12121
total mass of locomotive (t)	134
load mass (kg/wagon × no. of wagons)	90000 × 50
Gear Ratio	17/90
Primary suspension springs (N/m)	89×10^6
Vertical viscous dampers stiffness(N/m)	44×10^6
Secondary suspension springs (N/m)	5.2×10^6
Longitudinal stiffness(N/m)	5×10^6
Wheel contact stiffness (N/m)	2.4×10^9
Primary suspension vertical damping (kg/s)	10×10^3
Secondary suspension vertical damping (kg/s)	2×10^4
Rail damping (kg/s)	1×10^6
Locomotive body length (m)	22
Locomotive body height – without bogie (m)	1.93
Bogie length (m)	3.7
Bogie height (m)	0.733
Horizontal distance between bogies' mass centres (m)	13.7
Horizontal distance between axles (m)	1.3
Vertical distance between body bottom and bogie top (m)	0.3605
Vertical distance between bogie bottom and wheel top (m)	0.127
Wheel diameter (m)	1.016
Simulation time step (s)	5×10^{-6}
Creep threshold	4%

APPENDIX B

Detailed mathematical model for the longitudinal-vertical-pitch dynamics of the locomotive

Paper D

Investigation of the impact of full scale locomotive adhesion control on wear under changing contact conditions

Investigation of the impact of locomotive creep control on wear under changing contact conditions

Ye Tian^{1,2}, Sheng Liu¹, W.J.T. (Bill) Daniel^{1,2}, Paul A. Meehan^{1,2}

¹School of Mechanical and Mining Engineering, the University of Queensland, Queensland, Australia 4072

²Cooperative Research Centre for Railway Innovation (CRC Rail), Queensland, Australia

ABSTRACT

This paper presents the locomotive traction controller performance with respect to the track wear under different operation conditions. In particular, an investigation into the dynamic response of a locomotive under changing wheel-rail friction conditions is performed with an aim to determine the effect of controller setting on track wear. Simulation using a full scale longitudinal-vertical locomotive dynamic model shows that the appropriately designed creep threshold, controller, settings can effectively maintain high tractive effort while avoiding excessive rail damage due to wear, especially during acceleration under low speed.

Nomenclature

x_c	Locomotive body longitudinal displacement
z_c	Locomotive body vertical displacement
θ_c	Locomotive body pitch angle
$x_{b1,2}$	Locomotive front/rear bogie longitudinal displacement
$z_{b1,2}$	Locomotive front/rear bogie vertical displacement
$\theta_{b1,2}$	Locomotive front/rear bogie pitch displacement
$z_{w1\sim6}$	Wheelset 1~6 vertical displacement
$\theta_{w1\sim6}$	Wheelset 1~6 rotation angle
$M_c M_b M_w$	Mass of locomotive body, bogie and axle
$I_c I_b I_w$	Moment of inertia of locomotive body, bogie and axle along pitch direction
Q	Wheel load
μ	Friction coefficient
ε	Gradient of the tangential stress in the area of adhesion
k_A, k_S	Reduction factor in the area of adhesion, reduction factor in the area of slip
μ_∞	Friction coefficient at infinity slip velocity
μ_0	Maximum friction coefficient at zero slip velocity
s_x	Creep in longitudinal (x) directions
V	Vehicle speed
w_x	Creep (slip) velocity in longitudinal (x) direction
a, b	Half-axes of the contact ellipse
c_{11}	Coefficient from Kalker's linear theory
F, G	Tractive force, Shear modulus
T_{ti}	Torque generated by electric drive $i=1\sim6$
T_{li}	Torque acting on axle $i=1\sim6$ generated by longitudinal contact force

1. Introduction

The progressive application of high traction motors and control techniques based on power electronics has brought great benefits to the rail industry due to its high power capacity and efficiency. Therefore, an effective locomotive control system is demanded to suit the contemporary high speed railway network. Traditionally, the traction controller performance and dynamic impact on the rail are assessed under specific steady state conditions. In particular, traction controller performance under natural perturbations in friction/lubrication, wheel/rail profiles, track curvature, vehicle/track dynamics, wheel/track imperfections etc. has not been comprehensively investigated yet. Among those perturbations, the changes in friction or lubrication can cause sudden changes of creep and often leads to over/under traction/braking. In order to investigate this issue, a predictive locomotive dynamic model combining crucial dynamic components such as locomotive rigid body dynamics, contact dynamics and electric drive and control is needed.

Locomotive traction dynamics and rail wear have been investigated by several researchers. Bakhvalov et al. combined electrical and mechanical processes for locomotive traction simulation [1]. Senini et al. has also performed locomotive traction simulation at the electric drive level [2]. These works, however, are not focused on the effect of transient of the contact conditions and different controller settings on the rail wear; especially for a full-scale locomotive case. Modern development of mechatronics systems has improved rail vehicle operation under various conditions. The traction control system, also known as an adhesion or anti-slip control system is essential for the operational efficiency and reliability of these systems. A pattern-based slip control method has been applied and modified by Park et al. [3]. An anti-slip control method based on a disturbance observer was proposed by Ohishi et al. [4]. Yasuoka et al. proposed a slip control method [5] involving bogie oscillation suppression. Most recently Spiriyagin et al. employed a co-simulation approach with the Gensys multibody code and Simulink to investigate the heavy haul train traction dynamics [6] and fuzzy logic control [7] and adhesion estimation based control [8] to maximize adhesive forces. Yuan et al. proposed a fuzzy logic adhesion controller [9]. Mei et al. investigated a mechatronic approach to control the wheel slip based on the information on the torsional vibration of the wheelset [10]. Zhao et al. proposed an extended Kalman filter (EKF) based re-adhesion controller [11]. All these methods are reported to be effective in creep/traction control; however, the implementation of these methods to the rail industry can be challenging or costly as these methods require for the reliable high speed processors and/or high accuracy sensors. While on the other hand, a PI/PID controller has is one of the most widely used control methods in various industrial applications, comparing to methods such as fuzzy logic control, observer based control, extended Kalman filter based or torsional vibration based control. As a result, a PI controller is employed in this work to reveal the real case of locomotive operation and its possible effects on rail wear with different controller parameters. Wear phenomenon in the rail industry and its modelling has been studied for decades [12-15], however, the impact of locomotive dynamic response on wear phenomena under different conditions has not been investigated deeply.

In this paper, the dynamic response of a full scale locomotive model with a traction controller under different speed and/or contact conditions is investigated in relation to the rail wear. This work focus on longitudinal and vertical dynamics on tangent tracks as it is the most important part of locomotive dynamics closely related with traction/braking effort, passenger comfort and energy management [16]. A full scale locomotive longitudinal-vertical-pitch dynamic model with a PI creep controller combining all crucial dynamic components is developed and implemented using Matlab/Simulink and the wear rate [15] is compared before and after a change of contact conditions under a range of operational speed. A Newton-Euler method [17, 18] is used to obtain the motion equations of the locomotive model. For the contact mechanics, Polach's adhesion model [19] is adopted as it has been verified to be relatively accurate for the application in the field of locomotive traction analysis [20].

2. Simulation modelling

In order to study the impact of the operation of a full scale locomotive on rail damage due to wear phenomenon, a model considering all essential dynamic components needs to be developed. In this study, three major subsystems are taken into consideration for the modelling process; namely, a mathematical model representing the dynamics of a locomotive along longitudinal and vertical directions, electric drive/control dynamics, and contact mechanics. The structure of the model is shown in Figure 1. A dynamic

model of the mechanical system of an electric locomotive based on the Newton-Euler method [21] is developed. The wheel-rail contact in this model is based on Polach's model [19]. A simplified electric drive model with a PI creep controller is integrated into the electric drive/control dynamics block in this model.

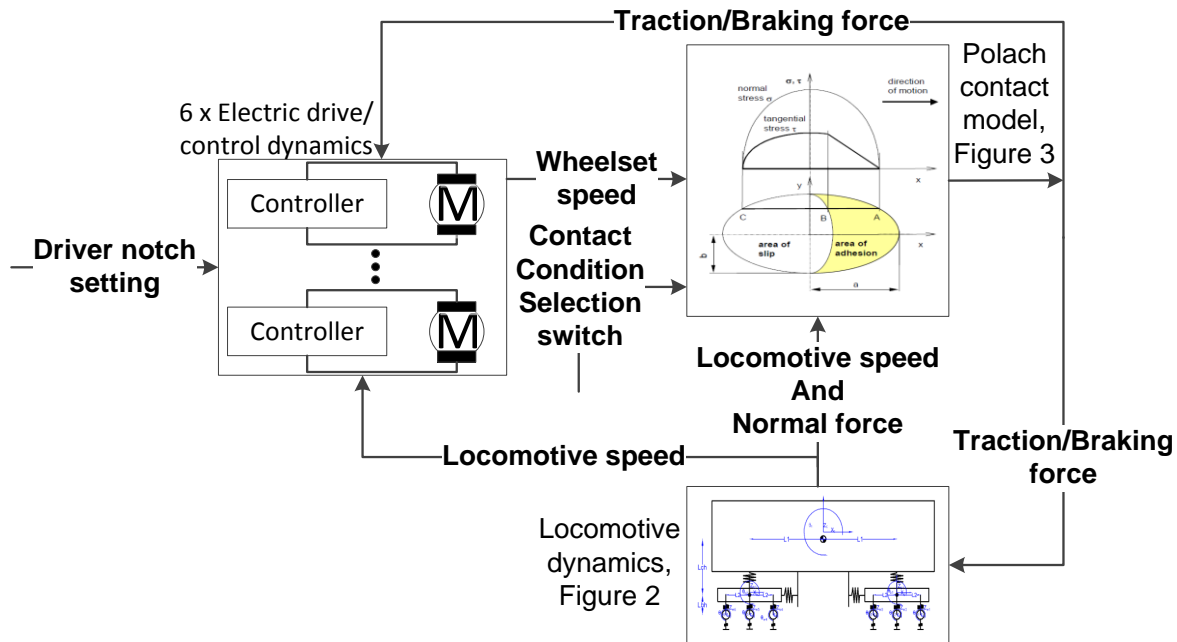


Figure 1: Schematic diagram of the overall system

The model may be described as a feedback system. The rotational speeds of axles are constantly measured by tachometers on the axles and used to generate reference creep. The position/speed information of the railway vehicle can be monitored by using a microwave ground speed sensor such as a Pegasem GSS20 [22, 23]. The creep value on each axle is also calculated with the information of the speed of each axle and the locomotive speed. The controller then adjusts the amount of torque generated by each electric drive separately. The electric drive and control system provides a torque acting on the motor shaft in the locomotive model. Torque also results from the longitudinal force due to the interaction between wheel-rail track contact mechanics. The resultant creep changes the longitudinal tractive force calculated using the Polach model, and the tractive force acts on the locomotive dynamic model and changes the displacements and velocities of the vehicle rigid bodies. Each of these components is detailed in the following sections.

2.1. Locomotive longitudinal-vertical dynamic modelling

A full scale 2-dimensional locomotive dynamics model is shown in Figure 2, which emphasizes longitudinal, vertical and pitch dynamics of locomotive motion. An assumption has been made that the motors are fixed on the bogie evenly and no relative displacement between the motors and bogie is considered in order to simplify the model. The reasons that there is no longitudinal motion between wheelsets and bogies in this study are: 1. To simplify the calculation and save simulation time while maintaining most of the essential dynamics; 2. As for a typical three-piece freight vehicle bogie, axles are mounted on the bogies via axleboxes (Figure 3.37, [24]). The stiffness between the axlebox and bogie tends to be relatively larger than that of other parts, thus the relevant motion between the axles and bogies tend to be very small; 3. The main purpose of this study is to investigate the effect of controller threshold on wear growth. While taking longitudinal motion between bogies and axles into consideration will give a more preferable and detailed dynamic model, it wouldn't change the main conclusion of this study.

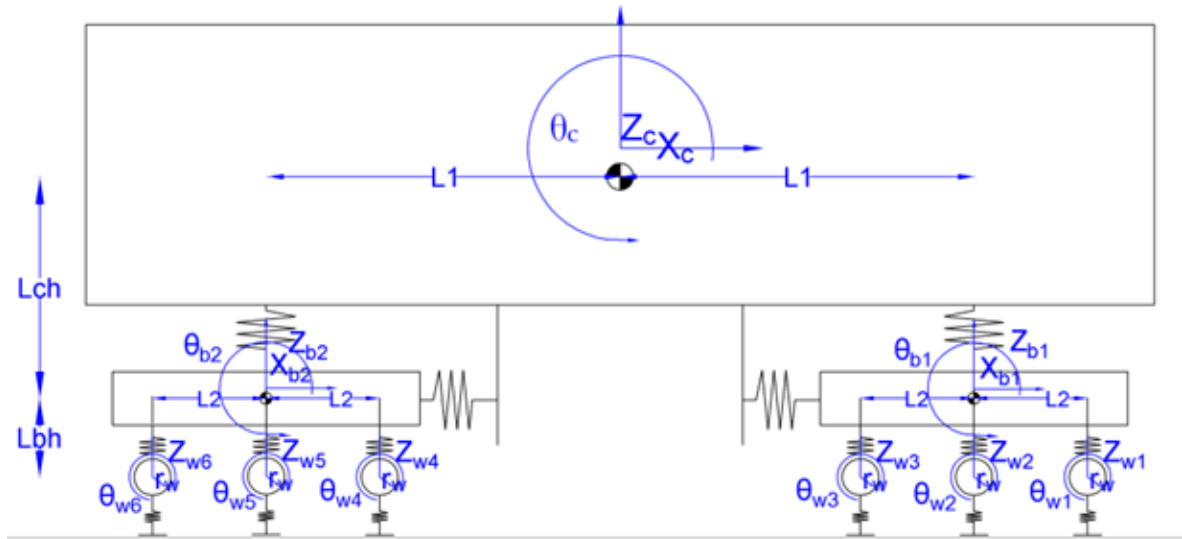


Figure 2: Locomotive longitudinal-vertical dynamic diagram

This model has 21 degrees of freedom (DOF), including 9 DOF for the longitudinal, vertical and pitch motion of locomotive body and two bogies, and 12 DOF for vertical and rotating motion of the six wheelsets. The connection between the car body and bogies, i.e. the secondary suspension, contains a set of springs and dampers along both longitudinal and vertical direction. The connection between wheelsets and bogies, i.e. the primary suspension, contains a set of springs and dampers along only vertical direction as the longitudinal connection between the wheelsets and bogies are assumed to be rigid as the longitudinal stiffness of the primary suspension is usually much higher than that of the secondary suspensions [25] and their effect to the dynamic response can be neglected. The longitudinal tractive force acting on the whole locomotive is caused by the friction force between the wheel and rail, providing longitudinal acceleration/deceleration dynamic component of the bogies and torque for bogie pitch motion. The relative motion between the bogies and car body provides the car body forces and torque for longitudinal, vertical and pitch motion.

The system variables are expressed as a vector containing 42 entries, representing the relative displacements and velocities between different nodes as,

$$X = [Z \quad \dot{Z}]^T, Z = [Z_c \quad Z_{bogie1} \quad Z_{bogie2} \quad Z_{axles}]^T, \quad (1)$$

in which $Z_c = [x_c \quad z_c \quad \theta_c]^T$ is a 3×1 vector representing the locomotive body longitudinal, vertical and pitch motion from the static positions, $Z_{bogie1} = [x_{b1} \quad z_{b1} \quad \theta_{b1}]^T$ and $Z_{bogie2} = [x_{b2} \quad z_{b2} \quad \theta_{b2}]^T$ are both 3×1 vectors representing longitudinal, vertical and pitch motion of the front and rear bogie separately, and $Z_{axles} = [z_{w1} \quad \theta_{w1} \quad z_{w2} \quad \theta_{w2} \quad \dots \quad z_{w6} \quad \theta_{w6}]^T$ is a 12×1 vector representing the vertical and rotating motion of wheelset 1~6. The state space representation of the dynamics can be expressed as:

$$\begin{aligned} \dot{X} &= A_m \cdot X + B_m \cdot u, A = \begin{bmatrix} \Theta & I \\ M^{-1}K_m & M^{-1}C_m \end{bmatrix}, \\ Y &= C \cdot X + D \cdot u \end{aligned} \quad (2)$$

where u is the longitudinal tractive force resulted from the interaction between the wheelsets and rail tracks, Y is a vector of displacement or velocity of each node from its static position, Θ is a zero matrix, I is an identity matrix of certain dimensions, K_m is the stiffness matrix, C_m is the damping matrix, and M is the diagonal mass and moment of inertia matrix in the form of,

$$M = \text{diag}(M_c \quad M_c \quad I_c \quad M_b \quad M_b \quad I_b \quad M_b \quad M_b \quad I_b \quad M_w \quad I_w \quad M_w \quad I_w \quad M_w \quad I_w \quad M_w \quad I_w \quad M_w \quad I_w \quad M_w \quad I_w). \quad (3)$$

Matrices B_m and D are shown in Appendix A.

The detailed parameters are listed in Table 1 for a full size GT46Ace locomotive.

Table 1: Detailed parameters of the locomotive model:

Parameter	Value
-----------	-------

Mass of each bogie frame (kg)	12121
Total mass of locomotive (t)	134
load mass (kg/carriage × no. of carriages)	90000 × 50
Load force (N)	4.8×10^6
Gear Ratio	17/90
Primary suspension springs (N/m)	89×10^6
Yaw viscous dampers stiffness (N/m)	45×10^6
Vertical viscous dampers stiffness (N/m)	44×10^6
Secondary suspension springs (N/m)	5.2×10^6
Longitudinal and lateral shear stiffness (N/m)	0.188×10^6
Central pivot longitudinal stiffness (N/m)	5×10^6
Wheel contact stiffness (N/m)	2.4×10^9
Primary suspension vertical damping (kg/s)	10×10^3
Secondary suspension vertical damping (kg/s)	2×10^4
Rail damping (kg/s)	1×10^6
Locomotive body length (m)	22
Locomotive body height – without bogie (m)	1.93
Bogie length (m)	3.7
Bogie height (m)	0.733
Horizontal distance between bogies mass centre(m)	13.7
Horizontal distance between axles (m)	1.3
Vertical distance between body bottom and bogie top (m)	0.3605
Vertical distance between bogie bottom and wheel top (m)	0.127
Wheel diameter (m)	1.016
Simulation time step (s)	5×10^{-6}
Wheelset mass (kg)	2850
Car body pitch moment of inertia (kg· m ²)	3610410
Front/rear bogie pitch moment of inertia (kg· m ²)	37007
Wheelset pitch moment of inertia (kg· m ²)	1200

2.1.1. Eigenmode frequency analysis

An eigenmode analysis was performed in Matlab to identify all the dynamic modes of vibration and to determine the stability of the system. The system eigenvalues are provided in Table 2. An eigenvalue is obtained for each possible mode of vibration of the system. The first part (real value) of each complex eigenvalue represents the amount of damping (if negative) of each mode of vibration. The second part (imaginary number) represents the part from which the frequency of vibration can be calculated. From the eigenvalues of the system, it can be seen that except for the car body horizontal mode, all modes of vibration have positive damping (negative real parts) which implies that the system is stable. A car body horizontal mode with zero damping is expected due to the rigid body longitudinal motion of the train.

Table 2: Modal frequencies of the locomotive dynamic system vibrations (Hz) and corresponding eigenvalues.

Modes	Frequency (Hz)	Eigenvalues	Modes	Frequency (Hz)	Eigenvalues
Car body vertical	0.4	$-2.9 \pm 2.8i$	Bogie 1 vertical	3.6	$-14 \pm 22.9i$
Car body pitching	1.8	$-2.1 \pm 11.4i$	Bogie 2 vertical	3.8	$-13 \pm 24.2i$
Bogie 1 pitching	3.3	$-1.7 \pm 20.8i$	Wheelset vertical	137.5	$-17 \pm 864i$
Bogie 2 pitching	3.3	$-1.6 \pm 20.6i$			

Corresponding bode diagram are shown in Appendix C.

2.2. Creep force modelling

The creep force is caused by the wheel-rail rolling contact and it is crucial in terms of the locomotive traction/braking operation. Polach provided an efficient formula to calculate the tangential force along the rail tracks based on his experimental data and Figure 3 as [19],

$$F = \frac{2Q\mu}{\pi} \left(\frac{k_A \varepsilon}{1+(k_A \varepsilon)^2} + \arctan(k_s \varepsilon) \right), \quad (4)$$

where F is the tangential force, Q is normal wheel load, k_A is the reduction factor in the area of adhesion and k_s is the reduction factor in the area of slip. ε is the gradient of the tangential stress in the area of adhesion which along the longitudinal direction (defined as x direction in Figure 1) can be calculated as,

$$\varepsilon_x = \frac{1}{4} \frac{G\pi a b c_{11}}{Q\mu} s_x, \quad (5)$$

where G is the shear modulus, a and b are the half-axes of the contact ellipse as shown in Figure 3. The contact area is calculated as in Appendix 3 in [26] as $a = 8.6 \text{ mm}$, $b = 4.4 \text{ mm}$ according to the dimension of the wheel in Table 1 and 60 kg rail profile from [27], c_{11} is derived from Kalker's work [28] and characterizes the longitudinal direction of the contact shear stiffness coefficient. Also s_x is the creep component in longitudinal direction defined as

$$s_x = \frac{w_x}{V}, \quad (6)$$

where w_x is the slip velocity in longitudinal direction and V is the vehicle speed.

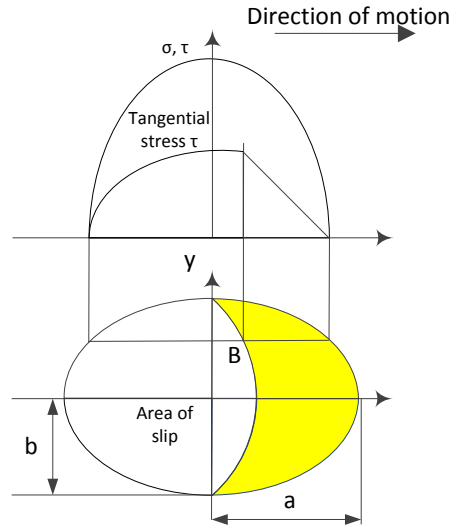


Figure 3: Wheel-rail contact area and distribution of normal and tangential stresses [19]

The Polach model employed is a regular form considering both longitudinal and lateral creep forces. However this is a simulation on a straight track, so only longitudinal dynamics need to be considered. Hence it is assumed the locomotive is tracking with no lateral displacement on the contact patch. As a result total creep s equals creep along the longitudinal direction s_x . μ is the coefficient of friction calculated as

$$\mu = \mu_0 [(1 - A_p) e^{-B_p w} + A_p], \quad (7)$$

where μ_0 is the maximum friction coefficient at zero slip velocity, A_p is the ratio of friction coefficient at infinity slip velocity μ_∞ and μ_0 , B_p is the coefficient of exponential friction decrease. Typical model parameters have been provided by Polach [19], as listed in Table 3.

Table 3: Typical parameters for dry and wet contact condition [19]

Parameters	Contact condition	
	Dry	Wet
k_A	1.00	0.30
k_s	0.40	0.10
μ_0	0.55	0.30
A_p	0.40	0.40
B_p	0.60	0.20

As it is shown in Figure 4, the optimum tractive force ratio shifts to lower values of creep as the speed of locomotive increases. As a result, setting the reference creep to be constant will cause traction performance degradation over different locomotive operation speeds. The degradation between low speed to medium speed is approximately 7% and 5% and up to 16% and 11% from low speed to high speed under dry wet conditions respectively.

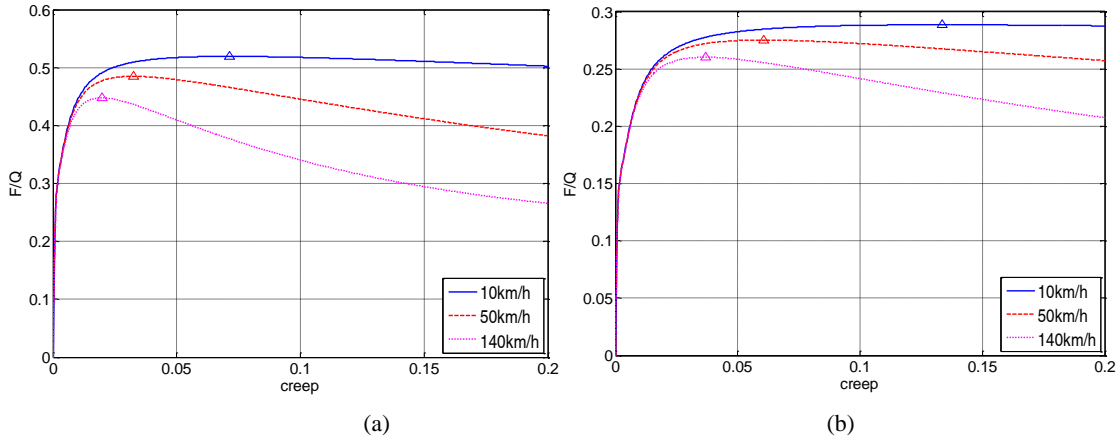


Figure 4: Polach tractive force curve at different speed under (a) dry contact condition; and (b) under wet contact condition

2.3. Wheel traction dynamic modelling

A simple wheel traction dynamic model characterizing the traction torque acting from the electric motor on a wheelset T_{ti} , mechanical loading T_{li} , the equivalent moment of inertia of the axles with the motor rotor I_w , and the angular acceleration of axles $\ddot{\theta}_{wi}$ can be described as [29]. The electrical modelling is not taken into account in this simplified model.

$$I_w \ddot{\theta}_{wi} = T_{ti} - T_{li}, i = 1, 2, \dots, 6 \quad (8)$$

3. Proposed control system

This study employs a basic PI based creep controller to limit the creep values under pre-set creep thresholds. The detailed controller diagram is shown in 5. Each wheelset has its own set of controller and motor so that the speed of the motors can be adjusted independently.

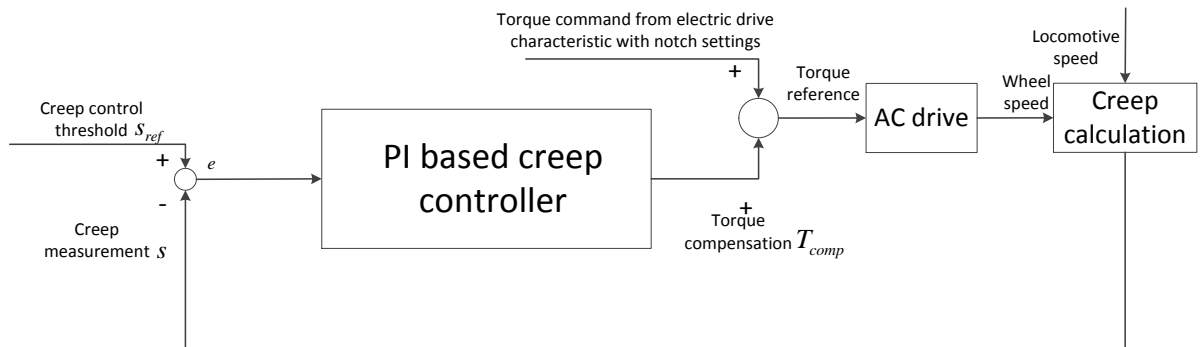


Figure 5: PI creep control diagram

In this study the creep threshold setting is assumed to be adjustable to investigate its impact on wear growth rate under different conditions, as shown in Figure 5. Different notch settings adjust the level of power supply to the motors and are controlled by drivers. The controller adjusts the torque generated by the motor if the creep measurement exceeds the creep threshold setting. If the creep measurement is lower than the pre-set threshold, the controller is not activated. Otherwise the creep controller gives a torque compensation signal to adjust the amount of torque generated by the electric drive. In this case, the parameter values of the PI controller are tuned to 1.5×10^7 and 2×10^5 , for the proportional (P) and integral (I) constants respectively, with consideration of the ratio of

$e = s_{ref} - s$ and the scale of torque to compensate. The resulting overshoot is about 2.5% with a steady state error of 2.3×10^{-4} . The torque compensation can be calculated as

$$T_{comp} = \begin{cases} 0 & \text{if } e \geq 0 \\ 1.5 \times 10^7 \times e + 2 \times 10^5 \times \int_{t_1}^{t_2} e dt & \text{if } e < 0 \end{cases} \quad (9)$$

where t_1 is the time when creep measurement starts exceeding threshold and t_2 is the current time when the creep is still larger than the threshold setting. The purpose of the proposed controller and its parameters is to reveal the possibility of controlling wear growth rate under change of operating conditions by means of choosing proper creep threshold, rather than to provide ‘optimal’ controller available. Simulations have been carried out using the creep controller with different creep threshold settings in order to investigate its impact on rail damage due to wear. Detailed simulation cases are listed in Table 4.

Table 4: Simulation cases

Creep Threshold	Speed case (dry-wet-dry)	
	Low (≈ 10 km/h)	Medium (≈ 50 km/h)
0.03	Yes	Yes
0.04	Yes	No
0.06	Yes	No
0.08	Yes	No

A threshold higher than 0.03 is not simulated for the medium speed case since the creep response will not activate the creep controller due to the electric drive constraints.

4. Results

The locomotive acceleration operation is investigated to simulate high tractional conditions that typically occur on straight track. Thus other dynamics such as lateral and rolling dynamics are excluded from this study. The results comparing locomotive response obtained with different creep controller settings are presented, focussing on tractive force and the transitional power parameter $T\gamma/A$, at speeds of about 10 km/h and 50km/h under the highest acceleration (notch 8) conditions. As the tractive effort of the electric drives is dependent of the operational speed, the change of contact condition is triggered when the locomotive reaches the same speed to ensure the result is comparable between different the control logics. The $T\gamma/A$ value is relevant to wear rate according to the mapping relation[14], as shown in Figure 6 below:

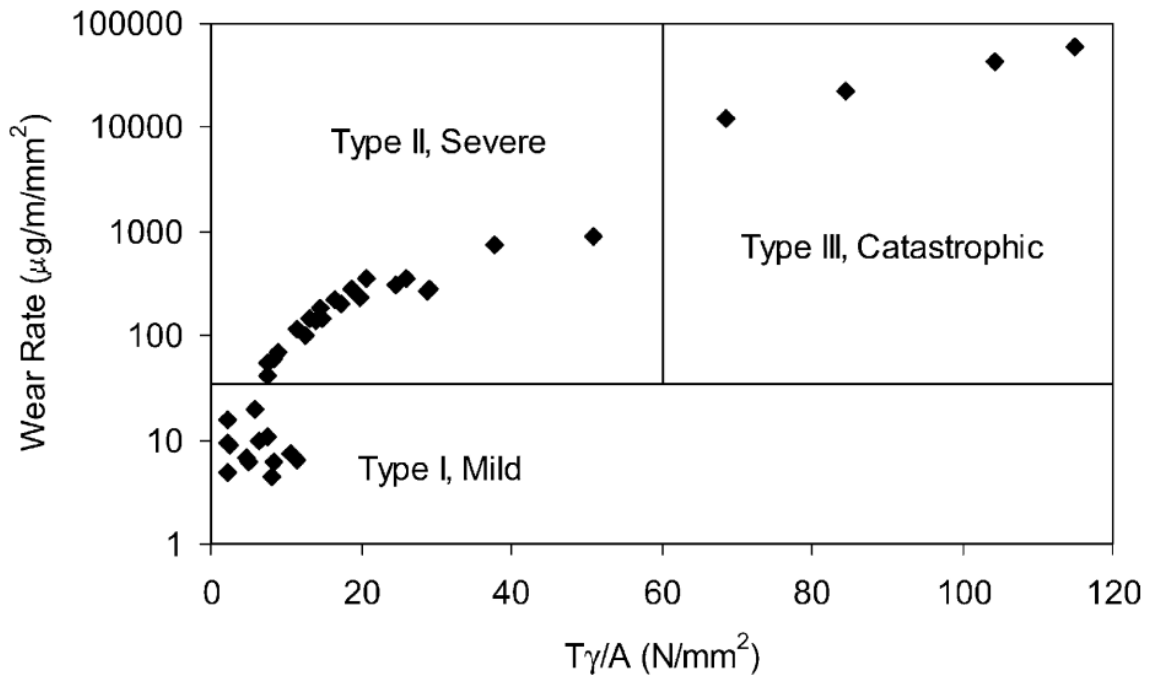


Figure 6: Wear regimes identified during twin disc testing of BS11 rail materials vs. Class D tyre material[14]

According to Figure 6, in order to avoid serious rail damage in Type III catastrophic region caused by wear, the $T\gamma/A$ value needs to be constrained below 60 N/mm^2 . Transient contact conditions are assumed to occur at 11 km/h from dry to wet and at 12.5 km/h from wet to dry for the low speed simulation. Similarly, for the medium speed simulation case, the contact condition changes at 51 km/h , and back to a dry condition at 52.5 km/h .

Case 1: low speed simulation

Figure 7 shows the tractive force of the front wheel under a change of contact conditions during low speed conditions.

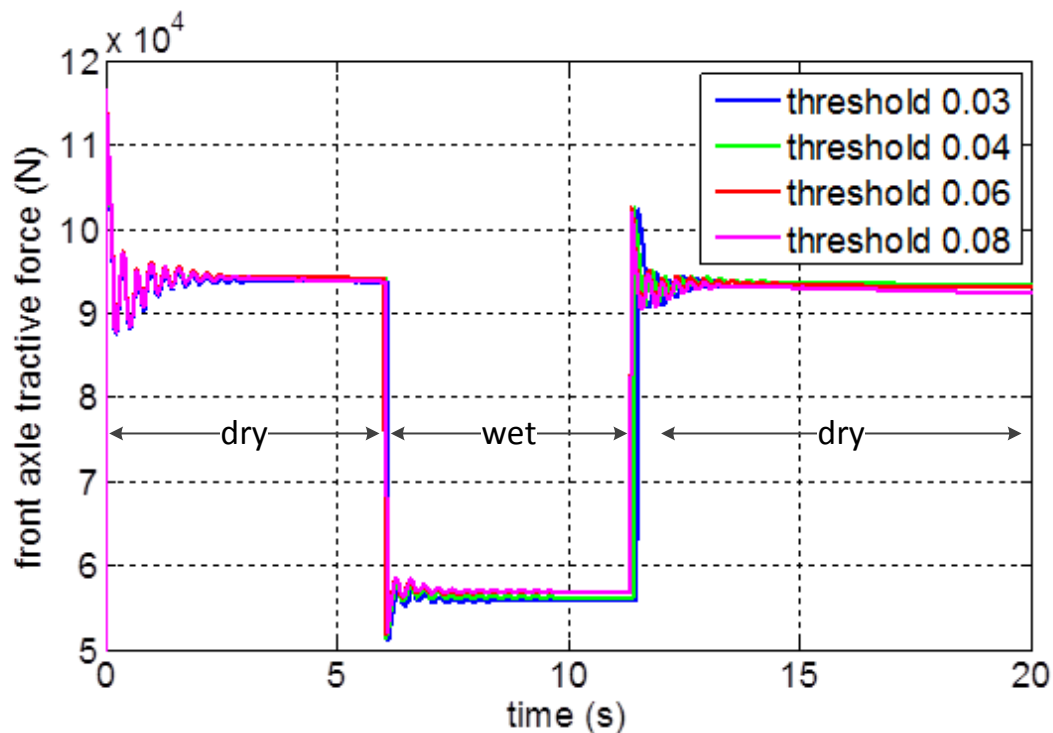


Figure 7: front wheel tractive force comparison under different controller thresholds at low speed

The difference of tractive force under different creep control threshold settings is very small as shown in Figure 7. The reason is the gradient of the tractive force from creep values 0.03 to 0.08 is small as shown in Figure 4 a), thus the change of tractive force is not sensitive to the change of creep value.

Figure 8 shows the front wheel set creep under different controller thresholds at low speed. It can be seen from the figure that the controller can effectively constrain the creep under the pre-set thresholds under various contact conditions.

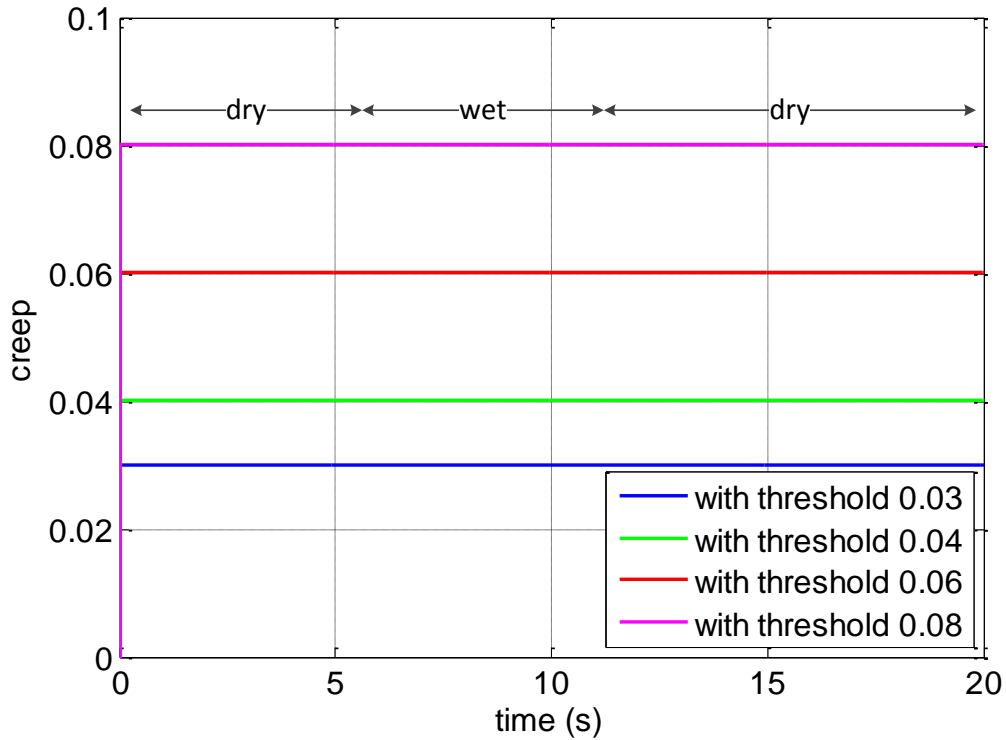


Figure 8: front wheel creep comparison under different controller thresholds at low speed

Figure 9 shows the front wheel $T\gamma/A$ value with different creep threshold settings under a change of contact conditions under low speed.

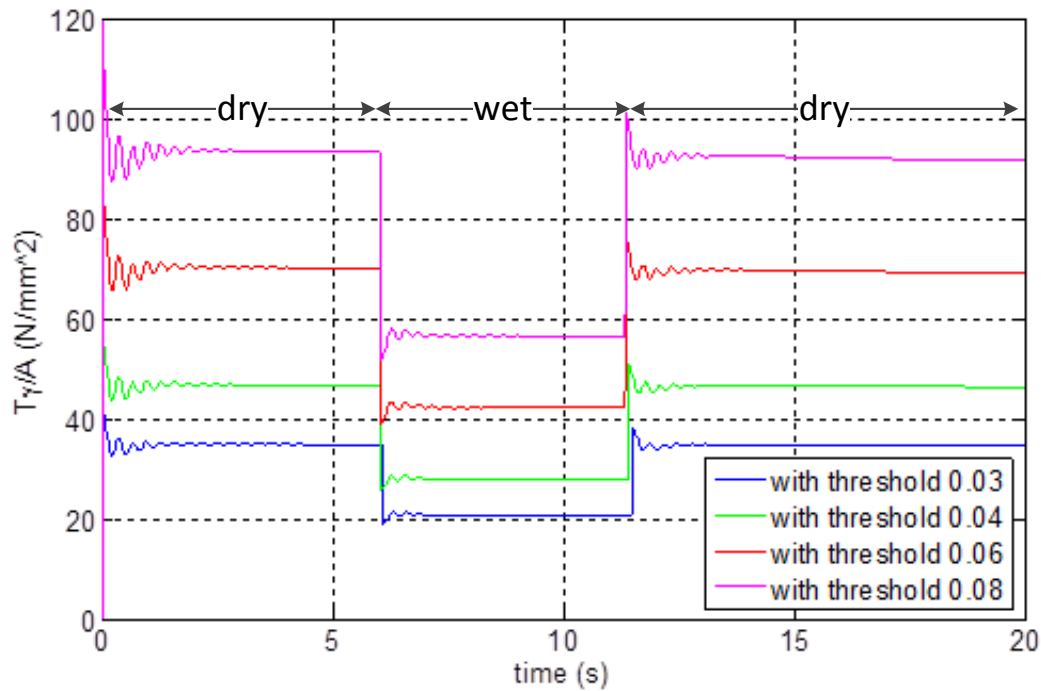


Figure 9: front wheel $T\gamma/A$ values comparison under different controller thresholds at low speed

As is shown in Figure 9, the $T\gamma/A$ value is mostly proportional to the value of creep thresholds due to the similarity of tractive forces in $T\gamma/A$ term under different threshold settings. From the simulation results in Figure 9, it can be seen that with a creep threshold below 0.04, the $T\gamma/A$ value is below 60 N/mm^2 and therefore according to Figure 6 the wear rate is constrained within the Type I and II (“mild” and “severe”) region. Similarly, with a creep threshold between 0.06 and 0.08, the wear rate is within the Type III (“catastrophic”) region, except under wet contact conditions. Therefore a creep controller threshold below 0.04 is desirable under low speed conditions.

Case 2: medium speed simulation

Figure 10 shows the front wheel tractive force response for medium speed simulation within constant power operation region. The changes of contact conditions occur at 51 km/h and 52.5 km/h.

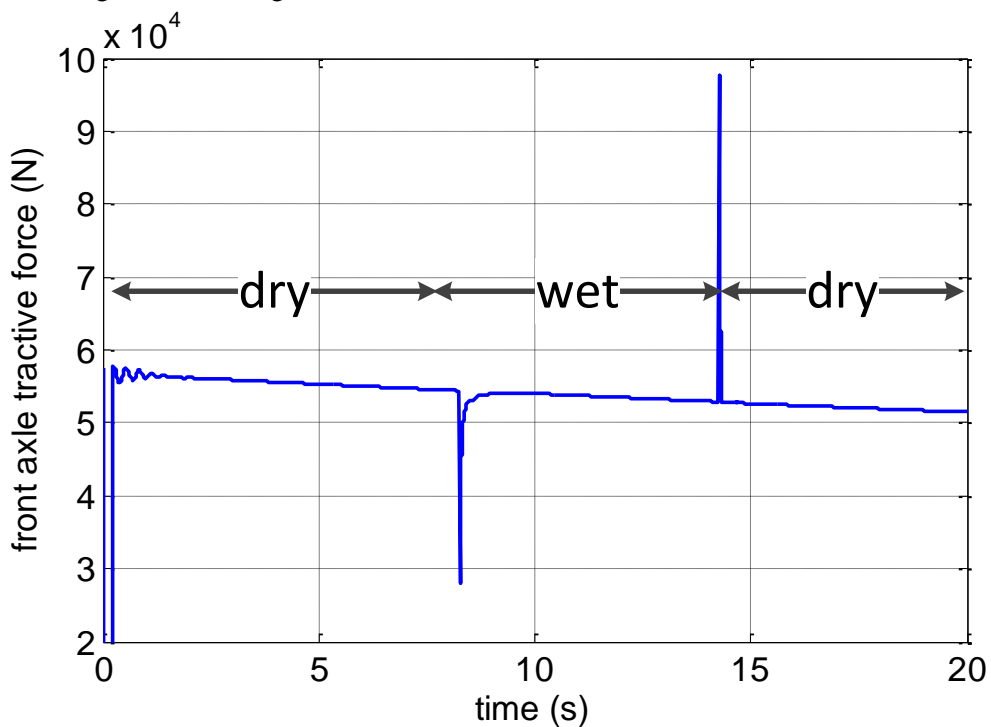


Figure 10: front wheel tractive force

The figure above shows that the front axle tractive force is not affected by the creep threshold setting at medium speed operation. This phenomenon can be explained by investigating the creep value on which the tractive force is dependant. Figure 11 shows the front axle creep response for medium speed simulation within constant power operation region.

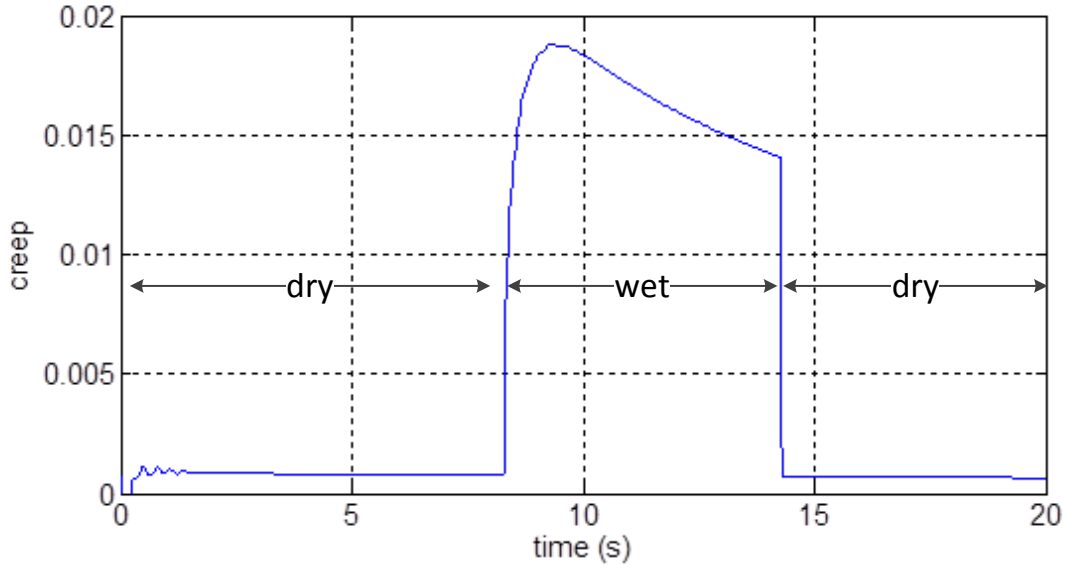


Figure 11: front wheel creep response for medium speed simulation under change of contact conditions

As it is shown in Figure 11, under the change of contact condition from dry to wet and from wet to dry for medium speed operation, the creep is always below 0.02, thus below the minimum threshold in Table 4, due to the force limit in the constant power region. As a result, the creep controller will not be activated under all creep threshold settings in Table 3. Thus the dynamic response and wear rate with different controller threshold settings should be the same. Figure 12 below shows the corresponding $T\gamma/A$ response for medium speed simulation under the change of contact conditions.

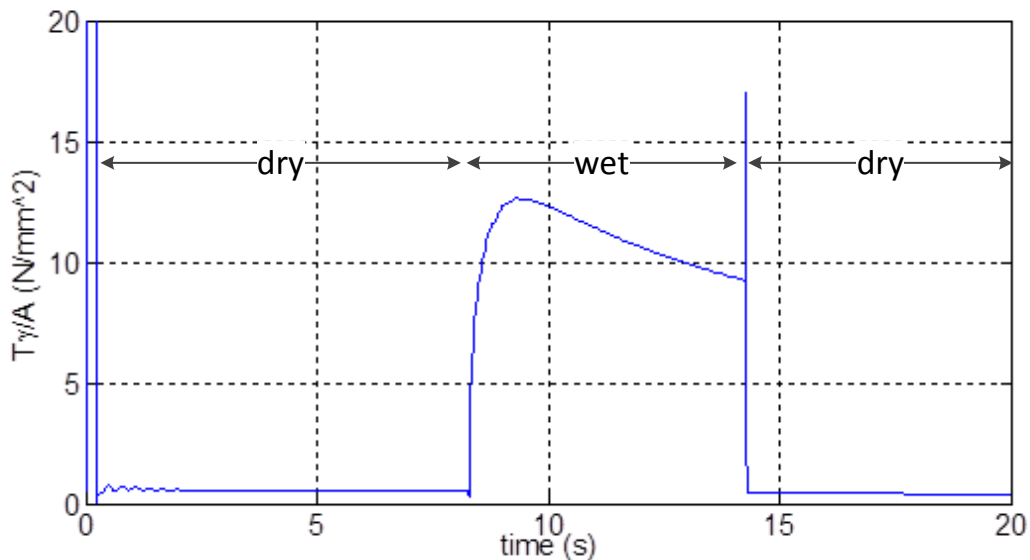


Figure 12: front wheel $T\gamma/A$ values at medium speed

In Figure 12, the $T\gamma/A$ value at medium speed is always below $20 N/mm^2$, thus the wear rate is within Type I and Type II region (see Figure 6). As a result, due to the impact of the torque-speed curve of the electric drives under constant power operating region, the wear rate is naturally constrained within the Type I and Type II region.

Comparing Figure 9 and Figure 12, it can be observed that at low speed operation where the tractive force is sufficient to activate the creep controller. The $T\gamma/A$ value is larger under dry contact condition than under wet condition as a result of very similar creep values under both dry and wet condition but different tractive force, under a certain creep threshold setting. While at medium speed operation where the tractive force is not large enough to activate the creep controller under both dry and wet contact conditions, the $T\gamma/A$ value is larger under wet contact condition than under dry condition, due to different creep values achieves similar tractive force as can be concluded from Figure 4.

5. Conclusion and future work

In this paper, wear rate with different PI creep control threshold settings under transient contact conditions have been compared by using a 21 DOF full-scale locomotive dynamic model under different operation speeds. Simulations have been carried out to compare tractive force and wear rate, focusing on the impact of operation speed and creep controller setting. Results show that by designing the creep controller threshold parameter, the wear rate can be effectively constrained within Type I and Type II regions, avoiding Type III ‘Catastrophic’ wear. Under higher speed operation, such as Case 2 in this paper, the wear rate is naturally constrained within region I and II due to the impact of the torque-speed characteristics of the electric drives, irrespective of the creep controller. Future work will include the investigation on modifying the controller so that optimal tractive force can be achieved to ensure the wear growth rate is constrained within Type I and II regions, automatically. Also more detailed dynamic model including lateral dynamics and relative motions between wheelsets and bogies will be employed for more accurate dynamic and control analysis on both straight and curved tracks.

Acknowledgements

The authors are grateful to the CRC for Rail Innovation (established and supported under the Australian Government's Cooperative Research Centres program) for the funding of this research Project No. R3.119 “Locomotive Adhesion”. The authors acknowledge the support of the Centre for Railway Engineering, Central Queensland University and the many industry partners that have contributed to this project, in particular staff from RailCorp, Fortescue Metals Group (FMG) and Brookfield Rail.

References:

- [1] Y. Bakhvalov, *et al.*, "Mathematical Modelling of Electromechanical Processes in Electric Locomotive," presented at the 16th IMACS World Congress, Lausanne (Switzerland), 2000.
- [2] S. Senini, *et al.*, "Dynamic simulation of wheel-rail interaction for locomotive traction studies," in *Railroad Conference, 1993., Proceedings of the 1993 IEEE/ASME Joint*, 1993, pp. 27-34.
- [3] P. Doh-Young, *et al.*, "Hybrid re-adhesion control method for traction system of high-speed railway," in *Electrical Machines and Systems, 2001. ICEMS 2001. Proceedings of the Fifth International Conference on*, 2001, pp. 739-742 vol.2.
- [4] K. Ohishi, *et al.*, "Anti-slip control of electric motor coach based on disturbance observer," in *Advanced Motion Control, 1998. AMC '98-Coimbra., 1998 5th International Workshop on*, 1998, pp. 580-585.
- [5] I. Yasuoka, *et al.*, "Improvement of re-adhesion for commuter trains with vector control traction inverter," in *Power Conversion Conference - Nagaoka 1997., Proceedings of the*, 1997, pp. 51-56 vol.1.
- [6] M. Spiriyagin, *et al.*, "Co-simulation of a mechatronic system using Gensys and Simulink," *Vehicle System Dynamics*, vol. 50, pp. 495-507, 2012.
- [7] M. Spiriyagin, *et al.*, "Control system for maximum use of adhesive forces of a railway vehicle in a tractive mode," *Mechanical Systems and Signal Processing*, vol. 22, pp. 709-720, 2008.
- [8] M. Spiriyagin, *et al.*, "Adhesion estimation and its implementation for traction control of locomotives," *International Journal of Rail Transportation*, vol. 2, pp. 187-204, 2014/07/03 2014.
- [9] Y. Yuan, *et al.*, "The dynamic study of locomotives under saturated adhesion," *Vehicle System Dynamics*, vol. 49, pp. 1321-1338, 2011/08/01 2011.
- [10] T. X. Mei, *et al.*, "A mechatronic approach for effective wheel slip control in railway traction," *Proceedings of the Institution of Mechanical Engineers, Part F: Journal of Rail and Rapid Transit*, vol. 223, pp. 295-304, May 1, 2009 2009.
- [11] Y. Zhao and B. Liang, "Re-adhesion control for a railway single wheelset test rig based on the behaviour of the traction motor," *Vehicle System Dynamics*, vol. 51, pp. 1173-1185, 2013/08/01 2013.
- [12] T. Jendel, "Prediction of wheel profile wear—comparisons with field measurements," *Wear*, vol. 253, pp. 89-99, 2002.
- [13] T. G. Pearce and N. D. Sherratt, "Prediction of wheel profile wear," *Wear*, vol. 144, pp. 343-351, 1991.
- [14] R. Lewis and U. Olofsson, "Mapping rail wear regimes and transitions," *Wear*, vol. 257, pp. 721-729, 2004.
- [15] F. Braghin, *et al.*, "A mathematical model to predict railway wheel profile evolution due to wear," *Wear*, vol. 261, pp. 1253-1264, 2006.
- [16] E. H. Law and N. K. Cooperrider, "A survey of railway vehicle dynamics research," *ASME Journal of Dynamic Systems, Measurement, and Control*, vol. 96, pp. 132-146, June 1974 1974.
- [17] R. Guclu and M. Metin, "Fuzzy Logic Control of Vibrations of a Light Rail Transport Vehicle in Use in Istanbul Traffic," *Journal of Vibration and Control*, vol. 15, pp. 1423-1440, September 1, 2009 2009.
- [18] D. S. Garivaltis, *et al.*, "Dynamic Response of a Six-axle Locomotive to Random Track Inputs," *Vehicle System Dynamics*, vol. 9, pp. 117-147, 1980/05/01 1980.
- [19] O. Polach, "Creep forces in simulations of traction vehicles running on adhesion limit," *Wear*, vol. 258, pp. 992-1000, 2005.
- [20] M. Spiriyagin, *et al.*, "Creep force modelling for rail traction vehicles based on the Fastsim algorithm," *Vehicle System Dynamics*, vol. 51, pp. 1765-1783, 2013/11/01 2013.
- [21] M. D. Ardema, *Newton-Euler Dynamics*: Springer, 2006.
- [22] I. J. Guy, "An analysis of the interaction between the front and rear axles of a four-wheel-drive tractor, and its contribution to power delivery efficiency," Harper Adams University College, 2011.
- [23] Pegasem. Pegasem GSS series ground speed sensors [Online]. Available: http://www.pegasem.com/english/datasheets_uk/gss_uk.pdf
- [24] S. Iwnicki, *Handbook of railway vehicle dynamics*: CRC press, 2006.
- [25] K. Abood and R. Khan, "Hunting phenomenon study of railway conventional truck on tangent tracks due to change in rail wheel geometry," *Journal of Engineering Science and Technology*, vol. 6, pp. 146-160, 2011.

- [26] K. L. Johnson, *Contact Mechanics*: Cambridge University Press, 1985.
 [27] *Rail Track Material Catalogue A5*. Available: <https://www.scribd.com/doc/92072909/Rail-Track-Material-Catalogue-A5#download>
 [28] J. Kalker, "On the Rolling Contact of Two Elastic Bodies in the Presence of Dry Friction," Ph. D Doctoral Thesis, Delft, 1967.
 [29] R. Marino, *et al.*, *Induction Motor Control Design*: Springer, 2010.

Appendix A: Matrix B_m and D in Equation (2)

$$B_m = \begin{bmatrix}
 \Theta_{24 \times 1} & \Theta_{24 \times 1} & \Theta_{24 \times 1} & \Theta_{24 \times 1} & \Theta_{24 \times 1} & \Theta_{24 \times 1} \\
 \frac{1}{M_b} & \frac{1}{M_b} & \frac{1}{M_b} & 0 & 0 & 0 \\
 0 & 0 & 0 & 0 & 0 & 0 \\
 \frac{L_{bh}}{I_b} & \frac{L_{bh}}{I_b} & \frac{L_{bh}}{I_b} & 0 & 0 & 0 \\
 0 & 0 & 0 & \frac{1}{M_b} & \frac{1}{M_b} & \frac{1}{M_b} \\
 0 & 0 & 0 & 0 & 0 & 0 \\
 0 & 0 & 0 & \frac{L_{bh}}{I_b} & \frac{L_{bh}}{I_b} & \frac{L_{bh}}{I_b} \\
 0 & 0 & 0 & 0 & 0 & 0 \\
 -\frac{r_w}{I_w} & 0 & 0 & 0 & 0 & 0 \\
 0 & 0 & 0 & 0 & 0 & 0 \\
 0 & -\frac{r_w}{I_w} & 0 & 0 & 0 & 0 \\
 0 & 0 & 0 & 0 & 0 & 0 \\
 0 & 0 & -\frac{r_w}{I_w} & 0 & 0 & 0 \\
 0 & 0 & 0 & 0 & 0 & 0 \\
 0 & 0 & 0 & -\frac{r_w}{I_w} & 0 & 0 \\
 0 & 0 & 0 & 0 & 0 & 0 \\
 0 & 0 & 0 & 0 & -\frac{r_w}{I_w} & 0 \\
 0 & 0 & 0 & 0 & 0 & 0 \\
 0 & 0 & 0 & 0 & 0 & -\frac{r_w}{I_w}
 \end{bmatrix}$$

$D = \Theta_{21 \times 6}$

Appendix B: Full equations of the dynamic model

$$m_c \cdot \ddot{x}_c = f_{b1cx} + f_{b2cx}$$

$$m_c \cdot \ddot{z}_c = f_{b1cz} + f_{b2cz}$$

$$I_c \cdot \ddot{\theta}_c = f_{b1cz} \cdot L_1 - f_{b2cz} \cdot L_1 - f_{b1cx} \cdot L_{ch} - f_{b2cx} \cdot L_{ch}$$

$$(m_b + 3 \cdot m_w) \cdot \ddot{x}_{b1} = f_{rw1x} + f_{rw2x} + f_{rw3x} - f_{b1cx}$$

$$m_b \cdot \ddot{z}_{b1} = f_{w1b1z} + f_{w2b1z} + f_{w3b1z} - f_{b1cz}$$

$$I_b \cdot \ddot{\theta}_{b1} = f_{w3b1z} \cdot L_2 - f_{w1b1z} \cdot L_2 - \sum_{j=1}^3 f_{rwjx} \cdot (r_w + L_{bh})$$

$$(m_b + 3 \cdot m_w) \cdot \ddot{x}_{b2} = f_{rw4x} + f_{rw5x} + f_{rw6x} - f_{b2cx}$$

$$m_b \cdot \ddot{z}_{b2} = f_{w4b2z} + f_{w5b2z} + f_{w6b2z} - f_{b2cz}$$

$$I_b \cdot \ddot{\theta}_{b2} = f_{w6b2z} \cdot L_2 - f_{w4b2z} \cdot L_2 - \sum_{j=4}^6 f_{rwjx} \cdot (r_w + L_{bh})$$

$$m_w \cdot \ddot{z}_{w1} = f_{rw1z} + f_{b1w1z}$$

$$I_w \cdot \ddot{\theta}_{w1} = T_{t1} - f_{rw1x} \cdot r_w$$

$$m_w \cdot \ddot{z}_{w2} = f_{rw2z} + f_{b1w2z}$$

$$I_w \cdot \ddot{\theta}_{w2} = T_{t2} - f_{rw2x} \cdot r_w$$

$$m_w \cdot \ddot{z}_{w3} = f_{rw3z} + f_{b1w3z}$$

$$I_w \cdot \ddot{\theta}_{w3} = T_{t3} - f_{rw3x} \cdot r_w$$

$$m_w \cdot \ddot{z}_{w4} = f_{rw4z} + f_{b2w4z}$$

$$I_w \cdot \ddot{\theta}_{w4} = T_{t4} - f_{rw4x} \cdot r_w$$

$$m_w \cdot \ddot{z}_{w5} = f_{rw5z} + f_{b2w5z}$$

$$I_w \cdot \ddot{\theta}_{w5} = T_{t5} - f_{rw5x} \cdot r_w$$

$$m_w \cdot \ddot{z}_{w6} = f_{rw6z} + f_{b2w6z}$$

$$I_w \cdot \ddot{\theta}_{w6} = T_{t6} - f_{rw6x} \cdot r_w$$

$$f_{b1cx} = -k_{bcx} \cdot (x_c - x_{b1}) - c_{bcx} \cdot (\dot{x}_c - \dot{x}_{b1})$$

$$f_{b2cx} = -k_{bcx} \cdot (x_c - x_{b2}) - c_{bcx} \cdot (\dot{x}_c - \dot{x}_{b2})$$

$$f_{b1cz} = -k_{bcz} \cdot (z_c - z_{b1} + L_1 \cdot \theta_c) - c_{bcz} \cdot (\dot{z}_c - \dot{z}_{b1} + L_1 \cdot \dot{\theta}_c)$$

$$f_{b2cz} = -k_{bcz} \cdot (z_c - z_{b2} - L_1 \cdot \theta_c) - c_{bcz} \cdot (\dot{z}_c - \dot{z}_{b2} - L_1 \cdot \dot{\theta}_c)$$

$$f_{w1b1z} = -k_{wbz} \cdot (z_{b1} - z_{w1} + L_2 \cdot \theta_{b1}) - c_{wbz} \cdot (\dot{z}_{b1} - \dot{z}_{w1} + L_2 \cdot \dot{\theta}_{b1})$$

$$f_{w2b1z} = -k_{wbz} \cdot (z_{b1} - z_{w2}) - c_{wbz} \cdot (\dot{z}_{b1} - \dot{z}_{w2})$$

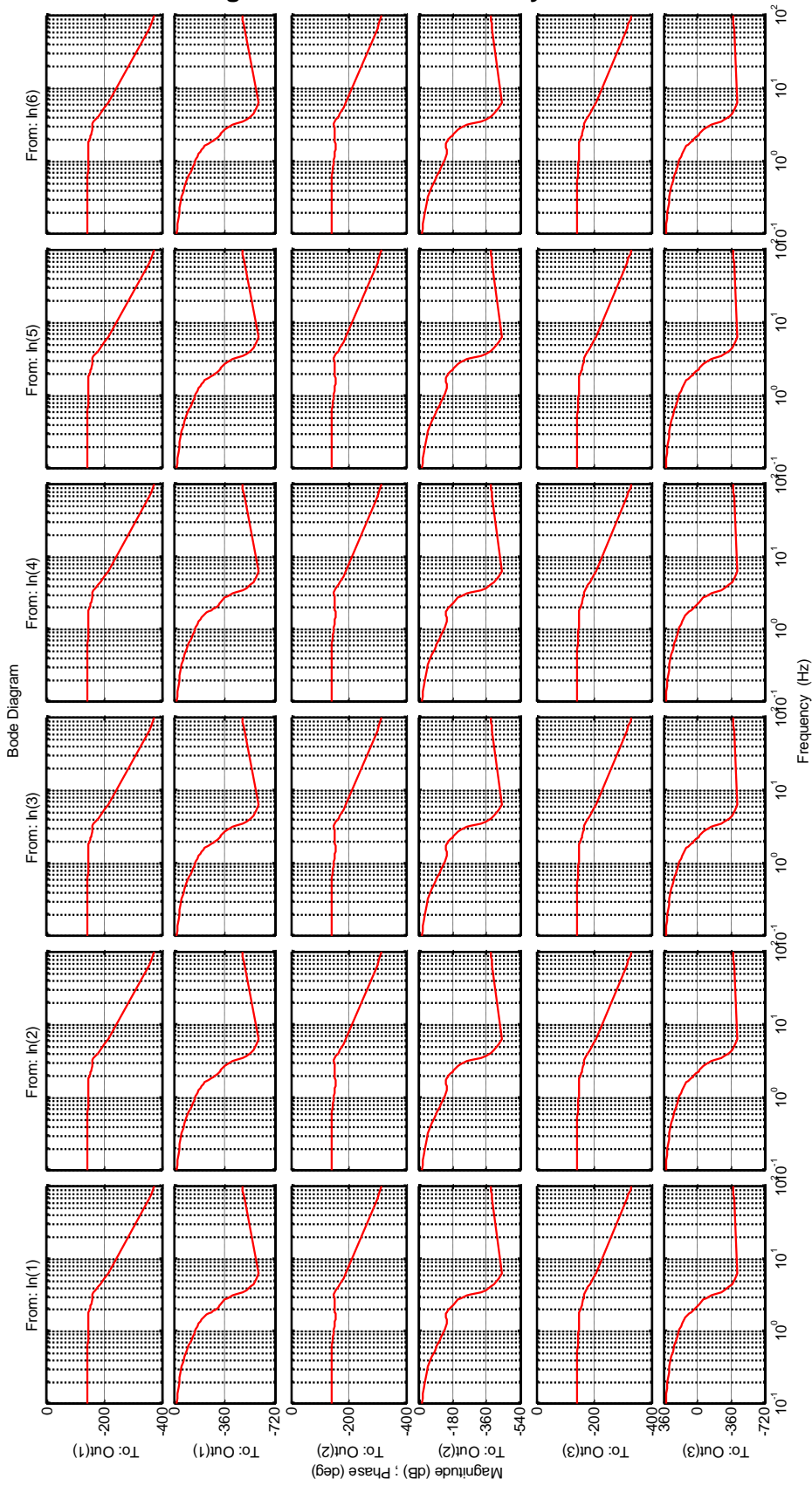
$$f_{w3b1z} = -k_{wbz} \cdot (z_{b1} - z_{w3} - L_2 \cdot \theta_{b1}) - c_{wbz} \cdot (\dot{z}_{b1} - \dot{z}_{w3} - L_2 \cdot \dot{\theta}_{b1})$$

$$f_{w4b2z} = -k_{wbz} \cdot (z_{b2} - z_{w4} + L_2 \cdot \theta_{b2}) - c_{wbz} \cdot (\dot{z}_{b2} - \dot{z}_{w4} + L_2 \cdot \dot{\theta}_{b2})$$

$$f_{w5b2z} = -k_{wbz} \cdot (z_{b2} - z_{w5}) - c_{wbz} \cdot (\dot{z}_{b2} - \dot{z}_{w5})$$

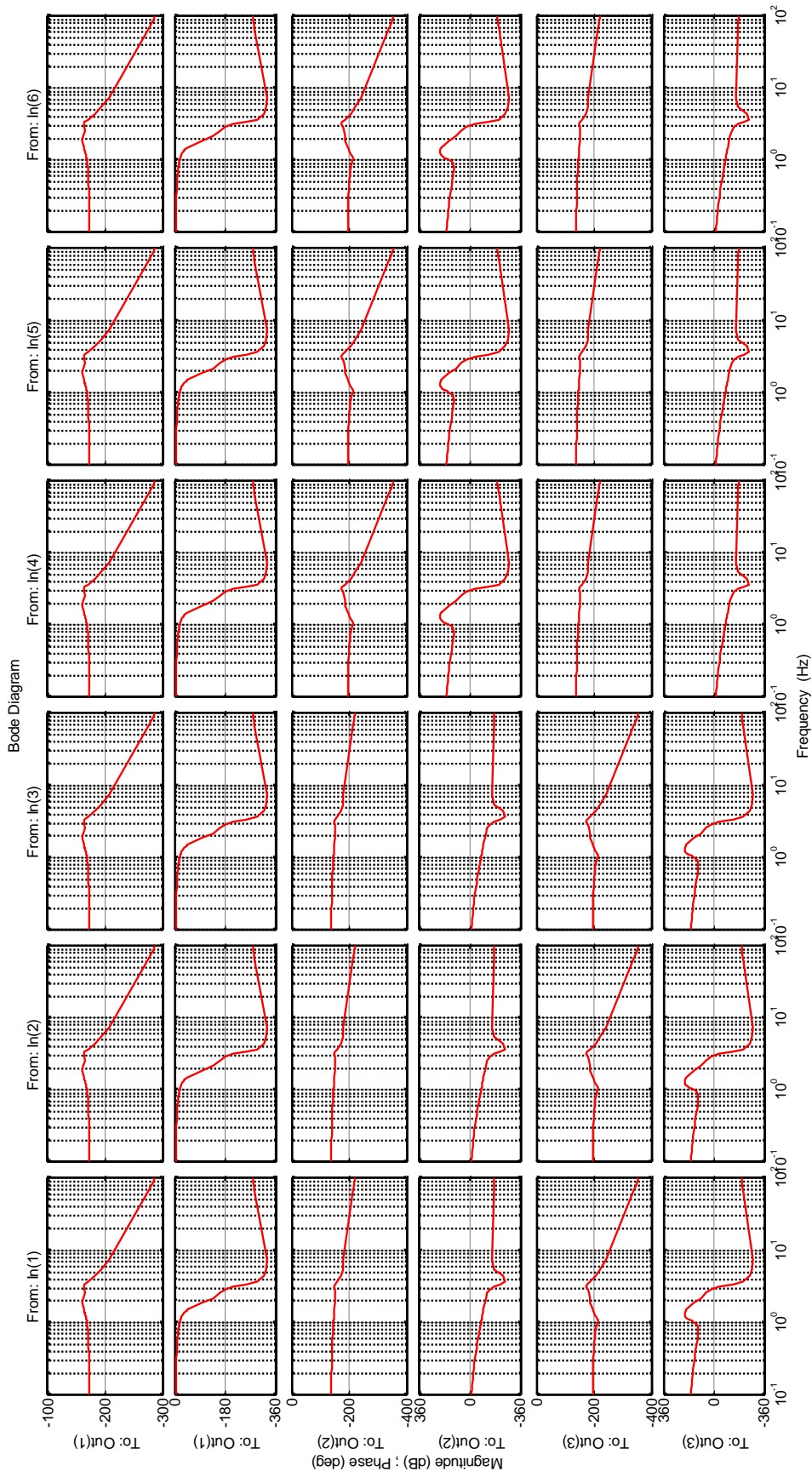
$$f_{w6b2z} = -k_{wbz} \cdot (z_{b2} - z_{w6} - L_2 \cdot \theta_{b2}) - c_{wbz} \cdot (\dot{z}_{b2} - \dot{z}_{w6} - L_2 \cdot \dot{\theta}_{b2})$$

Appendix C: Bode diagram of the locomotive dynamics



Bode diagram of vertical dynamics.

From: In(1)-In(6) implies tractive force from axle 1 to axle 6. Out(1), Out(2) and Out(3) are car body, front and rear bogie vertical responses



Bode diagram of pitch dynamics.

From: In(1)-In(6) implies tractive force from axle 1 to axle 6. Out(1), Out(2) and Out(3) are car body, front and rear bogie pitch responses respectively

Paper E

Real-time rail/wheel wear damage control

Real-time rail/wheel wear damage control

Ye Tian, W.J.T. (Bill) Daniel, Paul A. Meehan

School of Mechanical and Mining Engineering, the University of Queensland, Queensland, Australia 4072

This paper presents the performance of a real-time rail/wheel wear damage control system with respect to different operation conditions. In particular, an investigation into the wear growth rate control under changing wheel-rail friction conditions and different operation speeds is performed. Simulation using a mathematical model considering longitudinal-vertical-pitch dynamics of a locomotive running on straight tracks shows that the proposed controller can effectively reduce the rail/wheel wear damage by limiting mass loss rate, particularly during acceleration under low speed.

Keywords: wear control; railway; locomotive; wheel-rail

1. Introduction

Rail offers one of the most efficient forms of land-based transport [1], providing great carrying capacity. However, there is discussion as to whether the trend towards more powerful locomotives, particularly in the heavy haul rail industry, would contribute to considerable increase of rail track damage due to wear and increased track maintenance cost. Traditionally, friction modifiers (FM) have been employed on the rail/wheel contact patch to reduce such wear and rolling contact fatigue [2]. However this method depends on experiences and lacks understanding of the impact of locomotive dynamic traction creep behaviour. There is also additional cost. The American Association of Railroads estimates that the wear occurring at the wheel/rail interface as a result of ineffective lubrication costs in excess of \$US 2 billion per year [3]. Therefore, it is necessary to understand how wear growth is affected by different operation conditions and creep/adhesion control strategies. In particular, the transient state of locomotive operation due to external perturbations such as changes of wheel-rail contact conditions needs to be further investigated. As the most significant change of locomotive dynamic responses and oscillations are likely to occur during this transient state. Thus rail damage due to wear is likely to be controlled in a systematic way, potentially reducing or even excluding the use of friction modifiers for the purpose of wear reduction.

The study of patterns of wear behaviour was addressed by Beagley et al. [4]. Wear behaviour of wheel/rail steels was described as a 'wear regime'. The terms "mild" and "severe" regimes were used to describe wear characteristics according to the surface deformation observed in his experiments. A regime that arose from more severe contact conditions was observed by Bolton et al. [5] and was defined as the 'catastrophic' wear regime. A detailed review of this wear regime of steel was performed by Markov et al. in [6]. These three rolling-sliding wear regimes for wheel/rail steels have also been reconfirmed by Danks et al. [7]. He also suggested using the terms "type I wear", "type II wear" and "type III wear" for describing the "stages" of the wear in order to avoid the confusion between the mild and severe wear regimes and mild-oxidational and severe-oxidational wear mechanisms. For the wheel/rail steel, the material loss in wear process is defined as wear rate. It is determined by the loss of material mass per rolling distance ($\mu\text{g}/\text{m}$) [7]; or by the total loss of material mass per rolling distance, per contact area ($\mu\text{g}/\text{m}/\text{mm}^2$) [8]. Wear rate is often plotted against the 'wear index' $T\gamma/A_n$ [9]. A recent wear model considering the wear transitions has been developed by Vuong et al [10]. Both wheel and rail wear regimes can be illustrated in a similar mapping method [9, 11-15]. In this paper, the dynamic response of a full scale locomotive model with a traction controller under different speed and/or contact conditions is investigated in relation to the rail wear. This work focuses on longitudinal and vertical dynamics on tangent tracks as it is the most important part of locomotive dynamics closely related with traction/braking effort, passenger comfort and energy management [16]. A full scale locomotive longitudinal-vertical-pitch dynamic model with a PI creep controller and a wear controller combining all crucial dynamic components is developed and implemented using Matlab/Simulink and the wear rate [13] is

compared before and after a change of contact conditions under a range of operational speed. A Newton-Euler method [17, 18] is used to obtain the motion equations of the locomotive model. For the contact mechanics, Polach's adhesion model [19] is adopted as it has been verified to be relatively accurate for the application in the field of locomotive traction analysis [20].

2. Simulation modelling

In order to compare the wear damage with and without the proposed wear controller, a locomotive dynamic model considering all essential dynamic components needs to be developed, as shown in Figure 1.

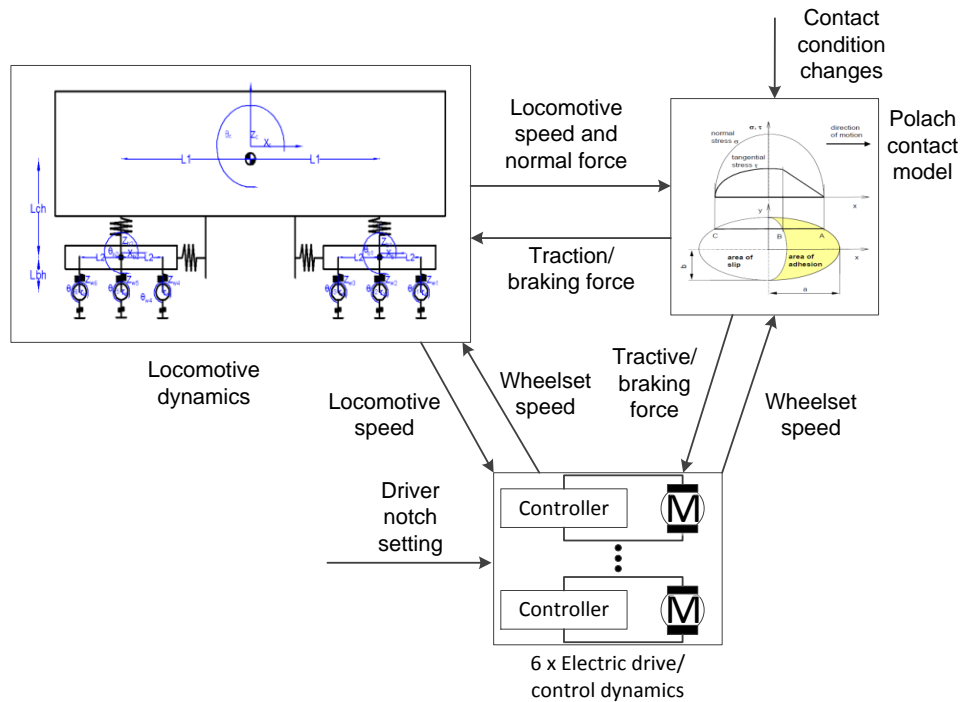


Figure 1. Schematic diagram of the overall system.

In this study, the locomotive dynamic model proposed in [21] is employed. Additionally, simplified electric drive models with a PI creep controller and a PI creep-wear controller are integrated into the electric drive/control dynamics block in this model. Each of these components is detailed in the following sections.

2.1. Locomotive longitudinal-vertical dynamic modelling

In this paper, the 2-dimensional locomotive dynamics model developed in [21] is employed. The model emphasizes longitudinal, vertical and pitch dynamics of locomotive motion. Details of the model is in [21].

2.2. Creep force modelling

The Polach model employed is a regular form considering both longitudinal and lateral creep forces. However this is a simulation on a straight track, so only longitudinal dynamics need to be considered. Hence it is assumed the locomotive is tracking with no lateral displacement on the contact patch. The formulae are detailed in [22]. Typical model parameters have been provided by Polach [19], as listed in Table 1.

Table 1: Parameters for dry [19] and friction modifier (FM) contact condition tuned according to the data in [10]

Parameters	Contact condition	
	Dry [27]	FM [66]
k_A	1.00	0.60
k_s	0.40	0.20
μ_0	0.55	0.23
A_p	0.40	0.50
B_p	0.60	0.30

2.3. Wear Control index

Wear of both rail and wheel can be categorized as Type I (Mild), Type II (Severe) and Type III (Catastrophic) regimes. Recent research [10, 23] shows that there are wear transitions between wear types of wheel/rail steel and models and proposed models for various rail materials.

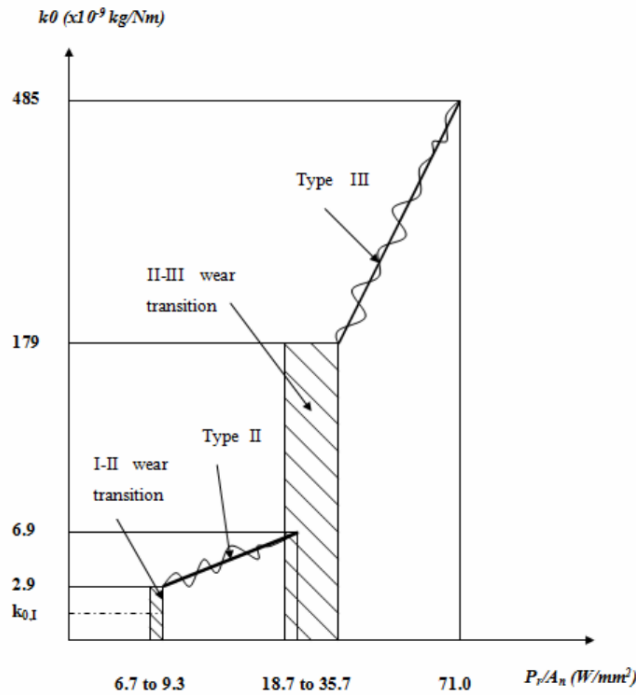


Figure 2. The wear coefficient versus the frictional power density for BS11 rail steel, running with class D wheel steel [10].

The frictional power density P_r/A_n is defined by $\frac{P_r}{A_n} = F_t V_s / A_n$, where F_t is the traction force, V_s is the relative slip velocity and A_n is the nominal contact area. The wear coefficient k_0 is determined by

$$k_0 = \frac{\Delta m}{\Delta W} \quad (1)$$

where Δm is the mass loss of rail disc after a certain time interval and ΔW is the frictional work dissipated in the rolling/sliding contact [10]. The wear coefficient under dry condition is about 4.7 times that under friction modifier condition [10]. In this work it is assumed the ratio is independent of the locomotive speed. The mass loss rate, the amount of mass loss caused by wear per unit time, indicates the level of wear damage. According to Vuong [10],

$$\Delta W = \mu N s V \Delta t \quad (2)$$

$$\frac{\Delta m}{\Delta t} = k_0 \frac{\Delta W}{\Delta t} = k_0 \mu N s V \quad (3)$$

where μ is the adhesion coefficient, N is the normal force, s is the creep and V is the locomotive velocity. The unit of the mass loss rate is kg/s.

In order to avoid excessive wear damage on the rail and wheel as in the Type III region in Figure 2 above, the wear index value separating Type II and III regions of Figure 2 is chosen as the wear control threshold. In this study the threshold is set at 35.7 N/mm^2 .

3. Proposed control system

The creep controller in this study is chosen to be the same as in [21]. The creep and wear control for the overall locomotive is shown in Figure 3. Each wheelset has its own set of controller and motor so that the speed of the motors can be adjusted independently.

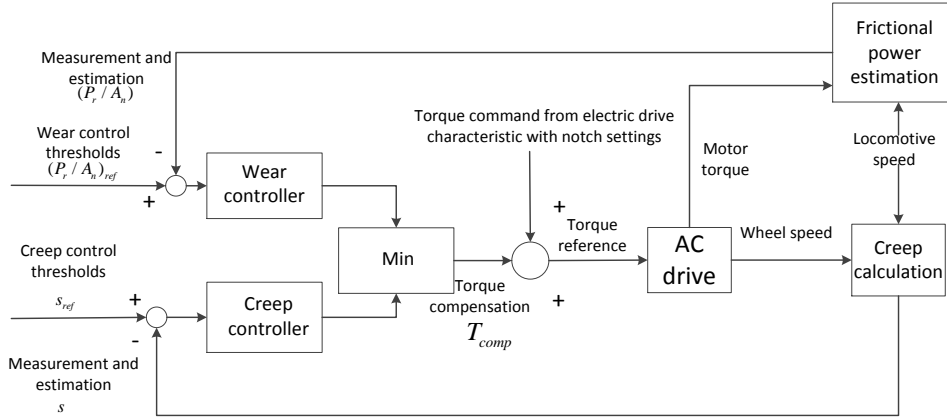


Figure 3. Creep and wear control diagram.

The details of the creep controller is provided in [21]. The torque compensation can be calculated as

$$T_{comp} = \begin{cases} 0 & \text{if } e \geq 0 \\ P_{creep} \times e + I_{creep} \times \int_{t_1}^{t_2} e dt & \text{if } e < 0 \end{cases} \quad (4)$$

where $e = s_{ref} - s$ is the difference between the creep threshold and the measured creep.

Similarly, the wear controller adjusts the torque generated by the motor if either the frictional power density estimation exceeds the frictional power density threshold setting or the creep measurement exceeds the creep threshold setting. If both the creep measurement and the frictional power density estimation are lower than their corresponding pre-set thresholds, the controller is not activated; otherwise the controller outputs the smaller negative value of the two as the torque compensation. The parameter values of the creep control subsystem are the same as that of the creep only controller. The PI wear control subsystem control parameters are $P_{wear} = 1.25 \times 10^7$ and $I_{wear} = 8 \times 10^3$ respectively. The torque compensation generated by the wear and creep controller can be calculated as

$$T_{comp} = \begin{cases} 0 & \text{if } e_s \geq 0 \text{ and } e_{P_r/A_n} \geq 0 \\ P_{creep} \times e_s + I_{creep} \times \int_{t_1}^{t_2} e_s dt & \text{if } e_s < 0 \text{ and } e_{P_r/A_n} \geq 0 \\ P_{wear} \times e_{P_r/A_n} + I_{wear} \times \int_{t_1}^{t_2} e_{P_r/A_n} dt & \text{if } e_s \geq 0 \text{ and } e_{P_r/A_n} < 0 \\ \min \left\{ P_{creep} \times e_s + I_{creep} \times \int_{t_1}^{t_2} e_s dt, P_{wear} \times e_{P_r/A_n} + I_{wear} \times \int_{t_1}^{t_2} e_{P_r/A_n} dt \right\}, & \text{if } e_s < 0 \text{ and } e_{P_r/A_n} < 0 \end{cases} \quad (5)$$

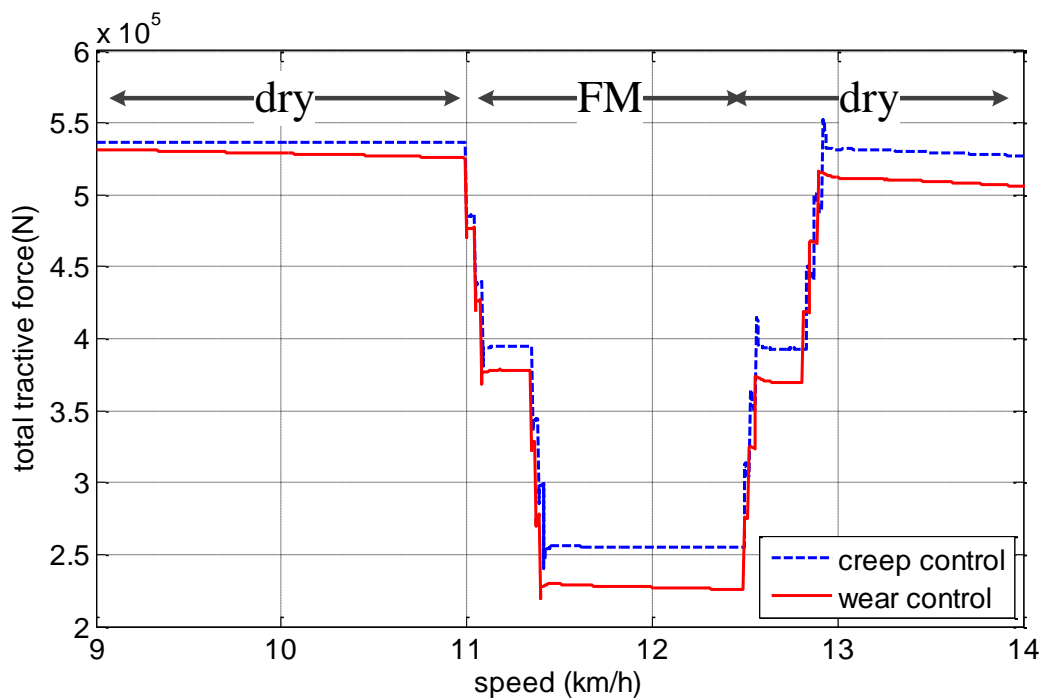
Simulations have been carried out using the creep controller and the wear controller. Simulation results are compared in order to show the effectiveness of the wear controller in terms of reducing wear damage on the rail tracks.

4. Results

The same assumptions are made as in [22]. The dynamic response comparison with creep and wear controllers employs speed rather than time as the horizontal axis because the adhesion coefficient, is determined by the creep and locomotive speed under the same wheel/rail contact condition. As a result the change of contact condition of the first axle is assumed to happen at a certain speed and sequentially at the rest of axles to ensure the same force condition.

Case I: Low speed operation simulation:

The comparison of total tractive force with creep and wear controllers under change of wheel/rail contact conditions between dry and friction modifier condition (FM) as shown in Table 2 under low speed operation is shown in Figure 4 below.



Figure

4. Comparison of total tractive forces with creep and wear controllers.

It can be seen that under low speed operation, the total tractive force is about 3.7% lower with wear control than that with creep control under dry wheel/rail contact condition, and about 11% under FM wheel/rail contact condition. Also when the wheel/rail contact condition changes from FM back to dry, the total tractive force with the wear controller has less overshoot than that with the creep controller. Also it can be noticed with the increase of locomotive speed, the total tractive force difference increases between the case with creep control and that with wear control. The reason of this is that the creep control takes slip velocity normalized by the speed of the locomotive as the control index; on the other hand, the wear control takes the frictional power density as the control index, which is directly affected by the slip velocity. As a result with the increase of the locomotive speed, the constant creep value means a larger slip velocity, which will result in a higher frictional power density ignoring the change of tractive force on the axle.

The comparison of front and rear bogie pitch with creep and wear controllers under a change of wheel/rail contact conditions under low speed operation is shown in Figure 5 below.

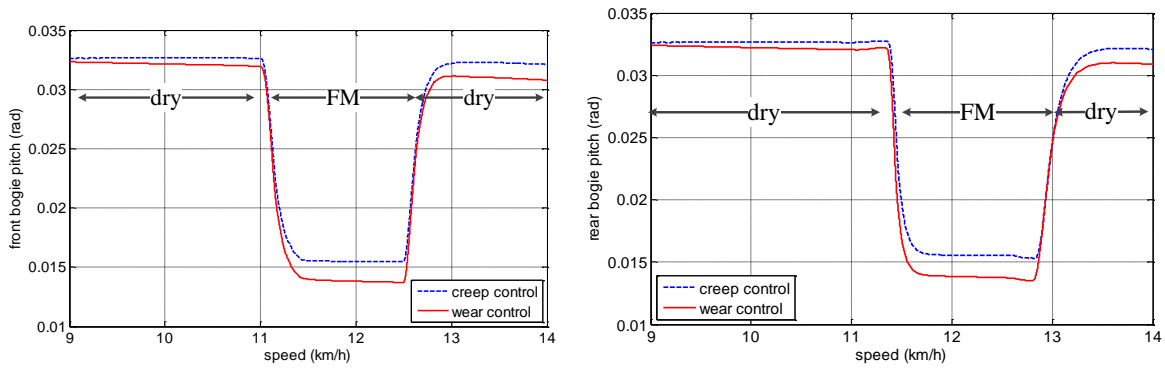


Figure 5. Comparison of front and rear bogie pitch with creep and wear controllers.

The front and rear bogie pitch motions show similar dynamic responses to that of the total tractive force. The difference of pitch angles increases with the increase of locomotive speed at low speed operation.

The comparison of car body pitch with creep and wear controllers under change of wheel/rail contact conditions under low speed operation is shown in Figure 6 below.

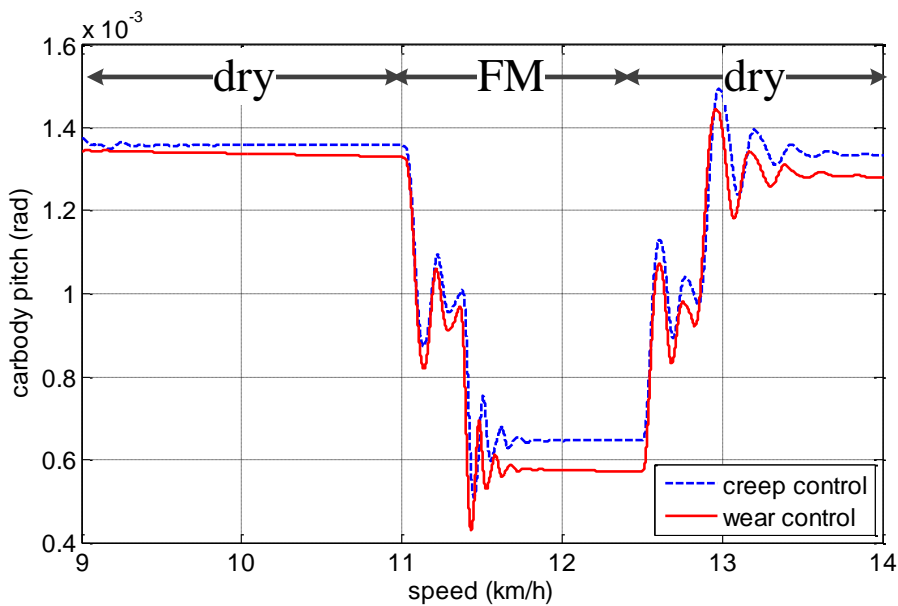


Figure 6. Comparison of car body pitch with creep and wear controllers.

The response of the car body pitch angle is closely correlated with that of the total tractive force. The change in car body pitch angles increases with locomotive operating speed. In addition, there are noticeable oscillations during the change of the wheel/rail contact condition, particularly when all axles on the front/rear bogie finish their contact condition transition. The reason for this is that after the last axle of the front bogie has run into the FM rail and before the first axle of the rear bogie runs into the FM area, the tractive force is relatively steady after a step change, forming a step-like tractive force variation as shown in Figure 4. This step-like tractive force change excites the mode of vibration of the car body pitch motion.

The comparison of axle 1 creep response with creep and wear controllers under change of wheel/rail contact conditions under low speed operation is shown in Figure 7 below.

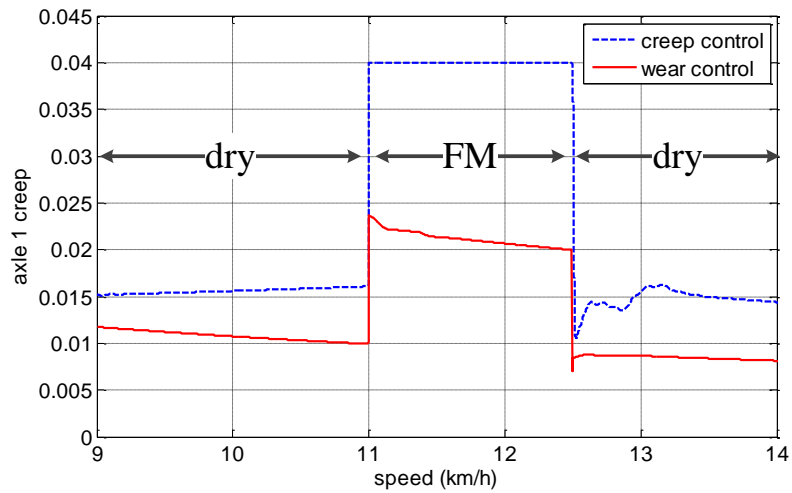


Figure 7. Comparison of axle 1 creep with creep and wear controllers.

The creep of axle 1 with the wear controller is about 43.4% and 59% lower than that with the creep controller under dry and FM wheel/rail contact conditions respectively.

The comparison of axle 1 frictional power density with creep and wear controllers under a change of wheel/rail contact conditions under low speed operation is shown in Figure 8 below.

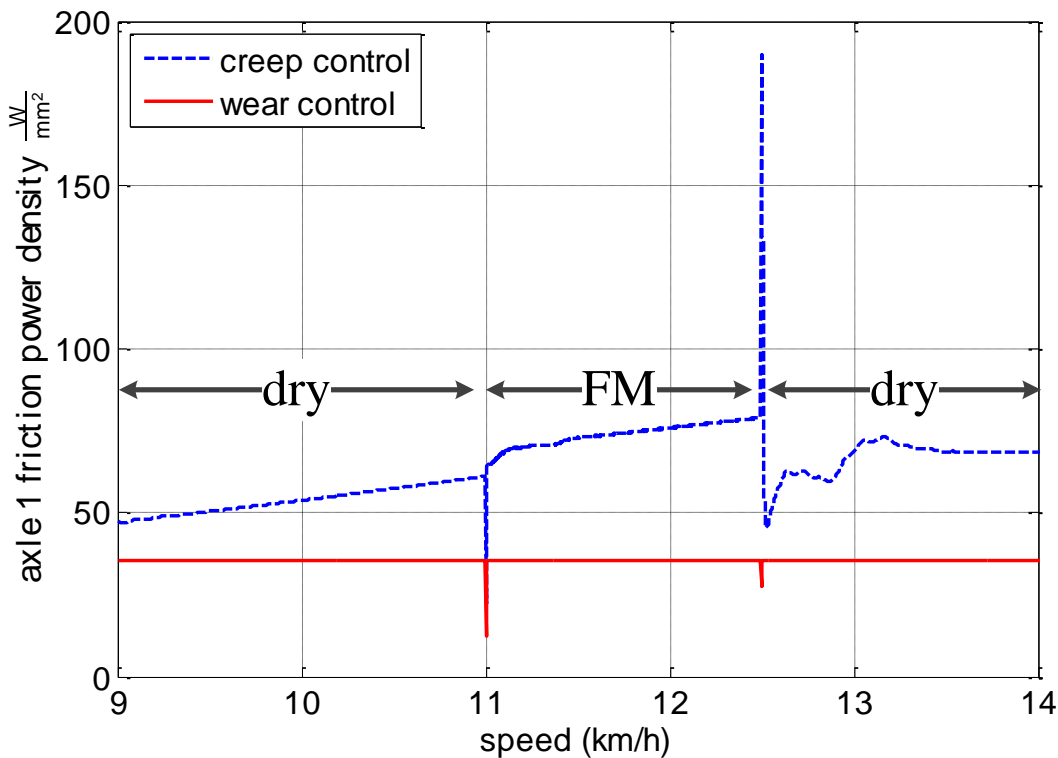


Figure 8. Comparison of axle 1 friction power density with creep and wear controllers.

As the wear controller employs a constant frictional power density as the control threshold, the value of the frictional power density is effectively constrained despite of the change of wheel/rail contact conditions. The frictional power density of axle 1 with creep controller, on the other hand, is about 1.92 and 2.1 times that with wear controller under dry and FM contact conditions respectively.

The comparison of axle 1 wear coefficient with creep and wear controllers under change of wheel/rail contact conditions under low speed operation is shown in Figure 9 below.

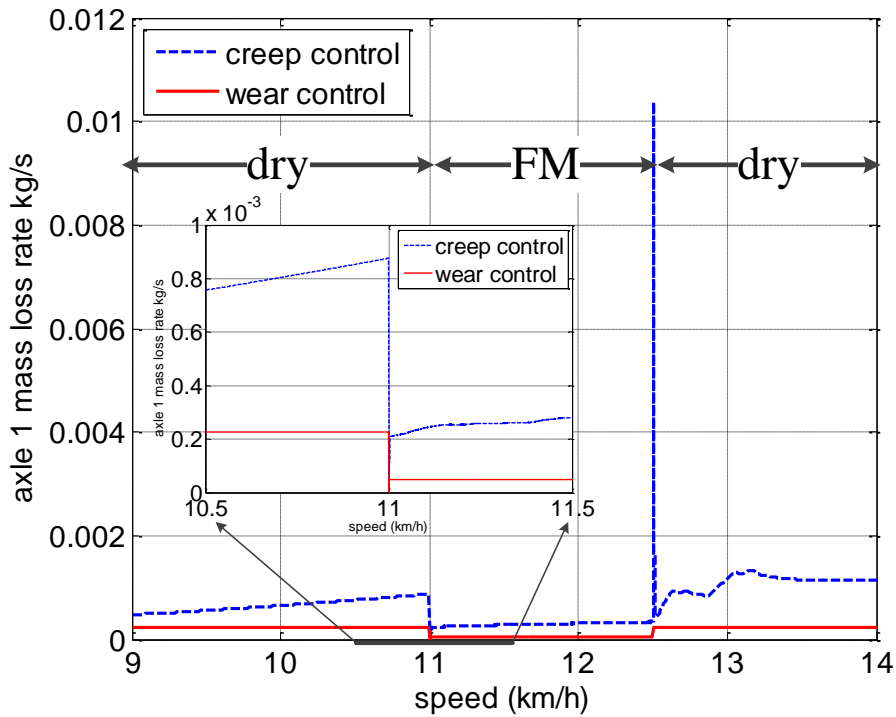


Figure 9. Comparison of axle 1 mass loss rate with creep and wear controllers.

As it is shown in Figure 9, the mass loss rate with the wear controller has been reduced to about 20% and 16% than that with the creep controller, under the dry and FM conditions respectively.

Case II: High speed operation simulation:

The comparison of total tractive force with creep and wear controllers under a change of wheel/rail contact conditions under high speed operation is shown in Figure 10 below.

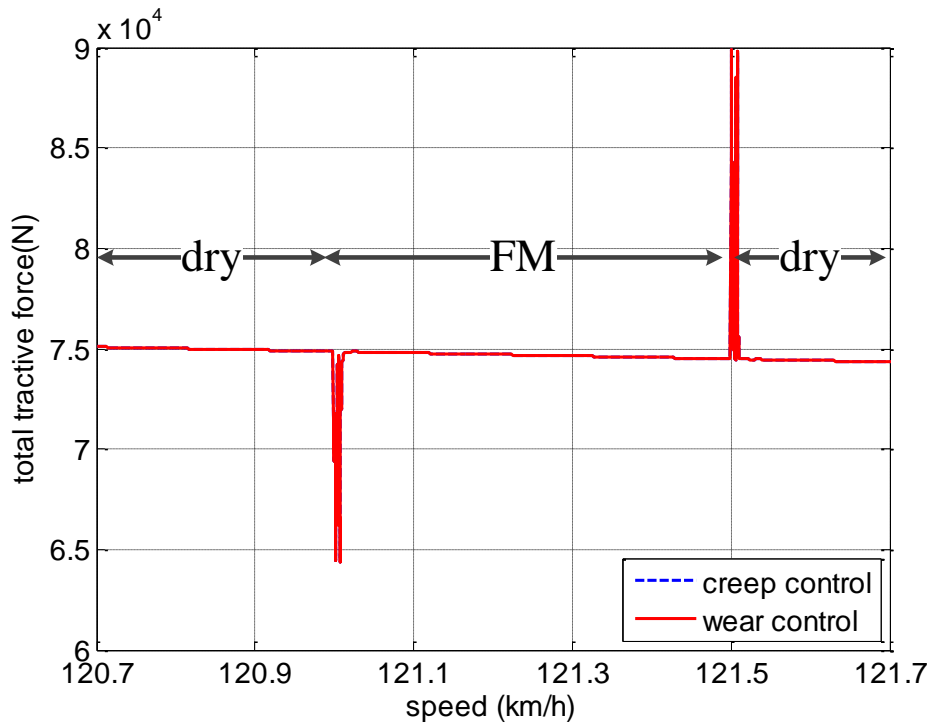


Figure 10. Comparison of total tractive forces with creep and wear controllers.

Due to the impact of the electric drive tractive effort characteristic, the total tractive force is much lower at high speed than that at low speed. Consequently under high speed operation the controllers do not take effect and there is no difference between the total tractive force with the creep controller and that with the wear controller under both dry and FM wheel/rail contact conditions.

The comparison of front and rear bogie pitch angles with creep and wear controllers under a change of wheel/rail contact conditions under high speed operation is shown in Figure 11 below.

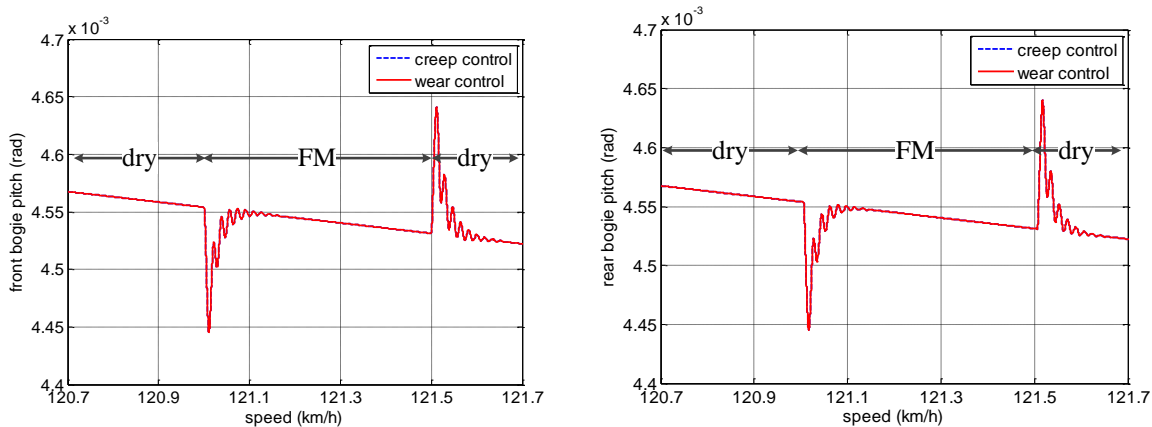


Figure 11. Comparison of front and rear bogie pitch with creep and wear controllers.

Since the same amount of low tractive force achieved under high speed operation, the actual creep and the frictional power density are below their control thresholds, as shown in Figure 13 and Figure 14. As a result of neither controller being activated, the pitch motions of the front and rear bogies show the same dynamics with the creep and wear controllers. The comparison of the car body pitch angles with creep and wear controllers under a change of wheel/rail contact conditions under high speed operation is shown in Figure 12 below.

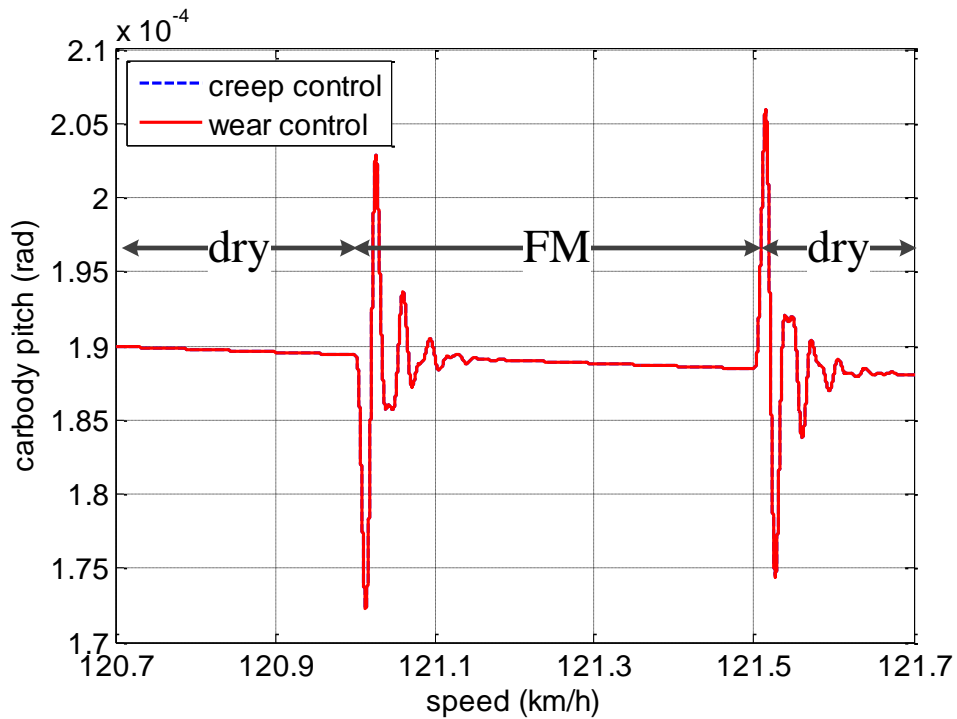


Figure 12. Comparison of car body pitch with creep and wear controllers.

The dynamic response of the car body pitch motion with the creep controller shows the same behaviour with that with the wear controller due to the same amount of tractive force.

The comparison of axle 1 creep response with creep and wear controllers under change of wheel/rail contact conditions under high speed operation is shown in Figure 13 below.

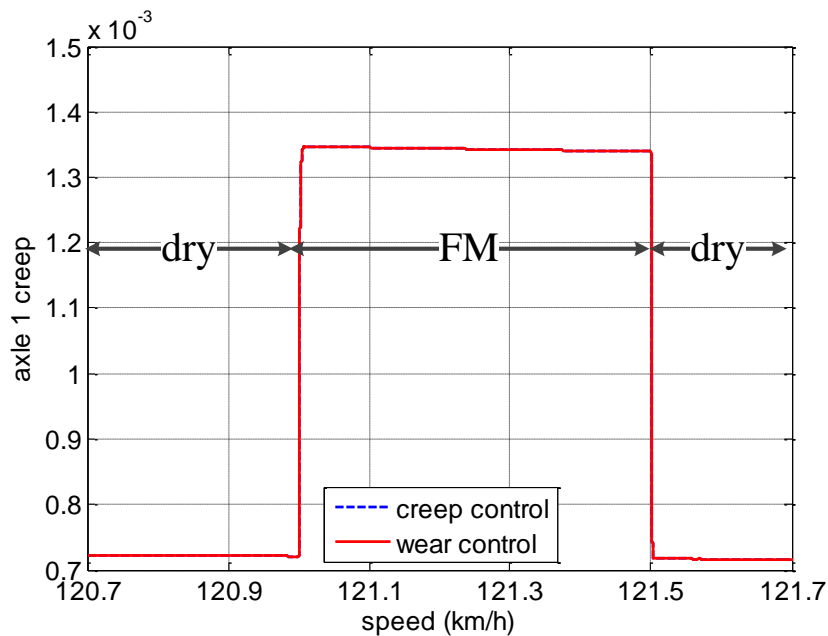


Figure 13. Comparison of axle 1 creep with creep and wear controllers.

The dynamic response of the axle 1 creep with the creep controller shows the same behaviour with that with the wear controller due to the same amount of tractive force.

The comparison of axle 1 frictional power density with creep and wear controllers under a change of wheel/rail contact conditions under high speed operation is shown in Figure 14 below.

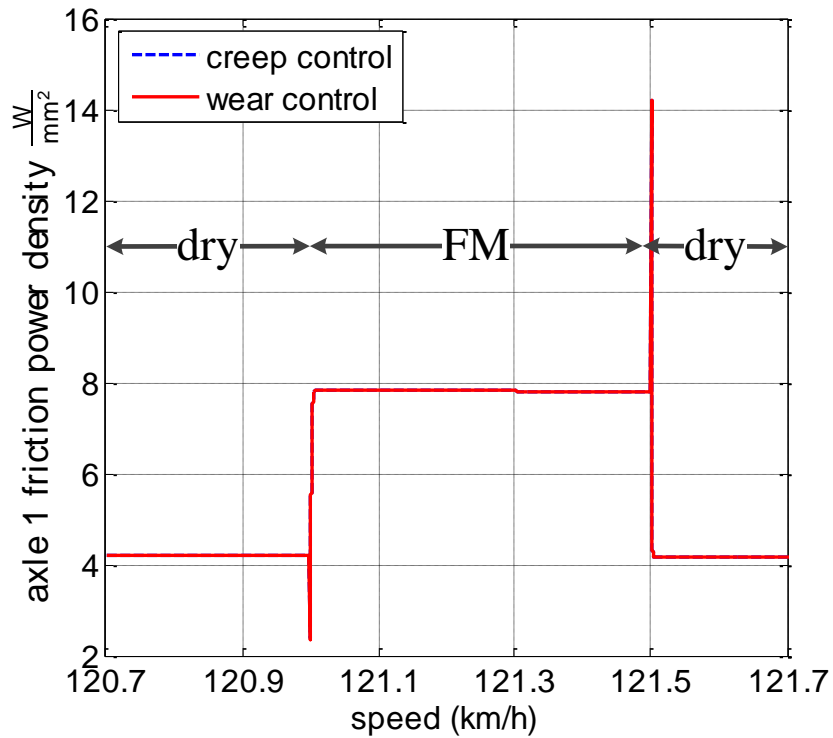


Figure 14. Comparison of axle 1 friction power density with creep and wear controllers.

The dynamic response of the axle 1 creep with the creep controller shows the same behaviour with that with the wear controller due to the same amount of tractive force. The comparison of axle 1 wear coefficient with creep and wear controllers under change of wheel/rail contact conditions under high speed operation is shown in Figure 15 below.

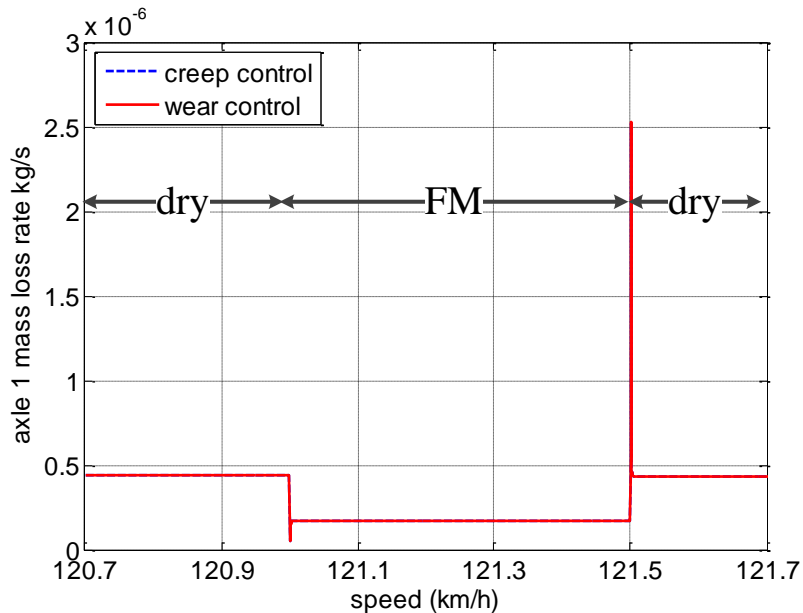


Figure 15. Comparison of axle 1 wear coefficient with creep and wear controllers.

The response of mass loss rate has similar behaviour with both controllers. Comparing Figure 12 and 18, it can be seen that the mass loss rate at high speed operation is much lower than that at low speed operation.

5. Conclusion

In this paper, a real-time rail/wheel wear damage control is developed. Simulations have been performed with a mathematical model of locomotive longitudinal, vertical and pitch dynamics, the Polach wheel/rail contact mechanics, and simplified electric drive dynamics. Simulations have been carried out to compare the locomotive dynamic response with a creep controller and the wear controller. Simulation results show that the proposed wear controller can reduce wear damage significantly under low speed operation, but has little effect on high speed operation. The cost of corresponding tractive force reduction is reasonably small.

References:

- [1] S. Hillmansen and C. Roberts, "Energy storage devices in hybrid railway vehicles: A kinematic analysis," *Proceedings of the Institution of Mechanical Engineers, Part F: Journal of Rail and Rapid Transit*, vol. 221, pp. 135-143, January 1, 2007 2007.
- [2] D. T. Eadie, et al., "The effects of top of rail friction modifier on wear and rolling contact fatigue: Full-scale rail-wheel test rig evaluation, analysis and modelling," *Wear*, vol. 265, pp. 1222-1230, 2008.
- [3] J. Mathew, et al., *Engineering Asset Management: Proceedings of the First World Congress on Engineering Asset Management (WCEAM) 2006*: Springer-Verlag, 2008.
- [4] T. M. Beagley, "Severe wear of rolling/sliding contacts," *Wear*, vol. 36, pp. 317-335, 1976.
- [5] P. J. Bolton and P. Clayton, "Rolling—sliding wear damage in rail and tyre steels," *Wear*, vol. 93, pp. 145-165, 1984.
- [6] D. Markov and D. Kelly, "Mechanisms of adhesion-initiated catastrophic wear: pure sliding," *Wear*, vol. 239, pp. 189-210, 2000.
- [7] D. Danks and P. Clayton, "Comparison of the wear process for eutectoid rail steels: Field and laboratory tests," *Wear*, vol. 120, pp. 233-250, 1987.
- [8] S. Zakharov, et al., "Wheel flange/rail head wear simulation," *Wear*, vol. 215, pp. 18-24, 1998.
- [9] R. Lewis and U. Olofsson, "Mapping rail wear regimes and transitions," *Wear*, vol. 257, pp. 721-729, 2004.
- [10] T. Vuong, "Investigation for the wear coefficient of the frictional-work wear model and feasibility of friction modifiers for wear-type corrugation control," 2011.
- [11] M. Ignesti, et al., "Development of a wear model for the prediction of wheel and rail profile evolution in railway systems," *Wear*, vol. 284–285, pp. 1-17, 2012.
- [12] R. Lewis, et al., "Mapping railway wheel material wear mechanisms and transitions," *Proceedings of the Institution of Mechanical Engineers, Part F: Journal of Rail and Rapid Transit*, vol. 224, pp. 125-137, 2010.
- [13] F. Braghin, et al., "A mathematical model to predict railway wheel profile evolution due to wear," *Wear*, vol. 261, pp. 1253-1264, 2006.
- [14] J. Pombo, et al., "A study on wear evaluation of railway wheels based on multibody dynamics and wear computation," *Multibody System Dynamics*, vol. 24, pp. 347-366, 2010/10/01 2010.
- [15] J. Pombo, et al., "Development of a wear prediction tool for steel railway wheels using three alternative wear functions," *Wear*, vol. 271, pp. 238-245, 2011.
- [16] E. H. Law and N. K. Cooperrider, "A survey of railway vehicle dynamics research," *ASME Journal of Dynamic Systems, Measurement, and Control*, vol. 96, pp. 132-146, June 1974 1974.
- [17] R. Guclu and M. Metin, "Fuzzy Logic Control of Vibrations of a Light Rail Transport Vehicle in Use in Istanbul Traffic," *Journal of Vibration and Control*, vol. 15, pp. 1423-1440, September 1, 2009 2009.
- [18] D. S. Garivaltis, et al., "Dynamic Response of a Six-axle Locomotive to Random Track Inputs," *Vehicle System Dynamics*, vol. 9, pp. 117-147, 1980/05/01 1980.
- [19] O. Polach, "Creep forces in simulations of traction vehicles running on adhesion limit," *Wear*, vol. 258, pp. 992-1000, 2005.
- [20] M. Spiryagin, et al., "Creep force modelling for rail traction vehicles based on the Fastsim algorithm," *Vehicle System Dynamics*, vol. 51, pp. 1765-1783, 2013/11/01 2013.
- [21] Y. Tian, et al., "Investigation of the impact of locomotive creep control on wear under changing contact conditions," *Vehicle System Dynamics*, pp. 1-18, 2015.
- [22] Y. Tian, et al., "Comparison of PI and fuzzy logic based sliding mode locomotive creep controls with change of rail-wheel contact conditions," *International Journal of Rail Transportation*, vol. 3, pp. 40-59, 2015/01/02 2015.
- [23] T. T. Vuong and P. A. Meehan, "Wear transitions in a wear coefficient model," *Wear*, vol. 266, pp. 898-906, 2009.

Paper F

Dynamic response of a locomotive with AC electric drives due to changes in friction conditions

Dynamic response of a locomotive with AC electric drives due to changes in friction conditions

Sheng Liu¹, Ye Tian^{1,2}, W.J.T. (Bill) Daniel^{1,2}, Paul A. Meehan^{1,2}

¹*School of Mechanical and Mining Engineering, the University of Queensland, Queensland, Australia 4072*

²*Cooperative Research Centre for Railway Engineering and Technology (CRC Rail), Queensland, Australia*

ABSTRACT

The locomotive traction control behaviour and its dynamic impact on the rail and vehicle have not been investigated deeply in respect to transient conditions. Such transient traction behaviour could be more significant to dynamic traction performance and track degradation (i.e. squat/corrugation formation etc.) than steady state behaviour. In order to study this, detailed numerical simulations are performed to investigate the locomotive dynamic response to a change in contact conditions. In particular, locomotive vibration, dynamic normal and tractive forces, and creep response are determined using a developed full scale locomotive dynamics model. The model includes the detailed AC motor dynamics, which was not considered in previous works. The result shows that the detailed model is capable of simulating the dynamic fluctuations of creep and traction forces that is not presented in the simpler model. Such transient response may cause damage to the track and vehicle components.

Keywords Locomotive traction, multibody dynamics, AC motor dynamics, friction

1. Introduction

The recent development of AC traction motor and control technology used on locomotives has allowed locomotives to be operated with much higher continuous traction forces and adhesion levels than previously achieved on locomotives with DC motors. Therefore it has attracted great attention from the rail industry due to the high power capacity, reliability and low maintenance. They however require precision traction control to achieve steady performance close to the adhesion limit i.e. from 30% to 46% [1]. It is especially important to understand and control the dynamic and creep response in the change of contact conditions due to natural perturbations in friction/lubrication, wheel/rail profiles, track curvature, vehicle/track dynamics, wheel/track imperfections etc. Such transient traction behaviour could be more significant to dynamic traction performance and track degradation (i.e. squat/corrugation formation etc.) than steady state behaviour. It is therefore important to understand the dynamic response due to a change in friction conditions. In order to study this, the vehicle/track dynamics, contact mechanics and traction and creep control behaviour of modern AC locomotive drives needs to be integrated and assessed as a total dynamic feedback interactive system.

To achieve this, the understanding of dynamic interactions between the locomotive structure, contact mechanics and traction control system is essential, especially the dynamic forces on the wheel-rail contact patch. Vehicle dynamics of locomotives has been previously studied in regard to wheel-rail contact mechanics, bogie self-steering etc. using different multibody software packages. The simplest model proposed to reveal the overall dynamics of a locomotive is a quarter rail vehicle model, which is preferred in many studies because of its simplicity and ease of application [2, 3]. Newton/Lagrangian full locomotive model for locomotive dynamic analysis is also built by means of basic newton principles or the Lagrangian method [4, 5]. However, these are either limited by modelling simplicity, particularly for the tractive and control dynamics, or simulation time. A rather complex locomotive model [6] has been built using the finite element method, though these FEM models are very time-consuming and computationally expensive. Spiryagin et al., proposed the multibody dynamics model on a bogie test rig compared with a locomotive

model, which further validated the accuracy of the high efficiency dynamics model [7]. Additionally, the integrated electric AC drive dynamics is expected to play a significant role in a locomotive dynamics system. A locomotive dynamics model with a simplified AC motor was proposed to simulate the transient dynamic response, from which the oscillation of the forces are linked to the corresponding vibration mode [8]. However the dynamic effect of the AC motor and creepage were not included, and the simulated time was not sufficient for the system to settle to a steady state. Therefore results of modelling a locomotive as a full mechatronic system combining the structural dynamics, contact mechanics and detailed AC motor dynamics for a relatively long time are required.

The aim of this research is firstly to develop a comprehensive numerical simulation based on a state-of-the-art locomotive dynamics model, which includes locomotive multibody dynamics, contact mechanics, detailed AC drive mechatronic systems, and creep controllers. The second aim is to use the developed model to investigate the dynamic response of a locomotive at a change of contact friction conditions to determine dynamic tractional forces that may cause excess damage to the vehicle and tracks.

2. Model establishment and validations

2.1. Overview

The locomotive dynamics model for a simplified dynamic model is based on Newton-Euler formulation, using a wheel-rail contact model based on Polach's method [9], an AC drive model based on direct torque control (DTC) with a creep controller. The locomotive model is comprised of three major components: locomotive multibody dynamics, AC drive & controller dynamics, and contact mechanics. The overall model structure is shown in Figure 1. Details of each block will be explained in the following sections. The input of the locomotive model is the traction or braking force acting on one of the wheelsets calculated with the Polach traction/adhesion model. Inputs of the Polach traction model are locomotive speed, wheelset speed, normal contact force and contact condition. Inputs of the AC drive are drive notch setting, traction or braking force as loading on the motor shafts and locomotive speed.

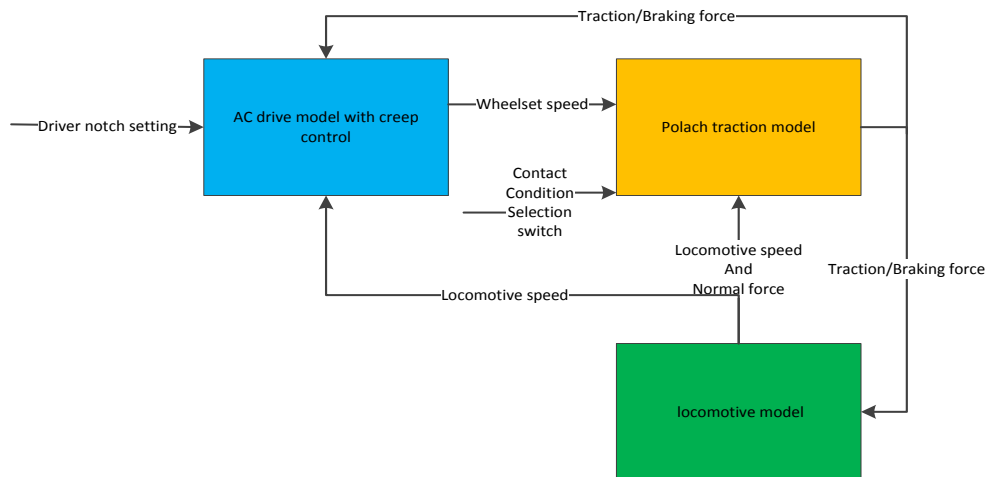


Figure 1: Overall model structure of the dynamic model of a locomotive.

The model is built in Matlab™ with the Simulink™ module. The efficiency of the model is optimized for real time use, and takes approximately 5 ~ 10 mins for compiling and 10 ~ 20 mins for simulating 10 s of real-time when run on a desktop computer, depending on whether the detailed AC motor dynamics is used. Given that this model is in completely monitored configuration, i.e., all dynamic response and AC drive conditions are continuously recorded, it is expected that the simulation time could be significantly reduced when deployed in real time circumstances.

2.2. Locomotive multibody dynamics

The locomotive has been modelled as shown in Figure 2 for the purpose of building its dynamic model. In this simplified model only dynamics along the longitudinal, vertical and pitching direction are considered. The figure also shows the structure of the simplified co-co locomotive which has two bogies. Each bogie has three axles attached. Key simulated parameters including geometry, velocity, displacement, and rotational motions are marked in the figure.

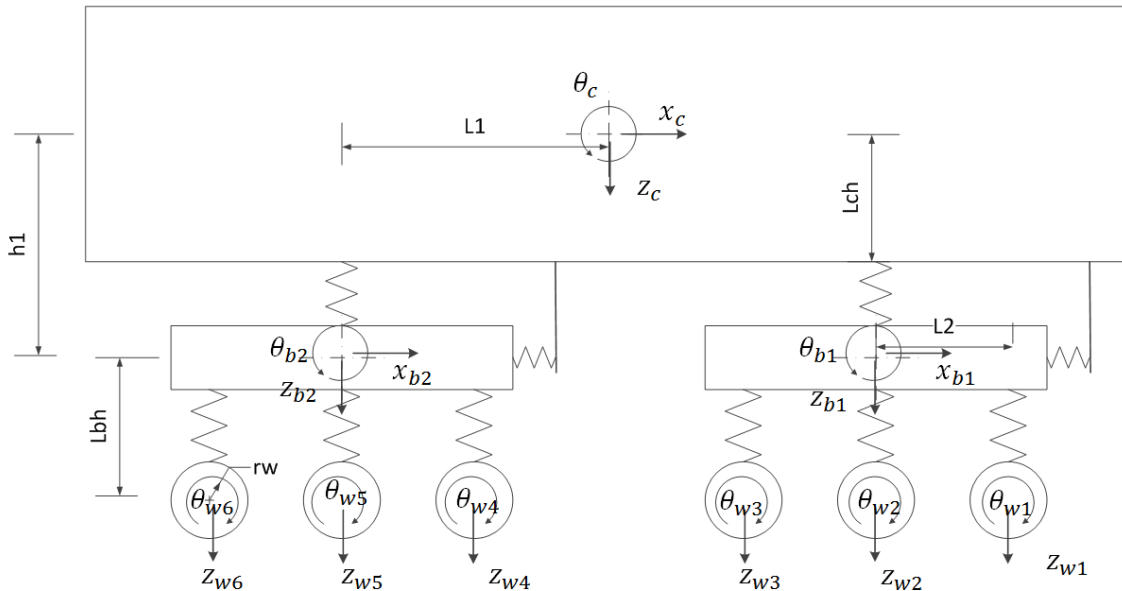


Figure 2: Diagram of simplified locomotive multibody structure

This simplified dynamic model has 21 degrees of freedom (DOF), including 9 DOF for the longitudinal, vertical and pitching motion of locomotive body and two bogies, and 12 DOF for the vertical and rotating motion of the six axles. The system variables are expressed as a vector containing 42 entries, representing the relative displacements and velocities between different nodes. The multibody dynamics model is built using Matlab Simulink and takes input such as the torque control signal, and outputs the resultant locomotive dynamic response to other modules.

An eigenmode analysis was performed in Matlab to identify all the dynamic modes of vibration and to determine the stability of the system. An eigenvalue is obtained for each possible mode of vibration of the system. The first part (real value) of each complex eigenvalue represents the amount of damping (if negative) of each mode of vibration. The second part (complex value) represents the part from which the frequency of vibration can be calculated. From the eigenvalues of the system, it can be seen that all modes of vibration except one, have positive damping (negative real parts) which implies that the system is stable. The one pair of eigenvalues with zero damping is expected due to the rigid body longitudinal motion of the train. The modal frequencies may be calculated as shown in Table 1 in (Hz).

Table 1: Modal frequencies of the multibody dynamic system vibration (Hz)

Vibration mode	Frequency
Car body vertical	0.8
Car body pitching	1.4
Bogie 1 horizontal	2.8
Bogie 2 horizontal	2.9

Bogie 1 vertical	7.2
Bogie 2 vertical	7.2
Bogie 1 pitching	12
Bogie 2 pitching	12
Wheelset 1 vertical	216
Wheelset 2 vertical	216
Wheelset 3 vertical	216
Wheelset 4 vertical	216
Wheelset 5 vertical	216
Wheelset 6 vertical	216

In the subsequent section full simulink simulations are performed from which the dominant modes of vibration in the response can be compared to the eigenvalue analysis.

2.3. Contact mechanics

The Polach contact mechanics model is widely used to determine the longitudinal tractive force due to the interaction between the wheelsets and rail tracks as it is efficient and compares well with field measurements and more complex models [9], [10]. Therefore the Polach model is employed in this research for efficiency. The implementation of the Polach model uses the inputs of locomotive velocity, normal contact force, wheel speed and a set of switchable parameters characterising different contact conditions (such as dry, wet or oil wheel-rail) including k_A , k_S , μ_0 , A and B . The output is the adhesion coefficient, defined as the ratio between the longitudinal force and normal contact force. The model is developed in Matlab Simulink based on the code provided in [11]. The parameters for dry and wet contact conditions are listed in Table 2, according to Polach's work, where A is the ratio of friction coefficient as defined as μ_∞/μ_0 , B is the coefficient of exponential friction decrease (s/m), k_A is the reduction factor in the area of adhesion and k_S is the reduction factor in the area of slip. The Polach model parameters k_A and k_S are tuned for different contact conditions as shown subsequently.

Table 2: parameters for different contact conditions [9]

Conditions Parameters	Dry	Wet
k_A	1	0.3
k_S	0.3	0.75
μ_0	0.55	0.3
A	0.4	0.4
B	0.25	0.09

2.4. Detailed AC drive controller dynamic model

The detailed AC drive co-co locomotive model includes 2 bogies, each with 3 wheelsets/AC drives. This component is used for the investigation of transient dynamic response of the locomotive connected to the AC drive dynamics. To achieve the required accuracy, a detailed AC drive model was developed, which includes the electric dynamics of the AC drives high frequency (thyristor) cycles [12]. An induction motor drive is a complicated nonlinear system, that has been the subject of a large body of research and the control schemes developed are complex [13]. The modelling allows for nonlinear inversion into a linear model, allowing the use of well understood linear control techniques [14]. The challenges with AC drive technology are accurately estimating rotor fluxes and load torques [15] and the cost associated with installing high accuracy sensors to measure rotation speed [16].

The direct torque control (DTC) method was used in the detailed AC drive [17] because it is fast in response and computationally inexpensive. The structure of a typical DTC controlled AC drive is shown in Figure 3. DTC is commonly used in controlling locomotive motors; for example DE502 and DE10023 diesel-electric locomotives, as well as some Siemens locomotives. Field-oriented control (FOC) is also widely used in

locomotive motor controls. It is suggested in the literature [18] that FOC and DTC would have very similar response. As a result, it is expected that the DTC model as described in this paper is generally able to represent FOC controlled locomotives such as the GT46. Figure 4 shows the Simulink diagram of the detailed AC drive with the DTC controller.

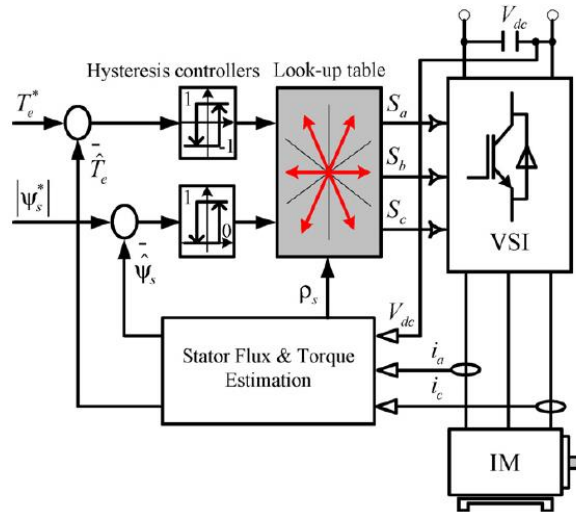


Figure 3: A typical DTC controlled AC drive structure [17]

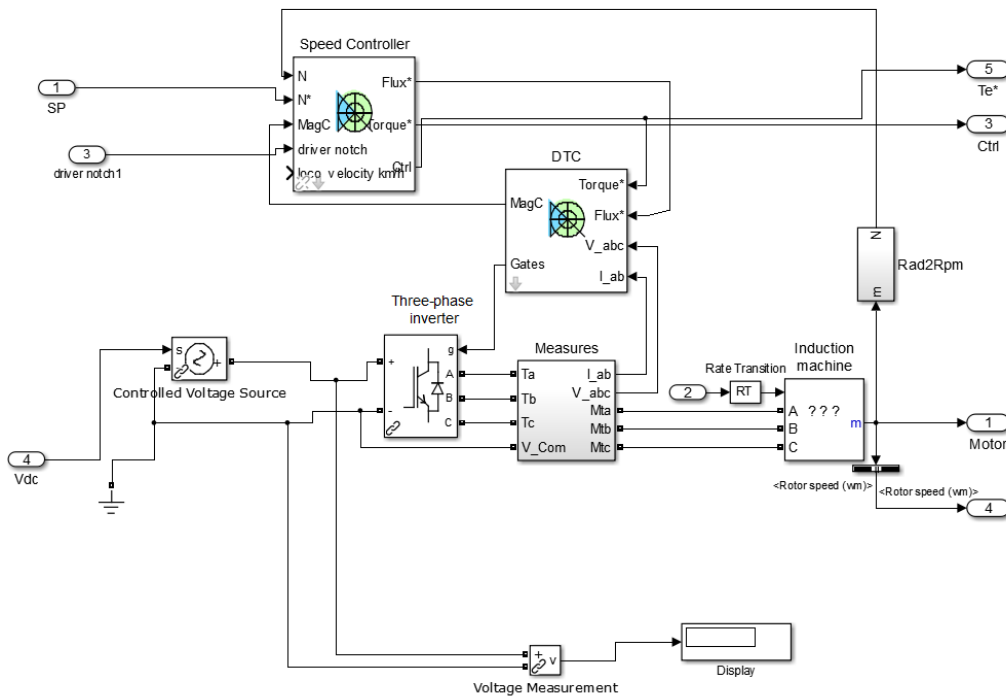


Figure 4: Simulink diagram of the detailed AC drive

The electromagnetic torque generated by the drive can be described by,

$$T_e = \frac{3}{2} p \frac{L_m}{\sigma L_s L_r} \bar{\psi}_s \times \bar{\psi}_r = \frac{3}{2} p \frac{L_m}{\sigma L_s L_r} |\bar{\psi}_s| |\bar{\psi}_r| \sin(\delta)$$

Details of the parameters and formulae used was published by Kumsuwan et al. [17].

The three phase voltage is controlled by the voltage source inverter (VSI) illustrated [19]. The control signal is generated by the look-up table where the selecting signal is determined by the difference between the reference electromagnetic torque T_e^* and the estimated electromagnetic torque T_e , and the difference between the flux Ψ_s^* and the estimated value Ψ .

2.5. Traction/creep controller

The PI controller, as shown in Figure 5, was used as the creep controller in this subsystem. It compares the measured creep value with the threshold setting and provides an electric signal to the DTC controlled AC drive rather than providing direct torque compensation when the threshold creep value is triggered. The standard PI controller is tuned to effectively control the creepage in different contact conditions including dry and wet conditions. Presently, a slightly lower creep value than the threshold is used as the target of the controller (threshold minus 0.5%).

The creep controller is based on the creepage with maximum traction effort according to the creep curve, which is set to 4% in this case. The design of the creep controller is very similar to the creep controller described in the patent document (US patent number 20130082626A [10]), which uses a threshold value of 3%. Based on the design of GT46Ace locomotive, only one creep controller is installed in each bogie. As a result, we deployed single controller logic for each bogie, which takes the maximum creep value of the three axles of the bogie as the input and generates a torque reduction signal only when the creep value exceeds the pre-set creep threshold. Otherwise the creep controller stays idle and doesn't provide a torque reduction signal. The controller includes a filter that keeps the excitation frequency within the limitation of the motor.

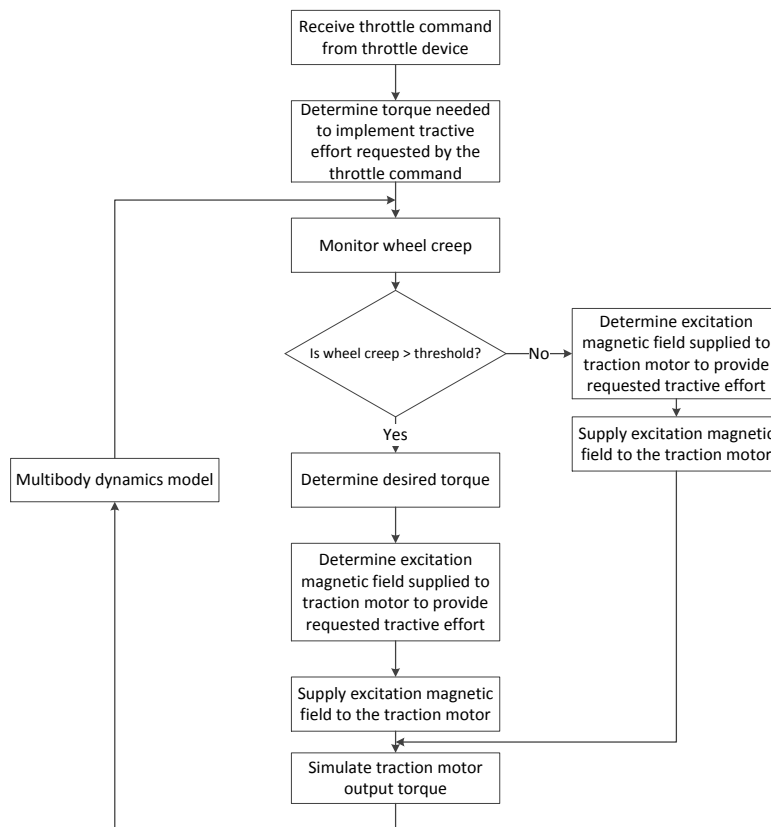


Figure 5: The creep controller in the detailed AC drive

2.6. Modelling details and locomotive specification

The locomotive model is built to simulate a full size GT46Ace locomotive. The detailed parameters for the GT46Ace locomotive dynamics model are listed in Table 3. The detailed and simplified electric AC drive dynamics, the multibody dynamics and contact mechanics module are detailed in the previous section. The traction curve of the traction motor 1TB2622 used in GT46Ace locomotive is provided by Siemens [20] as shown in Figure 6.

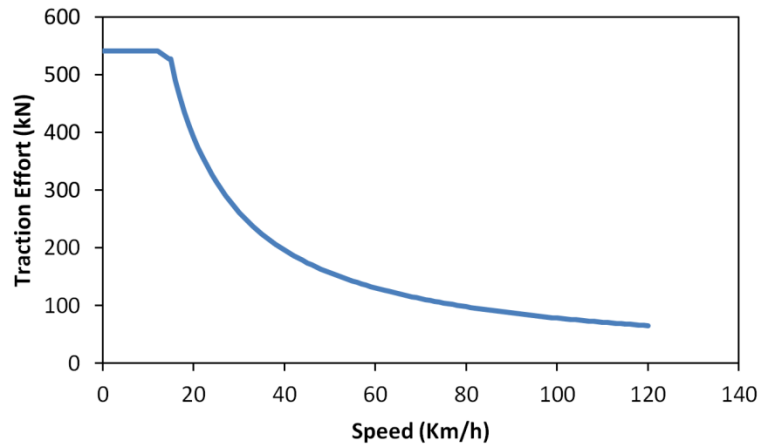


Figure 6: Traction curve of the locomotive (Notch 8) [20]

Table 3: Detailed parameters of the locomotive model:

Parameter	Value
Mass of each bogie frame (kg)	12121
Total mass of locomotive (t)	134
load mass (kg/carriage × no. of carriages)	90000 × 50
Load force (N)	4.8 × 10 ⁶
Gear Ratio	17/90
Primary suspension springs (N/m)	89 × 10 ⁶
Yaw viscous dampers stiffness (N/m)	45 × 10 ⁶
Vertical visvous dampers stiffness (N/m)	44 × 10 ⁶
Secondary suspension springs (N/m)	5.2 × 10 ⁶
Longitudinal and lateral shear stiffness (N/m)	0.188 × 10 ⁶
Traction rods stiffness (N/m)	5 × 10 ⁶
Wheel contact stiffness (N/m)	2.4 × 10 ⁹
Primary suspension vertical damping (kg/s)	10 × 10 ³
Secondary suspension vertical damping (kg/s)	2 × 10 ⁴
Rail damping (kg/s)	1 × 10 ⁶
Locomotive body length (m)	22
Locomotive body hight – without bogie (m)	1.93
Bogie length (m)	3.7
Bogie height (m)	0.733
Horizontal distance between bogies mass centre(m)	13.7
Horizontal distance between axles (m)	1.3
Vertical distance between body bottom and bogie top (m)	0.3605
Vertical distance between bogie bottom and wheel top (m)	0.127
Wheel diameter (m)	1.016
Simulation time step (s)	5 × 10 ⁻⁶
Creep threshold	4%

1. Dynamic response of a locomotive at the transient of friction condition

The full locomotive dynamic response under changing contact conditions from dry to wet are provided in this section. The structure and parameters of the simulation are described in the previous section. The notch setting is at 8. The torque generated by the electric drive together with the effect of the longitudinal force acting on the axle from the rail determine the angular acceleration of the rotor and consequently that of the axle. The change in creep in the transient response would directly affect the longitudinal traction force, and causes the dynamic change of acceleration, speed and position of all nodes in the system. The simulated dynamic response is reported below in terms of bogie and axle dynamic response, creep response and force response.

2.1. Bogie and axle dynamic response

Figure 7 shows the vertical displacement of each axle in response to a change from dry to wet conditions after 5s during acceleration. For direct comparison to the simplified model, parameters are chosen from [8]. The response on the same bogie is similar during the change of contact condition. The front and rear axle vertical displacements are dominated by the corresponding bogie pitching and the middle axle vertical displacements are dominated by the vertical motion of the bogies due to the acceleration. The vertical displacement response is different between the front (Bogie 1) and rear bogies (Bogie2). The front bogie has considerable higher amplitude compared with the rear bogie. The frequency of the car body pitching is about 1.5 Hz which is close to the eigenmode analysis result of 1.4 Hz. The system settled to a steady state after approximately 4s, after which, at 5s, the contact friction condition was changed from dry to wet. After this change large transient oscillations occur on all axles. For the front bogie, all 3 axles (yellow, light blue, and purple) respond in the same mode, which indicates the vibration of the front bogie is dominated by a bouncing caused by the car body pitching mode and the frequency is around 1.5 Hz. This agrees with the eigenmode analysis as listed in Table 1. There is also a higher frequency pitching vibration mode at roughly 13Hz (compared to 12Hz from Table 1) visible, but it is not very clear for the front bogie as the bouncing mode is dominant. For the rear bogie, the dynamic response is a combination of the bouncing/carbody pitching mode (1.5Hz) and the bogie pitching mode (12 Hz). The middle axle (light green) is in the same mode compared to the front bogie, however the leading and rear axles (red and blue) have high frequency pitching oscillations. It is noted that the oscillations of those two axles are out of phase, which is also consistent with bogie pitching. In general, it is demonstrated that after the change of friction condition, bouncing associated with the carbody pitching vibration mode will dominate the dynamic response, but for the rear bogie, the dynamic response is a combination of bouncing and bogie pitching.

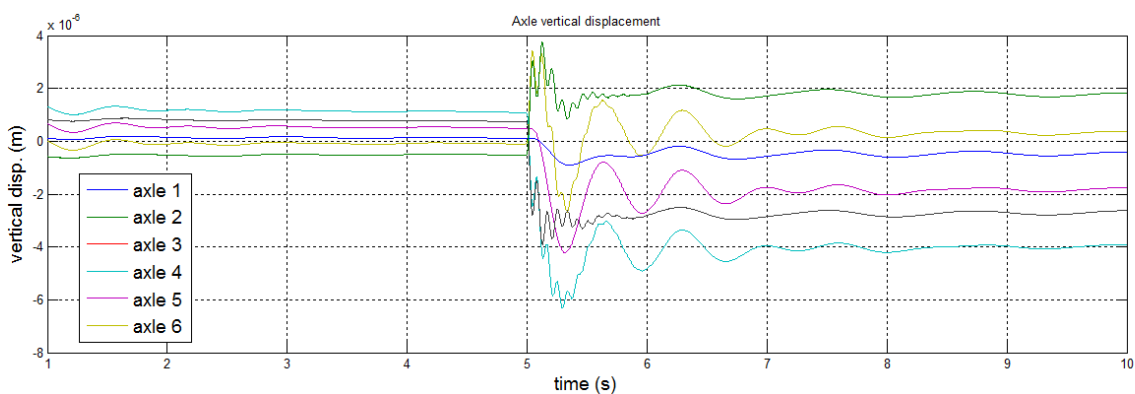


Figure 7: Vertical displacement of all axles during the change of contact condition

Figure 8 shows the pitching angle of the car body. It is shown in the figure that the locomotive body vibration in the pitching mode after the change of the friction condition is approximately 1.5 Hz that agrees with the car body pitching mode calculated in table 1. This is caused by the difference in amplitude of the vertical oscillations of the front and rear bogies shown in Figure 7. Additionally, it is shown that the stabilized pitching angle was reduced from approximately 5 mrad to 2.4 mrad. This indicates the acceleration

has reduced. Compared to the previous figures, it can be seen that the vertical displacement of the front and rear axle of each bogie is mainly determined by the pitching motion of each bogie.

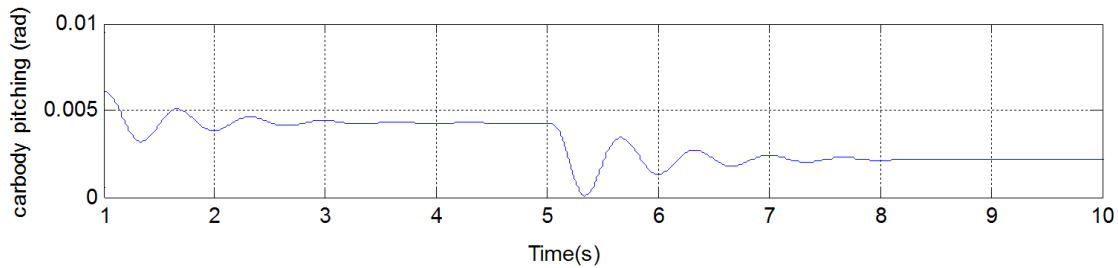
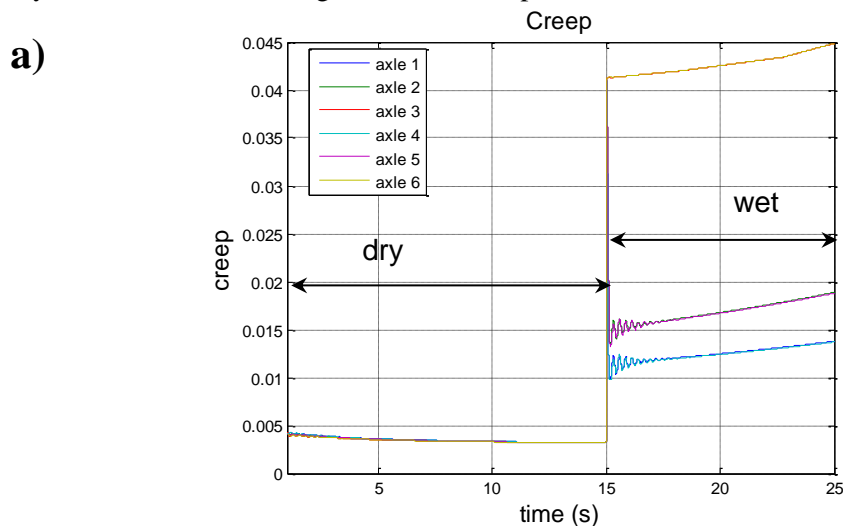


Figure 8: Pitching angles of car body and two bogies with the change of contact condition

2.2. Creep response

Figure 9 shows the creep on all six axes simulated by (a) the simplified model that was published previously [8] and (b) the detailed model developed in this work. It can be seen that the creep value of a certain axle and its counterpart on the other bogie are close to each other and change with the same pattern. Also it can be seen that the leading axles of each bogie have different dynamics from the other two axles on the same bogie. This is possibly because the creep controller takes the maximum value of all axles on a bogie as a control index, and provides a reduction of the torque command controlling all axles on the bogie. As the creep of the middle and rear axles is lower than the threshold, it doesn't affect the creep controller output. However, the creep value of the front axle on each bogie under acceleration is larger than the threshold and therefore the creep controller's output is directly affected by the creep of the leading axles. It is also shown that the creep result in both models is in good agreement before the change of friction condition at 15s. After the change of friction condition, it is indicated that, (similar to the results in the previous section), the detailed model shows significant random like high frequency oscillations, that are not seen in the simplified model result. The variation after the transient on axles other than the leading ones shown in the detailed model is caused by the effect of high frequency AC electric motor torque dynamics. This could be associated with significant wear or damage on the track. Hence it may be concluded that the simplified simulation has high efficiency compared to the detailed model. However, the detailed model is capable of revealing significant dynamic features affecting the locomotive performance.



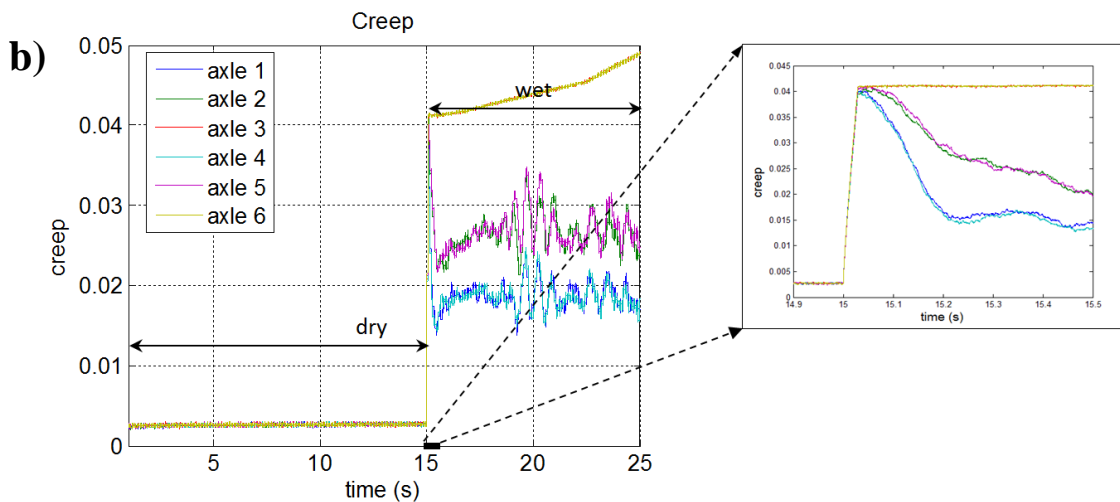


Figure 9: Constant speed under change of friction condition: Creep on each axle simulated by (a) the simplified and (b) the detailed model

The time around the change of friction is zoomed in to illustrate details of the creep change on each axle. It is also shown that after the change of friction, the creepage increased rapidly to around 0.43. The simplified model only takes 0.02s to reach the maximum creep while the detailed model takes roughly 0.13s for the increment. After that, the creep controller acts to reduce the creep. In comparison the detailed model delayed this process by 0.3s, whereas the simplified model creep controller acted almost instantly. This is likely because the simplified model directly controls the torque, while in reality and according to the detailed model, the creep controller only controls the electrical signal to the AC dynamics module that outputs the change of torque in a delayed response to the traction dynamics in Figure 9. It is shown that the creep response has not stabilized after the transient from dry to wet, although additional simulations have been performed to reveal creep response to settle to steady state after 50s as shown in Figure 10.

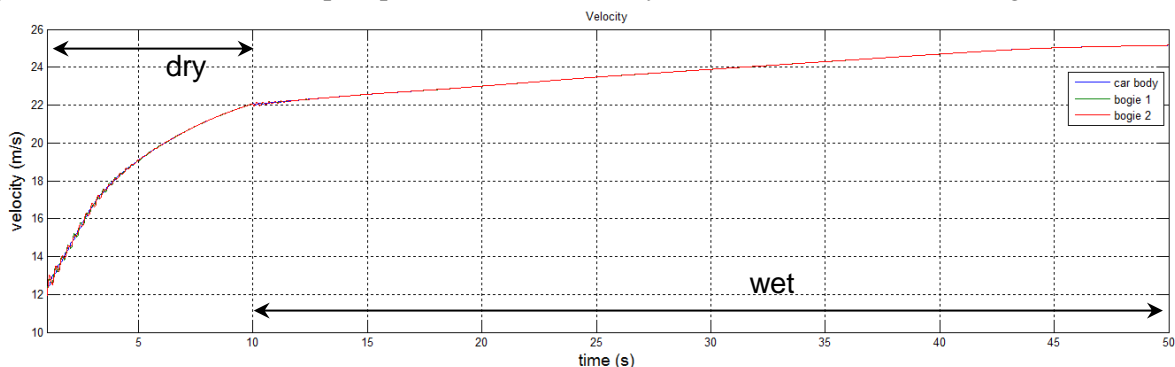


Figure 10: Velocity of the body and bogies on and after the transient of friction condition

In order to investigate further the longer term response of the detailed AC motor dynamics to a change a friction conditions, the creep response was simulated over a longer length of time to steady state as shown in Figure 11 and Figure 12. Figure 12 is a zoom in of the time right after the change of friction condition. In this case, the system is accelerating before the change of friction condition occurs at 10s. After the initial 2s, the creep of all axles, controlled by the creep controller, is reduced below 0.5%.

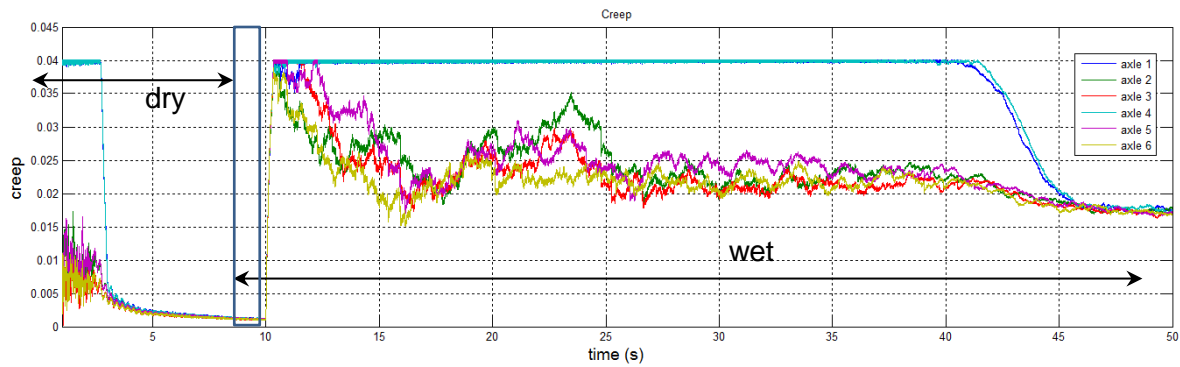


Figure 11: Creep on each axle for the entire simulation period

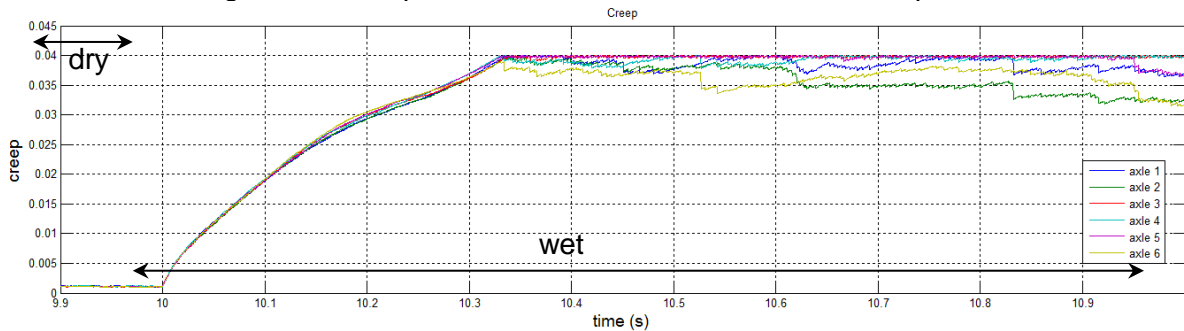


Figure 12: Creep on each axle on and after the change of friction condition (zoomup)

The following creep response has similar characteristics to the case described in Figure 9 in relation to the leading axles of each bogie having different dynamics from the other two axles on the same bogie which in turn show significant random like high frequency oscillations. However, no obvious high frequency oscillations can be seen during the dry condition, except the initial oscillation period (<2s). These high frequency oscillations are most likely associated with high frequency modes of the system, such as vibration of the wheelset-rail vertical vibration mode (mode frequency ~137Hz in Table 1). They do not appear in the vertical displacement response reported in the previous section since the high frequency response is beyond the frequency range of the multibody system.

After the change of friction conditions, the creep response can be divided into five stages. The first stage is when the creep increases dramatically, for 0.32s. This period of time from Figure 11 is zoomed in and plotted in Figure 12. After that (the second stage) the creep responses of all axles start to be reduced by the creep controller, while the leading axles of each bogie are kept at maximum/threshold creep 4%. During this stage (10.32s ~ 25s), the velocity of the bogies shows oscillations (barely discernable in Figure 10), this is mainly caused by the unstable creep response of the axles in this stage. From approximately 25s to 42s a steady acceleration stage occurs (the third stage), when the velocity oscillations of the bogies and the body are stabilized. The acceleration rate shown in Figure 10 is reduced significantly after the transient compared to the dry condition, because of the reduction of adhesion ratio from dry to wet condition. After 42s (the fourth stage), the creep of the leading axles start to converge to other axles; and after 45s (the fifth stage), the locomotive reached its maximum velocity and creep responses of all axles are stabilized.

2.3. Force response

The normal force of each axle was also investigated. Figure 13 shows the normal force for the entire simulation.

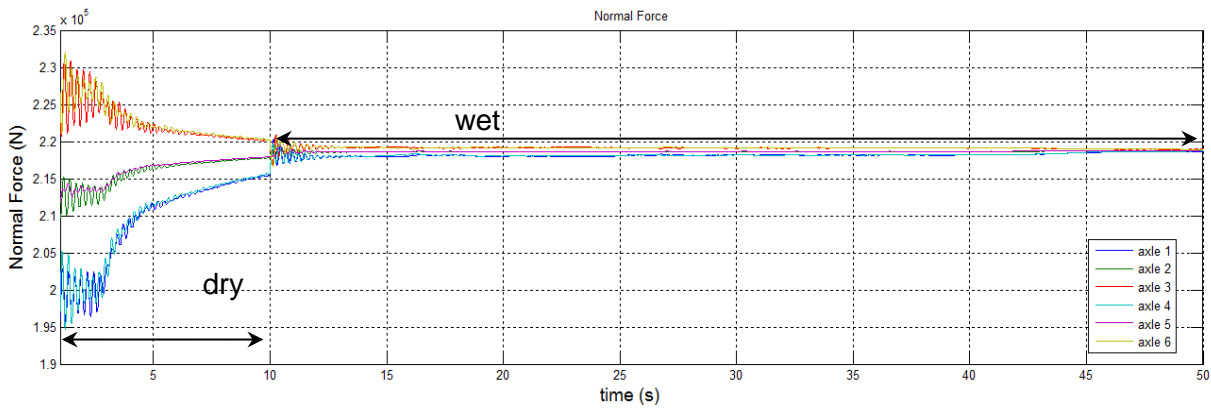


Figure 13: Normal force on each axle for the whole time

Similar to the creep response and the vertical displacement discussed previously, it can be seen that the normal force of a certain axle and its counterpart are similar. The oscillations on the normal force for each axle are approximately 3.7 Hz. It should be noted that the specification of this model is slightly different to the model discussed in section 3.1 [8]. The eigenmode analysis of the locomotive is as listed in Table 1. It is indicated that the oscillations at 3.7Hz agrees with the bogie vertical vibration mode at 3.72Hz. Since the contact between the wheel and rail was simplified as a spring-damper system, the normal force would be reflected in the vertical displacement. As a result, the oscillation frequency of the normal force should agree with the vertical vibration mode of the axles. The difference in normal force on separated axles results in the pitching of the bogies and the locomotive body as discussed in the previous section. It is also shown that the maximum amplitude of the normal force oscillation after the transient is approximately 2 kN per axle or 1% variation compared to the steady normal force ~ 220 kN per axle. The variation is considered relatively small and the damage to the wheel or the rail caused by such oscillations would be expected to be small.

Figure 14 shows the zoomup of Figure 13 normal force response after the change of the friction conditions. It is shown that large oscillations occurred for the first 5s after the transient, which agrees well with the creep response. After that, the normal forces stabilized with minor variations at the same frequency (~ 3.7 Hz). This could relate to the variations in creep response, as during 40-50s, when the creepage reduced, the normal force of all axles converged to each other.

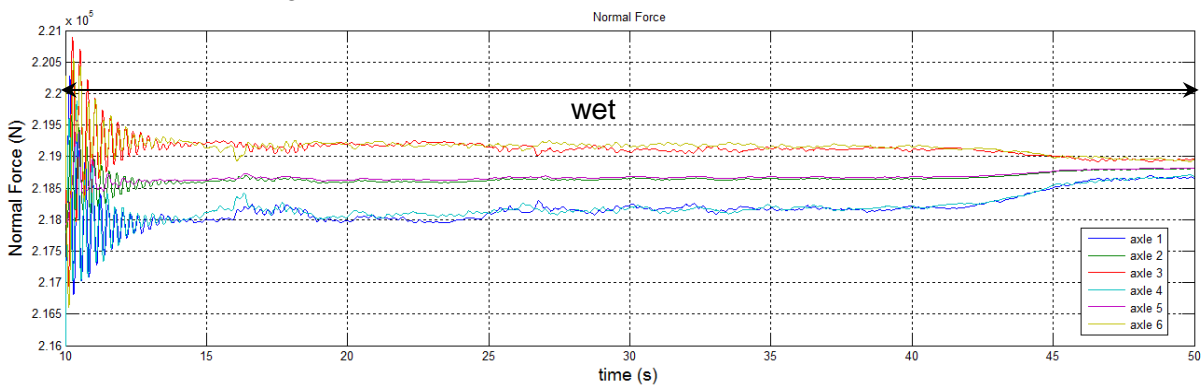


Figure 14: Normal force on each axle after the transient

Additionally, the traction forces of all axles are plotted in Figure 15 for the entire simulation. It is shown that the traction forces of all axles decrease before the change of the friction condition. This agrees with the traction curve indicating a hyperbolic relationship between the velocity and the traction effort. It is also noted that high frequency oscillations occur during the dry contact period even after the creep of all axles stabilized after 3s as shown in Figure 11. Further investigation into these high frequency oscillations shows that the frequency is over 1 KHz. This can only be caused by the torque variation of each 1/6 cycle of the AC motor ie due to the high frequency motor dynamics. After the change in friction condition, the traction force stabilized at the lower value. The reduction of the traction force is obviously caused by the reduction of the adhesion ratio from dry to wet. The high frequency oscillations still exist but the amplitude is reduced dramatically.

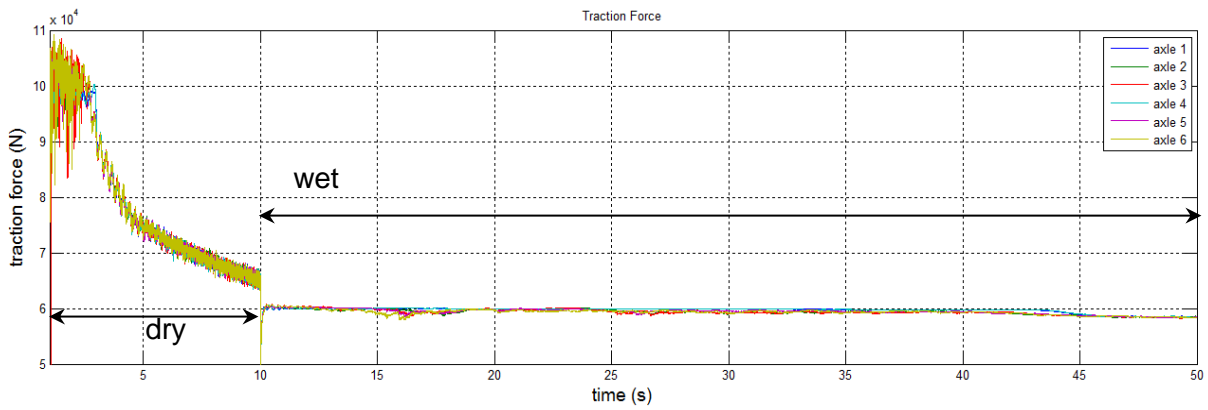


Figure 15: Traction force on each axle for the whole time

The traction/longitudinal force response after the change of the friction conditions are zoomed in and plotted in Figure 16.

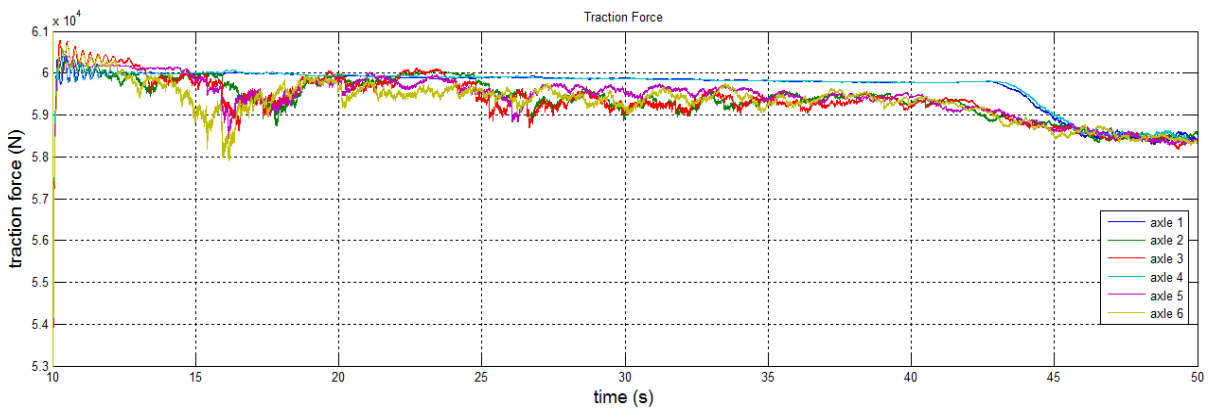


Figure 16: Traction force on each axle after the transient

It is shown that there are periodical oscillations on all axles from 10s to 13s at the frequency of approximately 3.7 Hz. This frequency is consistent with the normal force oscillations, and it occurs when the normal force oscillations have large amplitude. It can be calculated that the variation of traction force during this period of time is approximately 0.4 kN per axle or 0.6% compared to the steady traction force ~ 60 kN per axle. The variations of both forces are similar most likely because the creep interaction between traction and normal forces. It is demonstrated that the traction force follows the pattern of the creep response after 13s, consistent with the creep (Polach) law. The oscillations of both forces continue and are damped out for about 5s. After that, it is shown that the normal force stabilizes with minor oscillations occurring randomly until 40s. The random nature is most likely due to the interaction of the creep controller with the high frequency dynamics of the traction drive. It is noted that during this period, the locomotive is still under steady acceleration. This behaviour is consistent with the creep law and has caused a maximum variation on the traction force of 3 kN or 5% compared to the steady traction force ~ 60 kN. This variation is considerably larger than that of the normal force but is a decrease from critical values. A small scope sensitivity analysis shows this decrease appears to be consistent over changes in speed and controller strength. Such tractional oscillations will cause variations in wear and related defects but are expected not to be associated with excessive traction defects. However, the initial transients associated with vehicle dynamics (discussed above) could exceed critical creep excess traction damage particularly when the quasistatic traction levels are close to the limit of full sliding. In this case, these effects appear small to negligible (1%) when the locomotive creep controller has been tuned to achieve close to optimum performance. Under non-optimum performance and or largely different conditions the transient variations in forces are expected to be larger.

2. Conclusion and future works

An integrated dynamic model of a locomotive incorporating interactions between the structural dynamics, contact mechanics and traction/controller dynamics has been developed and tuned to investigate the response

under a change in frictional conditions. The dynamic response including creep response and forces, of the locomotive at and after a change in friction condition are investigated. The oscillation frequencies are compared with the eigenmode analysis and the related vehicle structural vibration modes are identified. By using the detailed AC motor dynamics model, both normal and traction force oscillations found in the first 3s after the change in friction condition are caused by the bogie structural vertical vibration. The amplitudes of these oscillations are approximately 1% of the steady force. After these vibrations are damped out, variations in creep dominate the changes in the traction force. These variations are relatively larger, up to 5%, compared to those caused by structural vibration, however they typically decrease the traction levels. These tractional oscillations, although small in this case, could result in dynamic wear defects and associated damage particularly when the quasistatic traction levels are close to the limit of full sliding and under less optimum creep controller performance. It takes approximately 30s for the creepage to stabilize. In this period of time, the locomotive will travel approximately 600m, and the track would possibly be affected by excessive transient forces.

Future research could be focused on the validation of the locomotive model dynamic response using field or test rig results. The model could also be further developed to simulate a larger range of locomotive models (if data is available from industry) and more frictional conditions. The efficiency of the model should be further improved to facilitate a sensitivity investigation of controller and locomotive structural parameters to dynamic force response.

Acknowledgements

The authors are grateful to the CRC for Rail Innovation (established and supported under the Australian Government's Cooperative Research Centres program) for the funding of this research Project No. R3.119 "Locomotive Adhesion". The authors acknowledge the support of the Centre for Railway Engineering, Central Queensland University and the many industry partners that have contributed to this project, in particular staff from RailCorp, Fortescue Metals Group (FMG) and Brookfield Rail.

References

- [1] N. Ramsey, F. Szanto, and P. Hewison, "Introducing the next generation locomotive to the Australian rail network," presented at the Conference on Railway Engineering, Perth, 2008.
- [2] R. U. A. Uzzal, A. K. W. Ahmed, and S. Rakheja, "Dynamic Analysis of Pitch Plane Railway Vehicle-Track Interactions Due to Single and Multiple Wheel Flats," *ASME Conference Proceedings*, vol. 2008, pp. 89-97, 2008.
- [3] M. R. U. A. Uzzal, "ANALYSIS OF A THREE-DIMENSIONAL RAILWAY VEHICLE-TRACK SYSTEM AND DEVELOPMENT OF A SMART WHEELSET," PhD, Mechanical Engineering, Concordia University, 2012.
- [4] R. Guclu and M. Metin, "Fuzzy Logic Control of Vibrations of a Light Rail Transport Vehicle in Use in Istanbul Traffic," *Journal of Vibration and Control*, vol. 15, pp. 1423-1440, September 1, 2009 2009.
- [5] D. S. Garivaltis, V. K. Garg, and A. F. D'Souza, "Dynamic Response of a Six-axle Locomotive to Random Track Inputs," *Vehicle System Dynamics*, vol. 9, pp. 117-147, 1980/05/01 1980.
- [6] X. Xin, B. K. Parida, A. K. Zaouk, N. Dana, and S. K. Punwani, "Impact Analysis of an Innovative Shock Energy Absorber and Its Applications in Improving Railroad Safety."
- [7] M. Spiryagin, Y. Q. Sun, C. Cole, T. McSweeney, S. Simson, and I. Persson, "Development of a real-time bogie test rig model based on railway specialised multibody software," *Vehicle System Dynamics*, vol. 51, pp. 236-250, 2013.
- [8] Y. Tian, W. B. Daniel, S. Liu, and P. A. Meehan, "Dynamic tractional behaviour analysis and control for a dc locomotive," in *World Congress on Rail Research (WCRR)*, Sydney, 2013.
- [9] O. Polach, "Creep forces in simulations of traction vehicles running on adhesion limit," *Wear*, vol. 258, pp. 992-1000, 2005.
- [10] M. Spiryagin, O. Polach, and C. Cole, "Creep force modelling for rail traction vehicles based on the Fastsim algorithm," *Vehicle System Dynamics*, vol. 51, pp. 1765-1783, 2013.
- [11] O. Polach, "A Fast Wheel-Rail Forces Calculation Computer Code," *Vehicle System Dynamics*, vol. 33, pp. 728-739, 1999.
- [12] V. R. Moorthi, *Power electronics: devices, circuits and industrial applications*: Oxford University Press, 2005.
- [13] I. Boldea and S. A. Nasar, *The Induction Machine Handbook*: CRC Press, 2002.
- [14] R. Marino, P. Tomei, and C. M. Verrelli, *Induction Motor Control Design*: Springer, 2010.
- [15] D. J. Atkinson, P. P. Acarnley, and J. W. Finch, "Observers for induction motor state and parameter estimation," *Industry Applications, IEEE Transactions on*, vol. 27, pp. 1119-1127, 1991.
- [16] S. Kadowaki, K. Ohishi, T. Hata, N. Iida, M. Takagi, T. Sano, and S. Yasukawa, "Antislip Readhesion Control Based on Speed-Sensorless Vector Control and Disturbance Observer for Electric Commuter Train Series 205-5000 of the East Japan Railway Company," *Industrial Electronics, IEEE Transactions on*, vol. 54, pp. 2001-2008, 2007.
- [17] Y. Kumsuwan, S. Premrudeepreechacharn, and H. A. Toliyat, "Modified direct torque control method for induction motor drives based on amplitude and angle control of stator flux," *Electric Power Systems Research*, vol. 78, pp. 1712-1718, 2008.
- [18] D. Casadei, F. Profumo, G. Serra, and A. Tani, "FOC and DTC: two viable schemes for induction motors torque control," *Power Electronics, IEEE Transactions on*, vol. 17, pp. 779-787, 2002.
- [19] P. Wach, *Dynamics and Control of Electrical Drives*: Springer, 2011.
- [20] S. N. EMU, "Rail Safety Investigation report No 2009/05, Platform overruns," Connex/Metro trains, Office of the Chief Investigator, transport Safety, Melbourne, Australia 2009.